REVALORIZACIÓN CATALÍTICA DE GLICERINA PARA UNA OBTENCIÓN MÁS RESPETUOSA CON EL MEDIO AMBIENTE DE ADITIVOS PARA COMBUSTIBLES

Mª Dolores González Candela

Dipòsit Legal: T. 1715-2011

María Dolores González Candela

REVALORIZACIÓN CATALÍTICA DE GLICERINA PARA UNA OBTENCIÓN MÁS RESPETUOSA CON EL MEDIO AMBIENTE DE ADITIVOS PARA COMBUSTIBLES

TESIS DOCTORAL

dirigida por
Dra. Yolanda Cesteros
Dra. Pilar Salagre

Departamento de Química Física e Inorgánica

UNIVERSITAT ROVIRA I VIRGILI

Tarragona
2011

UNIVERSITAT ROVIRA I VIRGILI
REVALORIZACIÓN CATALÍTICA DE GLICERINA PARA UNA OBTENCIÓN MÁS RESPETUOSA CON EL MEDIO AMBIENTE DE ADITIVOS PARA COMBUSTIBLES
Mª Dolores González Candela
DL:T. 1715-2011

UNIVERSITAT ROVIRA I VIRGILI

Departament de Química Física i Inorgànica
C/ Marcel·lí Domingo s/n
43007 Tarragona
Tel. 977558137
Fax 977559563

Dra. Yolanda Cesteros Fernádez, Catedrática de Universidad, y Dra. Pilar Salagre Carnero, Titular de Universidad, ambas del Departamento de Química Física e Inorgánica de la Universidad Rovira i Virgili,

HACEMOS CONSTAR:

Que este trabajo titulado "Revalorización catalítica de glicerina para una obtención más respetuosa con el medio ambiente de aditivos para combustibles", que presenta María Dolores González Candela, ha sido realizado bajo nuestra dirección en el Departamento de Química Física e Inorgánica de esta Universidad y que cumple los requisitos para poder optar a Mención Europea.

Tarragona, septiembre 2011

UNIVERSITAT ROVIRA I VIRGILI
REVALORIZACIÓN CATALÍTICA DE GLICERINA PARA UNA OBTENCIÓN MÁS RESPETUOSA CON EL MEDIO AMBIENTE DE ADITIVOS PARA COMBUSTIBLES
Mª Dolores González Candela
DL:T. 1715-2011

Agradecimientos

Es increíble que ya hayan pasado cuatro años, si parece que fue ayer cuando empecé esta aventura en el mundo de la investigación. Muchos de vosotros seguro que tenéis este mismo sentimiento porque habéis pasado junto a mí estos años, que sin duda alguna, no hubiera sido lo mismo sin vosotros.

En primer lugar quiero agradecer a mis directoras de tesis, las doctoras, Yolanda Cesteros y Pilar Salagre por todo su apoyo, ayuda y por haber hecho posible que este proyecto se llevara a cabo.

En particular a Yolanda le doy las gracias por su incondicional dedicación y esfuerzo en cada uno de los días de estos cuatro años, por siempre estar disponible en todo momento, por transmitirme todo su optimismo y ayudarme en los momentos más difíciles. Gracias por el trato que me has dado, la confianza y el respeto.

A Pilar gracias por ayudarme siempre que lo he necesitado y por ampliar mi conocimiento con preguntas e ideas que hacían que me esforzara más.

Agradecer a la Dra. María Linares del grupo de investigación dirigido por el Dr. David Serrano del departamento de Tecnología Química y Energética de la Universidad Rey Juan Carlos de Madrid por cederme la muestra de zeolita beta con porosidad jerarquizada. A la Dra. Elena Taboada por las muestras de aerogel y liogel sintetizadas en los laboratorios del Instituto de Ciencia de Materiales de Barcelona (ICMAB) en el grupo de investigación dirigido por el Dr. Elies Molins. Al Dr. Jordi Llorca de la Universitat Politècnica de Catalunya por los análisis de XPS.

Agradecer a todos los miembros del grupo de Organometálicos y Catálisis Homogénea, al igual que al grupo de Síntesis Orgánica estereoselectiva y Química de los carbohidratos, por toda la ayuda que me han dado durante estos años.

Todo esto no podría haber sido posible sin la ayuda de María José y Jordi, gracias por siempre estar disponibles y ayudarme con todo lo que he necesitado, las secretarias del departamento y al "Servei de Recursos científics i tècnics" de la Universidad, en especial a Ramón de RMN siempre buscando un hueco para el RMN de sólidos!! A Francesc de DRX siempre disponible a ayudar y a Mercè y Rita de Microscopia, gracias a todos!!!

Quiero agradecer a todos mis compañeros de seminario!! A los que empiezan, Laia mucha suerte en esta aventura!! Jorge y Tatiana gracias por vuestra simpatía, mucha suerte!! A las que hace poco empezaron y ya casi son veteranas! Jessica muchas

gracias por ser como eres, por ser tan simpática y atenta con todo el mundo, siempre intentado hacer una unión del seminario, esto te hace especial! y Eli, mi nueva compi de inglés! Muchas gracias por contar conmigo siempre aunque no pertenezca a vuestro grupo, me habéis hecho sentir una más. A las que estáis terminando, Angelica muchas gracias por tu buen humor, nunca dejes de sonreír! y por siempre ayudarme sin pedir nada a cambio, Mercè gracias por todos los buenos momentos que hemos vivido juntas! A las dos mucha suerte con la tesis, y sin duda alguna estaré ahí para lo que necesitéis. Oriol, Javi, Sabina, Jessica Cid mucha suerte en el futuro. Cristina Pubill! Gracias por siempre tener una sonrisa y hacer que días duros de trabajo acaben siendo muy divertidos!! Amadeu mucha suerte con la tesis, gracias por todos estos años, tanto en la carrera como durante la tesis, por ayudarme siempre que has podido y contar siempre conmigo! A los que ya han terminado Aitor, Carolina, Verónica gracias por los buenos momentos, Ariadna gracias por toda la ayuda que me has dado (no sé que hubiera hecho sin "la crack de la informática") y por los buenos momentos vividos! y Eva gracias por siempre estar cuando te he necesitado y compartir no solo un lado del seminario sino por las risas, días de estrés, de diversión, de cotilleos…see you soon!! Sin olvidarme de Ali, Cyril, Henrik y Bernabé, gracias!! Por último quiero dar las gracias a Raquel, que en tan poco tiempo te has convertido en una persona muy importante! Gracias por estar en todo momento cuando te he necesitado! Por escucharme, por las tardes en la plaza de la Font, cenas, risas…y lo que queda! muchas gracias!!

Quiero agradecer en especial a mis compañeras del laboratorio, a las "gatitas verdes". Que voy hacer sin vosotras!!! Gracias por estar cuando os he necesitado, por todos los momentos que hemos vivido en ese nuestro laboratorio, días de risas, de estrés, de diversión, de concentración…y como no días malos y buenos que acababan con una cerveza en la plaza de la Font, cenas, fiestas… en fin…imposible de olvidar! Gracias Isa por ayudarme en todo lo que era de tu alcance. Tati, que decirte…que sin duda alguna me llevo una buena amiga, que me da mucha pena que te marches, pero espero algún día ir a verte a Cali. Elena, la crazy del laboratorio, jeje! Gracias por alegrar el día poniendo siempre música en el lab, por las tardes en la plaza de la Font, por las cenas en tu pisito, gracias por ayudarme en todo, y espero que sean muchos años más juntas. Susana, muchas gracias por hacer que en el lab todo sea más fácil! María, mucha suerte por Alemania y gracias por los buenos momentos. Olga, gràcies pels teus consells! Y Xavi, aunque hemos coincidido poco gracias por los ratos que hemos pasado en el laboratorio.

A todos los de ingeniería: Álvaro, Anna, Sandra, Antón, Noelia, Mayra, Abel, Beteley, Kaveh, Iulana, Oscar y Luis -el presidente de la futura República de España, jeje- gracias por los buenos momentos!! Alex y Adriana mucha suerte!!y gracias por estos cuatro años, por vuestra ayuda y apoyo!! Y María Alba, mucha suerte en tu tesis!!

A todos los que han pasado por el seminario Nicolas, Olivier, Doris, Lourdes, Gawaine, Cara, Glòria, Vanessa, Alex, Norbert, Benjamin, Tatiana, Dagoberto, Sarah y Sheila. En especial a Cara, gracias por todos los buenos momentos vividos esos tres meses que estuviste de estancia en el labo, nunca lo olvidaré, que se convirtieron en otras visitas a Londres, Tarragona, Nottingham...

Mil gràcies Estefania! que sembla mentida que després de 4 anys de carrera, sense conèixer-nos, arribessis al nostre labo i et converteixis en una amiga molt especial!! Gràcies per tots el moments viscuts al labo, i en especial moltes gràcies per fer la meva estància en Nottingham molt fàcil. No oblidaré, les nits de soparets a casa veient una peli, les nits de cinema, de birres…Ara que has començat una nova etapa a Alemanya et desitjo lo millor, que tot vagi molt bé i lo més difícil ja l'has passat i que ara solament et queda la recta final!ens veiem aviat!muaass!

I would like to thank Prof. Robert Mokaya to accept me in his group. Thanks to Afaf, Nurul and specially Eric and Marta for helping me in the lab during my three months in Nottingham. Marion and Alice, my flatmates, thank you for making things easier. Como no al grupo de españoles que conocí que hicieron mi estancia tan fácil: Eduardo, Yolanda, Mara, Ana, Oscar, los que no era españoles Lee, Amrit, y en especial Marta y Pilar que fuisteis un gran apoyo y os convertisteis en grandes amigas, espero que nos veamos pronto y que las nuevas etapas que empezáis en Asturias e Inglaterra sean muy buenas, os deseo lo mejor!Sonia, madre mía!! quién mejor para conocer la experiencia que viví en Nottingham, mejor dicho que vivimos!! En poco tiempo te convertiste en una hermana, recuerdo las conversaciones que teníamos por las mañanas delante de la facultad tomando el primer café de la mañana, y ya hacia noviembre se trasladaron a tu despacho por el frio que hacía ya. Todo fue muchísimo más fácil, gracias por todo, y mucha suerte para la tesis que seguro que irá muy bien. Espero que cuando acabes no te olvides que en Tarragona tienes una amiga para siempre!

Dar las gracias a mis compañeros de carrera, Cristina Fernández, que se introdujo en el mundo de la quimiometria...Gracias por todos esos años, clases interminables, laboratorios, tardes de cartas y como no tantas noches de fiesta. Javi, el

orgánico por excelencia, gracias también por todos estos años siempre ayudándonos con el mundo de la orgánica.

En especial quiero agradecer a mis grandes amigas Cris e Irene por todo el apoyo, por toda vuestra ayuda fuera y dentro del laboratorio, habéis hecho que todo fuera más fácil. Gracias por escuchar mis ralladas, por esas noches de cine, fiesta…que puedo decir, tantos recuerdos inolvidables durante estos cuatro años…y todo lo que nos queda por vivir que nada sería igual sin vosotras!! A mis amigas de siempre Laura, Adela y Rocío, no sería nada sin ellas!! En estos años de tesis gracias por ser mi vía de escape y permitir poder desconectar en muchos momentos del mundo de la Química que muchas veces era muy difícil! A mi compi Lorena, muchas gracias por todos los momentos vividos durante la carrera y después de ella, sabes que tienes una amiga para siempre! En este grupo no podrían faltar Jordi, Alba, Joan (el primo), Oksana, Albert, Miguel, Hugo, Ángel, Elena, Eli…entre otros muchos, gracias!!

Gracias a toda mi familia, que sin ellos no sería nada. Aunque nací y soy de Tarragona mis raíces son de Villacarrillo, un pueblecito de Jaén, y de La Unión, ciudad minera y flamenca, de Murcia. Especial cariño tengo a La Unión ya que allí tengo a la mitad de mi corazón. La otra mitad, como no, está en Tarragona. Gracias a mis primos, tíos y abuelos por enseñarme, ayudarme y quererme tal y como soy. Estoy muy orgullosa de pertenecer a esta GRAN FAMÍLIA!!! Sin olvidarme de la familia Carrión Pedrol, gràcies per fer-m'he sentir com una més de la família des del primer dia!!

Por quién daría la vida sin dudarlo ni un segundo, mis padres, tan importantes en mi vida, Lola y Jose Mª, mamá y papá, mil gracias por todo lo que habéis hecho por mí, mil gracias por ayudarme en los buenos y malos momentos, me siento muy orgullosa de vosotros!! A mi hermanito Jose Mª, el pequeño de la casa y el futuro Físico de la familia!! Mil gracias por todos los buenos momentos que hemos vivido juntos y por ayudarme siempre en todo!! Os quiero muchisimooooOOO!!

Joanan que te puedo decir que no sepas, que eres la persona más importante en mi vida. Gracias por estar siempre a mi lado, ayudarme, por comprender esos días de estrés que conlleva la tesis, gracias por darlo todo por mí… te quiero.

Por último, quiero dedicar mi tesis a las personas que creo que son las que más me han enseñado e incluso querido en esta vida. Porque la sabiduría es la hija de la experiencia. A vosotros abuelos, Lola y Juan, Isabel y Ginés esto va dedicado a vosotros.

UNIVERSITAT ROVIRA I VIRGILI
REVALORIZACIÓN CATALÍTICA DE GLICERINA PARA UNA OBTENCIÓN MÁS RESPETUOSA CON EL MEDIO AMBIENTE DE ADITIVOS PARA COMBUSTIBLES
Mª Dolores González Candela
DL:T. 1715-2011

ÍNDICE

1. Introducción general 3

1.1. Importancia de la glicerina 3

1.2. Problemática del excedente de glicerina 4

1.3. Transformaciones catalíticas de la glicerina 6

2. Objetivos 9

3. Parte experimental 15

3.1. Descripción de las zeolitas y materiales mesoporosos ordenados utilizados 15

3.1.1. Zeolitas 15

3.1.2. Materiales mesoporosos ordenados 18

3.2. Tratamientos de modificación de zeolitas 21

3.2.1. Desaluminación 21

3.2.2. Intercambio catiónico 22

3.2.3. Desilicación 24

3.2.4. Fluoración 24

3.2.5. Sulfonación 26

3.2.6. Zeolita con porosidad jerarquizada 28

3.3. Tratamientos de modificación de materiales mesoporosos ordenados 29

3.3.1. Incorporación de aluminio 29

3.3.2. Incorporación de grupos fosfóricos 30

3.3.3. Sulfonación 31

3.4. Tratamiento de sulfonación en otro tipo de materiales: montmorillonita K10, aerogel y liogel de sílica 34

3.4.1. Montmorillonita K10 34

3.4.2. Aerogel y liogel de silica 35

3.5. Utilización de la radiación microondas en la preparación y modificación de materiales 36

3.6. Técnicas de caracterización 37

3.6.1. Difracción de Rayos X de polvo (DRX) 37

3.6.2. Fisisorción de N_2 39

3.6.3. Análisis termogravimétrico (TGA) 42

3.6.4. Valoración potenciométrica....43
3.6.5. Espectroscopia Fotoelectrónica de Rayos X (XPS) 43
3.6.6. Microscopía electrónica....44
Microscopía electrónica de barrido (SEM) 44
3.6.7. Desorción a Temperatura Programada (TPD)....45
3.6.8. Espectroscopía FT-IR....45
3.6.9. Resonancia Magnética Nuclear de ángulo mágico de espín (RMN AME)....47
3.6.10. Fluorescencia de Rayos X (FRX)....48
3.6.11. Determinación de tipos de centros ácidos mediante test catalíticos....48
3.7. Actividad Catalítica en la reacción de eterificación de glicerol con tert-butanol e isobuteno....49
3.7.1. Condiciones de reacción....49
3.7.2. Análisis de los productos de reacción....51

4. Results and Discussion 57
4.1. Background about dealumination studies of zeolites 57
4.1.1. Effect of microwaves in the dealumination of mordenite on its surface and acidic properties 63
Introduction 64
Experimental....65
Results and discussion 67
Conclusions 76
Acknowledgments 77
4.1.2. Comparison of dealumination of zeolites beta, mordenite and ZSM-5 by treatment with acid under microwave irradiation 79
Introduction 80
Experimental....81
Results and discussion 84
Conclusions 96
Acknowledgments 96

4.2. Background about glycerol etherification with tert-butanol or isobutene.....99
4.2.1. Establishing the role of Brønsted acidity and porosity for the catalytic etherification of glycerol with tert-butanol by modifying zeolites.....105
Introduction.....106
Experimental.....107
Results and discussion.....111
Conclusions.....127
Acknowledgments.....128
4.2.2. Effect of hierarchical porosity in zeolites on the catalytic etherification of glicerol.....129
Introduction.....130
Experimental.....131
Results and discussion.....134
Conclusions.....146
Acknowledgments.....146
4.2.3. Boosted selectivity towards high glycerol tertiary butyl ethers by microwave-assisted sulfonic functionalization of SBA-15 and Beta zeolite.....147
Introduction.....148
Experimental.....148
Results and discussion.....149
Conclusions.....152
Acknowledgments.....153
Supporting information.....153
4.2.4. Microwave-assisted synthesis of sulfonic acid-functionalized microporous materials for the catalytic etherification of glycerol with isobutene.159
Introduction.....160
Experimental.....161
Results and discussion.....164
Conclusions.....177
Acknowledgments.....178

4.2.5. Successfully conventional and microwave-assisted preparation of sulfonic acid-functionalized aerogels and liogels by a simple post-synthesis method 179
Introduction 180
Experimental 181
Results and discussion 183
Conclusions 189
Acknowledgments 190
4.2.6. Synthesis of modified MCM-41, SBA-15 and HMS to be used as catalysts for the catalytic etherification of glycerol with isobutene 191
Introduction 192
Experimental 194
Results and discussion 198
Conclusions 207
Acknowledgments 208

5. Conclusiones 211
6. Referencias bibliográficas 217

1. INTRODUCCIÓN GENERAL

UNIVERSITAT ROVIRA I VIRGILI
REVALORIZACIÓN CATALÍTICA DE GLICERINA PARA UNA OBTENCIÓN MÁS RESPETUOSA CON EL MEDIO AMBIENTE DE ADITIVOS PARA COMBUSTIBLES
Mª Dolores González Candela
DL:T. 1715-2011

1. Introducción general

1.1. Importancia de la glicerina

El glicerol (glicerina o 1,2,3-propanotriol, Figura 1) es un líquido incoloro, inodoro y viscoso, derivado de compuestos naturales o petroquímicos. En 1779, el químico sueco Carl W. Scheele descubrió esta molécula, la cual probó encontrándole un sabor muy dulce. Sin embargo, el descubrimiento de "el dulce de Scheele" no tuvo un gran impacto en la investigación científica e industrial durante años. No fue hasta 1811, cuando Michel Eugene Chevrel, un químico francés denominó a este líquido como "glicerol", que tiene su origen en la palabra griega *glykos,* que significa dulce. [1-2]

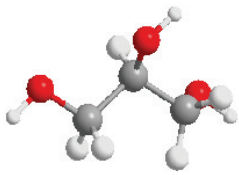

Figura 1. Molécula de glicerol.

La glicerina es una de las sustancias químicas conocidas más versátil, con más de mil aplicaciones y usos. [1,3] La primera aplicación que tuvo el glicerol fue en 1866 en la producción de nitroglicerol, que se utilizaba en la obtención de dinamita. Entre todas sus aplicaciones cabe destacar su uso en farmacia, cosmética, higiene personal, en la fabricación de tabaco, comestibles, o en la producción de resinas, o detergentes entre otras (Figura 2).

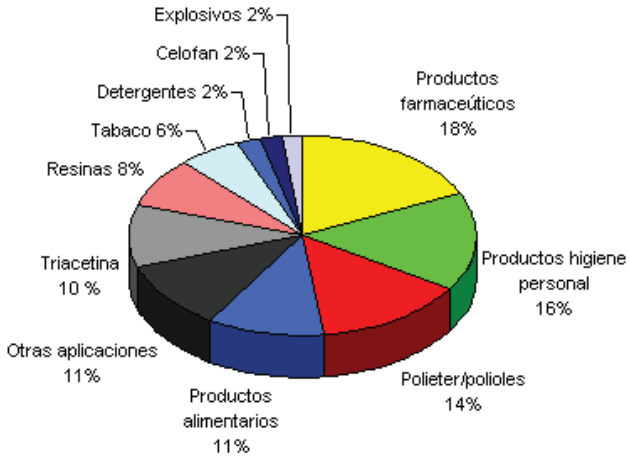

Figura 2. Mercado del glicerol. [3]

La cantidad de glicerol que se utiliza anualmente en estas aplicaciones es de alrededor de 160000 toneladas, y se espera un incremento anual de un 2.8%. Sin embargo, el mercado de la glicerina ha cambiado radicalmente en los últimos años debido a los excedentes que se generan en la producción de biodiesel.

1.2. Problemática del excedente de glicerina

Durante el siglo XXI ha aumentado el interés por el uso de nuevos combustibles obtenidos a partir de materias primas renovables y más respetuosos con el medioambiente (libres de azufre y de compuestos aromáticos, dando lugar a una reducción significativa de emisiones de partículas, hidrocarburos, CO y aldehídos) entre los que podemos destacar la producción de biocombustibles. [4] Hoy en día existen numerosas tecnologías para la fabricación de biocombustibles, destinados al transporte, a partir de biomasa. Se pueden considerar dos tipos principales de biocombustibles: el biodiesel y el bioetanol. [5] El bioetanol se obtiene a partir de la fermentación de azúcar o maíz, mientras que el biodiesel se obtiene mediante la transesterificación de aceites vegetales con metanol (Figura 3).

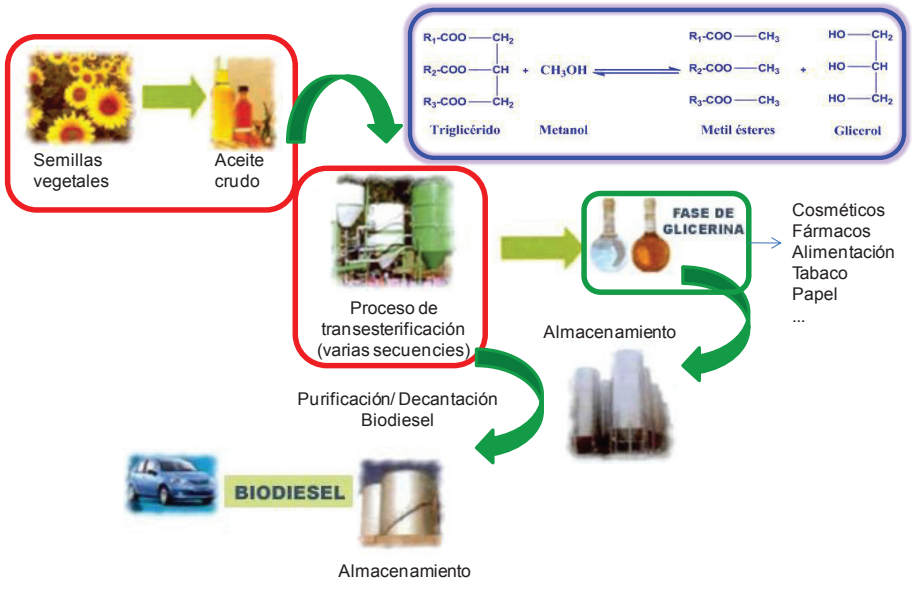

Figura 3. Transesterificación de aceites vegetales con metanol para la obtención de biodiesel.

Durante la fabricación de biodiesel se obtiene glicerina como subproducto (10 % en peso del producto total). Un incremento de la demanda de biodiesel en los últimos años ha dado lugar a importantes excedentes de glicerol (1 millón de toneladas de glicerina en 2007 comparado con las 600000 toneladas de 1992). A finales de 2010 la Unión Europea (UE) se había propuesto una aportación del 5.75 % de biocombustibles en el total de combustibles utilizados para el transporte. Este aumento se ha traducido en un incremento de la producción biodiesel de unos 10 millones de toneladas por año, produciendo alrededor de 1 millón de toneladas de glicerol como subproducto (Figura 4). El aumento de la producción de biodiesel dio lugar, a mediados de los años 2000, a una disminución del precio de la glicerina conforme iba aumentando la construcción de plantas de biodiesel (Figura 4). [6,7] Además, la UE mira hacia el futuro y pretende que la proporción de biocombustibles en el transporte aumente hasta un 10 % en 2020.

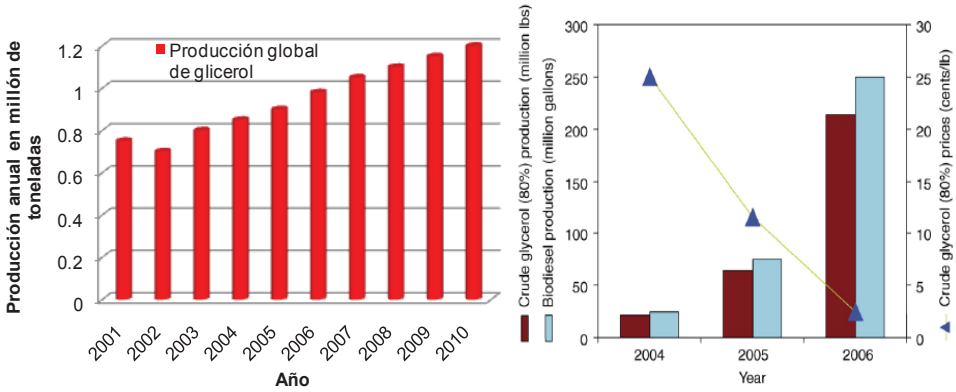

Figura 4. Influencia del incremento de la producción de biodiesel en el precio del glicerol. [7]

El glicerol que se obtiene durante la fabricación de biodiesel, contiene una mezcla de metanol, agua, sales inorgánicas (residuos del catalizador), ácidos grasos libres, reactivos sin reaccionar, etc. Por ello, es necesario purificarlo para su posterior utilización en sus aplicaciones tradicionales como en la industria farmacéutica, cosmética o alimentaria.

Este proceso de purificación tiene un elevado coste y difícilmente se puede aplicar en las plantas de biodiesel, ya que no resulta rentable teniendo en cuenta los grandes excedentes de glicerol obtenidos. Por tanto, es necesario buscar nuevas formas de transformar el glicerol en productos de alto valor añadido de manera que se pueda dar una salida rentable al exceso de glicerol generado.

1.3. Transformaciones catalíticas de la glicerina

Una alternativa altamente interesante es la utilización de la catálisis heterogénea para la transformación de la glicerina en derivados con importantes aplicaciones en diversos sectores como fueles, detergentes, productos farmacéuticos, productos químicos diversos o materiales de construcción. [2-3,5-11] Las primeras publicaciones sobre estas reacciones catalíticas comienzan en los años 80 del siglo pasado, algunas de ellas en forma de patentes, pero es a partir del 2002, a raíz del crecimiento en la producción del biodiesel, y por tanto, de la generación de excedentes de glicerina, cuando se ha incrementado la investigación, y en consecuencia el número de publicaciones.

En la bibliografía se constata que uno de los factores clave en la transformación catalítica selectiva de glicerol es el uso de catalizadores con las características adecuadas al proceso catalítico concreto. [3,11] En la siguiente figura se muestra un resumen de los principales productos químicos que se pueden obtener mediante conversión catalítica de glicerina.

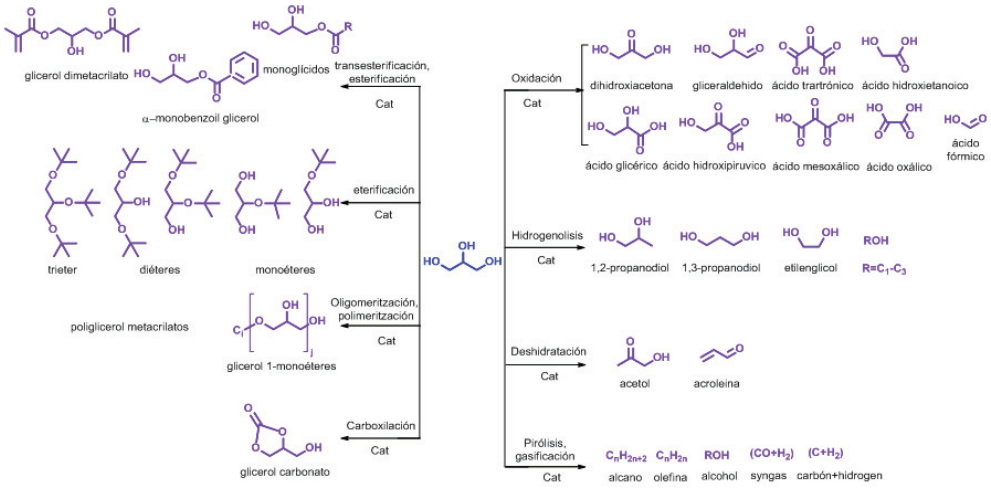

Figura 5. Transformación catalítica del glicerol en productos de alto valor añadido.

Una de las reacciones con mayor interés es la eterificación de glicerol con tert-butanol o isobuteno para la obtención de los di- y tri-tert-butil éteres de glicerol (h-GTBEs) ya que se pueden utilizar como aditivos oxigenados en combustibles reemplazando el metil tert-butil éter (MTBE), tóxico para el medio ambiente. Esta reacción está catalizada por centros ácidos de Brønsted. [5]

2. OBJETIVOS

UNIVERSITAT ROVIRA I VIRGILI
REVALORIZACIÓN CATALÍTICA DE GLICERINA PARA UNA OBTENCIÓN MÁS RESPETUOSA CON EL MEDIO AMBIENTE DE ADITIVOS PARA COMBUSTIBLES
Mª Dolores González Candela
DL:T. 1715-2011

2. Objetivos

El objetivo principal de esta tesis es preparar y caracterizar nuevos catalizadores heterogéneos ácidos activos y selectivos hacia la formación de di- y tri-tert-butil éteres de glicerol (h-GTBEs) en la reacción de eterificación de glicerol con tert-butanol o isobuteno.

Otro de los objetivos importantes de la tesis es el estudio del efecto de la radiación microondas en desaluminación de zeolitas y en sulfonación de zeolitas y materiales mesoporosos ordenados.

En base a lo comentado anteriormente, los objetivos parciales de esta tesis son:

1. **Realizar un estudio comparativo del efecto de la radiación microondas en la desaluminación de zeolitas respecto al método de calentamiento convencional.** El estudio se ha realizado con 3 zeolitas comerciales tipo pentasil: Na-mordenita, Na-Beta y Na-ZSM-5 tanto en autoclave como en reflujo.

2. **Preparar y caracterizar catalizadores con diferente cantidad y fuerza de centros ácidos de Brønsted y con diferente porosidad** (micro-, meso- y macroporosidad) con la finalidad de observar su efecto en la reacción estudiada. La presencia de meso- y macroporosidad debería favorecer la formación de los éteres de mayor volumen, especialmente el triéter así como la accesibilidad de los reactivos a los centros activos.

    - Zeolitas modificadas: H-zeolitas, La-zeolitas, zeolitas desaluminadas, zeolitas desilicadas y posteriormente protonadas, zeolitas fluoradas y zeolitas sulfonadas que se obtendrán a partir de 3 zeolitas comerciales tipo pentasil: Na-mordenita, Na-ZSM-5 y Na-beta. También se probará una zeolita beta con porosidad jerarquizada y esa misma muestra fluorada.
    - Arcilla modificada: se incorporarán grupos sulfónicos en una montmorillonita K10 comercial.

- Materiales mesoporosos ordenados sintetizados (HMS, MCM-41 y SBA-15) y modificados mediante incorporación de aluminio, grupos fosfóricos y sulfónicos.
- Aerogel y liogel de sílica modificados mediante sulfonación.

3. **Estudiar el efecto de la utilización del horno microondas en la sulfonación de la zeolita Beta, el material mesoporoso ordenado SBA-15, el aerogel y liogel de silica.** Comparar las propiedades de los materiales sulfonados con microondas con los correspondientes sulfonados mediante la utilización de calentamiento convencional.

4. **Caracterizar los catalizadores obtenidos** mediante las siguientes técnicas: fisisorción de N_2, difracción de Rayos X, análisis termogravimétrico, desorción a temperatura programada, infrarrojo, resonancia magnética nuclear de Al e H, fluorescencia de Rayos X, microscopía electrónica de barrido y transmisión y espectroscopía fotoelectrónica de Rayos X. Además, para la determinación de tipos de centros ácidos en zeolitas se realizarán tests catalíticos con dos reacciones modelo: la isomerización de óxido de estireno a fenilacetaldehído y la reacción de apertura del anillo de estireno a 2-etoxi-2-feniletanol.

5. **Estudiar la actividad catalítica de los catalizadores preparados en la eterificación de glicerol con isobuteno o con tert-butanol** en reactor batch autoclave. Los resultados catalíticos se compararán con los obtenidos con una resina de intercambio iónico ácida (Amberlyst-15), un típico catalizador comercial utilizado en esta reacción. Los productos de reacción se analizarán mediante cromatografía de gases.

6. **Estudiar la desactivación** de algunos de los catalizadores con el tiempo y comparar los resultados con los obtenidos con el catalizador Amberlyst-15. Además, se realizará el seguimiento de las propiedades superficiales de los catalizadores después de la reacción.

Esta tesis cumple con varios de los principios por los que aboga la "Química Verde", ya que por una parte se busca la revalorización de un excedente como la glicerina como materia prima para la obtención de productos químicos de alto valor añadido; por otra parte, los procesos propuestos son vías alternativas a los que utilizan productos derivados del petróleo (fuente no renovable); además, la síntesis de catalizadores (que sean altamente selectivos a los productos deseados) implica una disminución en la generación de residuos (disminución del factor E (kg de residuo /kg de producto obtenido)) y, por último, con la utilización de microondas en la preparación de catalizadores se persigue una disminución en los tiempos de preparación, con el consiguiente ahorro energético.

UNIVERSITAT ROVIRA I VIRGILI
REVALORIZACIÓN CATALÍTICA DE GLICERINA PARA UNA OBTENCIÓN MÁS RESPETUOSA CON EL MEDIO AMBIENTE DE ADITIVOS PARA COMBUSTIBLES
Mª Dolores González Candela
DL:T. 1715-2011

3. PARTE EXPERIMENTAL

UNIVERSITAT ROVIRA I VIRGILI
REVALORIZACIÓN CATALÍTICA DE GLICERINA PARA UNA OBTENCIÓN MÁS RESPETUOSA CON EL MEDIO AMBIENTE DE ADITIVOS PARA COMBUSTIBLES
Mª Dolores González Candela
DL:T. 1715-2011

3. Parte Experimental

3.1. Descripción de las zeolitas y de los materiales mesoporosos ordenados utilizados

Las zeolitas y los materiales mesoporosos ordenados comparten la característica común de tener estructuras porosas uniformes y regulares. Para describir una estructura porosa, los parámetros más utilizados son el tamaño y forma de poro. Siguiendo las reglas de la IUPAC, los compuestos porosos pueden clasificarse como materiales microporosos (diámetro de poro menor a 2 nm), mesoporosos (diámetro de poro entre 2 y 50 nm), y macroporosos (diámetro de poro mayor a 50 nm).

3.1.1. Zeolitas

Las zeolitas constituyen una de las familias más importantes en el grupo de los materiales microporosos. Las zeolitas naturales se descubrieron por primera vez en *1756* cuando el minerologista sueco Alex Cronsted describió la primera zeolita mineral, la estilbita. Cronsted las define como una nueva clase de minerales constituídos por aluminosilicatos hidratados. El nombre que les otorgó fue debido a la capacidad de éstas de perder fácilmente agua por calentamiento; así las denominó zeolitas que proviene de las palabras griegas: *zeo* que significa hervir y *lithos* que significa piedra. [12] El término "zeolita" se refiere a un aluminosilicato cristalino o sílica polimorfa basada en una estructura tridimensional formada por tetraedros de silicio y aluminio $[SiO_4]^{4-}$ $[AlO_4]^{5-}$ unidos por compartición de vértices formando puentes de oxígeno no lineales (Figura 6). Las posiciones de los átomos de Si y Al se asignan aplicando la regla de Loewnstein, que prohíbe la presencia de una unión Al-O-Al en la estructura.

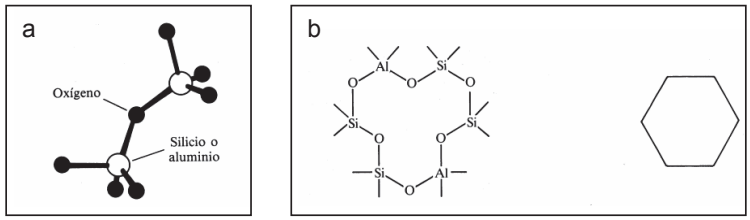

Figura 6. a) Unidades tetraédricas de construcción de una zeolita b) Esquema de un anillo de 6.

Las zeolitas poseen un esqueleto aniónico, ya que la sustitución de Si (IV) por Al (III) en la estructura crea un desequilibrio electrónico, y para preservar la neutralidad eléctrica total es necesario equilibrar cada $[AlO_4]^{5-}$ con una carga positiva. La carga

negativa que se genera queda compensada por la presencia de cationes que se sitúan en los canales o cavidades de las zeolitas. Estas cavidades y/o canales también alojan moléculas de agua y otras moléculas o sales. [13]

La fórmula empírica de la zeolita se puede expresar como $\mathbf{M_{x/n}[(AlO_2)_x(SiO_2)_y]\cdot mH_2O}$, donde M es el catión con carga n.

Los tetraedros $[SiO_4]^{4-}$ y $[AlO_4]^{5-}$ pueden unirse compartiendo dos, tres o los cuatro vértices, formando así una gran variedad de estructuras diferentes. Muchas zeolitas se basan en unidades de construcción superiores. Existen dos tipos de unidades: la sodalita y el pentasil (Figura 7).

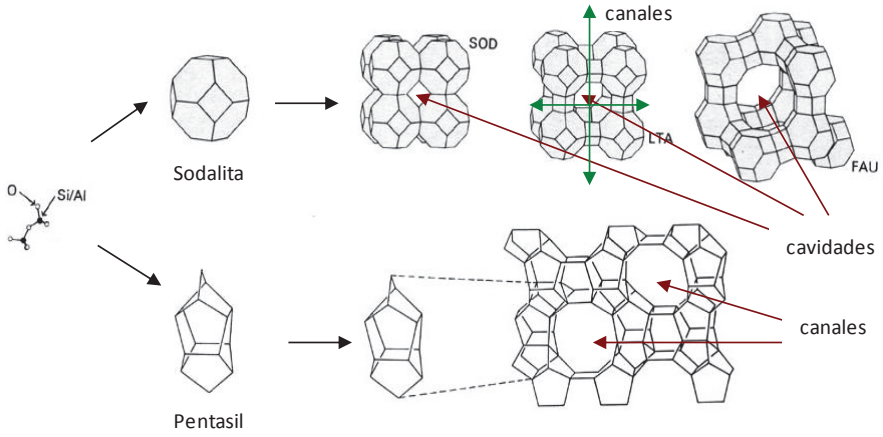

Figura 7. Ejemplo de zeolitas tipos sodalita y pentasil.

Las zeolitas utilizadas en esta tesis son: Mordenita, Beta y ZSM-5. La zeolita Mordenita presenta un sistema poroso unidimensional con dos tipos de canales con anillos de 8 y de 12, respectivamente. Los canales principales tienen un diámetro de poro de 6.7 x 7.0 Å y los canales más pequeños, denominados "side-pockets", de 2.6 x 5.7 Å (Figura 8). Por otro lado, la zeolita Beta presenta un sistema poroso tridimensional de canales con anillos de 12 y diámetros de poro de 6.6 x 6.7 Å y 5.6 x 5.6 Å (Figura 8), siendo su estructura muy flexible. Por último, la zeolita ZSM-5 tiene una sistema poroso tridimensional formado por canales con anillos de 10 y diámetros de poro de 5.1 x 5.5 Å y 5.3 x 5.6 Å. Su sistema poroso no conecta cavidades grandes pero si hay intersecciones con gran cantidad de espacio libre que puede permitir que se lleven a cabo interacciones moleculares (Figura 8). [14]

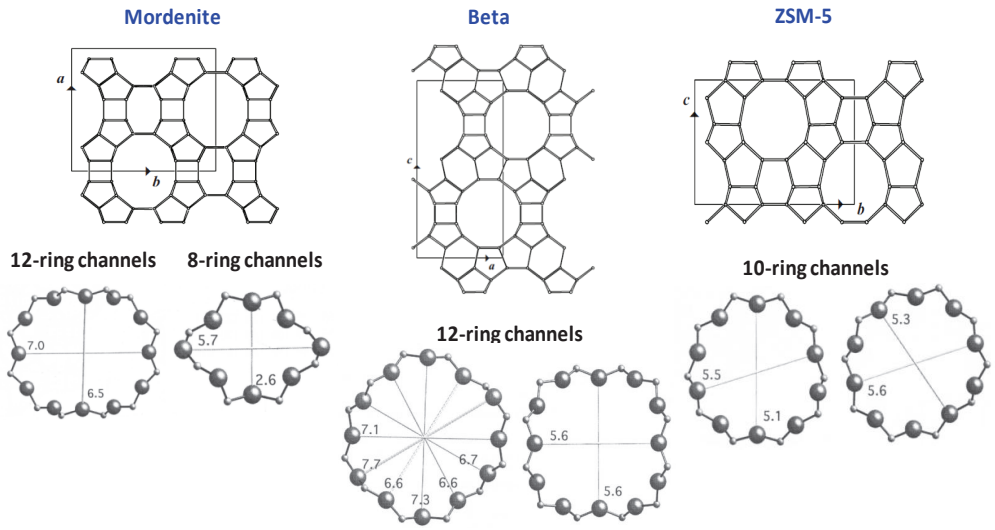

Figura 8. Estructura microporosa de poro de las zeolitas: Mordenita, ZSM-5 y Beta.

Las primeras aplicaciones industriales de las zeolitas datan de 1955 con su utilización para la deshidratación de gases refrigerantes y de gas natural así como intercambiadores de cationes para ablandar las aguas duras. En 1960 las zeolitas empezaron a ser empleadas como catalizadores en reacciones de cracking o isomerización de parafinas y como tamices moleculares en procesos de separación de moléculas de diferentes formas y tamaños. A partir de entonces la investigación de estos materiales se ha desarrollado con rapidez debido a su amplia aplicación en catálisis ya que por sus características ácidas y la selectividad de forma que presentan ("shape selectivity") se utilizan como catalizadores en la industria petroquímica. [15] Todas estas aplicaciones quedan principalmente determinadas por sus características estructurales, como son el tamaño de la ventana de poro, la accesibilidad a los centros activos, la dimensionalidad del sistema de canales, el número y lugar ocupado por los cationes, etc.

3.1.2. Materiales mesoporosos ordenados (MCM-41. SBA-15, HMS)

Unas de las principales limitaciones de las zeolitas son las dimensiones y accesibilidad de sus poros (~1.3 nm) que limitan sus aplicaciones a moléculas pequeñas, y a moléculas orgánicas o biológicas de cadena corta. Por ello, la síntesis de materiales mesoporosos ordenados con un sistema de tamaño de poro entre ~1.5-30 nm resulta altamente interesante. En la siguiente figura se muestra algunos ejemplos de la distribución de tamaño de poro de diferentes materiales porosos. [16-17]

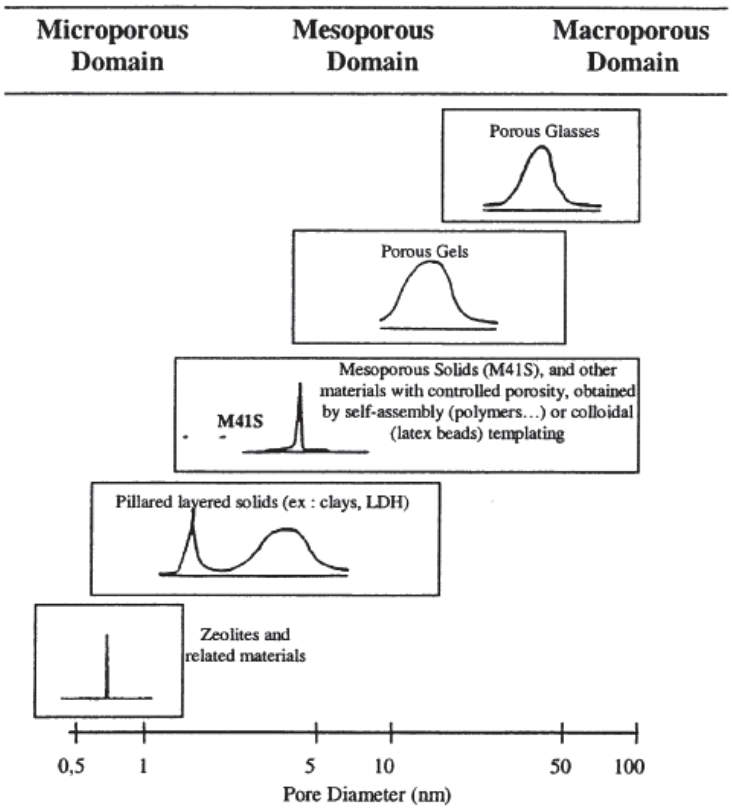

Figura 9. Distribución de tamaño de poro de diferentes materiales micro-, meso- y macroporosos. [17]

Los materiales mesoporosos ordenados poseen algunas propiedades que otros materiales porosos no tienen. Estas propiedades incluyen:

- Tamaños y forma de poro bien definidos, además de una distribución de tamaño de poro estrecha.
- Sistema de estructura de poro altamente ordenado a nivel de nanómetros.
- Tamaño de poro ajustable en un rango de ~1.3 a ~30 nm.
- Varias geometrías, composición de las paredes y formas de poro.
- Baja estabilidad térmica e hidrotérmica.
- Elevada área superficial y elevada porosidad.
- Existencia de microporos en la pared amorfa.
- Aplicación en la catálisis de moléculas grandes, procesos biológicos, adsorción selectiva y como material funcional.

La gran ventaja de un material mesoporoso ordenado es que presenta una elevada área superficial y un gran volumen de poro. Por otra parte, la mayor desventaja podría ser su pared amorfa y por tanto no ordenada a nivel atómico. Esto conlleva una baja estabilidad térmica y baja fuerza ácida, aunque hay muchos métodos que permiten mejorar estas propiedades. [16]

En la síntesis de materiales mesoporosos existen tres componentes principales: las especies inorgánicas para la formación de la pared inorgánica, el "template" o molde (en la mayoría de los casos un surfactante) el ensamblaje del cual guiará la formación de la mesofase, y el medio de reacción (solvente). En la siguiente figura se muestra un ejemplo del mecanismo de síntesis de un material mesoporoso ordenado.

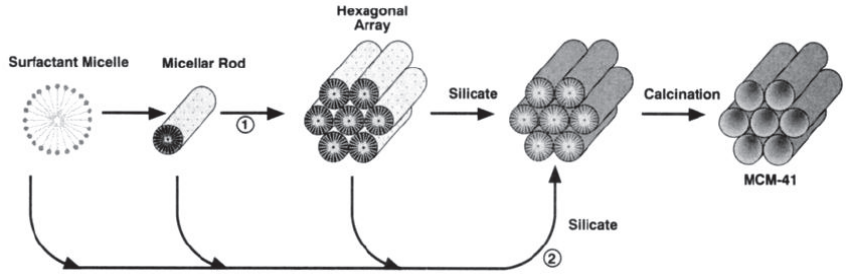

Figura 10. Síntesis de MCM-41 mediante el mecanismo LCT (Liquid Crystal Templating). [18]

En la síntesis de sílicas mesoporosas tanto el surfactante como la especie inorgánica tienen un efecto director en la obtención de un material específico. El sólido que se forma depende en gran medida de las interacciones entre los surfactantes y los precursores inorgánicos.

En el caso de surfactantes iónicos, la formación del material mesoestructurado está principalmente gobernado por interacciones electrostáticas. La carga del surfactante (S) y de la especie mineral (I) es opuesta. Existen dos rutas de síntesis directa: S^+I^- y S^-I^+. Otras dos rutas de síntesis, consideradas como indirectas, presentan también este tipo de interacciones, pero en este caso surfactante y especie inorgánica tienen la misma carga, por lo que se necesita incorporar otra especie. Así, se llevan a cabo interacciones $S^+X^-I^+$ en condiciones ácidas en presencia de aniones haluros ($X^- = Cl^-$, Br^-) mientras que la ruta $S^-M^+I^-$ se realiza en medio básico en presencia de cationes alcalinos ($M^+ = Na^+$, K^+). [19] Por último, la utilización de surfactantes no-iónicos, donde las interacciones entre el "template" y la especie inorgánica se produce mediante puentes de hidrógeno o interacciones dipolares: S^oI^o, N^oI^o y $N^oF^-I^+$. [20]

En esta tesis se han preparado y modificado tres tipos de materiales mesoporosos: MCM-41, SBA-15 y HMS.

En la siguiente figura se muestra el tipo de interacción entre el surfactante y el precursor de sílica en la síntesis de MCM-41, SBA-15 y HMS.

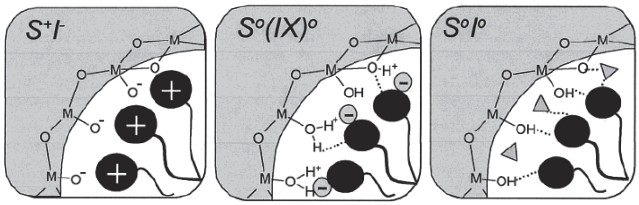

Figura 11. Representación esquemática de las dos tipos de interfases sílica-surfactante en la síntesis de la MCM-41 (S^+I^-), SBA-15 ($S^oX^-I^+$) y HMS (S^0I^0).

SBA-15 presenta una pared silícea (~2 a 6 nm) más fina que la de MCM-41, con un tamaño de poro mayor a 4 nm, elevada estabilidad térmica (> 900 ºC) y estabilidad hidrotermal. El pequeño tamaño de partícula de HMS (< 200 nm) tiene como consecuencia la presencia de mesoporosidad textural complementaria que los otros tipos de mesoporosos estudiados presentan en muy poca cantidad. Los mesoporos texturales son importantes ya que facilitan el transporte de masa hacia los poros de la estructura. Por esta razón la reactividad catalítica de HMS es normalmente superior a la de MCM-41, especialmente para conversiones que implican sustratos voluminosos en medio líquido donde la velocidad de la reacción está limitada por la difusión. [21-22]

3.2. Tratamientos de modificación de zeolitas

3.2.1. Desaluminación

La desaluminación consiste en la extracción de átomos de aluminio de la estructura de la zeolita. Puede producirse mediante hidrólisis del enlace Al-O-Si por tratamiento térmico o hidrotérmico con vapor de agua ("steaming") a temperaturas elevadas, tratamiento químico con HCl o por sustitución directa de aluminio por silicio con $SiCl_4$ en fase gas también a temperaturas elevadas. Otros tratamientos de desaluminación menos utilizados incluyen la reacción con agentes quelantes como el EDTA, que conducen a una complejación del aluminio, reacción con ácido oxálico, con $(NH_4)SiF_6$ acuoso o con F_2 gas. [23-47]

Barrer y Makki fueron los primeros en realizar desaluminación de zeolitas sin pérdida de la estructura zeolítica, demostrando que la zeolita clinoptilolita podía ser desaluminada mediante tratamiento con ácido clorhídrico. [48] Recientemente, una clinoptilolita desaluminada en medio ácido se ha aplicado en la adsorción y separación de n-parafinas. [49]

En la siguiente figura se muestra el mecanismo de desaluminación en medio ácido. [50]

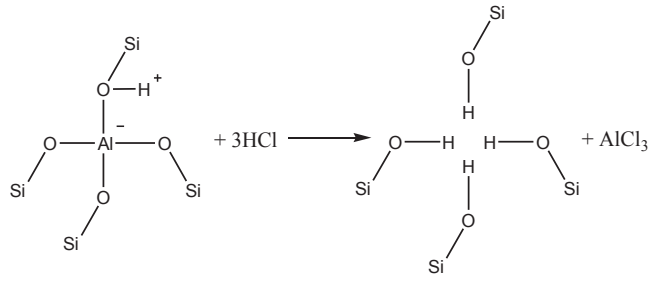

Figura 12. Mecanismo de desaluminación en medio ácido clorhídrico. [50]

En esta tesis, se ha utilizado una Na-Mordenita comercial (Zeolyst, Si/Al = 6.5, CBV 10A Lot. 1822-50) para el estudio del efecto de las microondas en su desaluminación en medio ácido (en autoclave y a reflujo). Para cada preparación se ha tratado 1 g de zeolita con 30 ml de HCl 6 M. Cuatro muestras se prepararon en microondas, dos en autoclave y dos a reflujo a 373 K durante 15 min y 2 h, respectivamente (MWA_{15min}, MWA_{2h}, MWR_{15min} y MWR_{2h}). Utilizamos un microondas ETHOS de la marca Millestone equipado con sonda de temperatura y controlador de temperatura programable (Figura 13). En cada tratamiento se programa una rampa de

temperatura durante 5 min hasta llegar a la temperatura deseada. A continuación la temperatura se mantiene el tiempo establecido. Por último la muestra se enfría mediante ventilación durante 15 min aproximadamente.

Figura 13. Microondas utilizado para la desaluminación.

Otras cuatro muestras se prepararon, dos en estufa convencional (en reactor cerrado de teflón) y otras dos en reflujo tradicional a la misma temperatura y tiempos que las muestras tratadas en microondas (A_{15min}, A_{2h}, R_{15min} y R_{2h}).

También se ha realizado un estudio comparativo del efecto del microondas en la desaluminación de tres tipos de zeolitas: Na-Mordenita (Zeolyst, Si/Al = 6.5, CBV 10A Lot. 1822-50), Na-ZSM-5 (Zeochem, Si/Al=20, PZ-2/40 Lot No. 6002827,01) y Na-Beta (Zeochem, Si/Al=10, PB Lot No. 6000186). Para la desaluminación se trató 1 g de zeolita con 30 ml de HCl 6M en microondas en autoclave a 373 K durante 15 min (MMW, ZMW, BMW, respectivamente). También se prepararon en el caso de la zeolita Beta a 5 min (BMW5), debido a que en 15 min observamos una elevada desaluminación tanto en convencional como en microondas. Además, se prepararon cuatro muestras en las mismas condiciones pero en una estufa convencional para comparar con las muestras desaluminadas mediante microondas (MA, ZA, BA, BA5).

Después del tratamiento, las muestras se filtran, se lavan con abundante agua destilada hasta pH neutro y se dejan secar en la estufa durante toda la noche.

3.2.2. Intercambio catiónico

Las zeolitas tienen cationes (normalmente Na^+, NH_4^+, H^+) en sus cavidades y canales que compensan la carga aniónica del esqueleto de la zeolita generada por la presencia de Al. Estos cationes se pueden intercambiar por otros cationes para su uso como adsorbentes y catalizadores. [51-53] Reacciones catalizadas por centros ácidos

pueden llevarse a cabo utilizando como catalizadores zeolitas con cationes H^+ (acidez de Brønsted) o con cationes La^{3+} (acidez de Brønsted y Lewis).

H-Zeolita

Se ha obtenido la forma ácida (H-zeolita) a partir de las zeolitas comerciales Na-Mordenita, Na-ZSM-5 y Na-Beta mediante intercambio catiónico. Se trataron 2 g de zeolita con una solución 1 M de NH_4NO_3 a 373 K durante 1 h. Después se lavaron con agua destilada y se dejaron secar en la estufa toda la noche. A continuación se calcinaron a 813 K durante 5 h para la obtención de las zeolitas protonadas (HM, HZ, HB, respectivamente). En la siguiente figura se muestra el mecanismo de protonación (Figura 14).

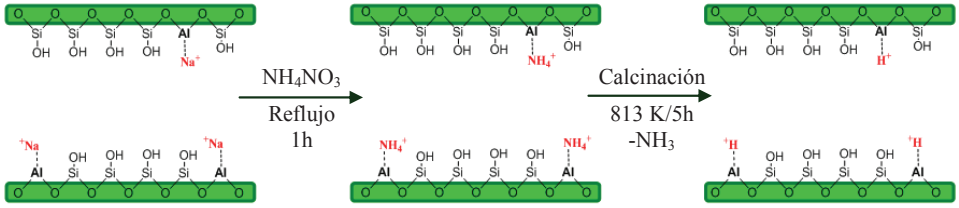

Figura 14. Preparación de zeolitas protonadas

La-Zeolita

Se trataron 2 g de zeolita (Mordenita y Beta) con $LaCl_3 \cdot 7H_2O$ (La/Al = 0.33) mediante intercambio catiónico (Figura 15). Se realizó en estado sólido para evitar la solvatación de los cationes lantanos que dificulta el intercambio (LaM y LaB).

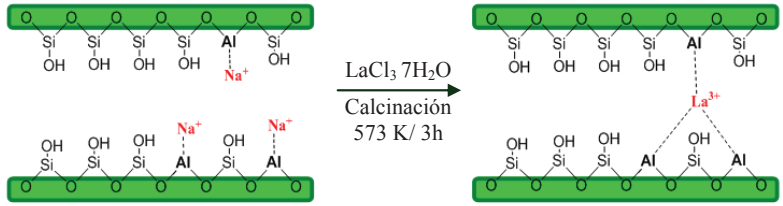

Figura 15. Preparación de La-zeolitas.

3.2.3. Desilicación

La desilicación consiste en la hidrólisis del enlace Si-O-Si mediante el tratamiento con medio básico (NaOH, normalmente) (Figura 16). Este tratamiento permite la formación de mesoporosidad mientras se preservan las propiedades ácidas de la zeolita. Fue en el año 2000 cuando se publicó por primera vez la generación de mesoporosidad en la zeolita ZSM-5 mediante tratamiento con NaOH. [54]

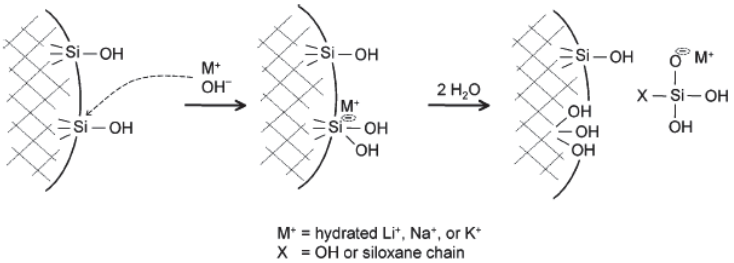

Figura 16. Representación esquemática de la hidrólisis del enlace Si-O-Si de una zeolita en medio básico. [55]

Se han observado diferentes comportamientos frente a la desilicación para diferentes tipos de zeolitas como son: Mordenita, [56] ZSM-5, [57] Beta. [58] La desilicación depende de la estructura de la zeolita. En las mismas condiciones de tratamiento presenta un mayor grado de desilicación: Beta > ZSM-5 > Mordenita. La relación Si/Al también es un factor a tener en cuenta ya que limita la desilicación. [57]

En esta tesis, se trataron tres zeolitas comerciales (Na-Mordenita, Na-ZSM-5 y Na-Beta) con NaOH 0.2 M a 338 K durante 30 min. Lavamos con abuntante agua hasta pH neutro, secamos e intercambiamos con NH_4NO_3 1 M a 373 K durante 1 h. Posteriormente, calcinamos a 813 K durante 5 h para obtener la forma ácida (DSHM, DSHB, DSHZ).

3.2.4. Fluoración

La fluoración de zeolitas puede incrementar su actividad catalítica en reacciones catalizadas por centros ácidos. Por ejemplo, en la reacción de isomerización de óxido de estireno catalizada por centros ácidos, la incorporación de fluor en la estructura de la

mordenita aumenta significativamente su actividad catalítica. [59] En la bibliografía, hemos encontrado estudios de fluoración de zeolitas en los que se han empleado como agentes fluorantes F_2 gas, HF, NH_4F o CH_3F. [60]

R. B. Borade y colaboradores propusieron dos posibles mecanismos de fluoración de la zeolita beta (Figura 17): a) la substitución de grupos hidróxidos (centros ácidos de Brønsted) por átomos de flúor con la formación de especies Si-F, y b) la substitución de átomos de oxígeno por átomos de flúor con la formación de especies Al-F. [61] El primer mecanismo implica la formación de fluorocomplejos de Si y la disminución de la relación de centros de Brønsted/Lewis mientras que el segundo mecanismo lleva a la formación de fluorocomplejos de Al y a un aumento en la acidez de Brønsted, debido a un efecto inductivo de los átomos de flúor introducidos en la estructura, que se tradujo en un aumento de la actividad catalítica en la reacción de craqueo de hexano.

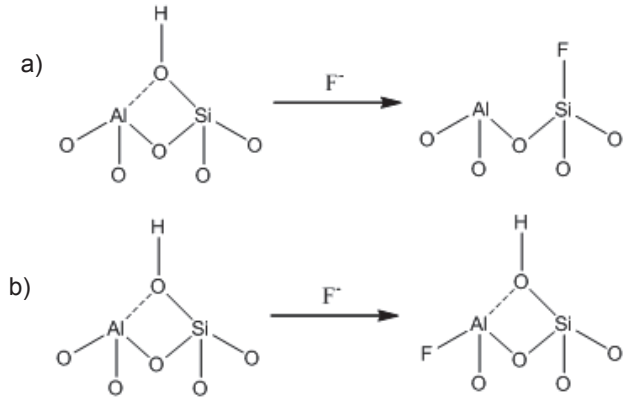

Figura 17. Fluoración de zeolitas. [61]

Para la fluoración tratamos 1 g de zeolita (Mordenita, ZSM-5 y Beta) con 3.5 ml de una solución 0.1 M de NH_4F a temperatura ambiente durante 42 h en agitación. Las muestras se lavaron con agua destilada y secaron en la estufa. Posteriormente, se calcinaron las muestras a 723 K durante 8 h para obtener la forma protonada (FHM, FHZ, FHB).

3.2.5. Sulfonación

La funcionalización de zeolitas permite incorporar centros ácidos muy fuertes (ej. $–SO_3H$) y por ello ampliar su aplicación en catálisis. Fue en 1998 cuando se sintetizó por primera vez una zeolita funcionalizada mediante síntesis directa. [62] Más adelante se incorporaron otro tipo de grupos ácidos como se muestra en la siguiente figura. [63]

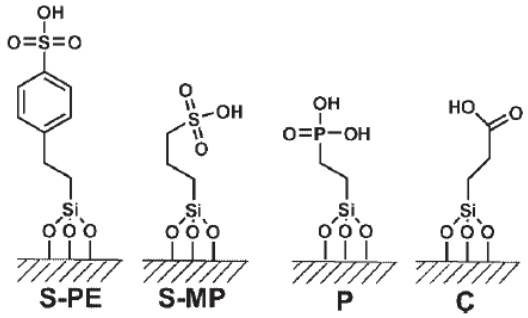

Figura 18. Incorporación de diferentes grupos ácidos en una zeolita beta. [63]

La funcionalización de materiales porosos se realiza por síntesis directa o post-síntesis. La síntesis directa se lleva a cabo mediante un método de co-condensación donde el grupo organosilano condensa o polimeriza junto a la fuente de sílica convencional. En el caso de la sulfonación mediante post-síntesis el material poroso se sintetiza en condiciones normales y posteriormente se trata con el agente organosilano donde este reaccionará con los silanoles (Si-OH) presentes en la superfície del material poroso. Los principales agentes sulfonantes utilizados son el (3-mercaptopropil)trimetoxisilano (MPTMS) y el fenetiltrimetoxisilano (PETMS) que necesitan un posterior tratamiento para obtener los grupos sulfónicos, y el 2-(4-clorosulfonilpropiltrimetoxisilano (CSPTMS) (Figura 19).

Estos agentes sulfonantes se han utilizado principalmente en la funcionalización de materiales mesoporosos y en algún caso en la funcionalización de zeolitas. De hecho, no hay referencias en la bibliografía sobre la sulfonación de zeolitas con CSPTMS ni sobre la utilización de microondas durante el proceso de sulfonación.

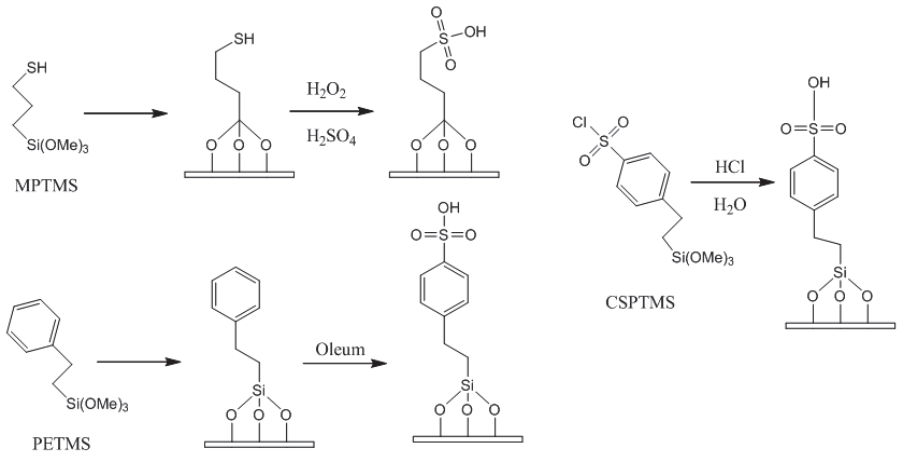

Figura 19. Principales organosilanos utilizados en la incorporación de grupos sulfónicos.

En el caso de las zeolitas es difícil incorporar grupos orgánicos mediante post-síntesis debido a su estructura microporosa (diámetro de poro < 2 nm). En cambio, la síntesis de zeolitas micro-/mesoporosas con gran cantidad de silanoles libres en las paredes de los mesoporos ha permitido funcionalizar estas zeolitas mediante post-síntesis. En este caso, los grupos silanoles pueden reaccionar con varios alcoxisilanos (Figura 20). [64]

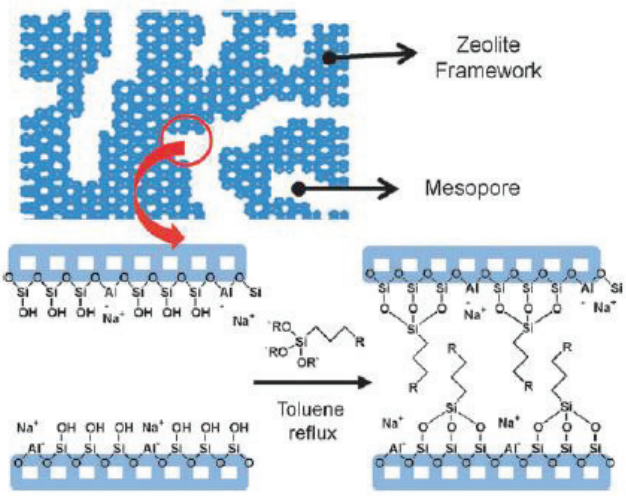

Figura 20. Funcionalización post-síntesis de una zeolita con mesoporosidad adicional. [64]

Se trataron las zeolitas Beta, ZSM-5 y Mordenita con diferentes cantidades de 2-(4-clorosulfonilfenil)etiltrimetoxisilano (CSPTMS, Gelest) a reflujo a 313 K durante 2 h en microondas. Las muestras se han nombrado como S-B(x), S-Z(x), S-M(x) donde x es la cantidad (en gramos) de CSPTMS utilizado durante la sulfonación. Con el fin de estudiar el efecto del microondas en la sulfonación de la zeolita Beta, se preparó una muestra sulfonada mediante la adición de 1.4 g de CSPTMS y calentamiento a reflujo convencional a 313 K durante 2 h (CS-B(1.4)). También se trató la zeolita Beta comercial con 1.4 g de CSPTMS bajo reflujo a 313 K durante 30 min con microondas (S-B(1.4)-30min) y mediante reflujo convencional en las mismas condiciones (CS-B(1.4)-30min). Todas las muestras se lavaron con agua destilada y se secaron en la estufa.

3.2.6. Zeolita con porosidad jerarquizada

En la búsqueda de materiales zeolíticos capaces de catalizar reacciones en que estén implicadas moléculas grandes, en los últimos años se ha investigado en la preparación de zeolitas que contengan mesoporosidad mediante su síntesis directa, diferentes tratamientos de post-síntesis, o mediante nuevas metodologías que utilizan "templates". [65, 66, 67]

Un método reciente para la síntesis de zeolitas con porosidad jerarquizada se basa en dificultar el crecimiento de los cristales zeolíticos mediante funcionalización de semillas zeolíticas para prevenir su posterior agregación y aglomeración. [68-69] Este método consta de las siguientes etapas: a) precristalización del gel de síntesis de la zeolita para formar los núcleos zeolíticos, b) funcionalización de las semillas zeolíticas mediante reacción con organosilanos que forman una barrera orgánica protectora contra la agregación, c) cristalización para completar la zeolización de las semillas funcionalizadas. Dependiendo de la estructura de la zeolita, las condiciones de cristalización y el agente sinalizante, el producto final que se obtiene estará formado por nanocristales muy pequeños de zeolita o por cristalitos con porosidad adicional en las regiones de supermicroporo-mesoporo generadas por los agentes silanizantes (Figura 21). Este tipo de materiales con porosidad jerarquizada han mostrado un efecto positivo mejorando los resultados catalíticos de su correspondiente zeolita estándar cuando se han utilizado como catalizadores en reacciones con moléculas voluminosas. [70-75]

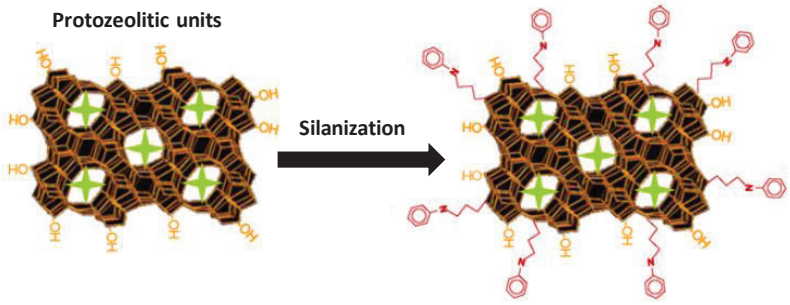

Figure 21. Esquema de la incorporación de organosilanos en la síntesis de una zeolita jerarquizada.

Una zeolita Beta con porosidad jerarquizada (H-Beta-hierarchical) y la correspondiente zeolita de referencia preparada en las mismas condiciones pero sin agente silanizante (H-Beta-27) fueron sintetizadas por la Dra. María Linares en el grupo de investigación dirigido por el Dr. David Serrano del departamento de Tecnología Química y Energética de la Universidad Rey Juan Carlos de Madrid.

Posteriormente, se ha realizado un tratamiento de fluoración a ambas muestras en nuestro laboratorio. Tratamos 1 g de zeolita Beta con porosidad jerarquizada (H-Beta-hierarchical) o 1 g de H-Beta-27 con 3.5 ml de una solución 0.1 M de NH_4F a temperatura ambiente durante 42 h en agitación. Las muestras se lavaron con agua destilada y se secaron en la estufa. Seguidamente se calcinaron a 723 K durante 8 h para obtener la forma protonada (FH-Beta-hierarchical y FH-Beta-27).

3.3. Tratamientos de modificación de materiales mesoporosos ordenados

3.3.1. Incorporación de aluminio

Se prepararon dos tipos de aluminosilicatos mesoporosos (Al-MCM-41 y Al-SBA-15) mediante la técnica sol-gel la cual incluye el uso de "templates" y posterior cristalización hidrotermal.

Síntesis directa: Al-MCM-41 se sintetizó mediante la utilización, como surfactantes de hidróxido de tetrametilamonio (TMAOH) y bromuro de cetiltrimetilamonio (CTAB), fumed sílica como fuente de silicio e isopropóxido de aluminio ($Al(O\text{-}i\text{-}Pr)_3$), como fuente de aluminio. Se le realizó una etapa de envejecimiento a temperatura ambiente durante 20 h. Posteriormente, el tratamiento hidrotérmico a 423 K durante 48 h y finalmente se calcinó a 823 K durante 8 h para la

eliminación del "template" (muestras Al-MCM-41(40), Al-MCM-41(20) y Al-MCM-41(10), en paréntesis la relación Si/Al). *Post-síntesis:* Sintetizamos la muestra MCM-41 siguiendo el procedimiento anteriormente explicado sin la incorporción de Al. Tratamos 1.0 g de MCM-41 con isopropóxido de aluminio (una cantidad necesaria para tener un relación Si/Al=5) en 50 ml de hexano seco a temperatura ambiente durante 24 h en agitación. A continuación filtramos, lavamos con hexano seco, secamos a temperatura ambiente y calcinamos a 823 K durante 4 h (muestra Al-MCM-41(5)-ps).

Síntesis directa: En la síntesis de SBA-15 se ha empleado como "template" Pluronic P123 ($EO_{20}PO_{20}EO_{20}$), el tetraetilortosilicato (TEOS, como fuente de silicio y el isopropóxido de aluminio ($Al(O\text{-}i\text{-}Pr)_3$), como fuente de aluminio, además de HCl para tener un pH ácido. Se envejeció a 308 K durante 20 h. Posteriormente, se realizó un tratamiento hidrotérmico durante 24 h a 373 K y calcinación a 773 K durante 6 h para la eliminación del "template" (Muestras Al-SBA-15(40) y Al-SBA-15(5), en paréntesis la relación Si/Al). *Post-síntesis:* Preparamos SBA-15 siguiendo el procedimiento anterior sin incorporar aluminio. Tratamos 1.0 g de SBA-15 con isopropóxido de aluminio en 50 ml de hexano seco a 343 K durante 24 h en agitación. A continuación filtramos, lavamos con hexano seco, dejamos secar a temperatura ambiente y calcinamos a 823 K durante 4 h (muestra Al-SBA-15(5)-ps).

Estos materiales se prepararon en la Universidad de Nottingham bajo la supervisión del Dr. Robert Mokaya durante la estancia de 3 meses.

3.3.2. Incorporación de grupos fosfóricos

Una vez sintetizadas MCM-41 y SBA-15, mediante el procedimiento anteriormente descrito, se incorporaron grupos fosfóricos en la superficie de la muestra mediante impregnación de 1 g de muestra con 4.5 ml de una solución H_3PO_4. La muestra impregnada con ácido fosfórico se secó rápidamente en agitación. A continuación secamos en una estufa a 373 K durante 8 h y calcinamos a 673 K durante 3 h (Muestras P-MCM-41 y P-SBA-15). En la figura 22 se muestra un esquema de la incorporación de grupos fosfóricos que puede generar centros ácidos de Brønsted.

Estos materiales se prepararon en la Universidad de Nottingham bajo la supervisión del Dr. Robert Mokaya.

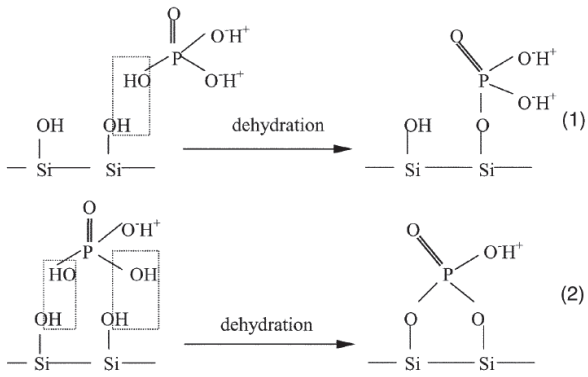

Figura 22. Dos posibles alternativas para la generación de centros de Brønsted en la incorporación de grupos fosfóricos. [76]

Otra manera de incorporar grupos fosfóricos es mediante la utilización de un organosilano como es el dietilfosfatoetiltrietoxisilano (DEPTES) mediante la formación de enlaces -O-Si-O- en la superficie del material. [63]

4.0 g de copolímero Pluronic P123 ($EO_{20}PO_{20}EO_{20}$) se añaden a 125 ml de HCl 2 M a temperatura ambiente en agitación. A continuación calentamos a 313 K y añadimos TEOS (9 g) gota a gota. Después de 45 min, 2.8 g de dietilfosfatoetiltrietoxisilano (DEPTES, Gelest) se añadem gota a gota. Seguidamente calentamos a 313 K durante 2 h en microondas con agitación. La mezcla de reacción se transfiere a un reactor autoclave de teflón y calentamos a 373 K en un horno convencional durante 24 h. Filtramos, lavamos con abundante agua y dejamos secar en aire toda la noche. Para la eliminación del surfactante realizamos una extracción con etanol a reflujo durante 24 h. Finalmente, los grupos dietilfosfato se convierten en grupos fosfóricos mediante el tratamiento de 1 g de muestra en 21 ml de HCl concentrado a 313 K durante 24 h en reflujo (muestra Ethyl-P-SBA-15-MW).

3.3.3. Sulfonación

Una gran ventaja de los materiales mesoporosos es su gran área superficial fácilmente modificable. La incorporación de grupos funcionales orgánicos puede llevarse a cabo principalmente mediante dos métodos: (a) por enlace covalente en las paredes inorgánicas del material (post-tratamiento) y (b) por incorporación directa de los grupos funcionales orgánicos, durante el proceso de síntesis “one-pot”.

En el primero de los casos, se emplean organoclorosilanos o organoalcoxisilanos para incorporar grupos orgánicos específicos, mediante reacciones de condensación con grupos silanoles o Si-O-Si de la estructura (Figura 23 a). [77-81] La concentración y distribución de los grupos funcionales está restringida por la superficie de silanoles y su accesibilidad. El grado de incorporación depende de la reactividad del precursor, limitado por la difusión y factores estéricos.

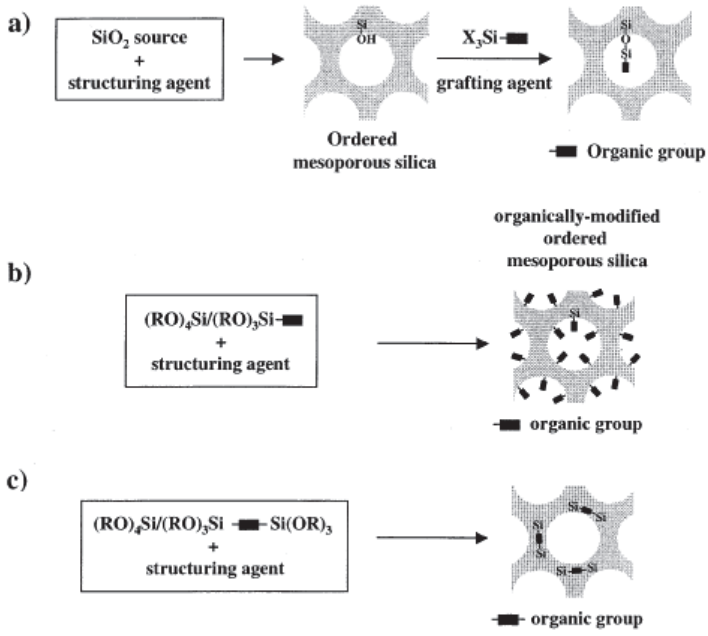

Figura 23. Incorporación de grupos orgánicos en sílica mesoporosa: (a) Mediante post-síntesis, (b) Mediante síntesis directa, (c) puentes de silsesquioxanos. [17]

Otra posible alternativa para la funcionalización de mesoporosos es mediante síntesis directa. Este procedimiento está basado en la co-condensación de precursores de siloxano y organosiloxano en un solo paso durante la síntesis de la MCM-41 (Figura 23 b). [80-85] Mientras los precursores de siloxano aseguran la formación de la red mineral, los organosilanos juegan doble papel: contribuyen a la construcción de la estructura inorgánica y aportan los grupos orgánicos.

Se prepararon dos SBA-15 funcionalizadas mediante síntesis directa estudiando a su vez el efecto de la radiación microondas. Para la síntesis de estos materiales se añadieron 4 g de Pluronic P123 en 125 ml de HCl 2 M. Una vez disuelto se llega a una temperatura de 313 K y seguidamente se añade 9 g de TEOS. Después de 45 min, se

añade 2.8 g de CSPTMS y se deja en agitación a 313 K durante 24 h (a reflujo convencional o en microondas). A continuación se lleva a un reactor de teflón para realizar el tratamiento hidrotérmico a 373 K durante 24 h. Una vez llegado a este punto, filtramos, lavamos y dejamos secar a la estufa durante toda la noche. La eliminación del "template" se realiza a reflujo con etanol durante 24 h y posterior calcinación a 473 K durante 24 h para evitar la destrucción de los grupos sulfónicos ($-SO_3H$). La nomenclatura de las muestras son: SBA-15-CS para la muestra sulfonda con reflujo convencional y SBA-15-MwS para la muestra sulfonada con reflujo microondas.

Se estudió el efecto de la porosidad en la sulfonación mediante la síntesis de una sílica mesoporosa HMS utilizando surfactantes con diferentes longitudes de cadena carbonada. Se prepararon estos materiales a 338 K durante 20 h en agitación, a partir de un gel que contenía tetraetilortosilicato (TEOS), como "templates" dodecilamina (dda), hexadecilamina (hda) y octadecilamina (oda), etanol y agua. La composición molar: 0.02 TEOS : 0.005 "template" : 0.088 EtOH : 2.56 H_2O. Para la eliminación del surfactante se calcinó la muestra a 873 K durante 4 h.

Posteriormente se realizó el tratamiento de sulfonación. 2 g de sílica mesoporosa HMS se trataron con 1.5 g de CSPTMS en una solución HCl 2M a 313 K durante 2 h en microondas. Seguidamente se filtraron, lavaron con agua destilada y dejaron secar en la estufa. Las muestras preparadas se denominaron Arene-S-HMS(dda), Arene-S-HMS(hda) y Arene-S-HMS(oda), respectivamente.

Durante la estancia de tres meses en la Universidad de Nottingham se realizó la incorporación de grupos sulfónicos mediante otra síntesis:

Síntesis directa: Añadimos mercaptopropiltrimetoxisilano (MPTMS) en la síntesis de la MCM-41 y seguimos el procedimiento anteriormente explicado para la síntesis de este material. La eliminación del "template" se realiza a reflujo con etanol durante 24 h para evitar la destrucción de los grupo tioles (-SH). A continuación los grupos tioles immovilizados en el material se oxidan con H_2O_2 en una mezcla metanol-agua. Finalmente, filtramos, acidificamos y dejamos secar a 333 K (Muestra Propyl-S-MCM-41).

3.4. Tratamiento de sulfonación en otros tipos de materiales: montmorillonita K10, aerogel y liogel de sílica

3.4.1. Montmorillonita K10

Las esmectitas son arcillas laminares microporosas. Sus láminas están constituidas de octaedros $M(O, OH)_6$ donde M= Al^{3+}, Mg^{2+}, Fe^{3+} o Fe^{2+} y tetraedros principalmente formados por Si(O, OH). La estructura tipo esmectita consiste en láminas formadas por una capa tetraédica seguida de una octaédrica y finalmente otra capa tetraédrica (TOT). En la siguiente figura se muestra la estructura tipo esmectita. Estos materiales presentan baja área superficial, cationes intercambiables y propiedades ácidas. La montmorillonita pertenece al grupo de las esmectitas y su fórmula general es $[Si_8(Al_{4-x}Mg_x)(OH)_4O_{20}]M_{n+x/\ n}{\cdot}mH_2O$ contiene, por tanto, cationes Al^{3+} y Mg^{2+} en posiciones octaédricas. En esta tesis se ha utilizado una montmorillonita K-10 que deriva de la montmorillonita a la que se le aplica un tratamiento ácido.

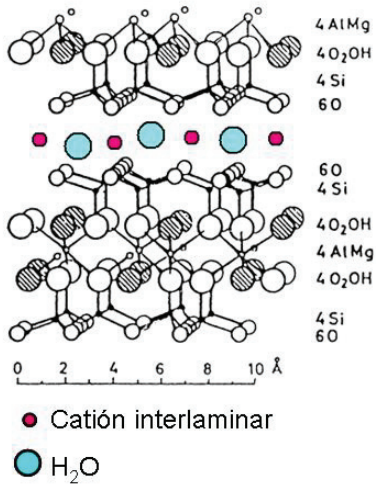

Figura 24. Estructura tipo esmectita.

En los últimos años se ha investigado en la funcionalización de esmectitas para la incorporación de grupos sulfónicos. [86-87] Sin embargo, no existen referencias en la bibliografía sobre sulfonación de esmectitas con CSPTMS.

2 g de montmorillonita K-10 comercial (Sigma-Algrich, Si/Al=2.7) se trataron con 1.4 g de CSPTMS en una solución de HCl 2M a 313 K durante 2 h a reflujo en

microondas (muestra S-Mont(1.4)). Posteriormente filtramos, lavamos con agua destilada y dejamos secar en una estufa durante toda la noche.

3.4.2. Aerogel y liogel de sílica

El procedimiento "sol-gel" constituye una de las rutas de preparación de materiales porosos a partir de soluciones líquidas de precursores moleculares. Este método se caracteriza por la formación, en una primera etapa, de soluciones coloidales estables ("sol") seguida por la condensación anisotrópica de partículas coloidales (micelas) que acaban dando lugar, tras la etapa de gelificación, a la formación de un "gel". [88] La eliminación del disolvente da lugar a la formación de "xero"-, "lio"- o "aerogeles" dependiendo del método de secado. Estos materiales presentan diferentes propiedades superficiales. Puede haber una última etapa, denominada de calcinación/sinterización que consiste en un tratamiento térmico para estabilizar las estructuras obtenidas y conseguir diferentes formas de sólido como monolitos, membranas etc.

Las 4 etapas principales en la preparación de materiales via sol-gel son: formación del gel, envejecimiento del gel, eliminación del disolvente y tratamiento térmico. [89]

Los precursores que se utilizan en la preparación sol-gel suelen ser sales o alcóxidos metálicos disueltos en un solvente apropiado. Los alcóxidos metálicos son los más utilizados ya que se encuentran disponibles comercialmente con elevada pureza. Las reacciones que se dan principalmente en las primeras etapas de formación del gel son las siguientes. [90]

Hidrólisis

$$Si(OR)_4 + H_2O \rightarrow (OH)Si(OR)_3 + ROH$$

Condensación

$$(OH)Si(OR)_3 + Si(OR)_4 \rightarrow (OR)_3Si - O - Si(OR)_3 + ROH$$

$$(OH)Si(OR)_3 + (OH)Si(OR)_3 \rightarrow (OR)_3Si - O - Si(OR)_3 + H_2O$$

En la siguiente figura se muestra un esquema de la estructura de una sílica aerogel.

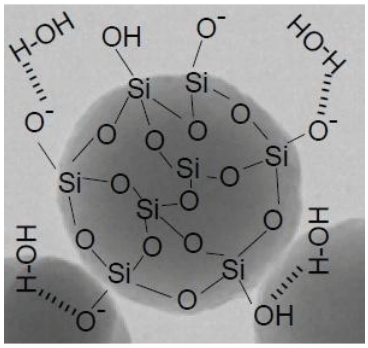

Figura 25. Sílica aerogel con grupos silanoles en superficie.

Los aerogeles y liogeles son materiales extremadamente ligeros y porosos obtenidos mediante la eliminación del solvente de los geles bajo condiciones supercríticas (aerogel) o bajo condiciones de liofilización (liogel) evitando presiones de capilaridad, responsables del colapso de los poros. El resultado es un material poroso abierto con elevada área superficial y excelentes propiedades de transferencia de masa.

Un aerogel y un liogel fueron sintetizados por la Dra. Elena Taboada en los laboratorios del Instituto de Ciencia de Materiales de Barcelona (ICMAB) en el grupo de investigación dirigido por el Dr. Elies Molins.

Posteriormente estos materiales se sulfonaron en nuestro laboratorio. Se trataron 2 g de aerogel o liogel con 1.4 g de CSPTMS en una solución de HCl 2M a 313 K durante 2 h en microondas (muestras SMw-AG(1.4) y SMw-LG(1.4)) o calentamiento convencional (muestras SC-AG(1.4) y SC-LG(1.4)). Se prepararon otras dos muestras aerogel sulfonadas con microondas en las mismas condiciones de temperatura y tiempo pero utilizando 0.7 g y 2.8 g de CPTMS (SMw-AG(0.7) y SMW-LG(2.8)). Todas las muestras se filtraron, lavaron con agua destilada y se dejaron secar en una estufa durante toda la noche.

3.5. Utilización de la radiación microondas en la preparación y modificación de materiales

Cuando se aplica radiación microondas, se produce una vibración y rotación de las moléculas polares generando calor. El calentamiento se produce principalmente a través de dos mecanismos: polarización dieléctrica y dipolar. El calentamiento mediante polarización dieléctrica se debe a la resistencia parcial de las cargas a seguir los cambios

rápidos de un campo eléctrico. En el mecanismo de polarización dipolar, las moléculas polares rotan para orientarse con el campo electromagnético producido por la radiación microondas, resultando en fricciones entre ellas que generan un incremento en la temperatura de la muestra. Para una frecuencia típica de 2450 MHz el alineamiento de las moléculas seguido por su relajación ocurre a 4.9 x 10^9 veces/s, dando lugar a un rápido calentamiento. A causa de esta elevada velocidad de calentamiento se pueden generar "hot spots". [91]

En esta tesis se ha utilizado un microondas Milestone Ethos Touch control (Figura 26) para la preparación y modificación de materiales. Se ha realizado el estudio a reflujo o autoclave. Los tratamientos en autoclave se han llevado a cabo en un rotor de 6 posiciones que contiene 6 reactores autoclave de 85 ml de capacidad. La temperatura se controló con un termopar situado en uno de los reactores. Cada uno de los reactores contenía un agitador magnético para homogeneizar el calentamiento. Además, el rotor también se mueve durante el experimento.

Figura 26. Microondas (Milestone Ethos Touch control).

3.6. Técnicas de caracterización

3.6.1. Difracción de Rayos X de polvo (DRX)

La técnica de difracción se fundamenta en hacer incidir una radiación X sobre un sólido cristalino que difracta si cumple las condiciones mostradas en la ley de Bragg.

$$2 \cdot d_{hkl} \cdot \sin \theta = n \cdot \lambda$$

Esta ecuación indica la relación entre el espaciado interplanar (d_{hkl}), la longitud de onda de la radiación X (λ) y el ángulo de incidencia del haz de rayos X (θ).

En el caso de la difracción de polvo se obtiene el llamado cono de radiación difractada ya que los cristales de las muestras en polvo presentan diferentes orientaciones (Figura 27).

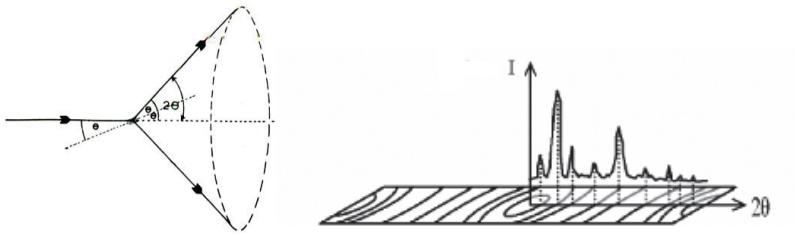

Figura 27. Método de Debye-Scherrer para la difracción de rayos X de polvo.

La difracción de rayos X nos ha permitido identificar las fases cristalinas presentes en las muestras, calcular los parámetros de celda, a partir de las distancias interplanares correspondientes a los picos característicos de cada fase cristalina así como determinar las diferencias de cristalinidad entre las muestras. Generalmente, para identificar las diferentes fases cristalinas obtenidas se utiliza la base de datos JCPDS (Joint Committee for Powder Diffraction Sources). En esta tesis se han utilizado las fichas JCPDS siguientes: 43-0171, 48-0074, 37-359 que corresponden a la mordenita, beta y ZSM-5, respectivamente.

Calculamos los parámetros de celda de cada muestra a partir de la ecuación que relaciona las distancias interplanares (d_{hk}) con los parámetros de celda (a,b,c) que son función de la simetría espacial de cada muestra.

La mordenita tiene una simetría ortorrómbica por lo que hemos calculado los parámetros de celda siguiendo la siguiente ecuación:

$$1/d^2 = h^2/\mathbf{a}^2 + k^2/\mathbf{b}^2 + l^2/\mathbf{c}^2$$

A partir de los valores de las distancias interplanares de los picos (200), (020) y (202) de la mordenita se han determinado los parámetros de celda a, b, c, siendo d la distancia interplanar y h,k,l los índices de Miller de cada pico.

La ZSM-5 cristaliza en un sistema monoclínico por lo que se han calculado los parámetros de celda a partir de la ecuación:

$$1/d^2 = 1/\sin^2\beta\ [h^2/\mathbf{a}^2 + (k^2\sin^2\beta)/\mathbf{b}^2 + l^2/\mathbf{c}^2 - (hl\cos\beta)/\mathbf{ac}]$$

A partir de las distancias interplanares de los picos (200), (020), (002) y (-103) de la ZSM-5 se han obtenido los parámetros de celda a, b, c, siendo d la distancia

interplanar, h, k y l los índices de Miller de cada pico y β el ángulo entre los parámetros a y c.

La cristalinidad se ha determinado comparando la suma de las áreas de los picos (150), (202), (350) y (402) (22-32º 2Θ) de las mordenitas modificadas respecto a la mordenita comercial. La cristalinidad de las muestras ZSM-5 modificadas se ha calculado a partir de la intensidad del pico (051) comparado con la zeolita comercial. Por último, integrando la intensidad del pico a 2θ = 22.4º se evaluó la cristalinidad de las muestras beta modificadas respecto a la comercial.

Los experimentos se realizaron en un difractómetro de polvo Siemens D-500 utilizando una radiación CuKα con filtro de Ni y detectando entre valores 2θ de 0-70º. La muestra que es un polvo cristalino hace falta triturarla antes de su análisis para tener una superficie de difracción completamente plana.

3.6.2. Fisisorción de N_2

Esta técnica nos permite determinar área superficial y distribución de tamaño de poro de un sólido. Se basa en la adsorción de un gas, en este caso N_2 a 77 K en la superficie de un sólido. Durante este proceso de adsorción se dan diferentes fenómenos: adsorción del gas en una monocapa y posteriormente en multicapas en función de la presión de N_2.

Las isotermas obtenidas (volumen de nitrógeno adsorbido en función de la presión relativa de nitrógeno) representan las curvas de adsorción-desorción del gas en la superficie de la muestra. Existen diferentes tipos de isotermas (Figura 28).

- La isoterma tipo I es característica de materiales microporosos con poca superficie externa.
- La isoterma tipo II se observa en sólidos no porosos o macroporosos. El punto B representa el estado en que la monocapa está completa y es cuando empieza la adsorción en multicapa.
- La isoterma tipo III no muestra el punto B. Este tipo de isotermas no son comunes. En este caso, las interacciones adsorbato-adsorbato son más importantes que las adsorbato-adsorbente.

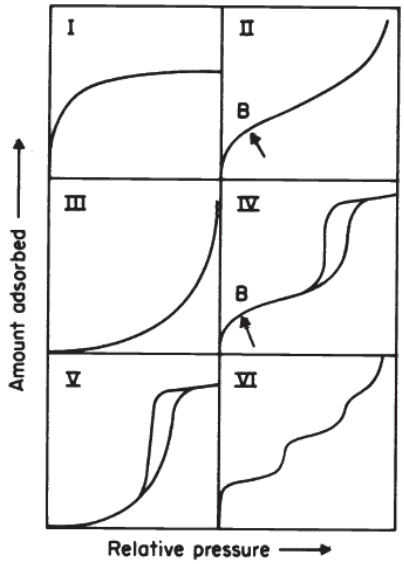

Figura 28. Tipos de isotermas de adsorción.

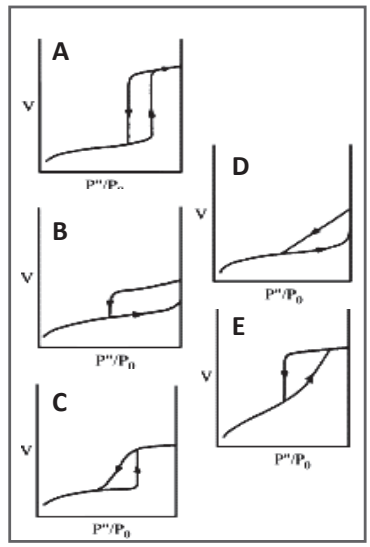

Figura 29. Tipos de histéresis.

- La isoterma IV presenta histéresis, asociada a condensación capilar que se da en los mesoporos, a presiones relativas (P/Po) altas. La primera parte la isoterma está relacionada con la adsorción monocapa-multicapa ya que sigue el mismo patrón que la isoterma tipo II. Este tipo de isoterma es característica de materiales mesoporosos.
- La isoterma tipo V no es muy común. Está relacionada con la isoterma tipo III en que la interacción adsorbente-adsorbato es débil.
- La isoterma tipo VI representa diferentes etapas de adsorción de multicapa en un área uniforme no porosa.

La histéresis aparece en el intervalo de multicapa de las isotermas de fisisorción y está asociada con fenómenos de condensación capilar en estructuras mesoporosas. Las curvas de histéresis presentan una gran variedad de formas (Figura 29).

- Histéresis del tipo A corresponde a poros tubulares abiertos por ambos lados.
- Histéresis del tipo B está relacionada con los poros de la forma de "hendiduras" es decir, son aquellos que se forman por la superposición de láminas cristalinas paralelas entre sí y separadas por pequeñas partículas o a veces, por ciertos defectos cristalinos.

- Histéresis tipos C y D derivan de los tipos A y B, respectivamente. Éstos corresponden a poros cónicos o piramidales (tipos C) o a poros formados entre láminas cristalinas no paralelas (tipos D). Estos dos tipos son bastante raros de encontrar.
- Histéresis del tipo E indica la presencia de poros en forma de botella, es decir, de un cuerpo bastante grande de diámetro y que termina con una boca muy estrecha.

El método Brunauer-Emmett-Teller (BET) es el más utilizado para la determinación de área superficial en materiales porosos. Para la determinación del área BET se utiliza la siguiente ecuación lineal:

$$\frac{\mathrm{P}}{\mathrm{V}(\mathrm{P}^\circ - \mathrm{P})} = \frac{1}{Vm \cdot C} + \frac{(C-1) \cdot P}{Vm \cdot C \cdot P^\circ}$$

donde V es la cantidad absorbida a una determinada presión relativa P/P^o y Vm es el volumen de monocapa. Según la teoría BET, el valor C está relacionado exponencialmente con la entalpia (calor) de adsorción en la primera capa adsorbida (monocapa). El intervalo de linealidad está restringido a una zona limitada de la isoterma que normalmente está entre valores de presión relativa P/P^o de 0.05-0.30.

El valor de área superficial BET se calcula a partir del volumen adsorbido en la monocapa mediante la siguiente ecuación:

$$A\ (BET) = \frac{Vm \cdot L \cdot Am}{M}$$

donde L es el número de Avogadro, Am es el área ocupada por cada molécula de nitrógeno adsorbida (0.162 nm^2 a 77 K) y M es la masa del gas adsorbido.

Se han utilizado tres aparatos de fisisorción de N_2, dos de la marca Micromeritics, modelos ASAP 2000 y 2010, y un Quadrasorb surface analyzer de la marca Quantrachrome.

Todas las muestras se han desgasificado a 393 K durante 12 h. La cantidad de muestra utilizada para los análisis fue la suficiente para tener un área BET superior a 10 m^2/g. La distribución de tamaño de poro de microporos y meso-macroporos se ha determinado a partir de las isotermas obtenidas empleando el método Horvath-Kawazoe y el BJH (Barret, Joyner y Halenda), respectivamente.

3.6.3. Análisis termogravimétrico (TGA)

Esta técnica consiste en observar diferencias de peso, debidos a eliminación, oxidación o reducción de especies químicas, en la muestra después de aplicarle calor con un flujo constante de gas (aire, O_2, N_2, H_2, etc).

A partir de la representación de la variación del peso en función de la temperatura (termograma) se pueden identificar diferentes etapas que tienen lugar durante en el tratamiento.

En esta tesis, esta técnica se ha utilizado para la determinación de centros ácidos de zeolitas mediante la adsorción de una molécula sonda con propiedades básicas (ciclohexilamina) [92] La muestra se deja en contacto con la molécula sonda que interacciona con los centros ácidos del material sólido. Después del proceso de impregnación, la muestra se somete a 353 K durante 2 h para eliminar el exceso de ciclohexilamina y a 523 K durante 2 h para eliminar la ciclohexilamina fisisorbida. Posteriormente, la muestra se analiza mediante análisis termogravimétrico (TGA) donde se observa una pérdida entre 553-723 K que corresponde a la pérdida de ciclohexilamina. [92] Podemos calcular así la cantidad de centros ácidos en la muestra en relación con la cantidad de ciclohexilamina que desorbemos de la muestra.

$$Acidez = \frac{(M1 - M2)}{M2} \cdot \frac{1000}{99.18} = mmoles\ ciclohexilamina/g\ muestra$$

M1 = % de masa a 553 K
M2 = % de masa a 723 K
1000 = Factor para obtener mmol/g
99.18 = Peso molecular de la ciclohexilamina

Se determinó la cantidad de centros ácidos de las zeolitas modificadas mediante desaluminación, desilicación, fluoración y intercambio catiónico mediante la adsorción de ciclohexilamina y posterior análisis termogravimétrico con un equipo TA instruments en las siguientes condiciones: de 323 K hasta 1073 K a 10 K/min en flujo de aire.

3.6.4. Valoración potenciométrica

Para la determinación de centros ácidos en muestras sulfonadas se pueden realizar intercambios con diferentes cationes (Na^+, Tetrametilamonio: TMA^+, Tetraetilamonio: TEA^+) y posterior valoración de los protones intercambiados con NaOH. [83]

En nuestro caso, se ha realizado la valoración mediante intercambio de H^+ con cationes Na^+:

$$-SO_3H + Na^+ \longrightarrow -SO_3Na + H^+$$

Para ello se añadieron 0.10 g de muestra en 20 ml de NaCl 2 M y se dejaron en agitación durante 24 h. Una vez los protones se intercambiaron, la solución se valoró con NaOH 0.01 M.

3.6.5. Espectroscopía Fotoelectrónica de Rayos X (XPS)

Esta técnica nos permite identificar y cuantificar átomos a nivel superficial. Se basa en un efecto fotoeléctrico: un átomo absorbe un fotón de rayos X de energía hν y un electron de valencia con una energía de enlace E_b es emitido con una energía cinética: $E_k = h\nu - E_b$. Debido a que cada energía de enlace es característica de cada elemento, esta técnica se puede utilizar para analizar la composición de una muestra a nivel superficial. El intervalo de detección es de 0.2-1.5 KeV de E_k.

Mediante esta técnica se han podido identificar las grupos sulfónicos de las zeolitas, montmorillonita K10, aerogel, liogel y materiales mesoporosos ordenados sulfonados. La señal del S 2p a 168-169 eV está asociada a especies sulfato (S^{6+}) que correspoden a los grupos sulfónicos ($-SO_3H$). [77, 87]

Los espectros de XPS se han obtenido con un sistema SPECS equipado con una fuente de ánodo de Al XR50 operando a 150 W con detector Phoibos 150 MCD-9. Se utilizó un paso de energía de 25 eV a 0.1 eV y presión por debajo de $6 \cdot 10^{-9}$ mbares.

3.6.6. Microscopía electrónica

La microscopía electrónica permite visualizar el tamaño y forma de las partículas. También, puede dar información de la composición de las partículas, por ejemplo, mediante la detección de los rayos X que se producen por la interacción de electrones con la materia, o mediante el análisis de cómo los electrones son difractados. En la siguiente figura se muestra el comportamiento que tiene la muestra al incidir un haz de electrones.

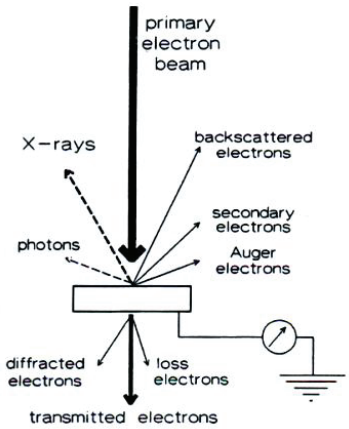

Figura 30. La interacción de un electrón primario con la muestra en microscopía electrónica produce una gran cantidad de señales detectables.

Microscopía electrónica de barrido (SEM)

La microscopía electrónica de barrido se fundamenta en el bombardeo mediante un haz de electrones de la superficie a visualizar. Este haz de electrones, enfocado por lentes electromagnéticas a través de una columna de alto vacío, se proyecta sobre la superficie de la muestra donde los electrones rebotan o provocan la emisión de electrones secundarios. Los electrones secundarios tienen energías bajas (10-50 eV) y se originan en la superficie de la muestra. Los electrones que son rebotados provienen de capas más profundas y proporcionan información de la composición de la muestra. Estos electrones dispersos o emitidos son recogidos por unos detectores y proyectados sobre una pantalla de televisión que proporciona una imagen tridimensional del objeto.

Se ha utilizado un microscopio JEOL JSM-35C. Se empleó un voltaje entre 20-25 kV y una distancia focal entre 10 y 17 mm, trabajando entre 3700-50000 aumentos dependiendo de la muestra.

3.6.7. Desorción a Temperatura Programa (TPD)

La desorción a temperatura programada se basa en la quimisorción de un gas, en este caso de amoníaco, sobre la muestra y posterior desorción del gas mediante un aumento de temperatura. La cantidad de especies adsorbidas se pueden detectar mediante diferentes tipos de detectores, ya sea el TCD (detector de conductividad térmica) o el espectrómetro de masas. A partir de esta información podemos conocer la fortaleza de los distintos centros ácidos de la superficie de nuestra muestra. Según la fuerza de las interacciones entre el gas y los tipos de centros presentes en la muestra se observarán diferentes máximos de temperaturas de desorción.

Se ha utilizado un TPD de la marca ThermoQuest, modelo TPD/R/O 1100 para conocer la variación de fuerza de los centros ácidos entre la mordenita comercial y las muestras desaluminadas. Las condiciones utilizadas son las que se muestran en la siguiente tabla.

Tabla 1: Condiciones utilizadas en el TPD.

Etapas	Gas	Flujo gas (ml/s)	T_{inicio} (K)	Rampa	T_{final} (K)	t_{final} (min)
Limpieza	Ar	40	off	off	off	5
1:	Ar	40	off	10 K/min	673	10
2:	5%NH_3	40	373	1 K/min	373	7
3:	He	40	off	off	off	40
Análisis	He	20	off	5 K/min	973	10

3.6.8. Espectroscopía FT-IR

Esta técnica se basa en la absorción de fotones, con frecuencias en la región infrarroja (longitud de onda entre 0.78-1000 μm), en la muestra donde las unidades y agrupaciones estructurales de los sólidos experimentan un cambio neto en su momento dipolar, el cual es consecuencia de sus movimientos de vibración y rotación. La espectrocopia FTIR se centra en la región del infrarrojo medio comprendida entre los 4000 y los 400 cm^{-1} (de 2.5 a 25 μm). Las unidades para medir la radiación infrarroja pueden ser la longitud de onda (μm) o el número de onda (cm^{-1}).

Los espectros de infrarrojos de zeolitas comerciales y modificadas que permiten observar las bandas correspondientes a T-O (Si-O, Al-O) se han obtenido con un equipo Bruker Equinox 33 a 32 scans, una resolución de 4 cm^{-1} en el rango de frecuencias

comprendido entre 400-4000 cm^{-1}. Las pastillas se prepararon con un 5% aproximadamente de muestra y 95% de KBr, y se dejaron en la estufa (373 K) varias horas para eliminar el agua que podría interferir con las bandas a observar.

Una de las aplicaciones más comunes de la espectroscopía infraroja en catálisis es para identificar especies adsorbidas y para estudiar como estas especies quedan quimisorbidas en la superficie del catalizador. La adsorción de una molécula sonda permite obtener información de los centros activos que están presentes en un catalizador.

En el presente trabajo se ha utilizado una molécula sonda básica (piridina) para determinar centros ácidos (Brønsted y Lewis) en algunas zeolitas. En la figura 31 se muestra las interacciones entre la molécula sonda y los centros ácidos. La piridina cuando interacciona con un ácido de Brønsted o de Lewis da lugar a unas bandas a 1545 cm^{-1} y 1465 cm^{-1}, respectivamente.

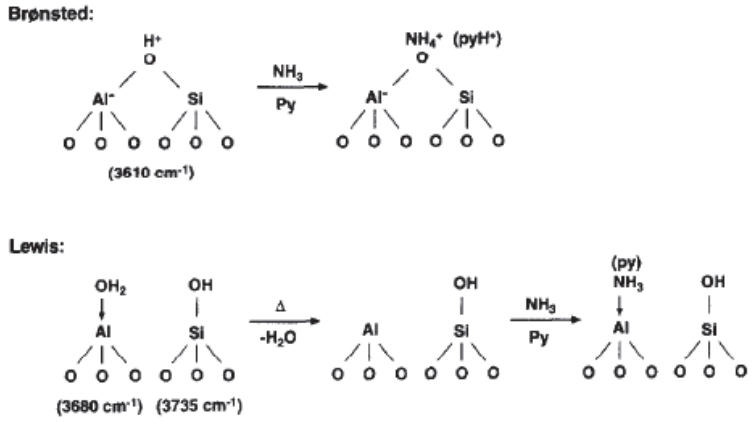

Figura 31. Adsorción de amoniaco o piridina en centros ácidos. [93]

Para el estudio de acidez se adsorbió la piridina a 298 K y el espectro de infrarojos se realizó a 64 scans, 4 cm^{-1} de resolución y en un intervalo de 400-4000 cm^{-1}.

3.6.9. Resonancia magnética nuclear de ángulo mágico de espín (RMN AME)

Un núcleo magnético puede absorber una energía correspondiente a una radio frecuencia cuando se le aplica un campo magnético con una fuerza específica para identificar el núcleo.

La resonancia magnética nuclear de ángulo mágico de espín elimina el ensanchamiento de las señales de RMN que se observa normalmente en los sólidos. El ensanchamiento de las líneas se debe a diversas interacciones anisotrópicas. Si giramos la muestra alrededor de un eje inclinado a este "ángulo mágico" con respecto a la dirección del campo magnético, eliminaremos estas fuentes de ensanchamiento y mejoraremos la definición del desplazamiento químico del espectro.

^{27}Al tiene una abundancia natural = 100% y un espín nuclear de I = 5/2, lo que produce una resonancia fuerte que se ensancha y se vuelve asimétrica por efectos cuadrupolares de segundo orden. Como la regla de Loewenstein descarta las uniones Al-O-Al, todos los entornos del Al tetraédrico en una zeolita son $Al(SiO)_4$. Encontraremos dos tipos de coordinación del Al: una señal entre 50-65 ppm que corresponde a aluminio tetraédrico (aluminio de la estructura) y una señal a 0 ppm que se asigna a aluminio en un entorno octaédrico (aluminio fuera la estructura).

En el espectro de RMN de ^{1}H podemos tener diferentes grupos OH. Estos grupos OH principalmente pueden derivar de la presencia de Al en la estructura, ya que conlleva la presencia de cationes que compensan su carga, o por la presencia de grupos silanoles (Si-OH). [94-95] En la siguiente tabla se muestran los desplazamientos químicos de los diferentes protones que se encuentran en zeolitas.

Tabla 2. Desplazamientos químicos de ^{1}H (ppm) de algunas especies presentes en zeolitas. [95]

Especies	Desplazamiento químico
NH_4^+ y aminas protonadas	6.0-8.1
Silanoles sin enlaces H	1.2-2.3
Centros ácidos de Brønsted	3.0-5.0
Especies Al-OH fuera de la estructura	1.2-3.6
Agua	4.6-5.0

Los espectros de RMN de ^{27}Al y ^{1}H se han obtenido con un aparato Mercury 400 a una frecuencia de 400 MHz utilizando una velocidad de giro de 3 kHz con una duración de pulso de 2ms y un tiempo de relajación de 5 segundos. Como referencia se han utilizado nitrato de aluminio para RMN de ^{27}Al y 3-trimetilsilil propansulfonato de sodio deuterado para RMN de ^{1}H.

3.6.10. Fluorescencia de rayos X (FRX)

La fluorescencia de rayos X se basa en la emisión de electrones secundarios de una material que ha sido bombardeado con rayos X de alta energía o rayos gama. Este fenómeno se utiliza para análisis elemental.

El análisis elemental para la determinación de la relación Si/Al de las zeolitas modificadas se ha obtenido con un analizador XRF Philips PW-2400 secuencial con un software Phiplips Super Q. Todas las medidas se realizaron por triplicado.

3.6.11. Determinación de tipos de centros ácidos mediante test catalíticos

Se estudiaron la reacción de isomerización de óxido de estireno y la reacción de apertura de anillo de óxido de estireno como reacciones modelo para la caracterización de centros ácidos ya que la isomerización de óxido de estireno está catalizada por centros ácidos de Brønsted mientras que la reacción de apertura del anillo de oxido de estireno a 2-etoxi-2-feniletanol está catalizada por centros ácidos de Brønsted y Lewis (Figura 32). [59]

Las dos reacciones se realizaron en fase líquida a presión atmosférica y temperatura ambiente durante 3 h. Se utilizaron 0.8 g de catalizador (para catalizadores Mordenita) o 0.4 g (para catalizadores Beta y ZSM-5), 20 ml de solvente (tolueno o etanol, para favorecer la isomerización y apertura de anillo de óxido de estireno, respectivamente) y 0.48 ml de óxido de estireno. Los productos de reacción fueron analizados mediante cromatagrafía de gases en un aparato Shimadzu GC-2010, equipado con una columna capilar DB-1 recubierta de fenilmetilsilicona, y un detector FID.

Isomerización de óxido de óxido de estireno

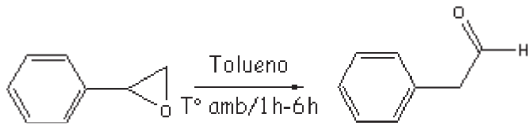

Apertura de anillo de óxido de estireno

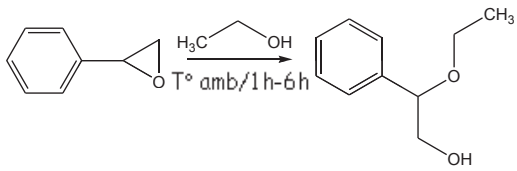

Figura 32. Esquema de las dos reacciones catalíticas utilizadas para la determinación de tipos de centros ácidos en zeolitas

3.7. Actividad Catalítica en la reacción de eterificación de glicerol con tert-butanol e isobuteno

3.7.1. Condiciones de reacción

En esta tesis se ha estudiado la reacción de eterificación de glicerol con tert-butanol o isobuteno para la obtención de di- y tri-tert-butil éteres de glicerol (h-GTBE).

La reacción se da en etapas consecutivas. En primer lugar se forman los monoéteres que por reacción con el tert-butanol o isobuteno presentes en el medio pueden convertirse en los diéters y posteriormente evolucionar hasta la formación del triéter (Figura 33).

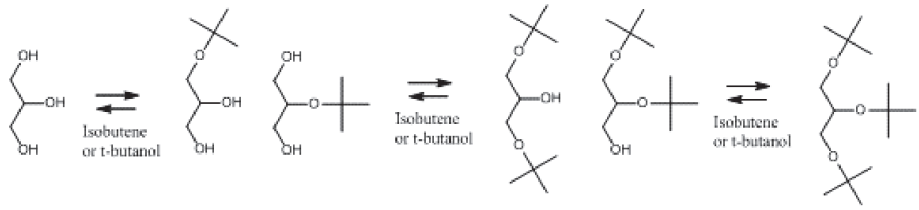

Figura 33. Eterificación de glicerol con tert-butanol o isobuteno.

En la reacción con isobuteno se observó en los catalizadores más activos la formación de diisobuteno en pequeñas cantidades.

Figura 34. Reactor batch autoclave

Reacción con tert-butanol

Las pruebas catalíticas se han llevado a cabo en fase líquida en un reactor autoclave en batch de 150 ml (Figura 34) equipado con controlador de temperatura y de presión. En la reacción de eterificación de glicerol con tert-butanol se utilizaron 20 g de glicerol, 1 g de catalizador y una relación molar glicerol/t-butanol = 1/4.

Reacción con isobuteno

En el caso de la eterificación con isobuteno, las pruebas catalíticas también se han realizado en un reactor autoclave en batch de 150 ml. El isobuteno presurizado en fase líquida se inyectó en el reactor (glicerol/isobuteno = 1/4), previamente cargado con glicerol (10 g) y catalizador (0.5 g) y bajo 10 bares de nitrógeno. Una vez se llega a la temperatura deseada la presión aumenta siguiendo el equilibrio líquido-vapor.

Las reacciones, tanto con tert-butanol como con isobuteno, se realizaron a 348 K entre 4 h y 96 h. Todos los experimentos se agitaron a 1200 r.p.m para evitar limitaciones de difusión externa. Los productos de reacción fueron analizados mediante cromatagrafía de gases en un aparato Shimadzu GC-2010 con una columna SupraWax-280 y detector FID.

3.7.2. Análisis de los productos de reacción

La conversión de glicerol y la selectividad hacia MTBG (monoéteres de glicerol) se determinaron a partir de rectas de calibrado obtenidas a partir de los productos comerciales. Para DTBG (diéteres de glicerol) y TTBG (Triéter de glicerol), que no son comerciales, se separaron, a partir de los productos obtenidos en la reacción de eterificación, mediante columna cromatográfica (1:9 acetato de etilo/hexano) y se identificaron mediante RMN de ^{13}C y de ^{1}H (Figuras 35-38) para su cuantificación con la ayuda de la caracterización publicada por Jamróz et al. [96]

Los espectros de RMN de ^{1}H y ^{13}C se realizaron a 400 MHz and 100.6 MHz, respectivamente, usando $CDCl_3$ como solvente, con un desplazamiento químico (δ) referenciado para patrones internos de $CDCl_3$ (7.26 ppm ^{1}H, 77.23 ppm ^{13}C).

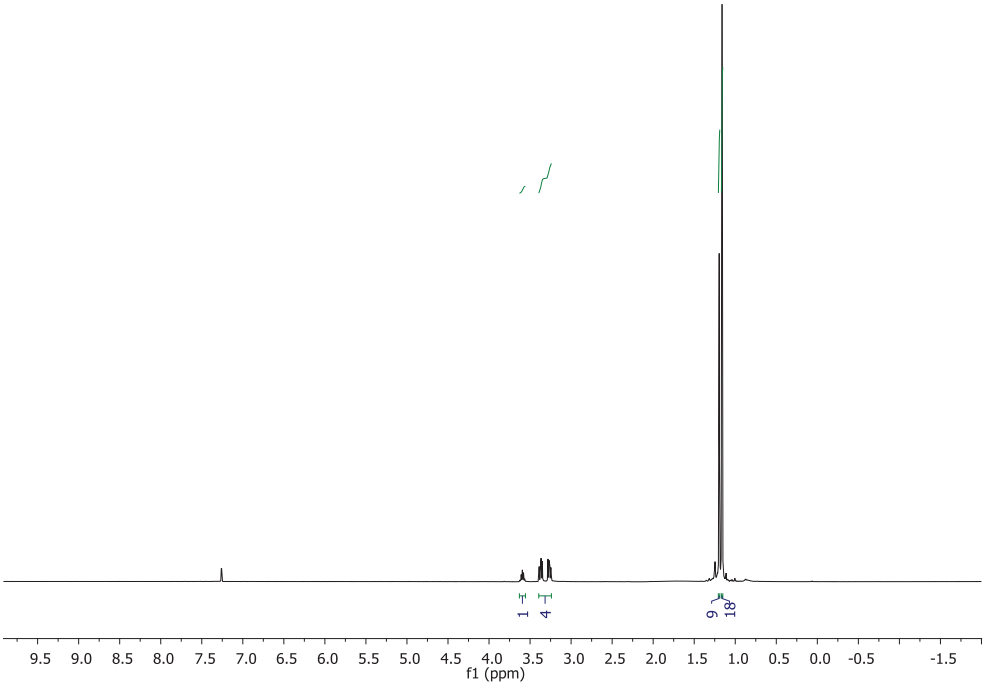

Figura 35. ^{1}H RMN de 1,2,3-tri-*tert*-butoxi-propano.
^{1}H NMR (400 MHz, $CDCl_3$) δ in ppm: 3.59 (m, 1H, C2-H); 3.37 (dd, 2H, *J* = 9.2 Hz, *J* = 5.9 Hz, C1-H and C3-H); 3.27 (dd, 2H, *J* = 9.2 Hz, *J* = 5.3 Hz, C1-H' and C3-H'); 1.20 (s, 9H, C2-$OC(CH_3)_3$); 1.16 (s, 18H, C1-$OC(CH_3)_3$ and C3-$OC(CH_3)_3$)

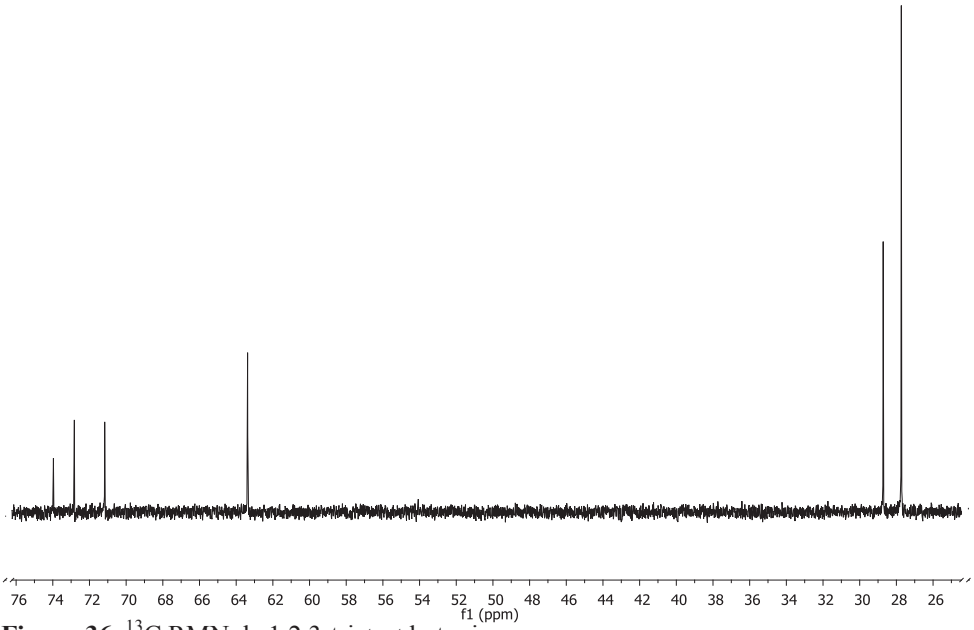

Figura 36. ^{13}C RMN de 1,2,3-tri-*tert*-butoxi-propano.
^{13}C NMR (100.6 MHz, $CDCl_3$) δ in ppm: 73.96 (C2-O**C**$(CH_3)_3$), 72.2 (C1-O**C**$(CH_3)_3$) and C3-O**C**$(CH_3)_3$); 71.17 (C2); 63.37 (C1 and C3); 28.72 (C2-OC(**C**$H_3)_3$); 27.73 (C1-OC(**C**$H_3)_3$) and C3-OC(**C**$H_3)_3$)

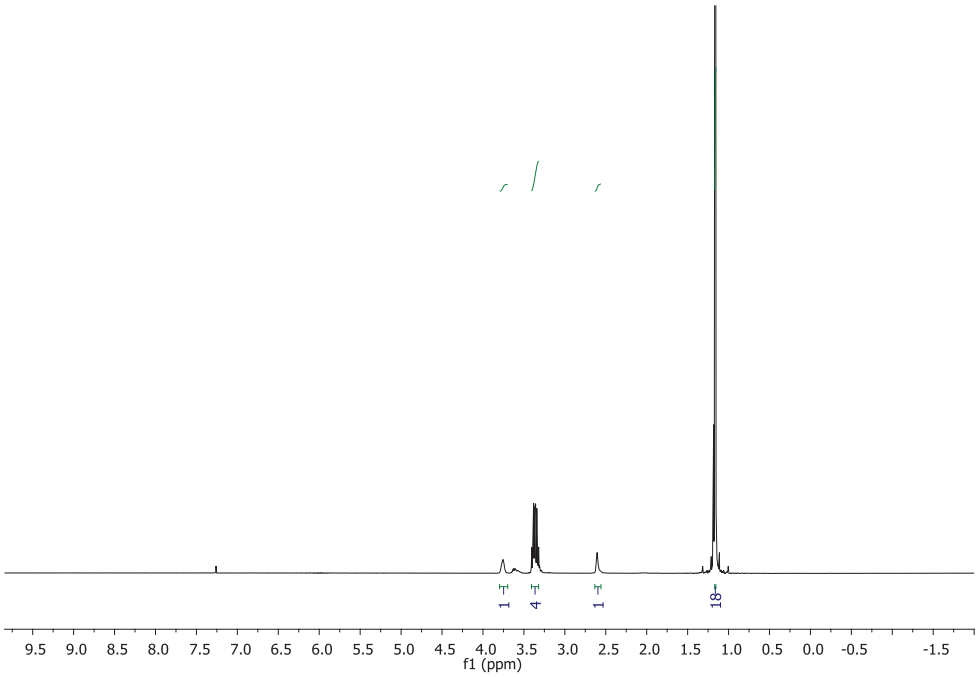

Figura 37. ^{1}H RMN de 1,3-di-*tert*-butoxi-2-propanol
^{1}H NMR (400 MHz, $CDCl_3$) δ in ppm: 3.76 (m, 1H, C2-H); 3.39 (dd, 2H, J = 9.0 Hz, J = 5.0 Hz, C1-H and C3-H); 3.34 (dd, 2H, J = 9.0 Hz, J = 5.9 Hz, C1-H' and C3-H'); 2.60 (s, 1H, -OH); 1.16 (s, 18H, C1-C$(CH_3)_3$ and C3-C$(CH_3)_3$)

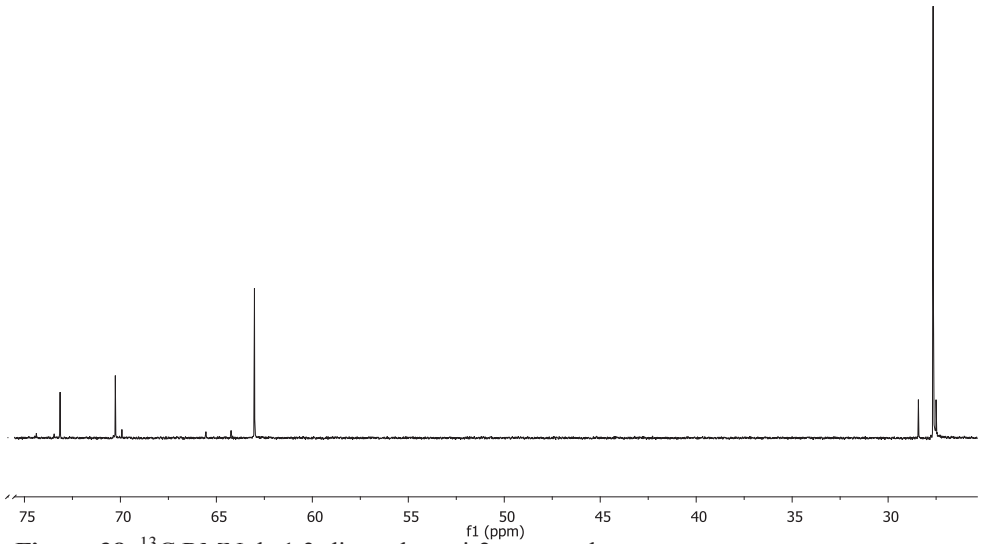

Figura 38. ^{13}C RMN de 1,3-di-*tert*-butoxi-2-propanol.
^{13}C NMR (100.6 MHz, $CDCl_3$) δ in ppm: 73.14 (C1-**C**$(CH_3)_3$) and (C3-**C**$(CH_3)_3$), 70.26 (C2), 63.02 (C1 and C3), 27.65 (C1-C(**C**$H_3)_3$) and (C3-C(**C**$H_3)_3$)

UNIVERSITAT ROVIRA I VIRGILI
REVALORIZACIÓN CATALÍTICA DE GLICERINA PARA UNA OBTENCIÓN MÁS RESPETUOSA CON EL MEDIO AMBIENTE DE ADITIVOS PARA COMBUSTIBLES
Mª Dolores González Candela
DL:T. 1715-2011

4. RESULTS AND DISCUSSION

4.1. Dealumination studies of zeolites

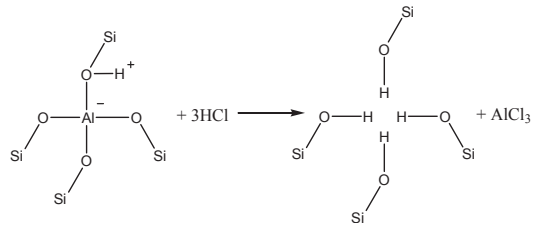

UNIVERSITAT ROVIRA I VIRGILI
REVALORIZACIÓN CATALÍTICA DE GLICERINA PARA UNA OBTENCIÓN MÁS RESPETUOSA CON EL MEDIO AMBIENTE DE ADITIVOS PARA COMBUSTIBLES
Mª Dolores González Candela
DL:T. 1715-2011

4. Results and Discussion

4.1. Background about dealumination studies of zeolites

Zeolites are well known microporous materials widely used as catalysts in petrochemical industry due to their large surface areas, shape selectivity, and controllable acidity. [37, 97] Dealumination of zeolites are useful to reduce acid site concentration, improve thermal stability, and modify pore structure.[37, 97-98] Although the number of Brønsted acid sites, directly related to the number of the framework Al atoms, decreases after dealumination, the acid strength of the remaining Brønsted acid sites can increase, at least up to certain Si/Al ratios. [99]

A considerable number of zeolite dealumination methods have been developed. Thus, we found dealumination studies by treatment of zeolites with steam or $SiCl_4$ vapour at elevated temperatures or treatment with $(NH_4)SiF_6$, mineral acids (i.e., HCl, HNO_3), organic acids (i.e., acetic acid, oxalic acid), F_2, chelating agents (i.e., EDTA), etc.[25-36, 38-39, 45-47, 100-114] Conventional heating is used when applying temperature during dealumination. Different zeolite structure types, such as beta, mordenite, ZSM-5, ferrierite, zeolite Y, zeolite 4A, are known to exhibit very different behaviour towards dealumination. Therefore, besides the dealumination method used, there are two major factors that influence the dealumination behavior of a zeolite sample: the synthesis conditions and the structure type.

With respect to the synthesis conditions, there is a preferred Si/Al ratio in the framework of every structure type during crystallization. For that reason, extraframework aluminum species could be formed, or the distribution of the aluminum atoms in the framework could be inhomogeneous if the synthesis gel deviates from the ideal Si/Al. Moreover, depending on the mineralizing agent (e.g. OH^- or F^- ions) used, more or less defects in the lattice could be generated.

The zeolite structure type is the second important factor, which can affect dealumination. The arrangement and size of the pores influence the accessibility of the aluminum atoms in the framework. Zeolite beta, for example, has a three-dimensional 12-ring pore system (straight channels of diameter 6.6 x 6.7 Å and sinusoidal channels of diameter 5.6 x 5.6 Å) and, because of this property, the framework is very flexible. Zeolite mordenite has a one-dimensional pore system with main channels of diameter 6.7 x 7.0 Å and compressed channels of diameter 2.6 x 5.7 Å whereas ZSM-5 has a three-dimensional 10-ring pore system with channels of diameter 5.1 x 5.5 Å. Both

these structures are less flexible than beta, and consequently, it is more difficult to dealuminate them. Additionally, zeolite beta crystallizes with many stacking faults [115] but mordenite samples, although less frequently, may also have structurally related stacking faults. [116] Stacking faults increase the probability of the presence of defect sites in the framework. Also, the number of the T-atoms in four-rings may have an influence on the stability towards dealumination because the tension in the smaller rings is larger. The more aluminum atoms there are in an environment with tension, the easier it is to dealuminate the zeolite sample. [45]

Zeolite Beta, before dealumination, presents both framework and extra-framework Al species. R. Srivastava et al. reported that some active sites enveloped by extra-framework Al species can become effective upon removal of these Al species by dealumination with acid oxalic (Figure 39). The extra-framework Al species (EFAL) are responsible for weak acid sites, while the framework Al species (FAL) for strong acid sites. The latter strong acid sites are efficient to catalyze acylation and esterification reactions. Dealumination caused an increase in the accessibility of large reactant molecules to the active sites, resulting in the enhancement of the overall activity of the zeolite beta catalyst. [102]

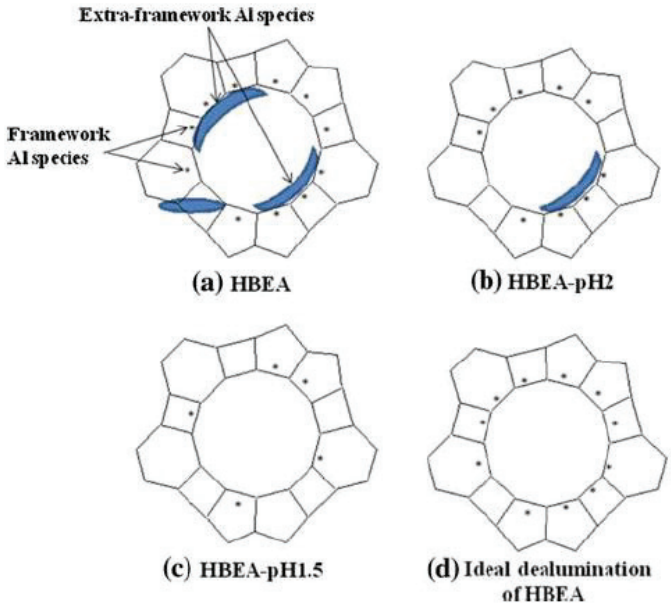

Figure 39. Schematic representation of HBEA samples before (a) and after dealumination (b), (c) and (d). [102]

J. P. Marques et al. concluded that dealuminated beta showed two domains, one essentially with extra-framework Al extraction at short leaching times, the other with essentially framework Al extraction for long leaching times. [103]

Three classical methods of dealumination were applied to a parent H-Beta sample: steaming, treatment with hydrochloric acid and treatment with ammonium hexafluorosilicate. M. M. L. R. Carrott and co-workers studied the adsorption of n-pentane and iso-octane in these dealuminated beta zeolites. Parent zeolite presented narrow pores outside the channel structure that behave as micropores towards the iso-octane molecules but as mesopores for nitrogen and n-pentane. The results suggested that these small pores must have formed upon calcination by deposition of EFAL species on intercrystalline voids and cracks on the external surface. These pores disappeared by the three treatments but as a consequence of different processes: widening of pores by dissolution of the EFAL (treatment with HCl) and pore blockage by deposition of silica (treatment with $(NH_4)_2SiF_6$) or further EFAL (treatment with steaming). [104] These dealuminated samples were used as catalysts in n-heptane cracking [105] and methylcyclohexane transformation. [106]

S. M. Maier and co-workers studied the effects of steaming treatment on zeolite beta with respect to the acidity and framework stability. 14 % of all Al T atoms were removed from the framework and transformed into extra-framework species. The cationic extra-framework Al species are located at the ion exchange positions and, thus, exchange the Brønsted acid sites. Note that one dealuminated Al atom leads to the loss of two Brønsted acid sites: one by the dealumination itself and one by the blockage of another framework Al atom as an extra-framework Al species. Extra-framework Al species in ion exchange positions stabilize the lattice and protect the remaining Al framework atoms from further dealumination. As a consequence, they are crucial to obtain a hydrothermally stable zeolite. [107]

On the other hand, there are few studies of dealumination of ZSM-5. In 1992, J. Kornatowski and co-workers studied the dealumination of ZSM-5 by several methods in order to compare the effectiveness of the various treatments and their influence on the crystal structure. They concluded that the best way to obtain the most open pore structure in dealuminated ZSM-5 is by leaching with acid followed by steaming and later second leaching. [108] More recently, ZSM-5 samples dealuminated by different methods (with HCl, acetylacetone and ammonium hexafluorosilicate) were used as catalysts in the isomerization of m-xylene increasing the catalytic activity. [109]

In the case of the mordenite structure, framework dealumination causes changes in both pore system and acidity. Several authors reported that dealumination of mordenite lead to an enlargement of pore sizes. Raatz et al. showed that it is possible to open up the porosity of the small-pore mordenite after removal of 20 % of framework alumina by dealumination. [26] J. Nagano et al. studied the microporous structure of dealuminated mordenite and observed that dealumination of mordenite led to an enlargement of pore sizes in both the main channels and the side pockets, more pronounced in the side-pockets. [27] Van Donk et al. reported the formation of mesopores in acid leached mordenite. [28] The accessibility of side pockets and acid sites of mordenite increased after dealumination. [30-31] N. Viswanadham et al. studied the dealumination of mordenite with nitric acid. The treatment resulted in the formation of secondary micropores larger than the main pore system (7-20 Å). The main reason for the increase in total micropore volume was explained by the opening of the side pockects of mordenite (Figure 40). [25]

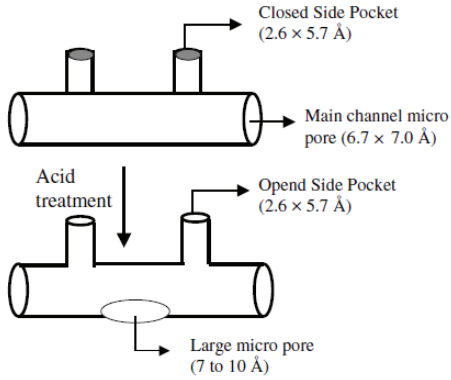

Figure 40. Effect of acid treatment on the pore system of H-mordenite. [25]

S. Moreno et al. investigated the dealumination of a large-pore and a small-pore mordenites with different crystallite size and morphology. Desalumination resulted in changes in the pore system, with development of macro-, meso- and secondary micropores, which increased by increasing Si/Al ratios. [33]

With respect to the acidity, the dealumination of mordenite involves the formation of new Lewis acid sites due to the presence of extra-framework aluminum species (EFAL), such as AlO^{+}, $Al(OH)^{2+}$, $Al(OH)_2^{+}$ or AlO(OH), which imparts, via an inductive effect, stronger acidity to the remaining Brønsted acid sites.[35-36, 38-39, 100] Sawa and co-workers found that dealumination improved the life of catalyst activity for

the methanol conversion, but deactivated it above 366 K of the dealumination temperature. The pore opening was partly enclosed in the samples prepared at high temperatures due to the presence of extra-framework Al. [39] In 1998, Z. M. M. Noronha and co-workers studied dealumination of mordenite by steaming. By varying the temperature and the water vapor partial pressure, the authors observed that steaming conditions had a great influence on the crystallinity and the extent of dealumination of mordenite samples. Moreover, the decrease in the micropore volume of the mordenite structure upon steaming could be ascribed both to a loss of crystallinity and a blockage of the openings of main channels due to the formation and deposition of EFAL species resulting from steam dealumination of the framework. [100]

It is of crucial importance to understand how framework Al is distributed over the zeolite framework, and whether and how this is changed upon dealumination. There are indications that it is possible to preferentially leach Al from specific positions. [25] This will have an important impact not only on the size and connectivity of the additionally created pores, but also on the location of the active acid sites for catalysis. Kinetic Monte Carlo simulations of the dealumination process have been studied to determine the mechanism of dealumination. [117] Experiments with simulations have been combined to achieve a detailed understanding of the effect of dealumination on the pore system of HMOR (Figure 41).

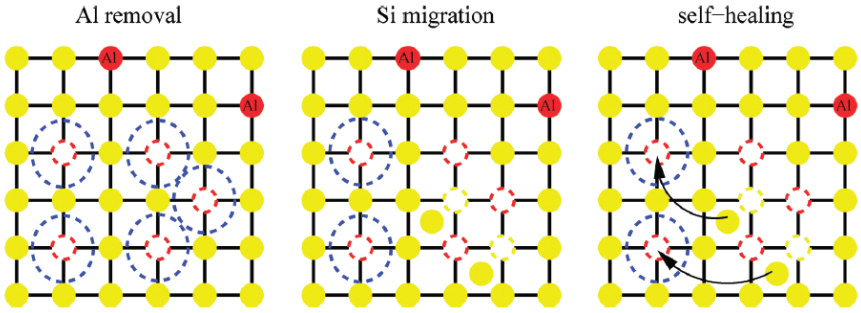

Figure 41. Schematic representation of the dealumination process. [117]

Dealumination procedure contains three stages: (1) the removal of framework Al. Framework Al is removed and transformed into extra-framework Al (this typically consists of AlO^{+}, $Al(OH)^{2+}$ and AlO(OH)). Typically extra-framework Al is removed using a mild acid. Due to the hydrolysis of Al-(O-Si-)$_4$ bonds, the removal of one framework Al atom results in the formation of a framework vacancy consisting of four (SiOH) groups. (2) The migration of framework Si. Framework Si is mainly extracted

from stacking fault domains. The generated Si atoms will migrate through the crystal and eventually heal the generated silanol nests. (3) The self-healing of a silanol nest. Silanol nests can be healed by migrating Si atoms extracted from stacking fault domains, in order to form a perfect local siliceous structure.

Nowadays, microwave irradiation is being applied for the dry, synthesis, and cation-exchange of zeolites. [91, 118-119] The use of microwaves considerably decreases the preparation times, with the subsequent energy saving, and modifies the samples properties. Therefore, microwave syntheses constitute valuable processes in Green Chemistry. At the beginning of this thesis, there was no reference about the use of microwaves for the dealumination of zeolites.

4.1.1 Effect of microwaves in the dealumination of mordenite on its surface and acidic properties.

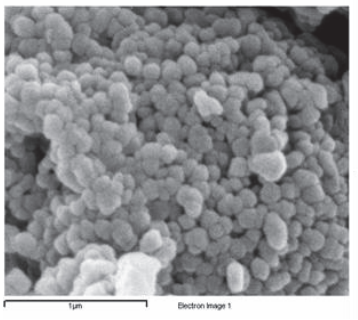

SO ring-opening		
% Conversion	% PA Selectivity	% EPE Selectivity
15	--	--

Microwaves
autoclave
15 min

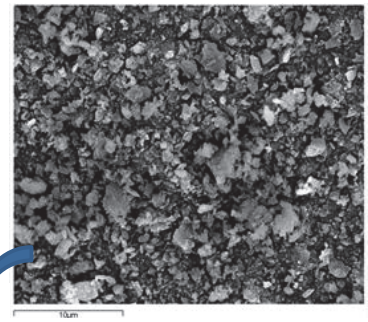

SO ring-opening		
% Conversion	% PA Selectivity	% EPE Selectivity
100	4	96

Abstract

Commercial mordenite was partially dealuminated in HCl medium by conventional heating or under microwaves by refluxing or autoclaving at 373 K at different times. Samples were characterized by AAS, XRD, N_2 physisorption, FT-IR, ^{27}Al NMR, NH_3-TPD, and SEM techniques. The acidity of the dealuminated samples was also determined by testing them as catalysts in two acid-catalyzed reactions: the isomerization of styrene oxide to obtain β-phenylacetaldehyde, and the styrene oxide ring-opening reaction to give 2-ethoxy-2-phenylethanol. The use of microwaves, under autoclave or refluxing conditions, enhances dealumination, favours the later elimination of the Al extracted during washing, and affects the surface and acidic characteristics of the resulting samples. All catalysts showed similar low amounts of Brønsted acid sites. However, the catalyst treated under microwaves by autoclaving at shorter time (15 min) presented active acid centres with medium strength, and, interestingly, lower amounts of strong Lewis acid sites (responsible for deactivation) than the rest of catalysts. These characteristics explain the total conversion obtained for this catalyst for the styrene-oxide ring opening reaction.

Microporous and Mesoporous Materials **2009**, 118, 341-347.

Introduction

Dealumination of zeolites is an essential step in the synthesis of a large number of commercial zeolite formulations. Barrer and Makki were the first to show that dealumination of zeolite frameworks could be achieved without loss of the zeolite structure, demonstrating that a natural zeolite clinoptilolite can be dealuminated by treatment with hydrochloric acid. [48]

Mordenite has been identified as suitable acid catalyst in several industrial processes, such as cracking and isomerization of hydrocarbons. [120] This zeolite is comprised of two straight channel types: i) larger channels, also called main channels, accessible through twelve member oxygen rings with an opening of 7.0 x 6.5 Å, and ii) smaller channels, often referred to as compressed channels, which include eight member oxygen rings with 2.6 x 5.7 Å. [14] On the whole, mordenite catalysts undergo rapid deactivation because of their uni-dimensional pore system with small side-pockets that are generally not accessible for reactant molecules, and limit the free diffusion of intermediate and product molecules. However, by applying dealumination methods, mordenite has been successfully used in industrial processes such as the DOW's process for cumene production [23], and the Shell's process for hydroisomerization of linear alkanes to branched alkanes. [24] A recent study showed that the dealumination of mordenite can improve the reactant molecules diffusion through its unidimensional pores, and results in higher resistance to deactivation catalyst for the isomerization of n-hexane. [25]

Framework dealumination of mordenite causes changes in both pore system and acidity. Several authors reported that dealumination of mordenite lead to an enlargement of pore sizes in the main channels as well as in the side pockets, and/or an increase of pore volume and surface area in mesopores. [26-34] With respect to the acidity, the dealumination of mordenite involves the formation of new Lewis acid sites due to the presence of extra-framework aluminum species (EFAl), such as AlO^{+}, $Al(OH)^{2+}$, $Al(OH)_2^{+}$ or AlO(OH), which imparts, via an inductive effect, stronger acidity to the remaining Brønsted acid sites. [35-38]

A considerable number of zeolite dealumination techniques have been developed. Thus, for mordenite we found dealumination studies by treatment with steam or $SiCl_4$ vapour at elevated temperatures or treatment with $(NH_4)SiF_6$, mineral acids (i.e., HCl, HNO_3), organic acids (i.e., acetic acid, oxalic acid), F_2, chelating

agents (i.e., EDTA), etc. [23-46] Conventional heating is used when applying temperature during dealumination.

Nowadays, microwave irradiation is being applied for the dry, synthesis, and cation-exchange of zeolites. [91, 118-119] The use of microwaves considerably decreases the preparation times, with the subsequent energy saving, and modifies the samples properties. Therefore, microwave syntheses constitute valuable processes in Green Chemistry. There is no reference about the use of microwaves for the dealumination of zeolites.

The aim of this work is to study the effect of using microwaves (in autoclave and by refluxing), during dealumination in HCl medium of commercial mordenite, on its resulting surface and acidic properties. Commercial mordenite was also dealuminated in acid medium by conventional heating (in autoclave and by refluxing) for comparison. All samples were characterized by a wide number of techniques.

Experimental

Preparation of partially dealuminated mordenite samples

The starting material was a commercial Na-Mordenite (Zeolyst, Si/Al = 6.5, CBV 10A Lot No. 1822-50), designated as M. We treated 1 g of mordenite with 30 mL HCl 6M for each preparation. Four samples were heated under microwaves (Milestone ETHOS-TOUCH CONTROL equipped with a temperature controller), two in an autoclave at 373 K for 15 min and 2 h (samples MWA_{15min}, MWA_{2h}, respectively), and the other two by refluxing at the same temperature and times (samples MWR_{15min} and MWR_{2h}). Four more samples were heated by autoclaving in a conventional oven at 373 K for 15 min and 2 h (samples A_{15min}, A_{2h}, respectively) or by traditional refluxing at the same temperature and times (samples R_{15min} and R_{2h}). After the acid treatment, samples were washed several times with deionized water, and dried in an oven overnight.

Elemental analyses

Elemental analyses of the samples were obtained with a Philips PW-2400 sequential XRF analyzer with Phillips Super Q software. All measures were made in triplicate.

^{27}Al MAS NMR

^{27}Al NMR spectra were obtained with a Varian Mercury Vx 400Mhz with a probe of 7mm CPMAS at a frequency of 400 MHz by spinning at 5kHz. The pulse duration was 2 μs, the delay time was 5s, and the chemical shift reference was high purity aluminium nitrate.

X-ray diffraction (XRD)

Powder X-ray diffraction patterns of the samples were obtained with a Siemens D5000 diffractometer using nickel-filtered Cu Kα radiation. Samples were dusted on double-sided sticky tape and mounted on glass microscope slides. The patterns were recorded over a range of 2θ angles from 5º to 40º. Crystalline phases were identified using the Joint Committee on Powder Diffraction Standards (JCPDS) files (43-0171 corresponds to mordenite). Cell parameters were calculated from (200), (020) and (202) peaks using a matching profile with WIN FIT 1.2 software. Crystallinity was determined by comparing the sum of the peak areas of (150), (202), (350) and (402) (22-32º 2θ) of the modified mordenites with respect to commercial Na-mordenite.

Nitrogen physisorption

BET areas were calculated from nitrogen adsorption isotherms obtained at 77 K using a Micromeritics ASAP 2000 surface analyser with a value of 0.164 nm^2 for the cross-section of the nitrogen molecule. Samples were pretreated in vacuum at 573 K for 6 h. Pore volumes and surface areas of micropores and mesopores were determined from their isotherms using the Horvath-Kawazoe method, and the BJH method, respectively.

FTIR

Infrared spectra were recorded on a Bruker-Equinox-55 FTIR spectrometer. The spectra were acquired by accumulating 32 scans at 4 cm^{-1} resolution in the range of 400–4000 cm^{-1}. Samples were prepared by mixing the powdered solids with pressed KBr disks in a ratio of 5:95, and dried in an oven overnight.

Temperature-programmed desorption-mass spectrometry experiments (TPD).

The acid properties of the samples were characterized by NH_3-TPD uSING A TPD/R/O 1100 Thermo Finnigan, equipped with a programmable temperature furnace and TCD detector. The gas outlet was couplet to a quadrupole mass spectrometer Pfeiffer GSD300 to identify the peaks. Experiments were performed with 3% NH_3/He flowing through the sample which was previously activated at 673 K for 1 hour. The desorption of NH_3 was made by flowing He 20 cm^3/min from room temperature to 1073 K at 5 K/min.

Scanning Electron Microscopy (SEM)-X-Ray microanalysis

This technique was used to observe the morphology and particle sizes of the samples. Experiments were performed on a scanning electron microscope, JEOL JSM6400, operating at accelerating voltage of 15 kV, work distances of 15 mm, and magnifications in the range 3700-50000x.

Catalytic activity studies

Isomerization of styrene oxide (SO), and styrene oxide ring-opening reactions were carried out in the liquid phase at atmospheric pressure at room temperature. The catalytic experiments were performed using 0.8 g of catalyst, 20 ml of solvent (toluene or ethanol to favour SO isomerization or SO ring-opening, respectively) and 0.48 ml of styrene oxide. The reaction products, taken at 3 h of reaction, were analysed by GC on a Shimadzu GC-2010 instrument equipped with a 30 m capillary column DB-1, coated with phenylmethylsilicon, and a FID detector.

Results and discussion

Table 3 shows the Si/Al ratio, and the Na_2O wt percentage of the acid-treated mordenites compared to the commercial one. We observed an increase of the Si/Al ratio accompanied by a decrease in the Na^+ content, as expected, for all the treated samples. Longer treatments times, and the use of microwaves resulted in an increase in the amount of Al removed, independently of using autoclave or refluxing methods. Therefore, there was a clear reduction of time by using microwaves to achieve similar dealumination degrees than by conventional heating, especially under autogenous

pressure. ^{27}Al NMR spectra (not shown here) exhibited the presence of non-tetrahedral Al for all the modified samples, confirming the presence of Al extra-framework for all of them.

Table 3. Chemical analyses results.

Sample	Si/Al (atomic ratio)	Na_2O (wt. %)
M	6.5	6.50
R_{15min}	14.9	0.10
R_{2h}	18.2	0.08
A_{15min}	11.2	0.11
A_{2h}	17.1	0.07
MWR_{15min}	15.5	0.11
MWR_{2h}	20.2	0.04
MWA_{15min}	15.8	0.08
MWA_{2h}	23.6	0.04

The acid and heating conditions used here did not cause drastic changes in the mordenite structure after acid treatment, although there was some decrease in the crystallinity of the mordenite structure, as deduced from the relative crystallinity values calculated from XRD results for the dealuminated samples (Table 4). These values were similar to those reported by other authors when dealuminating mordenite with mineral acids. [25, 33] This decrease in the crystallinity was slightly larger for the microwaved samples (Table 4), probably related to their higher dealumination (Table 3). XRD peaks appeared displaced to higher 2Θ values, and therefore, to lower interplanar distances for all treated samples with respect to commercial mordenite. This displacement was slightly higher for the mordenites treated under microwaves (Figure 42). This involved a variation of *a*, *b* and *c* parameters resulting in a decrease of the unit cell volumes for all the acid-treated samples (Table 4). Whatever the dealumination method, the variation of the *b* parameter was greater than that of *a* and *c*. This anisotropic contraction has been attributed to the fact that Al atoms occupy non-equivalent sites and, during dealumination, some of them would be removed before other ones. [33] Such contraction (Si-O bond length: 1.62 Å vs. 1.69 Å for Al-O) has been generally accounted for, in steam-dealuminated zeolites, by the migration of silicon atoms and filling of the structural defects created by the departure of Al ions (cicatrization effect), [33, 121] but also due to the presence of silanol groups. [122] The contraction of the unit cell

volume was slightly higher for the mordenites heated under microwaves, and increased at higher Si/Al ratio.

Table 4. Characterization of samples by XRD and FTIR techniques.

Sample	XRD					FT-IR Frequency of bands (cm^{-1})[b]	
	Critallinity (%)	a (Å)	b (Å)	c (Å)	Unit cell volume ($Å^3$)[a]	ν_1	ν_2
M	100	18.13(3)	20.48(2)	7.51(3)	2791	1068	629
R_{15min}	76	18.10(2)	20.15(2)	7.46(3)	2722	1087	639
R_{2h}	75	18.18(2)	20.25(3)	7.46(3)	2747	1093	646
A_{15min}	73	18.12(3)	20.21(2)	7.47(3)	2737	1084	635
A_{2h}	75	18.18(2)	20.25(3)	7.46(3)	2747	1093	644
MWR_{15min}	67	18.10(2)	20.16(3)	7.46(3)	2722	1090	638
MWR_{2h}	68	18.08(2)	20.19(3)	7.45(3)	2721	1093	644
MWA_{15min}	70	18.07(3)	20.13(2)	7.46(3)	2713	1091	641
MWA_{2h}	68	18.05(2)	20.11(3)	7.45(3)	2705	1093	643

[a] Calculated from XRD patterns.
[b] Frequencies of the main asymmetric stretch (υ_1), and the main symmetric stretch (υ_2) due to the T-O bond (T=Si, Al).

Infrared spectra of dealuminated mordenites and the starting mordenite were taken since it is well known that the symmetric and asymmetric stretching frequencies of the T-O bond (T= Si, Al) increases when the aluminium content is lower. [123] This is due to the increase of the strength of the T-O bond when the Al content decreases (the Si-O bond is shorter than the Al-O bond and Al has lower electronegativity than Si). The FT-IR spectra of the acid-treated mordenites showed a shift to higher values of the symmetric and asymmetric stretching frequencies of the T-O bond (T= Si, Al) (Table 4). This confirmed the removal of aluminium atoms from the framework.

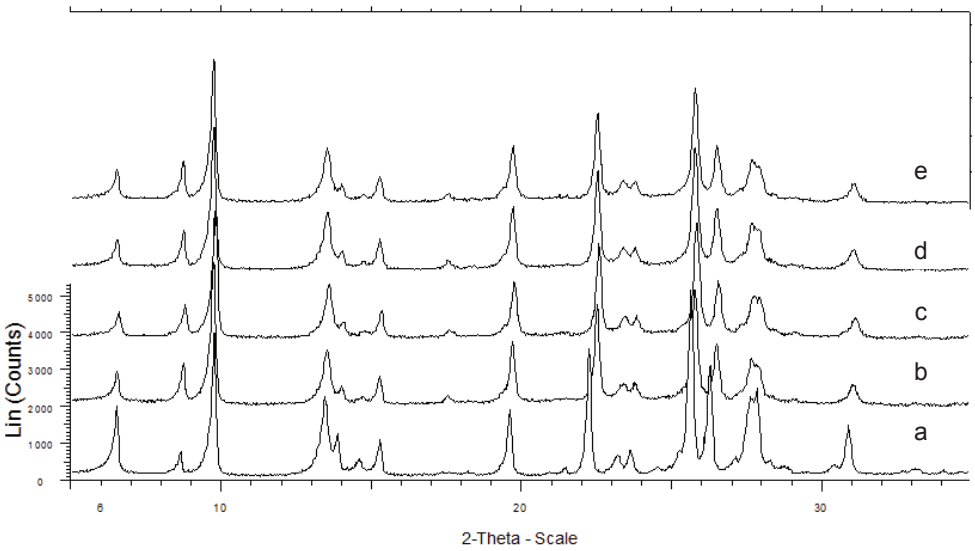

Figure 42. XRD patterns for the samples: a) M, b) MWA_{2h}, c) MWR_{2h}, d) A_{2h}, and e) R_{2h}.

Besides, the acid-treated samples showed higher BET areas, lower micropore area/non-micropore area ratios, and higher pore volumes than commercial mordenite (Table 5). These results can be associated to the loss of aluminum in the mordenite structure which lead to higher mesoporosity, and therefore, to higher surface areas. This is in agreement with the results reported by other authors. [25, 33, 46] Interestingly, this tendency appeared more marked for the microwaved samples. The appearance of hysteresis loops in the adsorption isotherm on the acid-treated mordenites confirmed the formation of mesopores by the acid treatment.

Table 5. Characterization of samples by nitrogen physisorption.

Sample	BET area (m^2/g)	micropore area/non-micropore area ratio	Volume pore (cm^3/g)
M	303	8.9	0.059
R_{15min}	384	5.7	0.109
R_{2h}	412	5.1	0.110
A_{15min}	376	6.1	0.096
A_{2h}	397	5.3	0.106
MWR_{15min}	388	5.1	0.102
MWR_{2h}	409	5.2	0.121
MWA_{15min}	419	5.9	0.110
MWA_{2h}	430	4.9	0.120

Scanning electron microscopy was used to monitor the morphologies and sizes of the particles of the acid-treated mordenites compared to commercial mordenite. Figure 43 shows the micrographs obtained for several samples. Commercial mordenite exhibited homogeneous rounded particles with sizes in the range 100-300 nm (Fig. 43a). Acid treatment under heating resulted in an agglomeration of the particles (Fig. 43b-43e), which presented heterogeneous sizes ranging from 100 to 3700 nm.

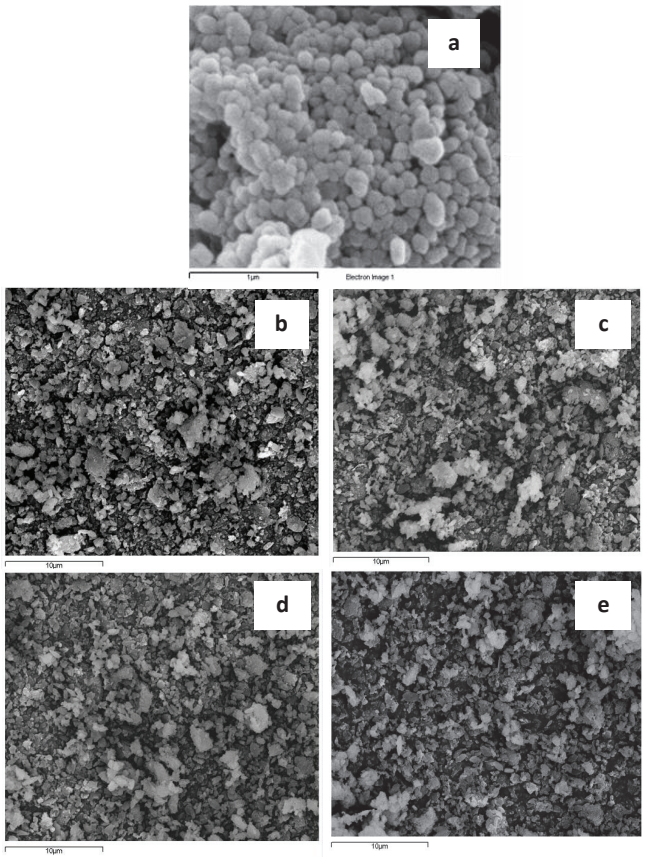

Figure 43. Scanning electron micrographs of samples: M (a), MWA_{2h} (b), A_{2h} (c), MWR_{2h} (d), and R_{2h} (e).

The acidity of all the partially dealuminated samples was evaluated by NH_3-TPD. Fig. 44 shows the NH_3-TPD thermograms of several representative samples whereas Table 6 depicts the TPD desorption temperature maxima obtained for all mordenites. The NH_3-TPD profile of Na-Mordenite only presented one peak with low intensity at 475 K. [59, 124] This peak has been assigned to ammonia weakly held or

physically adsorbed on the mordenite. [124] On the other hand, the partially dealuminated samples showed two non-symmetrical NH_3-TPD peaks (Fig. 44): one medium-high intense peak (peak 1) at 413 K-513 K, and a lower-medium intense peak (peak 2) at higher desorption temperatures (778-843 K). This is in agreement with the NH_3-TPD thermograms reported by other authors for dealuminated zeolites. [125] The peaks of the NH_3-TPD thermograms corresponding to the samples dealuminated under refluxing had less intensity than those of the autoclaved samples (Table 6, Fig. 44). Therefore, the refluxed samples have less acidity than the autoclaved ones. The use of atmospheric pressure favours more efficiently than autogeneous pressure the later elimination during washing of the Al removed from the zeolitic structure.

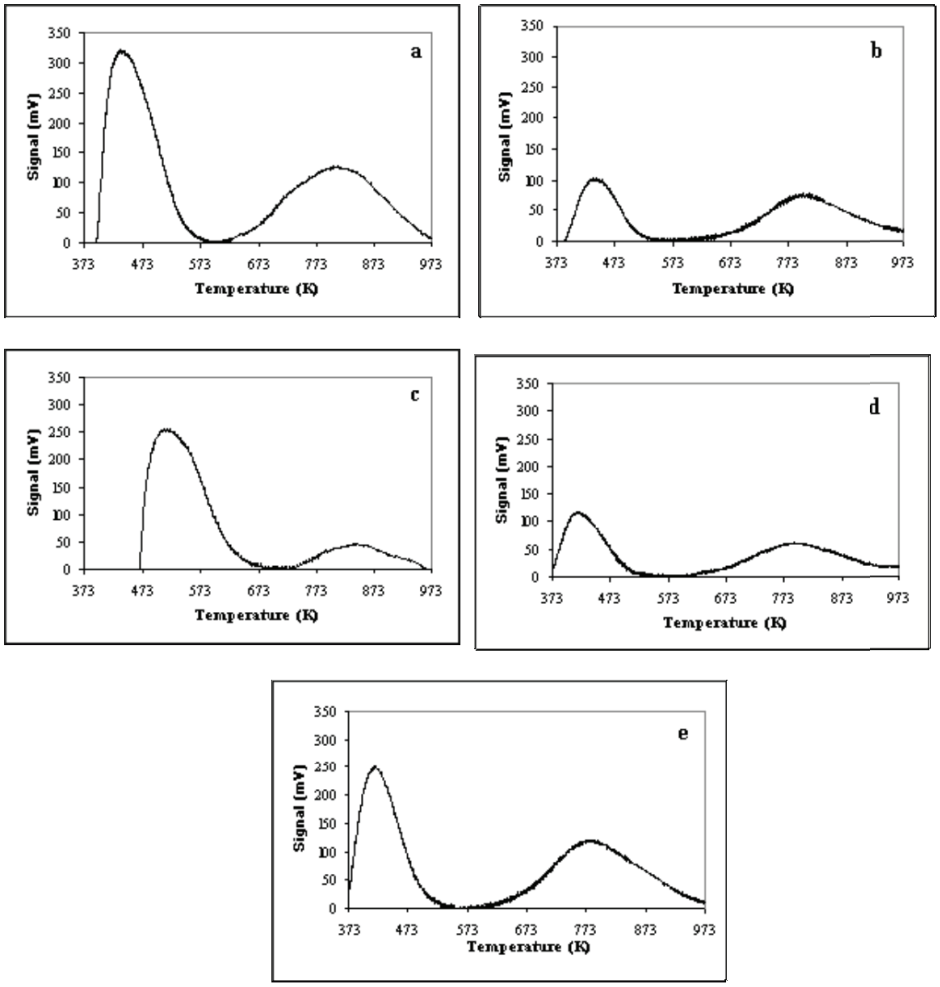

Figure 44. NH_3-TPD thermograms of several dealuminated samples: a) A_{15min}, b) R_{15min}, c) MWA_{15min}, d) MWR_{15min}, and e) MWA_{2h}.

In the literature, the assignment of the low temperature peak (peak 1) appears to be controversial. [125] This peak has been attributed to the release of NH_3 hydrogen-bound to NH_4^+ cations (readsorption of NH_3) [126] but also to weakly acid silanol groups (Brønsted acidity). [127] The possibility that weak Lewis acid sites were responsible for this peak has also been considered. [93, 128-129] It has been suggested that some extra-framework alumina species, such as $Al(OH)_2^+$ and $Al(OH)^{2+}$ could be sorption sites of a weak Lewis acid character. [93, 128] The non-symmetrical shape of this peak in our samples allowed us to think that this peak was formed for more than one contribution.

Table 6. NH_3-TPD results for the samples.

	NH_3 T_D (K)[a]	
Samples	Peak 1	Peak 2
M	475 (l)	-
R_{15min}	433 (m)	793 (m)
R_{2h}	433 (m)	803 (h)
A_{15min}	435 (h)	813 (m)
A_{2h}	423 (h)	835 (h)
MWR_{15min}	413 (m)	788 (m)
MWR_{2h}	413 (m)	783 (h)
MWA_{15min}	513 (h)	843 (l)
MWA_{2h}	418 (h)	778 (m)

[a] T_D: Maxima of NH_3 desorption temperature peaks. (l): low-intense peak; (m) medium-intense peak; (h): high-intense peak.

Mordenites dealuminated under refluxing had a less intense peak 1 than the autoclaved ones (Table 6, Fig. 44). The increase of the treatment time did not affect the intensity and the maximum of desorption temperature of peak 1 for the refluxed mordenites whereas for the autoclaved samples, we observed a decrease in the desorption temperature maximum at longer treatment times (2 h) (Table 6). The use of microwaves affects in a different way when using refluxing or autoclaving preparation methods. For the refluxed samples (MWR_{15min}, MWR_{2h}), and for the mordenite treated in autoclave for 2 h (MWA_{2h}) we saw a lower desorption temperature of peak 1 than the corresponding samples conventionally heated. However, sample MWA_{15min}, treated under microwaves in autoclave for 15 min, presented a maximum of peak 1 at higher desorption temperature than sample A_{15min}, treated in conventional autoclave for 15 min. Taking into account all these variations observed between the samples, we believe

that peak 1 can be assigned, on the whole, to weak acid sites (Brønsted and/or Lewis) associated to the dealumination procedure. Interestingly, microwaves led to weaker acidity than conventionally heated samples, except for sample MWA_{15min} (Table 6, Fig. 44), which showed medium acidity (higher desorption temperature). In this case, the shorter time used during dealumination was not enough to favour a later efficient elimination of the extracted Al (which was higher than for sample A_{15min} (Table 3)), that probably remained as extra-framework $Al(OH)_2^+$ and $Al(OH)^{2+}$ species. An inductive effect between both, these species and the silanols present, can explain the higher desorption temperature of peak 1 observed for this sample. This medium acidity, achieved by using microwaves at shorter times during the acid treatment, will play an important role on the catalytic results, as commented below.

With respect to peak 2, it had higher intensity for the samples dealuminated at longer times (2 h) (Table 6). Since commercial mordenite did not present peak 2, we can assume that this second peak can be related to some strong Lewis acid centres associated to extra-framework Al insoluble species generated from the zeolitic framework during dealumination. Interestingly, peak 2 was less intense for the samples prepared under microwaves, especially by autoclaving (Fig. 44c, 44d) than for the samples prepared by conventional heating (Fig. 44a, 44b). This seems to confirm that the use of microwaves allows us a better elimination during washing of the Al extracted during dealumination resulting in less amounts of strong Lewis acid centres.

In order to try to determine the nature of the acidity of the centres observed by NH_3-TPD, we tested the samples as catalysts in two reactions catalysed by different acid sites: the isomerization of styrene oxide to obtain β-phenylacetaldehyde, which is mainly catalysed by Brønsted acids sites, and the styrene oxide ring-opening to give 2-ethoxy-2-phenylethanol, which is catalysed by both Brønsted and Lewis acid sites. [59] Table 7 shows the catalytic activity of all samples for both reactions. All catalysts showed similar yield values to β-phenylacethaldehyde (PA), slightly higher than commercial mordenite, for the styrene oxide isomerization. Since Brønsted acid sites catalyse this reaction, as commented above, we can assume that the dealuminated samples have similar low amounts of Brønsted acid sites.

However, in the styrene oxide ring-opening reaction, catalysts presented different catalytic behaviour. There are two important features to remark: on the one hand, the samples treated at shorter times showed higher conversion and selectivity to EPE values than those treated at longer times, independently of the dealumination

method used; on the other, the samples dealuminated under microwaves exhibited higher conversion and higher selectivity to EPE values than the samples dealuminated under conventional heating. Thus, MWA_{15min} yield much higher conversion and much higher selectivity to 2-ethoxy-2-phenylethanol (EPE), followed by sample MWR_{15min}, than the rest of catalysts (Table 7).

Table 7. Catalytic activity for the two-acid catalyzed reactions

Catalysts	SO isomerization[a] % PA Yield	SO ring-opening[b]		
		% Conversion	% PA Selectivity	% EPE Selectivity
M	12	15	--	--
R_{15min}	42	36	44	56
R_{2h}	41	32	51	49
A_{15min}	36	49	46	54
A_{2h}	54	43	48	52
MWR_{15min}	43	73	16	84
MWR_{2h}	42	50	34	66
MWA_{15min}	50	100	4	96
MWA_{2h}	44	46	40	60

[a]Reaction time: 3h, solvent: toluene, [b]Reaction time: 3h, solvent: ethanol.
PA: β-phenylacethaldehyde; EPE: 2-ethoxy-2-phenylethanol.

The higher conversion and higher selectivity to EPE observed for sample MWA_{15min} can be explained by the presence of active acid centres (Lewis and Brønsted) with medium strength (peak 1) together with the existence of very low amounts of strong Lewis acid centres (peak 2), observed by NH_3-TPD (Fig. 44c). At higher treatment times, samples have weaker acid centres (peak 1) and higher amounts of strong acid centres (peak 2) (Table 6). Strong acid centres are responsible for deactivation, as previously reported. [59] In fact, we observed a higher deactivation with time (not shown here) for the catalysts acid treated at longer times (2 h), which presented higher amounts of these strong acid centres, as commented above. If we compare the catalytic activity results of catalysts R_{15min} and MWR_{15min}, prepared by refluxing under conventional heating and under microwaves, respectively, we observe that they have similar amounts of weak acid centres (Fig. 44b, 44d) but sample MWR_{15min} has lower amounts of strong acid sites, explaining its higher conversion value. The less amounts of these strong acid sites present in the microwaved samples

(especially at shorter times), explain the higher conversion values observed for these catalysts.

In this work, we report for the first time that the use of microwaves during dealumination of mordenite by acid treatment, not only enhances dealumination by decreasing considerably the time needed to achieve similar dealumination degrees than by conventional heating methods but also favours the later elimination of the Al extracted from the zeolite structure resulting in partially dealuminated mordenites with less strong acid sites than those conventionally dealuminated. In the literature, the mechanism of microwave heating of zeolite has been studied. Several authors reported that the heating proceeds in two steps; in the first step the hydrated zeolite absorbs microwaves through its adsorbed water, and in the second step the heated zeolite directly microwaves. [130-131] Therefore, the different heating process which involves the use of microwaves allow us to dealuminate mordenite in less time obtaining materials with different acidic properties, with their subsequent potential use in catalysis.

Conclusions

The use of microwaves for the dealumination of commercial mordenite affects the surface and acidic properties of the resulting partially dealuminated samples. Microwaves lead to faster dealumination than conventional heating by autoclaving as well as by refluxing.

Dealumination of the samples was observed by XRD, N_2 physisorption, IR, elemental analyses, ^{27}Al MAS NMR, and SEM techniques since the acid-treated samples showed higher Si/Al molar ratio, lower cell volume, higher BET area, and lower micropore area/non-micropore area ratio than commercial mordenite. These variations appeared more pronounced for the microwaved samples, confirming the effect of using microwaves on the surface characteristics of the mordenite samples.

NH_3-TPD thermograms presented two non-symmetrical desorption peaks for all the partially dealuminated samples. The first desorption peak has been related to the presence of weak-medium acid centres, which are a contribution of silanol groups (Brønsted acidity) together with $Al(OH)_2^+$ or $Al(OH)^{2+}$ Lewis species generated during dealumination. The second peak has been associated to strong Lewis acid centres due to extra-framework insoluble aluminium species also formed during dealumination.

Samples dealuminated under refluxing have less acidity than the autoclaved ones due to the best elimination, during washing, of the Al extracted at atmospheric pressure. The use of microwaves leads to lower acidity, due to the higher dealumination produced followed by a more efficient elimination of Al during washing, except for the sample prepared under autoclave at shorter time. Interestingly, in this sample the presence of acid sites with medium strength contributes decisively to the catalytic activity results. The partially dealuminated samples showed similar low amounts of Brønsted acid sites, as deduced from the catalytic results obtained for the isomerization of styrene oxide. Interestingly, from the catalytic results obtained for the styrene oxide ring-opening reaction, we observed that when the mordenite was dealuminated at shorter time (15 min) under microwaves, higher conversion values were obtained. The presence of active acid centres with medium strength together with the lower amounts of stronger Lewis acid sites, responsible for deactivation, observed for catalyst MWR_{15min} explains its total conversion for the styrene oxide ring-opening reaction.

Acknowledgements

The authors are grateful for the financial support of the Ministerio de Educación Ciencia and FEDER funds (CTQ2005-02384/PPQ).

UNIVERSITAT ROVIRA I VIRGILI
REVALORIZACIÓN CATALÍTICA DE GLICERINA PARA UNA OBTENCIÓN MÁS RESPETUOSA CON EL MEDIO AMBIENTE DE ADITIVOS PARA COMBUSTIBLES
Mª Dolores González Candela
DL:T. 1715-2011

4.1.2 Comparison of dealumination of zeolites beta, mordenite and ZSM-5 by treatment with acid under microwave irradiation

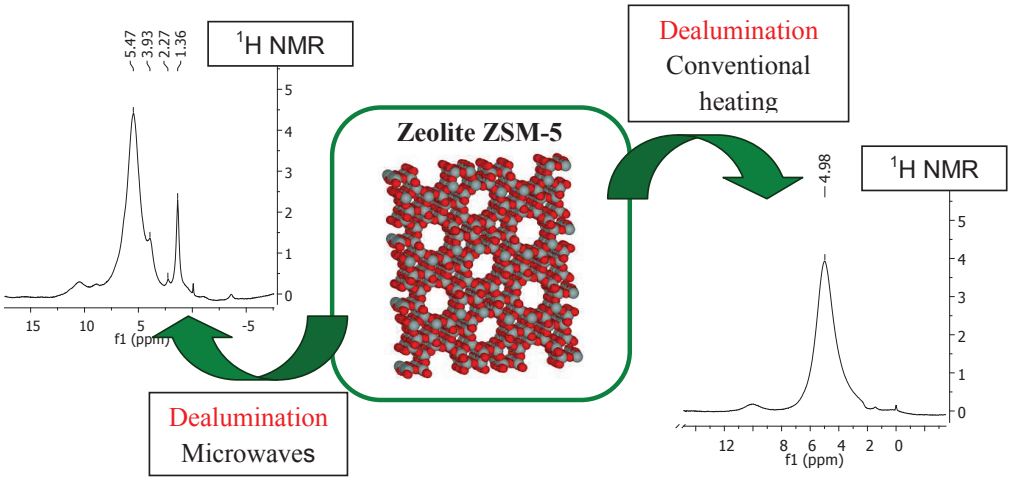

Abstract

Commercial mordenite, Beta and ZSM-5 zeolites were partially dealuminated in HCl medium in autoclave by conventional heating or under microwave irradiation at 373 K for 15 min. The extent of dealumination was function of the zeolite structure (beta > mordenite > ZSM-5), and the heating method used. Microwaves led to faster dealumination than conventional heating for the three zeolites. Besides, the use of microwaves affected the surface and acidic properties of the resulting dealuminated samples.

Microporous and Mesoporous Materials **2011**, 144, 162-170.

Introduction

Zeolites are well known microporous materials widely used as catalysts in petrochemical industry due to their large surface areas, shape selectivity, and controllable acidity. [37, 97] Dealumination of zeolites are useful to reduce acid site concentration, improve thermal stability, and modify pore structure. [37, 97-98] There are several factors that influence zeolites dealumination, such as the zeolite synthesis conditions, its structure type, and the dealumination treatment method.

During crystallization, there is a preferred Si/Al ratio in the framework of every structure type. When the Si/Al ratio of the synthesis gel deviates from the ideal ratio, extraframework aluminium species (EFAl) could be formed, or the distribution of the aluminum atoms in the framework could be inhomogeneous. [97] This can affect its behaviour towards dealumination.

Different zeolite structure types, such as beta, mordenite, ZSM-5, ferrierite, zeolite Y, zeolite 4A, are known to exhibit very different behaviour with respect to dealumination. [33, 45, 110-111] The arrangement and size of the pores influence the accessibility of the aluminum atoms in the framework. Zeolite beta, for example, has a three-dimensional 12-ring pore system (straight channels of diameter 6.6 x 6.7 Å and sinusoidal channels of diameter 5.6 x 5.6 Å) and, because of this property, its framework is very flexible. Zeolite mordenite has a one-dimensional pore system with main channels of diameter 6.7 x 7.0 Å and compressed channels of diameter 2.6 x 5.7 Å whereas ZSM-5 has a three-dimensional 10-ring pore system with channels of diameter 5.1 x 5.5 Å. Both these structures are less flexible than beta, and consequently, it is more difficult to dealuminate them. In addition, zeolite beta crystallizes with many stacking faults [115] while mordenite samples, although less frequently, may also have structurally related stacking faults. [116] Stacking faults increase the probability of the presence of defect sites in the framework. Also, the number of the T-atoms in four-rings may have an influence on the stability towards dealumination because the tension in the smaller rings is larger. Thus, a zeolite is easier to dealuminate as many aluminium atoms has in an environment with tension. [45]

A considerable number of zeolite dealumination techniques have been developed. We found dealumination studies by treatment of zeolites with steam or $SiCl_4$ vapour at elevated temperatures or treatment with $(NH_4)SiF_6$, mineral acids (i.e., HCl, HNO_3), organic acids (i.e., acetic acid, oxalic acid), F_2, chelating agents (i.e.,

EDTA), etc. [25, 31, 33, 45-47, 110-114] Conventional heating is used when applying temperature during dealumination.

Nowadays, microwave irradiation is being applied for the dry, synthesis, and cation-exchange of zeolites. [91, 118-119] The use of microwaves considerably decreases the preparation times, with the subsequent energy saving, and modifies the samples properties. Therefore, microwave syntheses constitute valuable processes in Green Chemistry. There are only two references about the use of microwaves for dealumination of zeolites. [132-133]

In a previous paper, we observed that the use of microwaves for mordenite dealumination in acid medium resulted in faster dealumination than when using conventional heating. The sample treated by autoclaving under microwave irradiation at shorter time (15 min), presented active acid centres with medium strength, and lower amounts of strong Lewis acid sites than the rest of samples. [132]

The present work aims to extend the investigation of the use of microwaves during dealumination in HCl medium in autoclave to other two zeolite structures: ZSM-5 and Beta. Dealumination experiments were performed at short treatment time (15 min) to compare with the mordenite dealumination results, some of which have been also included here. Zeolites were also dealuminated in acid medium by conventional heating in autoclave under identical conditions for comparison.

Experimental

Preparation of dealuminated samples

Na-Mordenite (Zeolyst, Si/Al=6.5, CBV 10A Lot No. 1822-50), Na-Beta (Zeochem, Si/Al=10, PB Lot No. 6000186), and Na-ZSM-5 (Zeochem, Si/Al=20, PZ-2/40 Lot No. 6002827,01), designated as M, B and Z, respectively, were treated with HCl 6M under microwave irradiation (Milestone ETHOS-TOUCH CONTROL equipped with a temperature controller) at 373 K for 15 min (samples MMW, BMW and ZMW, respectively), and in the case of Beta, also for 5 min (sample BMW5). Autoclaves were magnetic stirred and the rotor turned on while the microwave equipment was working in order to maximize the homogeneity of heating and to avoid local hotspots. Besides, these zeolites were also acid-treated by autoclaving in a conventional oven at the same temperature and times (samples MA, BA, ZA, and BA5).

Then, all samples were washed several times with deionized water, and dried in an oven overnight.

Elemental analyses

Elemental analyses of the samples were obtained with a Philips PW-2400 sequential XRF analyzer with Phiplips Super Q software. All measures were made in triplicate.

X-ray diffraction (XRD)

Powder X-ray diffraction patterns of the samples were obtained with a Siemens D5000 diffractometer using nickel-filtered Cu Kα radiation. Samples were dusted on double-sided sticky tape and mounted on glass microscope slides. The patterns were recorded over a range of 2θ angles from 5º to 40º and crystalline phases were identified using the Joint Committee on Powder Diffraction Standards (JCPDS) files (43-0171, 48-0074, 37-359 corresponds to mordenite, beta and ZSM-5, respectively). For mordenite, cell parameters were calculated from (200), (020) and (202) peaks, and for ZSM-5 from (200), (020), (002) and (-103) peaks, using a matching profile with WIN FIT 1.2 software. Crystallinity of the modified mordenites was determined by comparing the sum of the peak areas of (150), (202), (350) and (402) (22-32º 2θ) with respect to commecial Na-mordenite. Crystallinity of the modified ZSM-5 samples was calculated using the (051) peak intensity compared with the parent zeolite sample. The integrated intensity of the signal at 2θ = 22.4º was used to evaluate the crystallinity of beta samples.

FTIR

Infrared spectra were recorded on a Bruker-Equinox-55 FTIR spectrometer. The spectra were acquired by accumulating 32 scans at 4 cm^{-1} resolution in the range of 400–4000 cm^{-1}. Samples were prepared by mixing the powdered solids with pressed KBr disks in a ratio of 5:95 and dried in an oven overnight.

Nitrogen physisorption

BET areas were calculated from the nitrogen adsorption isotherms at 77 K using a Micromeritics ASAP 2000 surface analyser and a value of 0.164 nm^2 for the cross-section of the nitrogen molecule. Samples were pretreated in vacuum at 573 K for 6 h. Pore size distribution of micropores and meso-macropores were determined from isotherms using the Horvath-Kawazoe method and the BJH method, respectively.

Scanning Electron Microscopy (SEM)

This technique was used to observe the morphology and particle sizes of the samples. Experiments were performed on a scanning electron microscope, JEOL JSM6400, operating at accelerating voltage of 25 kV and work distances of 10 mm, and magnifications of 10,000x.

^{1}H MAS NMR and ^{27}Al MAS NMR.

^{1}H NMR and ^{27}Al NMR spectra were obtained with a Varian Mercury Vx 400Mhz with a probe of 7mm CPMAS at a frequency of 400 MHz by spinning at 5kHz. The pulse duration was 2 μs and the delay time was 5s. The chemical shift reference was trimethyl silil-3 propionic acid d_4-2,2,3,3 sodium salt for ^{1}H NMR, and high purity aluminium nitrate for ^{27}Al NMR.

Catalytic activity determination

Isomerization of styrene oxide, and styrene oxide ring-opening reactions were carried out in the liquid phase at atmospheric pressure at room temperature. Catalytic experiments were performed using 20 ml of solvent (toluene or ethanol, respectively), 0.8 g of catalyst (for mordenite catalysts) or 0.4 g (for beta and ZSM-5 catalysts), and 0.48 ml of styrene oxide. A lower catalyst amount was used when testing beta and ZSM-5 catalysts to decrease their conversion values below 100 %, observing better the differences in the selectivity values. The reaction products, taken at 3 h of reaction, were analysed by GC on a Shimadzu GC-2010 instrument equipped with a 30 m capillary column DB-1 coated with phenylmethylsilicon and a FID detector.

Results and discussion

We observed dealumination for all the acid-treated zeolites since they showed higher framework Si/Al ratio, lower cell volumes, and a shift to higher values of the IR bands assigned to symmetric and asymmetric stretching of the T-O bond (T= Si, Al) than their corresponding commercial ones (Table 8). The increase of the strength of the T-O bond when the Al content decreases was explained by the fact that Si-O bond is shorter than the Al-O bond, and Al has lower electronegativity than Si. [123] The extent of dealumination was function of the zeolite structure and the heating method used. Thus, beta zeolite was easier to dealuminate than mordenite, whereas dealumination of ZSM-5 was very low. This order can be related to the flexibility of each zeolite framework, and the accessibility of the aluminium atoms depending on the pores arrangement and sizes, according to the results reported by other authors. [45, 115-116] Interestingly, the samples treated with acid under microwave irradiation showed higher dealumination than the samples dealuminated in a conventional oven. In the case of Beta zeolite, where very high Si/Al ratio values were obtained after dealumination for 15 min, this effect was confirmed by dealuminating commercial beta at shorter heating time (5 min) since, again, the Si/Al ratio of the microwaved sample (BMW5) was higher than the Si/Al ratio of the sample conventionally heated (BA5) (Table 8).

Table 8. Characterization of samples by XRF, XRD, and FT-IR techniques.

Samples	Si/Al (XRF)	Crystallinity [a] (%)	Unit cell volume [a] ($Å^3$)	IR bands (cm^{-1}) [b] υ_1	υ_2
M	6.5	100	2791	1068	629
MA	11.2	73	2737	1091	641
MMW	15.8	70	2713	1084	635
B	10.0	100	--	1068	629
BA	110.8	62	--	1091	641
BMW	121.9	69	--	1084	635
BA5	84.7	87	--	1094	626
BAMW5	98.9	78	--	1096	632
Z	20.0	100	5209	1063	797
ZA	21.3	99	5125	1096	797
ZMW	22.4	100	5192	1097	797

[a] Calculated from XRD patterns. [b] Frequencies of the main asymmetric stretch (υ_1), and the main symmetric stretch (υ_2) due to the T-O bond (T=Si, Al).

^{27}Al NMR spectra of commercial zeolites (not shown here), showed tetrahedral Al for commercial mordenite, tetrahedral Al for commercial ZSM-5, and both tetrahedral Al and octahedral Al (this later in low amount) for commercial beta zeolite. The peaks corresponding to tetrahedral and octahedral aluminium appear around 50 ppm and 0 ppm, respectively. The presence of octahedral Al in commercial Beta can be attributed to extraframework aluminium species or to aluminium coordinated in defect sites taking into account the characteristic stacking faults of this zeolite structure. [103, 115] ^{27}Al NMR spectra of modified mordenite and modified ZSM-5 samples showed octahedral Al, in higher relative amounts for mordenite samples, confirming dealumination (Fig. 45).

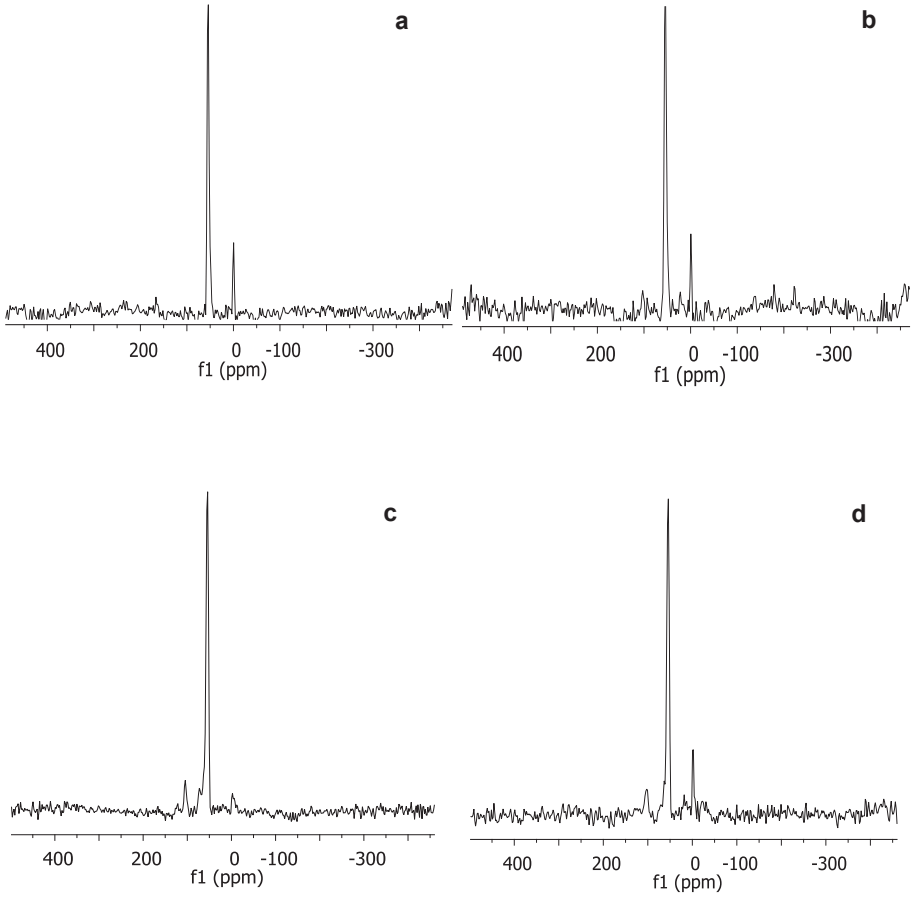

Figure 45. ^{27}Al NMR spectra of samples: (a) MA, (b) MMW, (c) ZA, and (d) ZMW.

For acid-treated ZSM-5 samples, we can conclude that although some aluminium was extracted from the framework upon acid treatment, dealumination was not very efficient. It is important to note the higher relative amounts of octahedral aluminium for the samples treated under microwave irradiation (ZMW and MMW) with respect to those dealuminated under autoclave at the same conditions (ZA and MA). For beta zeolites (not shown here), we observed a considerably decrease both in the tetrahedral and octahedral Al when compared with commercial Beta due to the high dealumination underwent.

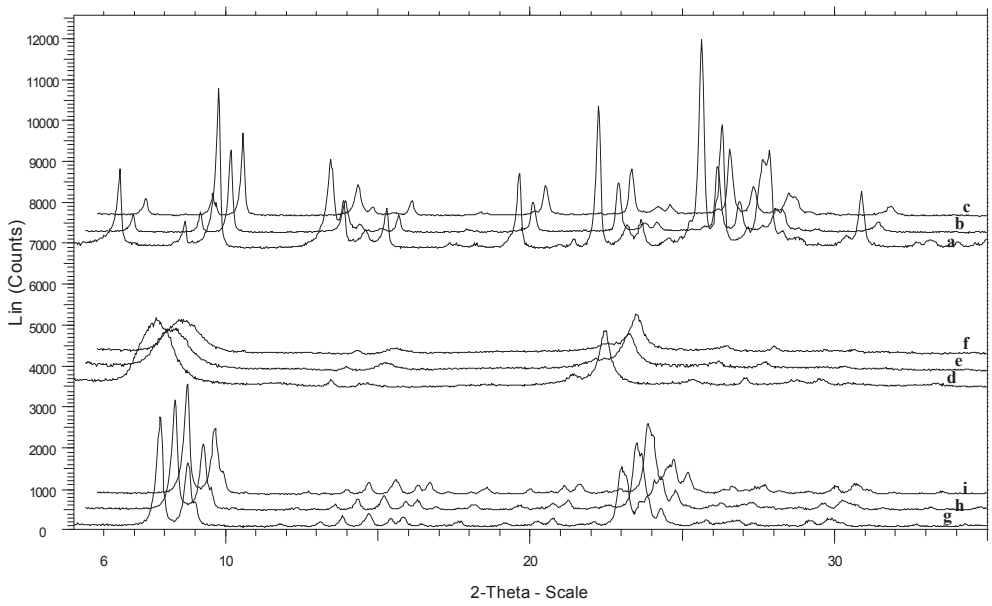

Figure 46. XRD patterns of the samples: (a) M, (b) MA, (c) MMW, (d) B, (e) BA, (f) BMW, (g) Z, (h) ZA, (i) ZMW.

The acid and heating conditions used here did not cause drastic changes in the zeolite structures (Figure 46), although there was some decrease in the crystallinity of the mordenite and beta zeolites after acid treatment (Table 8). The crystallinity of ZSM-5 samples practically did not change according to their low dealumination.

Table 9 and Figure 47 show several characterization results obtained from nitrogen physisorption for all samples. The acid-treated mordenites presented higher surface area, lower micropore area/non-micropore area ratios, and higher pore volumes than commercial mordenite. This can be associated to the loss of aluminium in the mordenite structure, which results in higher mesoporosity, and therefore, higher surface area. Also, a slight increase in the micropore size was observed. This is in agreement with the results reported by other authors. [25, 33, 46] Interestingly, this variation was more marked for the microwaved sample.

Table 9. Characterization of samples by nitrogen physisorption

Samples	BET area (m^2/g)	Micropore area/ non-micropore area ratio	Pore volume (cm^3/g)
M	303	8.9	0.059
MA	376	6.1	0.096
MMW	419	5.9	0.110
B	573	1.8	0.228
BA	554	1.8	0.244
BMW	451	1.5	0.242
BA5	527	1.6	0.322
BAMW5	507	1.5	0.359
Z	300	2.4	0.063
ZA	306	2.0	0.072
ZMW	300	1.7	0.073

On the other hand, after dealumination of Beta zeolite, we observed a decrease in the BET surface area accompanied to some variations in the micro-mesoporosity (Figure 47) which can be attributed to the loss of crystallinity after treatment, as reported by other authors. [134] Finally, for acid-treated ZSM-5 samples, slight differences in surface and porosity characteristics were detected when compared with commercial ZSM-5 due to their very low dealumination. The slight higher decrease in the micropore/non-micropore area ratio observed for the three zeolites when treated under microwave irradiation, could be related to their higher dealumination.

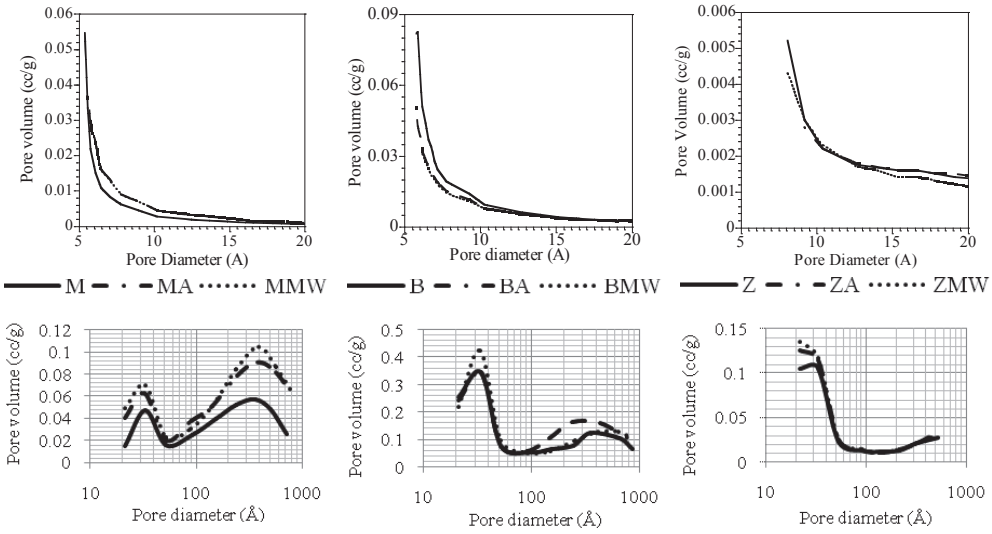

Figure 47. Micropore and mesopore size distribution graphics for all samples.

Scanning electron microscopy was used to monitor the morphologies and sizes of the particles of the acid-treated samples with respect to the starting commercial zeolites (Figures 48-50). Dealuminated mordenite and beta samples appeared less agglomerated, with less densely packed crystallites, than their corresponding commercial ones, especially those treated under microwave irradiation (Figures 48, 49) whereas the micrographs of ZSM-5 samples were very similar. (Fig. 50). No significant changes in the particle sizes were observed in any case.

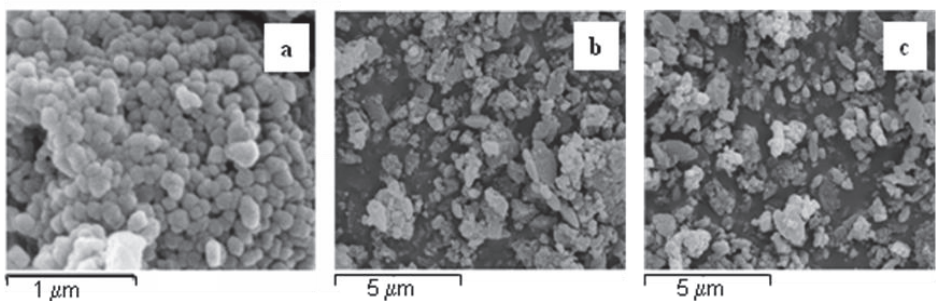

Figure 48. Scanning electron micrographs of samples: (a) M, (b) MA and (c) MMW.

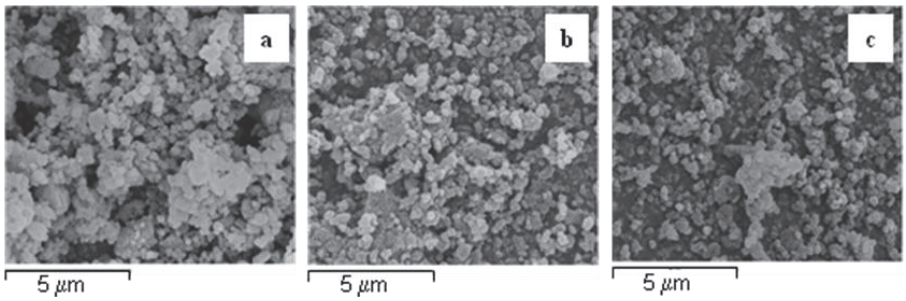

Figure 49. Scanning electron micrographs of samples: (a) B, (b) BA and (c) BMW.

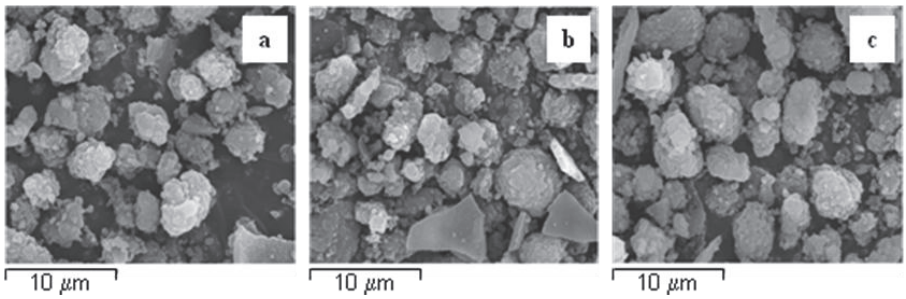

Figure 50. Scanning electron micrographs of samples: (a) Z, (b) ZA and (c) ZMW.

The effect of microwaves on dealumination, when compared with conventional heating, can be mainly explained taking into account that chemicals do not interact equally with the commonly used microwave frequencies for dielectric heating, and consequently selective heating may be achieved. [91, 135] This may lead to a significantly different temperature regime, caused by microwave dielectric heating, being the main contributing factor to the acceleration observed with respect to conventional heating.

Figures 51-53 show the ^{1}H NMR spectra of mordenite, beta and ZSM-5 samples, respectively. For commercial Na-zeolites (Figs. 51a, 52a and 53a), we observed one peak around 4 ppm, which can be associated to free Brønsted protons. [94] After acid treatment of mordenite (Figs. 51b and 51c), one broad peak appeared at higher ppm values (5.0-5.1 ppm) than that of commercial mordenite, indicating stronger acidity. [136] This peak could be attributed to Brønsted protons, formed during dealumination in HCl medium, that are interacting with the zeolite framework. [45, 134] The acidity was slightly higher for the microwaved sample.

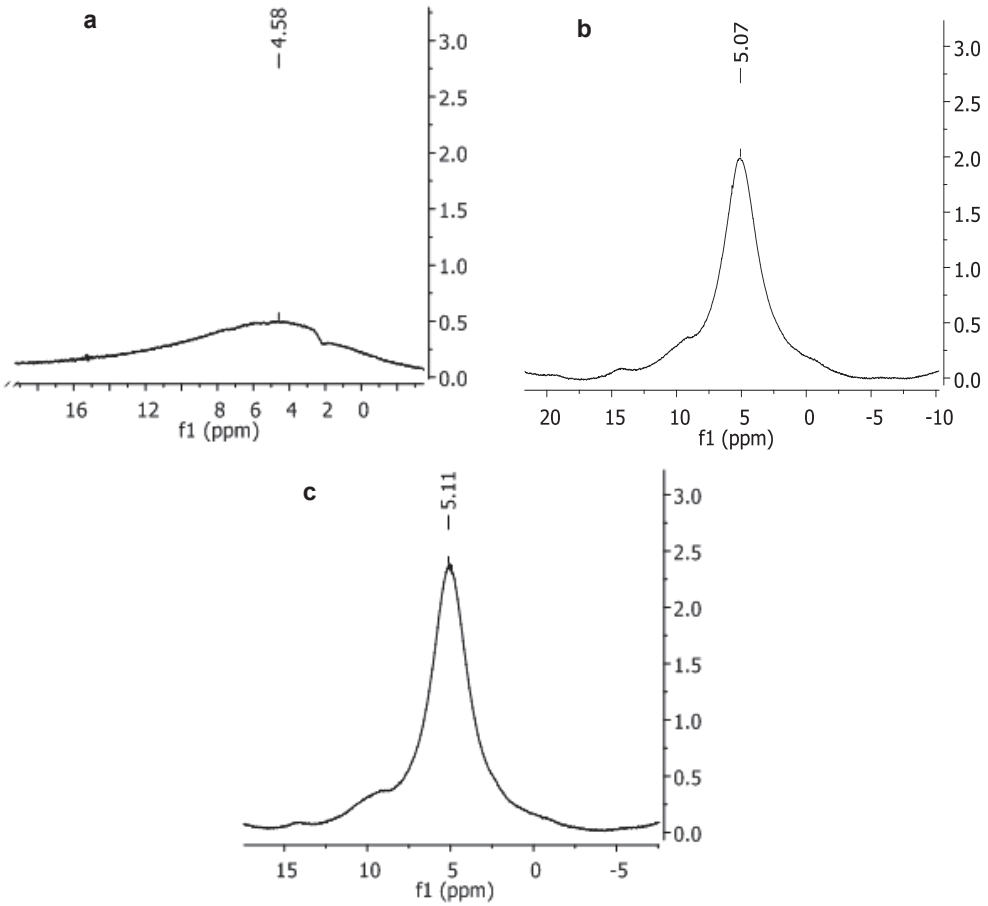

Figure 51. ^{1}H NMR spectra of samples: (a) M, (b) MA and (c) MMW.

For acid-treated beta samples, we observed one main peak in the ^{1}H NMR spectra (Figs. 52b, 52c and 52d) with a shift similar to that of commercial beta (around 4 ppm). This can be explained by the higher dealumination suffered by these samples. Therefore, there are not protons interacting with the framework since practically the zeolite framework has not negative charge. Interestingly, the sample treated under microwave irradiation (BMW) showed, in addition to this main peak, a second much less intense peak at 2.2 ppm (Fig. 51c) attributed to internal silanols groups [137], which were formed during acid dealumination of the framework, as indicated in scheme 1.

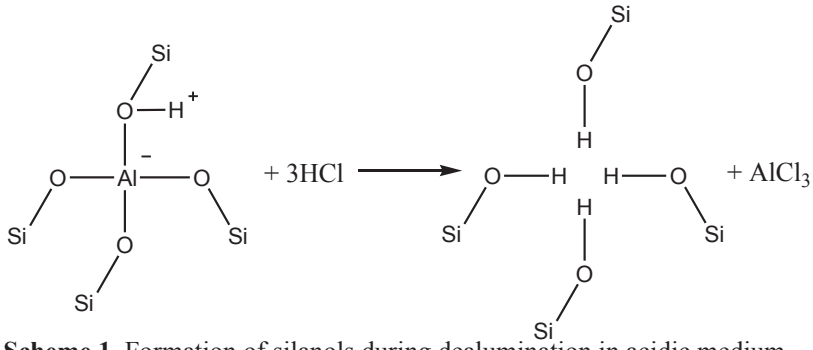

Scheme 1. Formation of silanols during dealumination in acidic medium.

FTIR (not shown here) confirmed this since an increase of the silanol band was observed after treatment for this sample. This peak at 2.2 ppm was also pointed out in the ^{1}H NMR spectrum of the sample treated under microwave irradiation at shorter time (BMW5) (Fig. 52d).

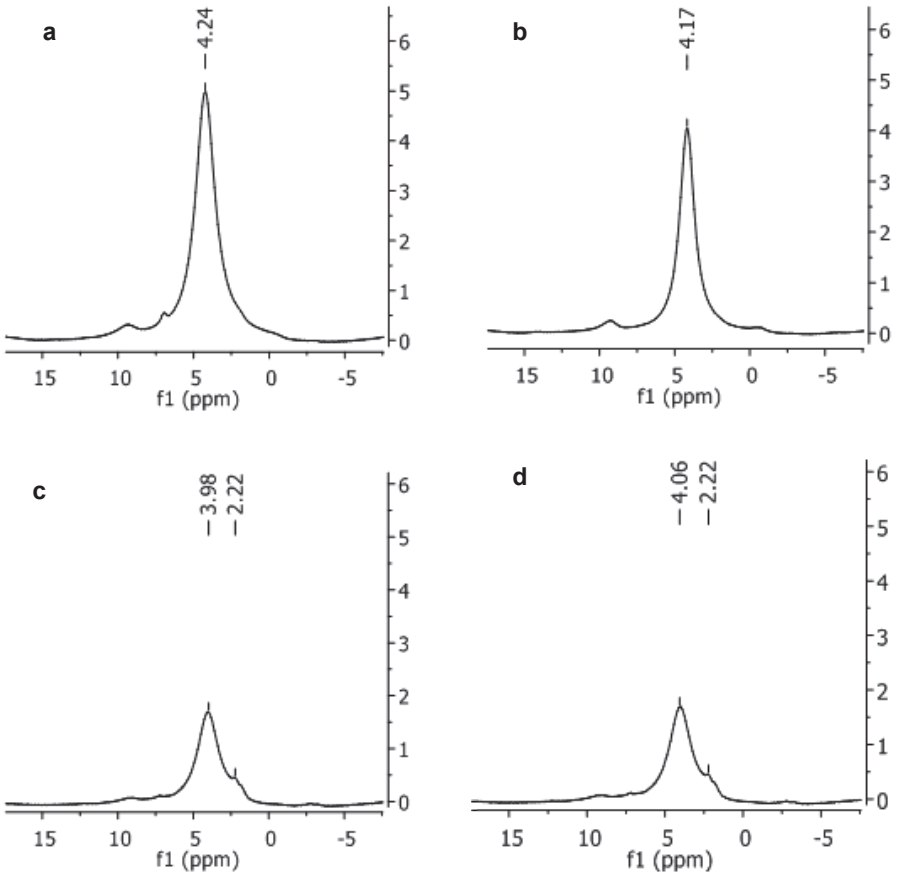

Figure 52. ^{1}H NMR spectra of samples: a) B, (b) BA, (c) BMW, and d) BMW5.

Finally, although the acid-treated ZSM-5 samples exhibited very low dealumination, we observed differences in their acidic properties by ^{1}H MAS NMR (Fig. 53). After treatment, both samples showed one peak at higher shift (around 5 ppm) than its corresponding Na-ZSM-5 sample. Again, this can be attributed to the presence of Brønsted protons interacting with the framework. This could be explained by some proton exchange occurred during dealumination due to the high acid medium, as reported by other authors. [138] Interestingly, after treatment under microwave irradiation new signals appeared between 1.2-2.2 ppm which can be associated to the presence of some external/internal silanol groups (Fig. 49c). [45, 137]

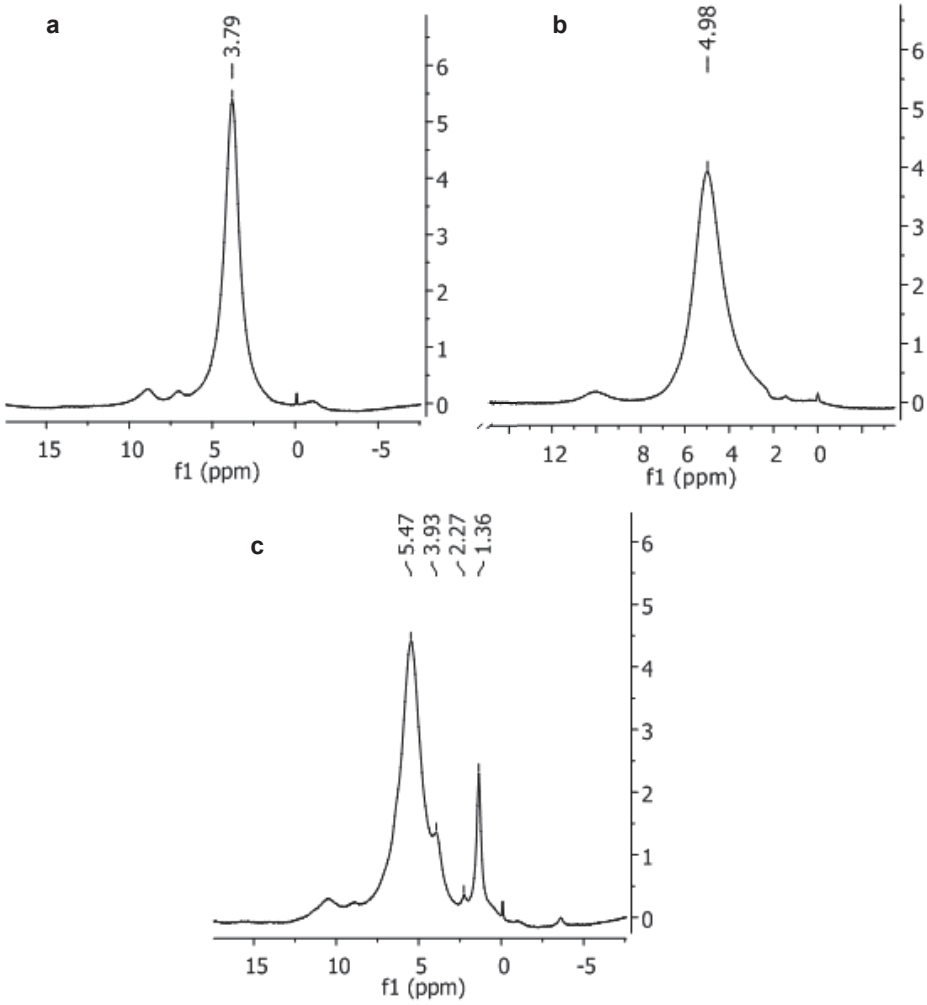

Figure 53. ^{1}H NMR spectra of samples: (a) Z, (b) ZA and (c) ZMW.

All samples were tested as catalysts in two reactions catalysed by different acid sites: the isomerization of styrene oxide to obtain β-phenylacetaldehyde (PA), which is mainly catalysed by Brønsted acid sites, and the styrene oxide ring-opening reaction to give 2-ethoxy-2-phenylethanol (EPE), which is catalysed by both Brønsted and Lewis acid sites but mainly by Lewis acid sites. [59, 132, 139]

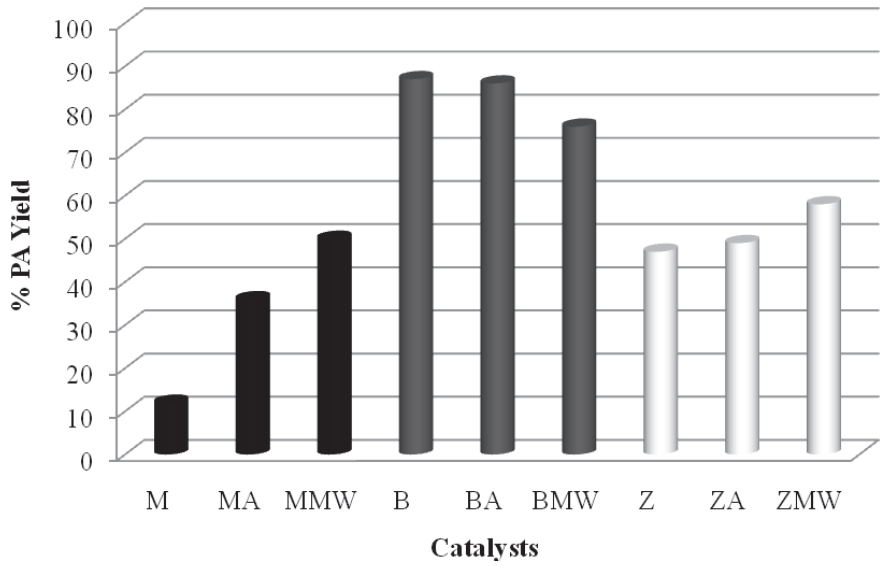

Figure 54. Catalytic activity of all catalysts for the isomerization of styrene oxide.

Fig. 54 depicts the catalytic activity of all catalysts for the styrene oxide isomerization reaction in terms of % yield to β-phenylacetaldehyde (PA). Modified mordenite, specially that treated with microwaves, showed higher yields to PA than commercial mordenite due to the presence of Brønsted acid sites with higher strength appeared after dealumination in HCl medium, as observed by ^{1}H NMR (Fig. 51). All beta catalysts had similar high yield values to PA for the styrene oxide isomerization. This agrees with the similar ^{1}H NMR spectra obtained for these samples. In this case, the microwaved sample presented slight lower PA yield than the conventionally autoclaved one. This can be explained by the slight lower strength of the protons related to its main ^{1}H NMR peak taking into account that silanols groups, obtained in low amounts for this sample, in zeolites with high density of defect sites, as beta zeolites, give very weak acidity. [134, 137] Modified ZSM-5 catalysts showed similar PA yields to

that obtained for the commercial one. Interestingly, sample treated with microwaves gave higher yield to PA. This can be attributed to the higher strength of the protons associated to the main ^{1}H NMR peak.

The differences in the activity between the three types of zeolites for this reaction could be explained by the number of Brønsted acid sites (related to the Si/Al ratio) and their strength together with the higher accessibility of the reactants to the active sites in beta and ZSM-5 samples because of their three-dimensional pore structure compared with the one-dimensional pore structure of mordenite.

For the styrene oxide ring-opening reaction, the three types of catalysts exhibited very different behaviour (Figs. 55-57). Besides 2-ethoxy-2-phenylethanol (EPE) and β-phenylacetaldehyde, other products of this reaction were no identified products of high molecular weights (condensation products), which are responsible for catalyst deactivation, as reported in previous studies. [59, 132, 139]

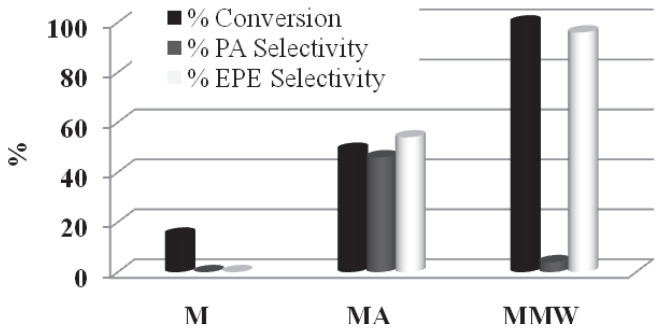

Figure 55. Catalytic activity of mordenite catalysts for the styrene oxide ring-opening reaction.

With respect to mordenite samples (Fig. 55), MMW presented higher conversion and higher selectivity to 2-ethoxy-2-phenylethanol (EPE) than M and MA. The presence of higher amounts of Lewis (Al extra-framework) and Brønsted acid sites with medium strength together with the existence of very low amounts of strong Lewis acid sites, which are responsible for catalyst deactivation in this reaction, can explain these results, as previously reported. [132]

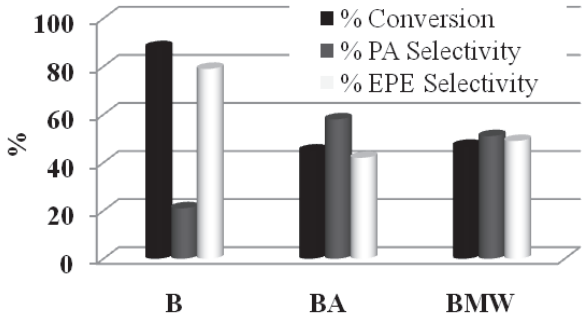

Figure 56. Catalytic activity of beta catalysts for the styrene oxide ring-opening reaction.

On the other hand, modified beta samples had lower conversion and lower selectivity to EPE than commercial Na-beta. This can be explained by the high elimination of aluminium after acid treatment, having in mind that the starting commercial Beta had aluminium partially coordinated on defect sites, which can act as Lewis acid sites [140-142], favouring the formation of EPE. This explanation also agrees with several characterization results reported by other authors who stated that the acid leaching of beta zeolite eliminates much faster the Lewis acid sites than the Brønsted ones. [103, 143]

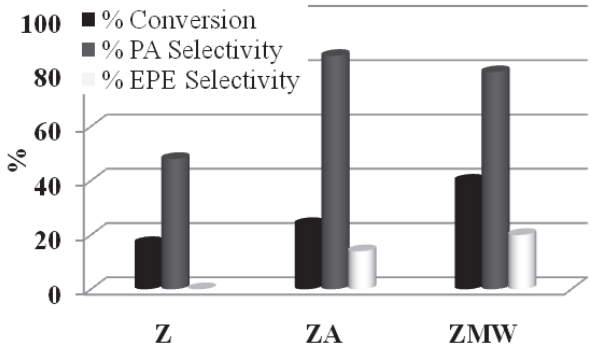

Figure 57. Catalytic activity of ZSM-5 catalysts for the styrene oxide ring-opening reaction.

Finally, modified ZSM-5 samples showed higher conversion than commercial ZSM-5 due to the presence of Brønsted acid sites with higher strength, as observed by ^{1}H NMR. The very low dealumination and, therefore, low generation of Al extraframework justifies the low selectivity values to EPE observed. The slightly higher

amount of Al extraframework, observed by ^{27}Al NMR (Fig. 45) for the microwaved sample, agrees with the slightly higher selectivity to EPE obtained for this sample.

Conclusions

The extent of dealumination was function of the zeolite structure and the heating method used. Beta zeolite was easier to dealuminate than mordenite whereas dealumination of ZSM-5 was very low. This can be related to the flexibility of each zeolite framework, and the accessibility of the aluminium atoms depending on the pores arrangement and sizes. Microwaves led to faster dealumination than conventional heating for the three zeolites. Besides, the use of microwaves affected the surface and acidic properties of the resulting dealuminated samples.

Mordenite treated with HCl under microwave irradiation showed higher mesoporosity, higher surface area, and Brønsted acid sites with higher strength than the mordenite treated by conventional heating. After acid treatment with microwaves, beta zeolite exhibited lower surface area accompanied with some variations in the micro-mesoporosity, and similar Brønsted acidity than the conventionally acid-treated beta. However, some silanols, with very weak acidity, were only detected for the microwaved sample. Lastly, ZSM-5 treated in acidic medium with microwaves had similar surface and porosity characteristics than the conventionally heated sample, probably due to the very low dealumination achieved. Interestingly, for the microwaved ZSM-5 sample, some accessible external silanol groups appeared after acid treatment, resulting in slightly higher Brønsted acididity. Besides, slightly higher amount of extraframework Al, and therefore, slightly Lewis acidity, was observed for this sample.

Acknowledgments

The authors are grateful for the financial support of the Ministerio de Ciencia e Innovación and FEDER funds (CTQ2008-04433/PPQ). Dolores González acknowledges Ministerio de Educación y Ciencia for a FPU grant (AP2007-03789).

4. RESULTS AND DISCUSSION

4.2. Glycerol etherification with tert-butanol or isobutene

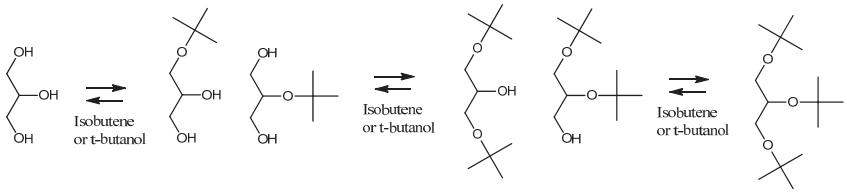

UNIVERSITAT ROVIRA I VIRGILI
REVALORIZACIÓN CATALÍTICA DE GLICERINA PARA UNA OBTENCIÓN MÁS RESPETUOSA CON EL MEDIO AMBIENTE DE ADITIVOS PARA COMBUSTIBLES
Mª Dolores González Candela
DL:T. 1715-2011

4.2. Background about glycerol etherification with tert-butanol or isobutene

Glycerol cannot be added directly to transportation fuel because of its decomposition and polymerisation, which may cause engine problems at high temperatures. Its low solubility in hydrocarbons also limits the direct addition of glycerol to fuels. Besides, it can be partly oxidized to toxic acrolein. Consequently, glycerol must be modified and converted to other derivatives, which can be compatible with diesel and biodiesel. [2, 6, 8, 144]

Special interest is focused on the preparation of alkyl ethers of glycerol by etherification with isobutene or tert-butanol. Isobutene (IB) or tert-butanol (TBA) reacts with glycerol in the presence of acid catalysts to obtain a mixture of mono-, di- and tri-tert-butyl glycerol ethers (MTBG, DTBG, TTBG, respectively) (Figure 58).

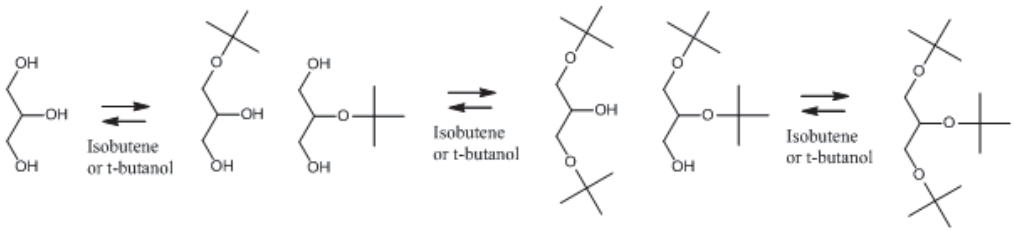

Figure 58. Synthesis of GTBE *via* reaction of glycerol with isobutene or t-butanol.

Nowadays, oxygenated molecules such as methyl tertiary butyl ether (MTBE) are used as valuable fuel additives because of their antidetonant and octane-improving properties. One challenging option is the catalytic etherification of glycerol with tert-butanol or isobutene to obtain di- and tri- tertiary butyl ethers of glycerol (h-GTBE), which is an excellent additive with a large potential for diesel and biodiesel reformulation. The etherification of glycerol is preferred on primary hydroxyl groups, favouring the formation of 1-GTBE and 1,3-GTBE. However, monoethers (MTBG) have low solubility in diesel fuel. For this reason, etherification of glycerol must be directed to the maximum formation of di- and tri-ethers. Thus, a mixture of 1,3-di, 1,2-di, and 1,2,3-tri-tert-butyl glycerol, the so-called "higher ethers" (h-GTBE), when incorporated in standard 30-40% aromatic-containing diesel fuel, led to significantly reduced emissions of particulate matter, hydrocarbons, carbon monoxide, and unregulated aldehydes.[145-146] Additionally, these high glycerol ethers are reported to reduce the viscosity of biodiesel and act as cold flow improvers. In an aim to replace the

use of MTBE, which is toxic to the environment and now is banned in 20 states of USA, studies about glycerol etherification to obtain h-GTBE have been carried out.

The first studies about the etherification of glycerol, the most part as patents, were published from middle of 90s, and were performed with isobutene. [145, 147-152] Etherification of glycerol with isobutylene (IB) or with tertiary butanol (TBA) has been studied in the presence of acid catalysts. [5,153-163] Etherification with isobutene yielded better conversion and better selectivity values to h-GTBE than etherification with tert-butanol. [158] Water formation, in the case of using TBA as reagent, inhibits the glycerol etherification since water molecules compete with reactants for the adsorption on the active sites. This effect limits the access of reactants to the acid sites due to the formation of solvated sites (Figure 59). [164-165]

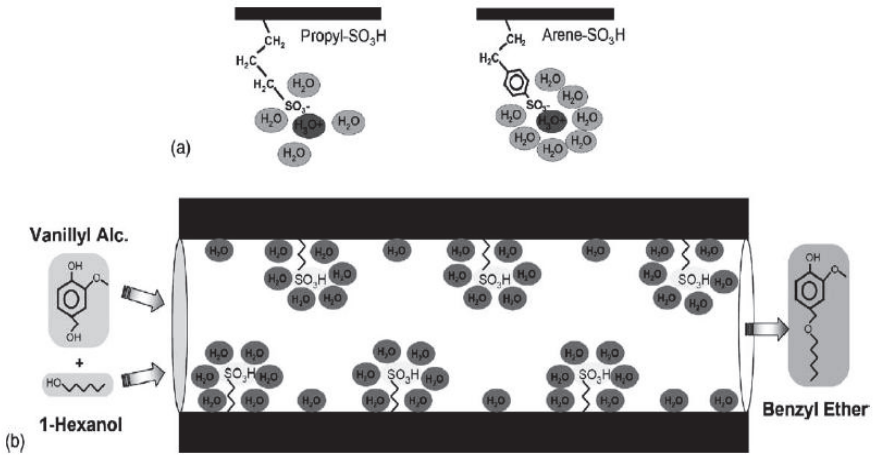

Figure 59. (a) Simplified scheme of water/sulfonic interaction for propyl-sulfonic acid group and arene-sulfonic acid group. (b) Schematic representation of a mesopore in sulfonic acid-modified SBA-15. [165]

However, the use of tert-butanol, as both reactant and glycerol solvent, instead of gaseous isobutylene, overcomes the technological problems arising from the need to use solvents able to dissolve glycerol (i.e. dioxane, dimethyl sulfoxide) and typical drawbacks of a complex three-phase system (mass transfer phenomena). [156, 163] Also, the simpler reaction system when using tert-butanol can be very useful to the activity systematic study of new catalytic systems.

Catalytic etherification of glycerol with isobutene have been studied at temperatures between 333-373 K with isobutene excess (from 2:1 to 4:1

isobutene/glycerol molar ratio) under moderate pressure of 15-20 bar to have isobutene in liquid phase. This reaction was first investigated in 1994 by Behr and Lohr at the Henkel Company. [150] In these studies, the reaction was performed in a batch reactor under nitrogen at low pressures with acid homogeneous catalysts (e.g. *p*-toluene sulfonic acid or methanesulfonic acid) as well as with acid heterogeneous catalysts type acid ion-exchange resins (Amberlysts). Although homogeneous catalysts yielded high conversion and moderate selectivity to the desired products, the difficulty in the separation of the catalyst form the reaction medium becomes an important restriction to project this process at industrial scale. With respect to heterogeneous catalysts, the best results were achieved by using an acid ion exchange resin, Amberlyst 15. However, the methanol formed during reaction must be eliminated to avoid catalyst poisoning. [152]

At the beginning of the reaction the system consists of two immiscible phases, the polar glycerol and the unpolar isobutene phase (Figure 60). Due to the two remaining hydroxyl groups the monoethers (m-GTBE) are still soluble in polar solvents, whereas the mixture of the di- and triethers (h-GTBE), are soluble in unpolar media, for instance in hydrocarbons. For this reason, when the concentration of monoethers and diethers in the isobutene phase rises, the solubility of glycerine on this phase increases. Once the glycerol conversion reaches 60-70 % the two phases coalesce and form a single phase. [153]

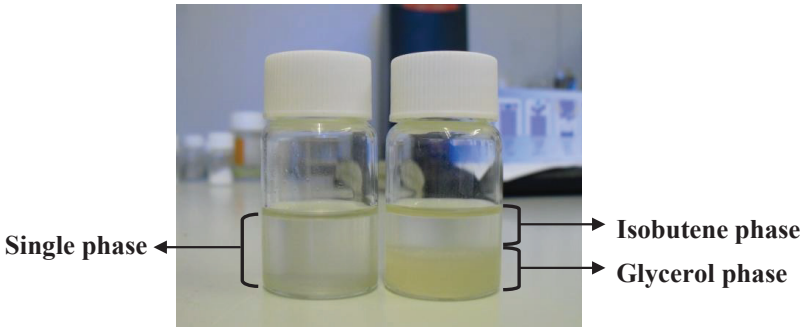

Figure 60. One or two liquid phases during the reaction.

Later, Behr and Obendorf reported a kinetic model for this reaction, which was performed in a batch reactor at 263 K, 2MPa with an isobutene/glycerol ratio of 2/1, and using heterogeneous and homogeneous catalysts. [153] This paper presents the estimated rate coefficients and activation energies for three consecutive equilibrium reactions of glycerol etherification corresponding to the mono-ether, di-ether and tri-ether formation,

respectively. The yield can be improved by optimizing the reaction conditions, such as temperature, molar ratio, and type and amount of catalyst. From these results, the authors developed an alternative technical process for the production of h-GTBE to that proposed until that moment by Arco Chemical. [147]

From 2003, Klepáčová et al. studied the catalytic activity and selectivity of ion-exchange resins of Amberlyst type (Amberlyst 15 and 35) and the large-pore zeolites (H-Y and H-Beta) on *tert*-butylation of glycerol with isobutylene. The higher conversion of glycerol was reported for H-Beta (almost 100 %), but the bulkier glycerol triether (TTBG) was not formed. This was attributed to steric hindrance due to the microporosity of zeolites. The higher amount of di- and tri-ethers was formed over Amberlyst 35 (88.7 %). This selectivity increased until 94.7 % when the resin was swollen in glycerol before put it into the reaction medium. [155] The authors concluded that the most appropriate temperature for the etherification is 333 K since at higher temperatures the dimerization of isobutene takes place. It is important to remark that although the ion-exchange resins had nearly five times higher total acidity than H-zeolites, they did not show five time higher initial reaction rates. These authors also reported the study in the liquid phase in a batch reactor of these same catalysts but in the presence of dioxane as solvent. [156] At these conditions, the best conversion of glycerol was achieved with H-Beta with high selectivity to di-ethers but again without the formation of the tri-tert-butyl ether. The highest amount of h-GTBE (di + tri-ethers) was obtained with catalyst Amberlyst 35. The solvent affects the polarity of the reaction mixture and favours the homogenization of reactants.

Karinen and Krause studied the effect of the isobutene/glycerol ratio using Amberlyst 35 as catalyst. [157] The formation of the tri-ether was favoured when the initial isobutene/glycerol molar ratio was high while the optimal conditions for the formation of the di-ethers were a stoichiometric initial isobutene/glycerol molar ratio. Finally, mono-ethers were the main products when using a low initial isobutene/glycerol molar ratio. It is important to note than an excess of isobutene increased undesired oligomerization reactions while an excess of glycerol increased the viscosity of the reaction mixture limiting the reaction rate. [157]

More recently, Melero et al. reported the etherification of glycerol with isobutylene over different sulfonic acid-modified mesoestructured silicas in comparison with sulfonic acid resins (Amberlyst and Nafion type). Optimal conditions were established to be isobutylene/glycerol molar ratio 4/1 and temperature of 348 K. Arene-

sulfonic acid-modified SBA-15 silica gave the highest production of DTBG and TTBG. In terms of selectivity towards di- and tri-ethers, a value of 92 % was obtained after 4 h. In contrast to macroporous commercial sulfonic acid resins, no presence of oligomerisation products was detected over this silica-based catalyst. [158] In this study, the authors used response factors of DTBG and TTBG extrapolated from that of glycerol monoethers (MTBG, available commercially) to calculate the selectivities to di- and tri-ethers.

On the other hand, there are few studies about the catalytic etherification of glycerol with tert-butanol. [154-155, 164, 166-167] Klepáčová et al. reported that acidic resin catalysts (Amberlyst type) exhibited higher conversion (88 %) than zeolites H-Y and H-Beta but, on the whole, low selectivity to h-GTBE (around 25 %) was achieved for this reaction, which were performed in a batch reactor at 338 K with a TBA/glycerol ratio of 4, at reaction times of 300 min. [154-155] However, triether was not detected when using these H-zeolites. This has been attributed to steric hindrance effects because of the microporosity of the zeolites. [155] Luque et al. evaluated a new family of mesoporous carbonaceous materials, denoted as Starbon, as catalysts for this reaction. Etherification reaction was carried out in a microwave-irradiated tube under continuous stirring for short time periods. The authors reported a conversion of 66 % with almost total selectivity to the monoether. [166] Frusteri et al. did not improve the catalytic results of Amberlyst when using lab-made silica supported acid catalysts. [164] More recently, Ozbay et al. studied this reaction in a flow reactor at short residence time using Amberlyst, Nafion and alumina catalysts. [167] Again, the best results were achieved with an Amberlyst catalyst but with lower conversion and selectivity to h-GTBE than the studies performed in a batch reactor.

Therefore, the number and strength of Brønsted acidity and the pore size of catalysts appear as key factors for this reaction. Other important aspect to study will be the catalyts deactivation with time, which is not practically commented in the literature.

UNIVERSITAT ROVIRA I VIRGILI
REVALORIZACIÓN CATALÍTICA DE GLICERINA PARA UNA OBTENCIÓN MÁS RESPETUOSA CON EL MEDIO AMBIENTE DE ADITIVOS PARA COMBUSTIBLES
Mª Dolores González Candela
DL:T. 1715-2011

4.2.1 Establishing the role of Brønsted acidity and porosity for the catalytic etherification of glycerol with tert-butanol by modifying zeolites

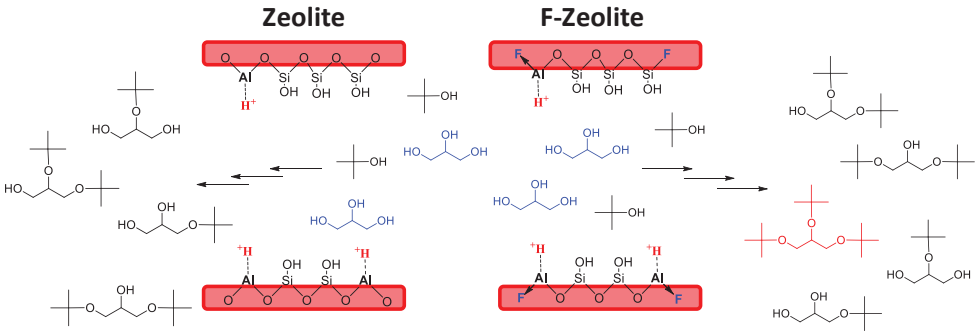

Abstract

The role of Brønsted acidity and porosity for the etherification of glycerol with tert-butanol was studied by modifying the surface and acidic characteristics of three commercial Na-zeolites (mordenite, beta and ZSM-5) by protonation, dealumination, desilication-protonation, lanthanum-exchange and fluorination. The amount and strength of Brønsted acid centres affected glycerol conversion whereas the acidity strength significantly influenced the formation of di- and specially tri-ethers of glycerol, independently of the porosity of the catalysts. However, the accessibility of the reactants to the acid sites must be guaranteed so that they can act. The introduction of fluorine in the zeolite framework generated higher amounts of stronger acid sites which yielded the best conversion and selectivity to h-GTBE results with the formation of the glycerol triether. The activity results of fluorinated beta, and fluorinated beta mixed with zeolite A were comparable to those obtained with Amberlyst-15, which is an acid catalyst traditionally used for this reaction. Additionally, fluorinated beta showed lower deactivation than Amberlyst-15.

Introduction

Glycerine (glycerol or 1,2,3-propanetriol) has over 1500 known end uses, including applications in cosmetics, pharmaceuticals and food products. [3, 168] During biodiesel manufacture, by transesterification of vegetable oils with methanol, glycerine is formed as by-product (10 weight % of the total product). [3, 11, 168] The price of glycerol is falling as fast as biodiesel plants are being built. Research is currently starting to find new outlets to convert the surplus of glycerol into high-added value products that improve the economy of the whole process. [2-3, 6, 9-10, 169]

One challenging option is the catalytic etherification of glycerol with tert-butanol or isobutene to obtain di- and tri- tertiary butyl ethers of glycerol (h-GTBE), which is an excellent additive with a large potential for diesel and biodiesel reformulation. [144-146] Thus, when h-GTBE was incorporated in standard 30-40% aromatic-containing diesel fuel, emissions of particulate matter, hydrocarbons, carbon monoxide, and unregulated aldehydes decreased significantly. [145-146] Besides, h-GTBE can replace methyl tertiary butyl ether (MTBE), which is used as valuable additive because of their antidetonant and octane-improving properties, but is detrimental to the environment.

Etherification of glycerol with isobutylene (IB) or with tertiary butanol (TBA) has been studied in the presence of acid catalysts. [5, 154-162] Etherification with isobutene yielded to better conversion and better selectivity values to h-GTBE than etherification with tert-butanol. [155, 158] The water formed when using TBA as reagent seems to have an inhibition effect on glycerol terbutylation. However, the use of tert-butanol, as both reactant and glycerol solvent, instead of gaseous isobutylene, overcomes the technological problems arising from the need to use solvents able to dissolve glycerol (i.e. dioxane, dimethyl sulfoxide) and typical drawbacks of a complex three-phase system (mass transfer phenomena). [155, 163] Also, the simpler reaction system with tert-butanol can be very useful to the systematic study of new catalytic systems.

There are few studies about the catalytic etherification of glycerol with tert-butanol. [154-155, 164, 166-167] Klepáčová et al. reported that acidic resin catalysts (Amberlyst type) exhibited higher conversion (88 %) than zeolites H-Y and H-Beta but, on the whole, low selectivity to h-GTBE (around 25 %) was achieved for this reaction, which were performed in a batch reactor at 338 K with a TBA/glycerol ratio of 4, at reaction times of 300 min. [154-155] However, triether was not detected when using these H-

zeolites. This has been attributed to steric hindrance effects because of the microporosity of the zeolites. [155] Luque et al. evaluated a new family of mesoporous carbonaceous materials, denoted as Starbon, as catalysts for this reaction. Etherification reaction was carried out in a microwave-irradiated tube under continuous stirring for short time periods. The authors reported a conversion of 66 % with almost total selectivity to the monoether. [166] Frusteri et al. did not improve the catalytic results of Amberlyst when using lab-made silica supported acid catalysts. [164] More recently, Ozbay et al. studied this reaction in a flow reactor at short residence time using Amberlyst, Nafion and alumina catalysts. [167] Again, the best results were achieved with an Amberlyst catalyst but with lower conversion and selectivity values to h-GTBE than those obtained in a batch reactor.

The aim of this work was to explore the influence of the amount, strength and accessibility of Brønsted acid sites on the conversion and selectivity to h-GTBE for the catalytic etherification of glycerol with tert-butanol by modifying the acidic and porosity characteristics of three pentasil-type zeolites by different treatment procedures: protonation, dealumination, desilication-protonation, lanthanum exchange and fluorination. Special attention was paid to study deactivation of catalysts.

Experimental

Catalysts preparation

Three commercial zeolites were modified by protonation, dealumination, desilication-protonation, lanthanum exchange and fluorination. Na-Mordenite (Zeolyst, Si/Al=6.5, CBV 10A Lot No. 1822-50), Na-Beta (Zeochem, Si/Al=10, PB Lot No. 6000186) and Na-ZSM-5 (Zeochem, Si/Al=20, PZ-2/40 Lot No. 6002827,01) were designated as M, B and Z, respectively.

Each commercial zeolite was treated with NH_4NO_3 1 M at 373 K for 1 h. Samples were washed several times with deionised water and calcined at 813 K for 5 h to obtain the corresponding H-zeolites (HM, HB and HZ). Dealuminated zeolites were prepared from commercial Na-zeolites by refluxing with HCl 6 M at 373 K for 2 h (DAM, DAB and DAZ, respectively).

Samples DSHM, DSHB and DSHZ were obtained by desilication of commercial zeolites with NaOH 0.2 M under refluxing at 338 K for 30 min. After

treatment, samples were washed until pH 7, dried, exchanged with NH_4NO_3 1 M at 373 K for 1 h and later calcined at 813 K for 5 h.

La-mordenite and La-beta were prepared by solid cation exchange adding $LaCl_3 \cdot 7H_2O$ (La/Al=0.33) to 2 g of zeolite. After treatment, samples were filtered and washed several times with deionised water. Then, modified samples were calcined at 573 K for 3 h (samples LaM and LaB).

Finally, fluorinated mordenite, beta and ZSM-5 samples were obtained by adding 3.5 mL of NH_4F 0.1 M to 1 g of commercial zeolite to have 0.3 wt % fluorine in the final sample. The slurry formed was stirred and kept at room temperature for 42 h. Lastly, samples were calcined at 723 K for 8 h (samples FHM, FHB and FHZ).

Two more beta samples were prepared combining fluorination and desilication treatments. Sample FHB was desilicated with NaOH 0.2 M by refluxing at 338 K for 30 min. Sample was filtered, washed and dried overnight to obtain sample HB(F-DS). The other sample was prepared by desilication of commercial beta with NaOH 0.2 M by refluxing at 338 K for 30 min. Then, the sample was cation exchanged with NH_4NO_3 1 M at 373 K for 1 h, and later fluorinated at the same conditions as for preparing sample FHB, resulting in the sample HB(DS-F).

One commercial Amberlyst-15 (sample A), supplied by Aldrich (39 m^2/g, pore size of 103 Å, pore volume of 0.34 cc/g) was also tested for comparison.

Catalysts characterization

Elemental analyses of the samples were obtained with a Philips PW-2400 sequential XRF analyzer with Phillips Super Q software. All measures were made in triplicate.

Structural characterization was completed by powder X-ray diffraction patterns of the samples which were obtained with a Siemens D5000 diffractometer using nickel-filtered Cu Kα radiation. Samples were dusted on double-sided sticky tape and mounted on glass microscope slides. The patterns were recorded over a range of 2θ angles from 5º to 40º and crystalline phases were identified using the Joint Committee on Powder Diffraction Standards (JCPDS) files (43-0171, 48-0074, 37-359 corresponds to mordenite, beta and ZSM-5, respectively). Crystallinity of the modified mordenites was determined by comparing the sum of the peak areas of (150), (202), (350) and (402) (22-32º 2θ) with respect to commecial Na-mordenite. Crystallinity of the modified

ZSM-5 samples was calculated using the (051) peak intensity compared with the parent zeolite sample. The integrated intensity of the signal at 2θ = 22.4º was used to evaluate the crystallinity of beta samples.

BET areas were calculated from the nitrogen adsorption isotherms at 77 K using a Micromeritics ASAP 2000 surface analyser and a value of 0.164 nm^2 for the cross-section of the nitrogen molecule. Samples were pretreated in vacuum at 573 K for 6 h. Pore size distribution of micropores and meso-macropores were determined from isotherms using the Horvath-Kawazoe method and the BJH method, respectively.

Infrared spectra were recorded on a Bruker-Equinox-55 FTIR spectrometer. The spectra were acquired by accumulating 32 scans at 4 cm^{-1} resolution in the range of 400–4000 cm^{-1}. Samples were prepared by mixing the powdered solids with pressed KBr disks in a ratio of 5:95 and dried in an oven overnight. For adsorbed pyridine FTIR studies, samples were pressed into self-supported wafers, and activated at 573 K. Pyridine was adsorbed at 298 K, and infrared spectra were acquired by accumulating 64 scans at 4 cm^{-1} resolution in the range of 400–4000 cm^{-1}.

X-ray photoelectron spectra were taken with a SPECS system equipped with an Al anode XR50 source operating at 150 W and a Phoibos 150 MCD-9 detector with pass energy of 25 eV at 0.1 eV steps at a pressure below 6 10^{-9} mbar.

The acid content of commercial and modified zeolites was measured using established procedures employing thermal desorption of cyclohexylamine. [92, 170] Samples were exposed to liquid cyclohexylamine at room temperature, after which they were kept overnight (at room temperature) and then in an oven at 353 K for 2 h. [92, 170] Cyclohexylamine desoption TGA curves were obtained using a Perkin Elmer TGA 7 microbalance equipped with a programmable temperature furnace. Each sample was heated from 323 to 973 K at heating rate of 10 K/min under nitrogen flow (25 mL/min). The weight loss associated with desorption of the base from acid sites was used to calculate the acid content in mmol of cyclohexylamine per gram of sample. [92, 170]

^{1}H NMR and ^{27}Al NMR spectra were obtained with a Varian Mercury Vx 400Mhz with a probe of 7mm CPMAS at a frequency of 400 MHz by spinning at 5kHz. The pulse duration was 2 μs and the delay time was 5s. The chemical shift reference was trimethyl silil-3 propionic acid d_4-2,2,3,3 sodium salt for ^{1}H NMR, and high purity aluminium nitrate for ^{27}Al NMR.

Catalytic Activity

Etherification experiments were performed in the liquid phase in a stainless steel stirred autoclave (150 mL) equipped with temperature controller and a pressure gauge. Stirring was fixed for all experiments at 1200 rpm to avoid external diffusion limitations. Typically, the composition of the reaction mixture was: 20 g of glycerol, glycerol/t-butanol molar ratio of 0.25, and constant catalyst loading of 5 wt.% (referred to glycerol mass). Catalysts were dried before testing. The reaction temperature used was 348 K. Some experiments were performed at 363 K, or with a glycerol/t-butanol molar ratio of 0.125. Samples were usually taken at 24 h of reaction. Samples were taken also at 1, 3, 6, 24, 48 and 96 h for catalyst FHB. The reaction products were analyzed by gas chromatography using a chromatograph model Shimadzu GC-2010 equipped with a SupraWax-280 column and a FID detector.

Glycerol conversion and selectivity to MTBG (glycerol monoethers) were determined from calibration lines obtained from commercial products. For DTBG (glycerol diethers) and TTBG (glycerol triether), which were not available commercially, we isolated them from the products of the etherification reaction by column chromatography (1:9 ethyl acetate/hexane) and identified them by ^{13}C and ^{1}H NMR for proper quantification with the assistance of the characterization data reported by Jamróz et al. [96]

Results and discussion

Catalysts characterization

H-zeolites (HM, HZ and HB) showed slightly higher Si/Al ratio than the starting Na-zeolites (Table 10). Besides, a shift to higher frequency values of the IR bands assigned to symmetric and asymmetric stretching of the T-O bond (T= Si, Al) was observed for the protonated samples (Table 10). This can be explained by some dealumination occurred because of the temperature used during calcination, as reported by other authors. [45] The increase of the strength of the T-O bond when the Al content decreases was explained by the fact that Si-O bond is shorter than the Al-O bond, and Al has lower electronegativity than Si. [123] H-zeolites maintained the zeolite structure (e.g. Fig. 61b) with similar crystallinity than the starting Na-zeolites (Table 10, e.g. Fig. 61a). In addition, protonated zeolites showed slightly higher surface areas than their corresponding commercial ones (Table 10). This can be related to the slightly increase of mesoporosity (e.g. Fig. 62b) generated in these samples due to the slight dealumination occurred. The acidity of H-zeolites was higher than for Na-zeolites (Table 10), as expected, due to the presence of H^+ compensating the negative charge of the zeolite framework. ^{1}H NMR spectra of commercial zeolites showed one peak around 4 ppm (e.g. Fig. 63a), which can be associated to free Brønsted protons. [137, 171] After protonation, this peak, related to the protons formed during the treatment, shifted to higher ppm values (Table 10, e.g. Fig. 63b), indicating stronger acidity. [136]

We observed dealumination for all the acid-treated zeolites (DAM, DAZ and DAB) since they showed higher Si/Al ratio, lower cell values, and a shift to higher frequencies of the IR bands assigned to symmetric and asymmetric stretching of the T-O bond (T= Si, Al) than their corresponding Na-zeolites (Table 10). The extent of dealumination was function of the zeolite structure. Thus, beta zeolite was easier to dealuminate than mordenite, whereas dealumination of ZSM-5 was very low. This order can be related to the flexibility of each zeolite framework, and the accessibility of the aluminium atoms depending on the pores arrangement and sizes. [45, 171] The acid and heating conditions used here did not cause drastic changes in the zeolite structures (e.g.

Table 10. Characterization of commercial and modified zeolites by XRF, XRD, N_2 physisorption, FTIR, TGA and ^{1}H NMR techniques.

Catalyst	Si/Al (XRF)	Crystallinity [a] (%)	Unit cell volume [a] (Å^3)	BET area [b] (m^2/g)	Micropore area/no micropore area ratio	IR bands (cm^{-1}) [c] ν_1	ν_2	Acidity capacity (mmol H$^+$/g)	^{1}H NMR (ppm)
M	6.5	100	2791	303	8.9	1068	629	0.10	4.6
HM	6.9	93	2790	312	7.1	1075	630	0.18	6.1
DAM	18.2	75	2747	412	5.1	1093	646	0.08	5.1
DSHM	4.7	62	2776	319	6.0	1075	636	0.15	4.4
LaM	6.5	67	2793	149	1.6	1069	627	0.16	6.4
FHM	7.0	88	2784	304	8.1	1070	628	0.11	6.5
B	10.0	100	----	573	1.8	1068	629	0.41	4.2
HB	11.0	89	----	579	1.7	1086	633	0.60	4.4
DAB	110.7	61	----	554	1.5	1091	641	0.18	4.0
DSHB	4.2	56	----	663	1.2	1078	630	0.50	3.9
LaB	10.1	44	----	384	1.5	1068	628	0.55	4.5
FHB	11.8	82	----	496	1.7	1073	629	0.46	4.7
Z	20.0	100	5209	300	2.4	1063	797	0.25	3.8
HZ	20.2	100	5186	307	2.3	1068	797	0.37	4.2
DAZ	22.3	99	5172	334	2.1	1096	797	0.21	4.5
DSHZ	14.2	97	5122	353	1.6	1073	795	0.28	3.7
FHZ	20.3	100	5154	305	1.8	1065	797	0.26	4.8

[a] Calculated from XRD patterns. [b] Calculated from N_2 physisorption results. [c]Frequencies of the main asymmetric stretch (υ_1), and the main symmetric stretch (υ_2) due to the T-O bond (T=Si, Al).

Fig. 61c), although there was some decrease in the crystallinity of mordenite and beta zeolites after acid treatment (Table 10). The crystallinity of ZSM-5 samples practically did not change as a result of their low dealumination. From nitrogen physisorption results, acid-treated mordenite and acid-treated ZSM-5 presented higher surface area and lower micropore area/non-micropore area ratios. This tendency appeared more marked for the mordenite sample. This can be attributed to the loss of aluminium in the zeolite structure, which results in higher mesoporosity, and therefore, higher surface area. However, after dealumination of beta zeolite, we observed a decrease in the BET surface area accompanied by some variations in the mesoporosity (Fig. 62c), which can be attributed to the loss of crystallinity observed after treatment, as reported by other authors. [134] Partially dealuminated samples showed lower amounts of Brønsted acidity than their starting zeolites (Table 10), as expected, due to the loss of extraframework cations as a consequence of the dealumination. ^{1}H NMR spectra of DAM and DAZ presented one broad peak at higher ppm values than that observed for M and Z,

respectively (Table 10), indicating stronger acidity. This peak could be attributed to Brønsted protons, formed during dealumination in HCl medium, that are interacting with the zeolite framework. [45, 171] For DAB, we observed one peak in the ^{1}H NMR spectrum (Fig. 63c) with a shift similar to that of commercial beta (Fig. 63a). This can be explained by the higher dealumination suffered by this sample. Therefore, there are no protons interacting with the framework since practically the zeolite framework has no negative charge.

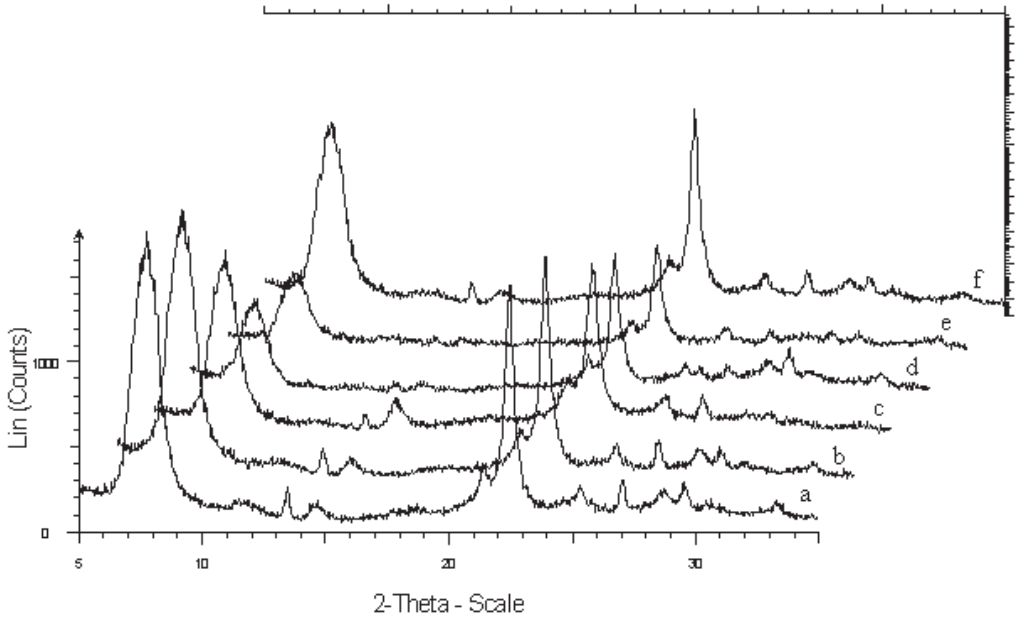

Figure 61. XRD patterns for commercial and modified beta samples: a) B, b) HB, c) DAB, d) DSHB, e) LaB, and f) FHB.

All basic-treated and later protonated samples (DSHM, DSHB, DSHZ) showed desilication since they had lower Si/Al ratios and lower cell volume values than commercial zeolites (Table 10). The frequencies of the IR bands assigned to symmetric and asymmetric stretching of the T-O bond (T= Si, Al) had similar values (Table 10) to those reported by other authors for desilicated zeolites. [172] Besides, some aluminium loss cannot be discarded due to the temperature used during calcination in the last step of protonation. Desilication was higher for beta than for ZSM-5 and mordenite. This can be related to the low stability of framework aluminium in beta compared to ZSM-5 and mordenite taking into account that lattice aluminium controls silicon extraction of the zeolite framework. [58] The zeolite structure maintained after desilication-protonation

treatment (e.g. Fig. 61d), although some decrease in the crystallinity of mordenite and beta was observed (Table 10). Desilicated-protonated samples showed higher surface area and higher mesoporosity (e.g. Fig. 62d) than their corresponding starting zeolites, as expected, due to the loss of silicon in the zeolite structure. Interestingly, acidity was slightly higher (Table 10) but less strong (Table 10, e.g. Fig. 63d) for the desilicated samples than for the commercial ones. The slight higher acidity can be explained by the second step of protonation applied to desilicated samples that led to the presence of H^+ in these modified zeolites whereas the less strength of these acid sites could be related to variations in the zeolite structure due to the treatment.

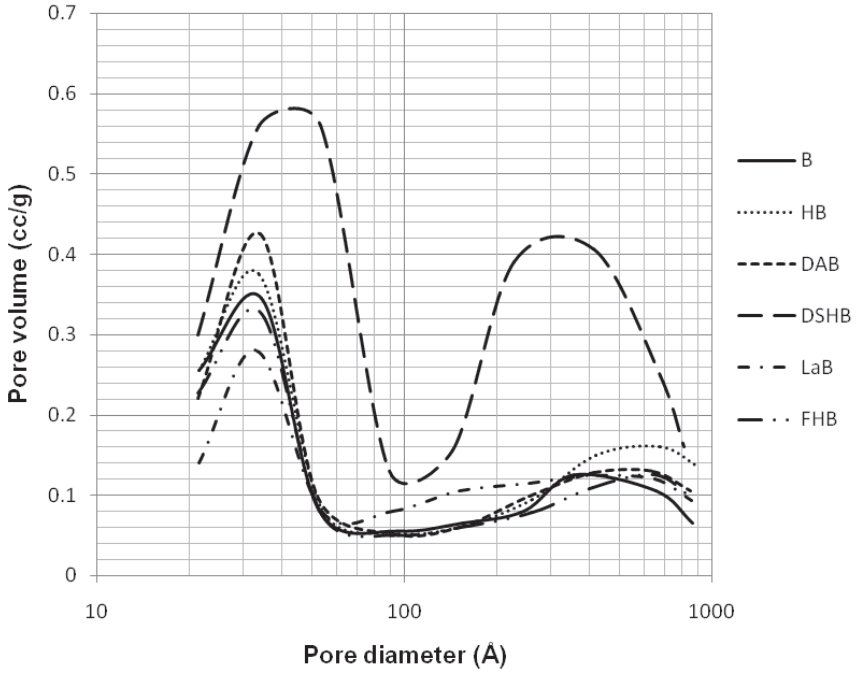

Figure 62. Mesopore size distribution graphics for commercial and modified beta samples: a) B, b) HB, c) DAB, d) DSHB, e) LaB, and f) FHB.

La-containing samples exhibited similar Si/Al ratio than their corresponding commercial zeolites (Table 10). This agrees with the similar frequencies values of the IR bands assigned to symmetric and asymmetric stretching of the T-O bond (T= Si, Al) obtained for these samples (Table 10). XRD patterns of LaB and LaM showed the maintenance of the zeolite structure (e.g. Fig. 61e) although a considerable decrease of crystallinity was observed for both samples (Table 10).

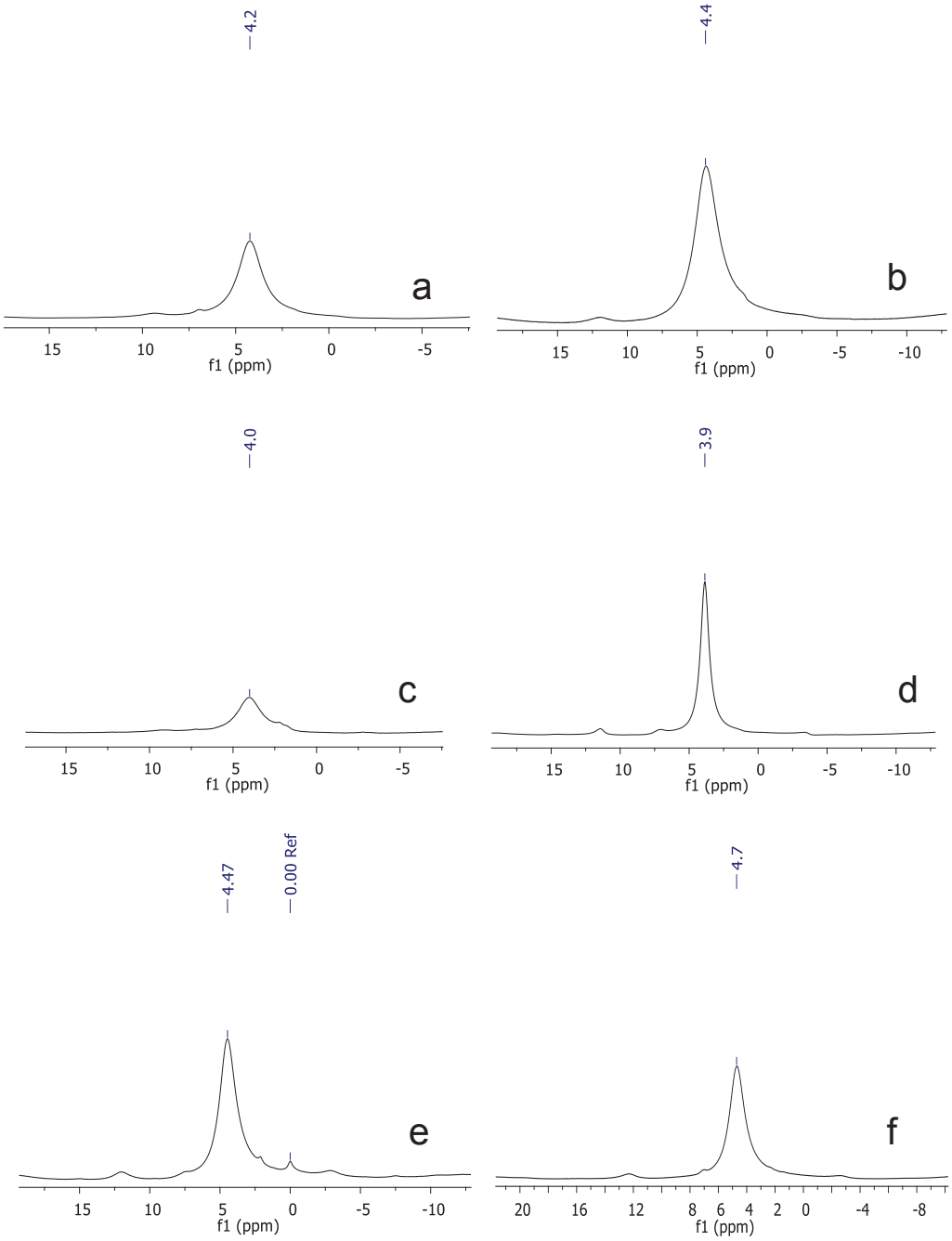

Figure 63. [1]H NMR spectra of the samples a) B, b) HB, c) DAB, d) DSHB, e) LaB, and f) FHB.

The lower surface areas accompanied by some decrease of micro- and mesoporosity (e.g. Fig. 62e) observed for La-modified samples can be attributed to the presence of bulky hydrolized lanthanum cations ($La(OH)_2^+$) blocking the pores. The introduced hydrolized lanthanum cations led to similar amount of acid sites than the corresponding H-zeolites (Table 10) but with slightly stronger Brønsted acidity (a shift to higher ppm values was observed in the ^1H NMR spectra, e.g. Fig. 63e) according to the results reported by other authors. [173-174] The lanthanum exchanged in the zeolites can cause a polarization of the zeolite framework. This increases the strength of the Brønsted acid sites. [175]

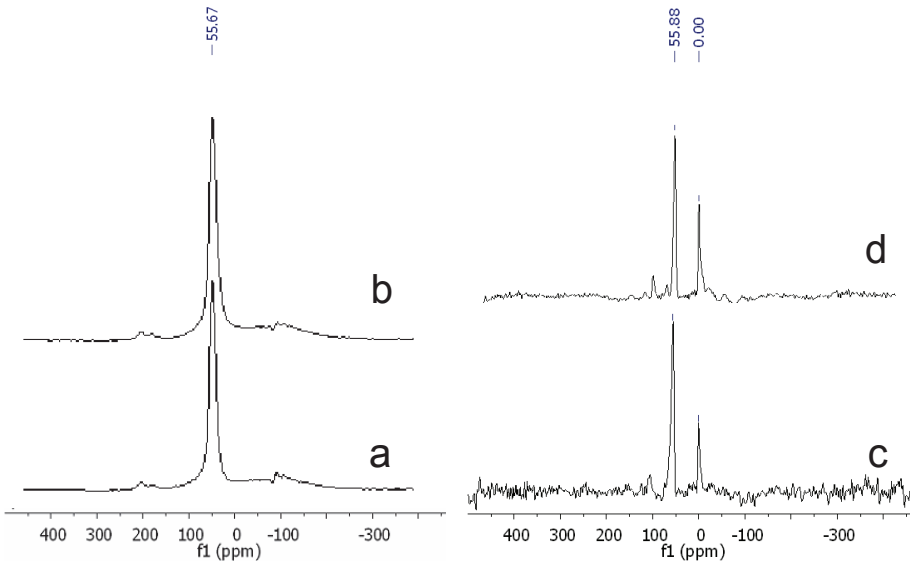

Figure 64. ^{27}Al MAS NMR for a) NaM, b) FHM, c) NaB, and d) FHB samples.

Zeolite modification by treatment with NH_4F practically did not affect the zeolite structure (e.g. Fig. 61f), except for some decrease in the crystallinity detected for FHM and FHB (Table 10). Besides, the Si/Al ratio, the position for the symmetric and asymmetric TO_4 tetrahedra bands in the mid-IR region (Table 10) and the nitrogen adsorption-desorption isotherm shapes of the fluorinated samples were very similar to those observed for the commercial ones with just some slight higher mesoporosity for the treated samples (Table 10, e.g. Fig. 63f). ^{27}Al NMR spectra of commercial zeolites showed tetrahedral Al for commercial mordenite, tetrahedral Al for commercial ZSM-5, and both tetrahedral Al and octahedral Al (in less amount) for commercial beta zeolite.

The signals corresponding to tetrahedral and octahedral aluminium appear around 50 ppm and 0 ppm, respectively. The presence of octahedral Al in commercial beta can be attributed to extraframework aluminium species or to aluminium coordinated in defect sites taking into account the characteristic stacking faults of this zeolite structure. [103, 115] ^{27}Al NMR spectra of fluorinated samples were very similar to those of the starting zeolites (e.g. Fig. 64). This confirms that fluorination at mild conditions did not cause appreciable dealumination. XPS results indicated that fluorination had no significant influence on the surface composition in terms of the Si/Al ratio. However, the O/Si ratio was found to be slightly lower for the fluorinated samples than in the parent zeolite. This confirms the incorporation of fluorine in the three zeolite structures. The F 1s XP spectra of fluorinated samples showed one peak with two components at ca. 686 and 688 eV (e.g. Fig. 65), which corresponds to fluoride species interacting with Al atoms, and with Si atoms, respectively. This is in agreement with the results reported by other authors for fluorinated zeolites. [61] Acidity capacity values of fluorinated samples were slightly higher than those of their corresponding Na-zeolites (Table 10). Besides, from ^{1}H NMR results, we observed that, after fluorination, the peak attributed to Brønsted protons, which are interacting with the zeolite framework, shifted to higher ppm values (e.g. Fig. 63f). This means that fluorinated samples had stronger Brønsted acid sites. This only can be explained by an inductive effect by F confirming the introduction of fluorine atoms in the zeolite framework.

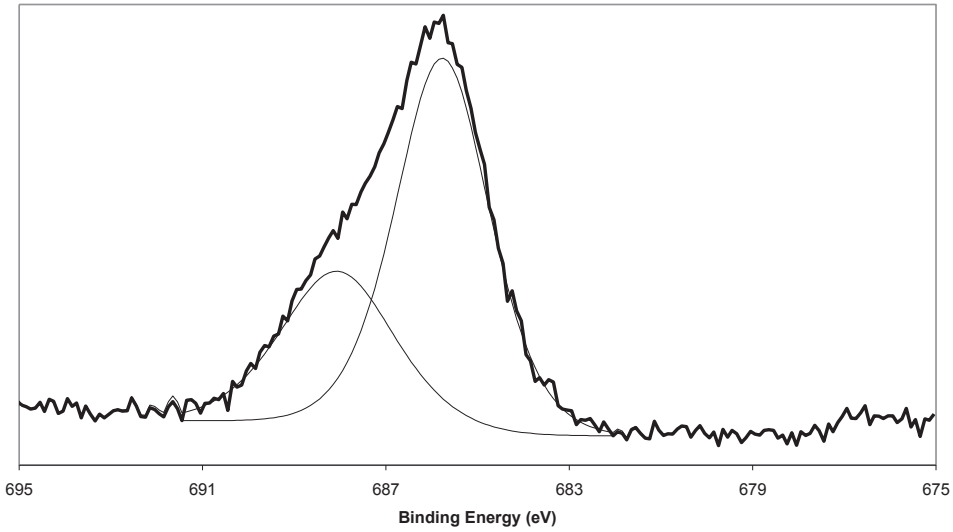

Figure 65. Deconvoluted F 1s XP spectrum of the sample FHB.

Catalytic Activity

Table 11 shows the catalytic activity results obtained for all zeolite catalysts for the etherification reaction of glycerol with tert-butanol. One acid ion-exchange resin (Amberlyst 15, here named as A), which is a typical acid catalyst used for this reaction, has been also tested at the same reaction conditions for comparison. The reaction products obtained were mono-tert-butyl glycerol ether (MTBG), di-tert-butyl glycerol ether (DTBG) and some times low amounts of tri-tert-butyl glycerol ether (TTBG). No other reaction products were detected in any case.

Table 11. Catalytic activity of Amberlyst-15, commercial and modified mordenite, beta and ZSM-5 catalysts after 24 h of reaction

Catalyst	Conversion (%)	MTBG (%)	h-GTBE (%)
A	81	64	36 (1)
M	10	77	23
HM	29	89	11
DAM	27	100	0
DSHM	8	95	5
LaM	23	100	0
FHM	32	81	9
B	63	74	26
B[a]	83	74	26
HB	66	66	34
HB[b]	71	70	30
DAB	29	100	0
DSHB	61	82	18
LaB	16	78	22
FHB	75	63	37 (1)
Z	35	100	0
HZ	58	96	4
DAZ	22	100	0
DSHZ	22	97	3
FHZ	33	92	8

[a]glycerol/t-butanol molar ratio of 0.125. [b]glycerol/t-butanol molar ratio of 0.125 and reaction temperature of 363 K.
MTBG: glycerol monoethers; h-GTBE: glycerol diethers + glycerol triether. In parenthesis, selectivity to glycerol triether (%).

Zeolite Na-beta was more active than Na-ZSM-5 and Na-mordenite in this order. The differences in the activity between the three types of zeolites could be explained by the number of Brønsted acid sites (related to the Si/Al ratio) and their strength together with the higher accessibility of the reactants to the active sites in beta and ZSM-5 samples because of their three-dimensional pore structure compared with the one-dimensional pore structure of mordenite. Thus, zeolite beta has a three-dimensional 12-ring pore system (straight channels of diameter 6.6 x 6.7 Å and sinusoidal channels of diameter 5.6 x 5.6 Å), zeolite mordenite has a one-dimensional pore system with main channels of diameter 6.7 x 7.0 Å and compressed channels of diameter 2.6 x 5.7 Å whereas ZSM-5 has a three-dimensional 10-ring pore system with channels of diameter 5.1 x 5.5 Å. Regarding selectivity results, the three Na-zeolites led to lower amounts of high-glycerol tert-butyl ethers (h-GTBE) than Amberlyst-15 (catalyst A). When NaB was tested at lower glycerol/t-butanol ratio, conversion increased and was comparable to that of Amberlyst 15 but the products selectivity values did not change (Table 11).

H-zeolites showed higher conversion than Na-zeolites, as expected, taking into account the higher amount and strength of their Brønsted acid sites (Table 10). H-Beta and H-ZSM-5 gave higher amounts of h-GTBE than Na-Beta and Na-ZSM-5, respectively, whereas H-mordenite yielded lower amounts of h-GTBE than Na-mordenite. This can be explained by the lower accessibility of the reactants to the acid sites in the mordenite channels, due to its lower dimensionality, as commented on above. When HB catalyst was tested at higher reaction temperature (363 K) and lower glycerol/t-butanol ratio, conversion increased but again the selectivity to h-GTBE did not improve (Table 11). One important feature to note is that triether was not detected for any Na-zeolite or H-zeolite. This has been attributed by other authors to steric hindrance effects because of the microporosity of the zeolites. [155]

Partially dealuminated zeolites showed lower conversion than their corresponding Na- and H-zeolites, except for dealuminated mordenite, and null selectivity to h-GTBE (Table 11). This can be related to the low amount of Brønsted acid sites observed for these samples due to dealumination (Table 10). This reveals the importance of acidity for this reaction since the additional mesoporosity generated during dealumination was not enough to favour the formation of the high-glycerol tert-butyl ethers (di- and triether). In the case of the mordenite, the higher conversion of DAM with respect to initial M can be related to the low Si/Al of the starting commercial mordenite (Si/Al = 6.5), since the loss of aluminium in these less siliceous zeolites

decreased the number of acid sites but they became stronger [136], as confirmed by ^{1}H NMR (Table 10).

Desilicated-protonated zeolites also showed lower conversion and lower selectivity to h-GTBE than the previously discussed catalysts (Table 11). This was surprising since these catalysts had slight higher acidity and higher mesoporosity to avoid possible steric hindrance than Na-zeolites (Table 10). These results can be explained by the lower strength of the Brønsted acid sites of desilicated samples, as observed from ^{1}H NMR (Table 10). Therefore, the acid strength of the catalytic sites influences significantly the catalytic performance, both conversion and selectivity to h-GTBE.

The incorporation of lanthanum in mordenite and beta zeolites reduced considerably the conversion and did not improve the selectivity values, especially for LaM where total selectivity to the glycerol monoethers was obtained (Table 11). The presence of bulky hydrolized lanthanum cations ($La(OH)_2^+$) blocking the pores increased steric hindrances despite the higher strength of the Brønsted acid sites of these catalysts (Table 10). Thus, the accessibility of the reagents to the catalytic sites strongly affects the catalytic results.

Finally, fluorination of zeolites at mild conditions resulted in catalysts, which yielded the best conversion values in all cases, due to the higher amounts of the strongest Brønsted acid sites generated because of the incorporation of fluorine in the zeolite framework. Regarding selectivity values, FHB and FHZ led to higher amounts of h-GTBE than the other catalysts prepared with the same zeolite whereas FHM did not improve the best selectivity results, probably because of the lower accessibility of the reactants to the acid sites in the mordenite channels, due to its lower dimensionality. Interestingly, FHB allowed us to detect the presence of tri-tert-butyl glycerol ether (TTBG) in low amounts. This is the first time that the formation of glycerol triether in a zeolite, for the glycerol etherification with tert-butanol, has been reported. Taking into account that this catalyst has similar porosity than NaB or HB (Table 10, Fig. 62), we can conclude that the modification of the acidity of the zeolite through the introduction of low amounts of fluorine in the zeolite structure is more important than porosity to favour the production of the bulky triether. In addition, catalytic activity of this catalyst was comparable to that obtained with Amberlyst-15 (Table 11).

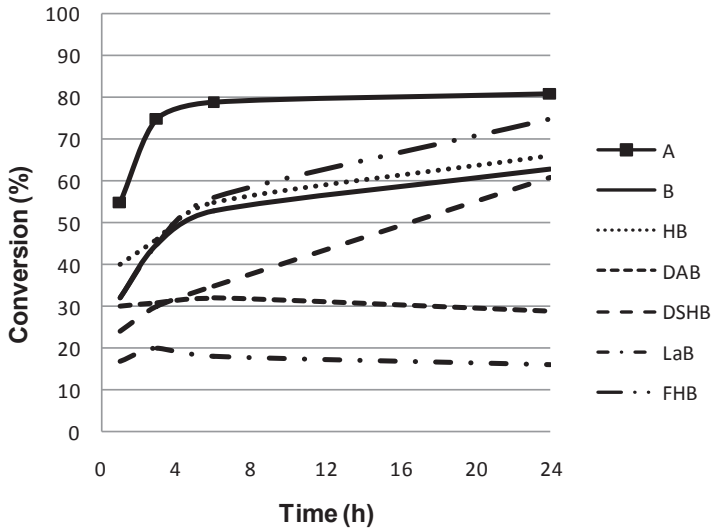

Figure 66. Deactivation studies of beta catalysts

Fig. 66 shows the catalytic deactivation studies performed for beta-zeolite catalysts and for catalyst A. Deactivation was accompanied by a decrease of the surface areas (Table 12) and a considerably decrease of Brønsted acid sites (e.g. Fig. 67). However, XRD did not show significant changes in the zeolite structure after reaction in any case except for some decrease in the crystallinity (e.g. Fig. 68). From these results, we can conclude that there is no collapse of the structure during reaction, but blocking of pores by reaction products. Interestingly, we clearly observed that NaB, HB, DSHB and FHB deactivated much less than the acid ion-exchange resin. This can be explained because of the nature of the zeolite, which can partially adsorb the water formed during reaction in contrast with Amberlyst, which was strongly affected by the presence of water, as reported by other authors. [164] The profile of DSHB was quite different than those of NaB, HB and FHB catalysts since the increase in the conversion with time was more gradual (Fig. 66). This can be related to the higher mesoporosity of this catalyst, which led to higher accessibility to the acid centres although their lower strength required longer time to act. In contrast, beta-zeolite modified by dealumination or La-exchange exhibited total deactivation after 1 h of reaction. This can be explained by the lower amount of acid centres of catalyst DAB, and because of the effect of bulky $La(OH)_2^+$ cations blocking the pores for LaB.

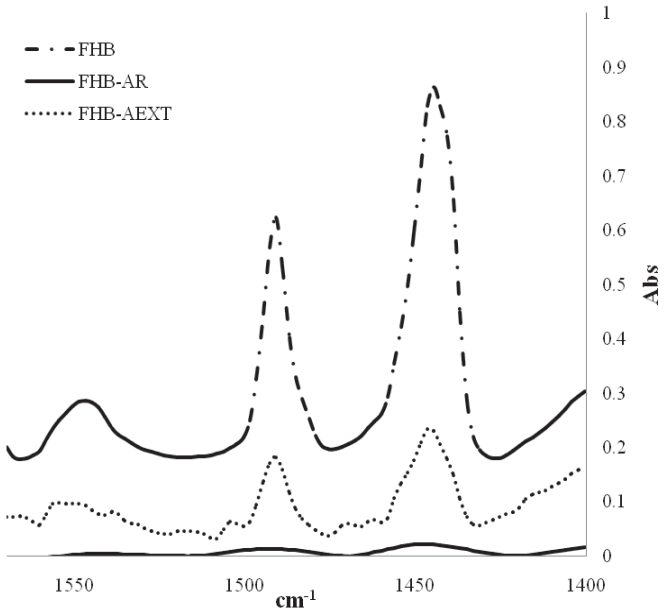

Figure 67. FTIR spectra of adsorbed pyridine for FHB, FHB-AR (after reaction) and FHB-AEXT (after extraction) B: Brønsted acid sites; L: Lewis acid sites.

In order to evaluate the nature of the products remaining in the catalytic pores after reaction, several used catalysts, after filtration, were submitted to extraction by refluxing with 50 mL of ethanol for 1 h. After rotary evaporation of the solvent, the resulting solution was analyzed by gas chromatography. All chromatograms showed the presence of several peaks corresponding to glycerol and products of reaction (monotethers and diethers in less proportion). Interestingly, surface areas and the amount of Brønsted acid sites of the catalysts were partially recovered after extraction (Table 12, e.g. Fig. 67). All these results explain the deactivation process since the presence of reagents and reaction products in the pores decreases the accessibility of the reagents to the acid sites.

Table 12. Characterization of several beta-zeolite catalysts before reaction, after reaction, and after extraction.

Catalyst	BET area before reaction (m^2/g)	BET area after reaction (m^2/g)	BET area after extraction (m^2/g)
B	573	361	457
HB	579	364	429
DAB	554	99	387
DSHB	663	124	498
LaB	384	45	276
FHB	496	334	164

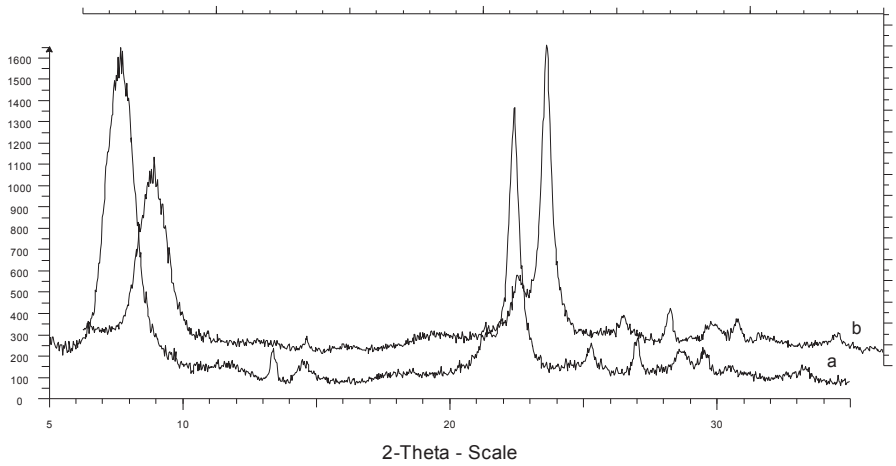

Figure 68. XRD patterns of catalyst FHB: a) before reaction, and b) after reaction.

Fig. 69 shows the variation of conversion and selectivity towards the three types of glycerol ethers with the reaction time for catalyst FHB. The most important feature to note is that, after 24 h of reaction, conversion values made a plateau, as mentioned above, but selectivity to the glycerol ethers vary in an interesting way since at reaction times > 24 h, we observed a gradual slight increase of the selectivity to the triether, which was more clearly visualized regarding the intensity of the chromatogram peak corresponding to this compound. This means that when glycerol conversion stopped the tert-butanol molecules remaining in the reaction medium react with monoethers and diethers formed previously evolving with time to higher selectivity to the triether.

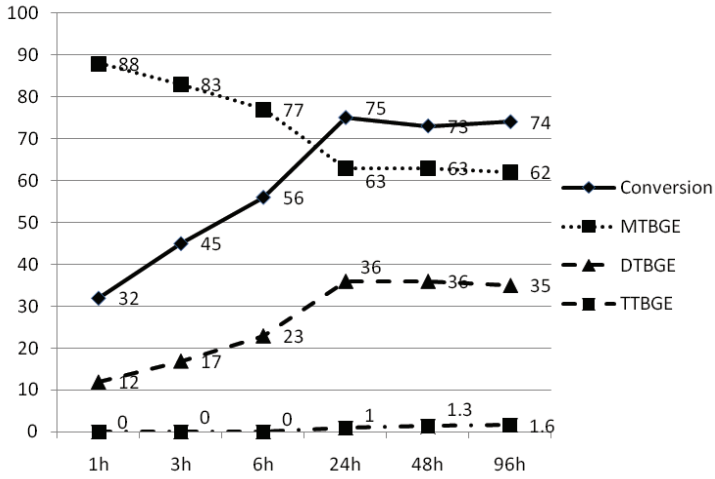

Figure 69. Evolution of conversion and selectivity to the three-glycerol ethers with time for catalyst FHB.

From all these results, we tried to improve the selectivity towards the triether detected with FHB. Thus, four new fluorinated beta catalysts were synthesized at different conditions and tested for this reaction. Two samples were prepared by the same method as FHB but increasing the theoretical fluorine content to obtain 1%wt F (FHB(1%)) and 10 %wt F (FHB(10 %)), with the idea to increase the number of stronger acid sites. The other two samples were synthesized by combining desilication and fluorination procedures (HB(DS-F) and HB(F-DS)), as described in the experimental section, with the aim to increase acidity and mesoporosity at the same time. The catalytic results of these four new catalysts are shown in Table 13.

As we can observe, the increase in the percentage of theoretical fluorine did not improve the catalytic results obtained for sample FHB. This suggests that not all the theoretical fluorine was introduced in the zeolite structure and some framework dealumination occurred for both samples (especially for FHB(10%)). Dealumination was confirmed by the decrease of the cell volumes, the gradual increase of octahedral aluminium observed by ^{27}Al NMR, the higher mesoporosity and the shift to higher frequencies of the IR bands, assigned to symmetric and asymmetric stretching of the T-O bond (T= Si, Al) of these two samples when comparing with the starting zeolite. Therefore, fluorination treatment with higher amounts of fluorine did not increase

significantly the introduction of fluorine in the structure, and for this reason, the catalytic results of these catalysts were very similar to those of FHB.

Table 13. Catalytic activity results of several fluorinated beta catalysts for the glycerol etherification with tert-butanol after 24 h of reaction.

Catalyst	Conversion (%)	MTBG (%)	h-GTBE (%)
FHB(1 %)	72	64	36 (1)
FHB(10 %)	70	66	34 (1)
HB(DS-F)	51	90	10 (< 1)
HB(F-DS)	74	70	30 (1)

MTBG: glycerol monoethers; h-GTBE: glycerol diethers + glycerol triether. In parenthesis, selectivity to glycerol triether (%).

Si/Al ratios, determined by XRF, were 4.0 and 4.1 for HB(DS-F) and HB(F-DS), respectively, confirming desilication. The sample first desilicated and later fluorinated had less % wt fluorine (0.1) than the sample first fluorinated and later desilicated (0.25) as determined by chemical analysis. This explains the catalytic results obtained since catalyst HB(DS-F) showed lower conversion and lower selectivity to h-GTBE whereas catalyst HB(F-DS) had similar conversion and slight lower selectivity to h-GTBE than FHB (Table 11). Interestingly, low amounts of tri-tert-butyl glycerol ether (TTBG) were detected for all four catalysts. This confirms the influence of the introduction of fluorine in the zeolite structure on the acidity, and therefore, the significant effect of the stronger Brønsted acidity, generated by fluorination, on the formation of the triether, independently of the porosity.

As commented above, one of the problems of this reaction is that the formation of water during reaction inhibits the glycerol etherification since water competes with tert-butanol and glycerol on the active site adsorption. [164] The higher water acidity in relation to tert-butanol results in a lowering of catalyst activity due to the formation of solvated sites, as reported in the literature. [176-177] Frusteri et al. proposed that the removal of water from the reaction medium could increase the formation of high glycerol ethers. [164] These authors performed one experiment by stopping the etherification reaction after 6 h, dehydrated the reaction mixture by zeolites, and then continued with the reaction for 6 more hours. The results showed an important increase in the formation of diethers. [164] From this idea, we designed one similar catalytic

experiment using a mixture of sample FHB and commercial zeolite 4A (Sigma-Aldrich) in a weight ratio of 1/1 as catalyst. Zeolite A was inactive for this reaction.

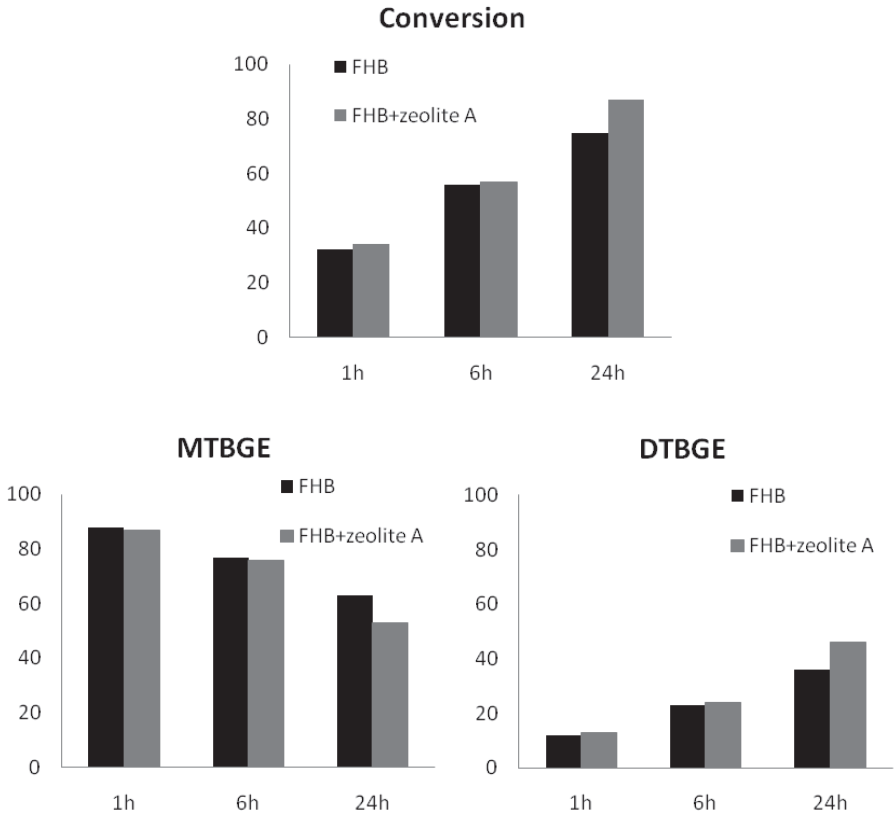

Figure 70. Comparison of conversion and selectivity to the three-glycerol ethers with the reaction time for catalysts FHB and FHB mixed with zeolite A.

Fig. 70 shows the comparative evolution with time of conversion and selectivity towards the three-glycerol ethers for catalyst FHB and the mixture FHB/zeolite A. After 1 h of reaction, the catalytic results were just slightly better for the catalyst mixed with the molecular sieve. This improvement in the conversion and selectivity to h-GTBE were more marked at higher reaction times. This confirms that the presence of zeolite A in the medium helped to adsorb the water generated during the etherification reaction allowing a better approach of the reagent molecules to the Brønsted acid sites of catalyst FHB, and therefore favouring the formation of high ethers. We also observed a higher

slight increase of the triether amount with time for the catalyst mixed with zeolite A (not shown here).

Therefore, the activity behaviour of catalyst FHB and FHB mixed with zeolite A were comparable to that of Amberlyst-15. Additionally, FHB showed lower deactivation than Amberlyst-15. Taking into account that the glycerol etherification with isobutene led to higher selectivity values to h-GTBE, these results are promising for using zeolytic materials for the production of these fuel additives.

Conclusions

Beta catalysts were more active than ZSM-5 and mordenite catalysts. This could be related to the number of Brønsted acid sites (related to the Si/Al ratio) and their strength together with the higher accessibility of the reactants to the active sites in beta and ZSM-5 samples because of their three-dimensional pore structure compared with the one-dimensional pore structure of mordenite.

Protonation of zeolites led to higher conversion and, on the whole, higher selectivity to h-GTBE due to their higher amounts of stronger Brønsted acid centres. Partially dealuminated zeolites had worse catalytic results due to their low amount of Brønsted acid sites whereas desilicated-protonated zeolites also showed lower conversion and lower selectivity to h-GTBE than Na-zeolites despite their slightly higher acidity and higher mesoporosity. This can be explained by the lower strength of the Brønsted acid sites of these catalysts.

The incorporation of lanthanum into mordenite and beta zeolites reduced considerably conversion and did not improve selectivity values because of the presence of bulky hydrolized lanthanum cations blocking the pores, which increased steric hindrances despite the higher strength of the Brønsted acid sites of these catalysts.

Finally, zeolites fluorinated at mild conditions resulted in catalysts, which yielded the best conversion and selectivity to h-GTBE (37 % for a conversion of 75 % with the formation of the triether) due to the higher amounts of stronger acid sites generated because of the incorporation of fluorine in the zeolite framework. This result was improved by mixing this catalyst with zeolite A, which adsorbed water from the reaction medium, and was comparable to the catalytic activity of Amberlyst-15. Additionally, fluorinated beta showed lower deactivation than Amberlyst-15.

From all these results, we can establish that the amount and strength of Brønsted acid sites affects conversion whereas the acidity strength significantly influences the formation of di- and tri-ethers of glycerol, independently of the porosity of the catalyst. However, the accessibility of the reactants to the acid sites must be guaranteed so that they can act.

Acknowledgments

The authors are grateful for the financial support of the Ministerio de Ciencia e Innovación and FEDER funds (CTQ2008-04433/PPQ). Dolores González acknowledges Ministerio de Educación y Ciencia for a FPU grant (AP2007-03789).

4.2.2 Effect of hierarchical porosity in zeolites on the catalytic etherification of glycerol

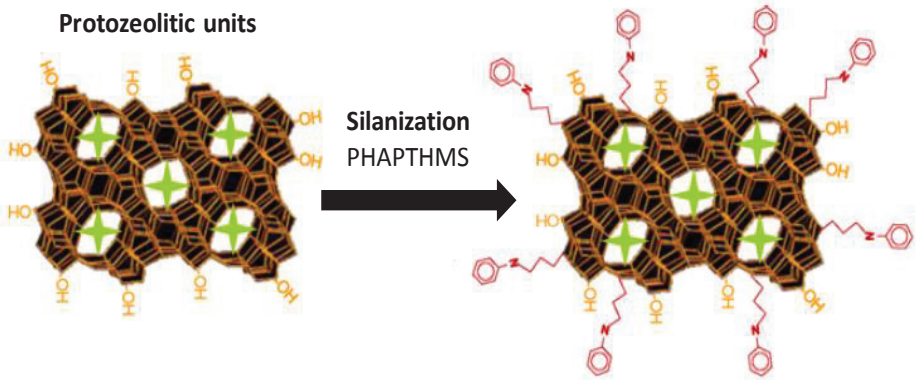

Abstract

The effect of hierarchical porosity in zeolites on the catalytic etherification of glycerol with tert-butanol or isobutene has been studied by comparing the catalytic behaviour of two conventional beta zeolites, with different Si/Al ratio, with one beta zeolite with hierarchical porosity. Besides, the three samples were fluorinated at mild conditions to modify their acidity. The higher selectivity to the bulkier glycerol triether obtained for the H-Beta with hierarchical porosity and its fluorinated form for both reactions only can be explained because of their additional porosity, which favor the diffusion of the reactants to the Brønsted acid sites, since these catalysts showed lower acidity amount and strength than a conventional H-Beta with lower Si/Al ratio. Fluorination of beta samples led to slight higher selectivity to h-GTBE (di- and triethers of glycerol). This has been related to their slightly stronger acidity achieved by the inductive effect of the fluorine introduced in the zeolite framework.

Introduction

Glycerine (glycerol or 1,2,3-propanetriol) has over 1500 known end uses, including applications in cosmetics, pharmaceuticals and food products. [3, 168] During biodiesel manufacture, by transesterification of vegetable oils with methanol, glycerine is formed as by-product (10 weight % of the total product). [3, 11, 168] The price of glycerol is falling as fast as biodiesel plants are being built. Research is currently starting to find new outlets to convert the surplus of glycerol into high-added value products that improve the economy of the whole process. [2-3, 6, 9-10, 169]

One challenging option is the catalytic etherification of glycerol with tert-butanol or isobutene to obtain di- and tri- tertiary butyl ethers of glycerol (h-GTBE), which is an excellent additive with a large potential for diesel and biodiesel reformulation. [144-146] Besides, h-GTBE can replace the highly toxic to the environment methyl tertiary butyl ether (MTBE).

Etherification of glycerol with isobutylene (IB) or with tertiary butanol (TBA) has been studied in the presence of acid catalysts. [5, 154-164, 166-167] Etherification with isobutene yielded to better conversion and better selectivity values to h-GTBE than etherification with tert-butanol. [155, 158] The water formed when using TBA as a reagent seems to have an inhibition effect on glycerol terbutylation. Regarding heterogeneous catalysis, the best activity results were achieved with acid ion-exchange resins of Amberlyst type (Amberlyst 15 and 35) [154-157] and with silicas functionalized with organosulfonic groups. [5, 158] In the first studies performed with zeolites as catalysts for this reaction, Klepáčová et al. concluded that the formation of the triether was sterically hindered in H-Beta and H-Y zeolites due to their microporosity. [156]

Beta is a large pore zeolite with a three-dimensional 12-ring pore system (straight channels of diameter 6.6 x 6.7 Å and sinusoidal channels of diameter 5.6 x 5.6 Å). In the last years, several works have been focused on the synthesis of either beta zeolite having crystals in the nanometer range (nanocrystalline zeolite beta) or beta zeolite with an additional porosity (hierarchical zeolites). [178-179] Mesopore-containing zeolites have been prepared by direct synthesis, different post-synthesis treatments, and novel dual templating methods. [65]

One recent method for the synthesis of hierarchical zeolites is based on hindering the growth of the zeolitic crystals by organo-functionalization of the zeolitic seeds in order to prevent their further aggregation and agglomeration. [68-69] This method

consists of the following steps: (i) precrystallization of the zeolite synthesis gel to form zeolite nuclei, (ii) functionalization of the zeolite seeds by reaction with organosilanes, which form a protective organic barrier against aggregation, (iii) crystallization to complete the zeolitization of the functionalised seeds. Depending on the zeolite structure, the crystallization conditions and the seed silanization agent (SSA), the product finally obtained applying this new strategy may consist of ultra-small zeolite nanocrystals or may be formed by crystallites having and additional porosity in the supermicro-mesopore regions generated by the silanization agents. These kinds of materials possess improved textural properties regarding to the standard zeolite, which may affect positively to their performance as catalysts in reactions involving bulky molecules. [69-70]

The aim of this work was to study the effect of hierarchical porosity by comparing the catalytic behaviour of one commercial Na-beta zeolite (Si/Al = 10), and their protonated form with one synthesized H-Beta (Si/Al = 27) and one H-beta zeolite with hierarchical porosity (Si/Al = 27), prepared from organofunctionalized seeds, for the etherification of glycerine with tert-butanol or isobutene. Additionally, these three zeolites were fluorinated to modify their acidity and observe the effect of fluoridation on the catalytic activity.

Experimental

Catalysts preparation

One commercial Na-beta (Zeochem, Si/Al=10, PB Lot No. 6000186), designated as Na-Beta-10, was treated with NH_4NO_3 1 M at 373 K for 1 h and later calcined at 813 K for 5 h to obtain H-Beta-10. Fluorinated beta was obtained by adding 3.5 mL of NH_4F 0.1 M to 1 g of commercial zeolite to have 0.3 wt % fluorine in the final sample. The slurry formed was stirred and kept at room temperature for 42 h. Finally, the sample was calcined at 723 K for 8 h (FH-Beta-10).

Zeolite beta with hierarchical porosity was prepared from a solution with the following molar composition: Al_2O_3: 60 SiO_2: 15.5 TEAOH: 1000 H_2O. Fumed silica (Fluka), tetraethylammonium hydroxide (TEAOH, 35 %; Alfa), aluminium flakes (Aldrich) and distilled water were used as starting materials. The precursor solution was precrystallized in a teflon-lined stainless steel autoclave under autogenous pressure at 408 K for 3 days. The solid formed was mixed with an aqueous solution containing the

phenylaminopropyltrimethoxysilane (PHAPTMS, 97 wt %, Aldrich) and TEAOH (13 % w/w) (TEAOH/SiO_2 = 0.5). The resulting mixture was kept in a reflux system under stirring (100 rpm) at 363 K for 6 h. Thereafter, the crystallization of the functionalized seeds was carried out in a stainless steel reactor under autogeneous pressure at 443 K for 7 days. The solid obtained was separated by centrifugation, washed several times with distilled water, dried overnight at 383 K and calcined in air at 823 K for 5 h (H-Beta-hierarchical). H-Beta hierarchical was fluorinated by adding 3.5 mL of NH_4F 0.1 M to 1 g of the synthesized beta with hierarchical porosity to have 0.3 wt % fluorine in the final sample. The slurry formed was stirred and kept at room temperature for 42 h. Finally, the sample was calcined at 723 K for 8 h (FH-Beta-hierarchical).

Lastly, one H-Beta zeolite (Si/Al = 27) was synthesized following the same procedure as for preparing H-Beta-hierarchical but omitting the precrystallization and silanization steps (H-Beta-27). H-Beta-27 was fluorinated by adding 3.5 mL of NH_4F 0.1 M to 1 g of the synthesized beta with hierarchical porosity to have 0.3 wt % fluorine in the final sample. The slurry formed was stirred and kept at room temperature for 42 h. Finally, the sample was calcined at 723 K for 8 h (FH-Beta-27).

One commercial Amberlyst-15 (sample A), supplied by Aldrich (39 m^2/g, pore size of 103 Å, pore volume of 0.34 cc/g) was also tested for comparison.

Catalysts characterization

Elemental analyses of the samples were obtained with a Philips PW-2400 sequential XRF analyzer with Phillips Super Q software. All measures were made in triplicate.

Structural characterization was completed by powder X-ray diffraction patterns of the samples which were obtained with a Siemens D5000 diffractometer using nickel-filtered Cu Kα radiation. Samples were dusted on double-sided sticky tape and mounted on glass microscope slides. The patterns were recorded over a range of 2θ angles from 5º to 40º and crystalline phases were identified using the Joint Committee on Powder Diffraction Standards (JCPDS) files (48-0074 corresponds to beta). The integrated intensity of the signal at 2θ = 22.4º was used to evaluate the crystallinity of beta samples.

BET areas were calculated from the nitrogen adsorption isotherms at 77 K using a Micromeritics ASAP 2000 surface analyser and a value of 0.164 nm^2 for the cross-

section of the nitrogen molecule. Samples were pretreated in vacuum at 573 K for 6 h. Pore size distribution of micropores and meso-macropores were determined from isotherms using the Horvath-Kawazoe method and the BJH method, respectively.

Infrared spectra were recorded on a Bruker-Equinox-55 FTIR spectrometer. The spectra were acquired by accumulating 32 scans at 4 cm^{-1} resolution in the range of 400–4000 cm^{-1}. Samples were prepared by mixing the powdered solids with pressed KBr disks in a ratio of 5:95 and dried in an oven overnight.

The acid content of the samples was measured using established procedures employing thermal desorption of cyclohexylamine. [92, 170] Samples were exposed to liquid cyclohexylamine at room temperature, after which they were kept overnight (at room temperature) and then in an oven at 353 K for 2 h. Cyclohexylamine desoption TGA curves were obtained using a Perkin Elmer TGA 7 microbalance equipped with a programmable temperature furnace. Each sample was heated from 323 to 973 K at heating rate of 10 K/min under nitrogen flow (25 mL/min). The weight loss associated with desorption of the base from acid sites was used to calculate the acid content in mmol of cyclohexylamine per gram of sample. [92, 170]

^{1}H NMR and ^{27}Al NMR spectra were obtained with a Varian Mercury Vx 400 Mhz with a probe of 7mm CPMAS at a frequency of 400 MHz by spinning at 5kHz. The pulse duration was 2 μs and the delay time was 5s. The chemical shift reference was trimethyl silil-3 propionic acid d_4-2,2,3,3 sodium salt for ^{1}H NMR, and high purity aluminium nitrate for ^{27}Al NMR.

Catalytic Activity

Etherification experiments were performed in a stainless steel stirred autoclave (150 mL) equipped with temperature controller and a pressure gauge. Stirring was fixed for all experiments at 1200 rpm to avoid external diffusion limitations. For the etherification of glycerol with tert-butanol, the composition of the reaction mixture was: 20 g of glycerol, glycerol/t-butanol molar ratio of 0.25, and constant catalyst loading of 5 wt.% (referred to glycerol mass). Catalysts were dried before testing. The reaction temperature used was 348 K. Samples were taken at 24 h of reaction.

For the therification of glycerol with isobutene (glycerol/isobutene molar ratio = ¼) Liquid phase pressurized isobutylene was injected into the reactor, previously charged with glycerol and catalyst (0.5 g), at the beginning of the reaction using

nitrogen at 8 bar as pushing agent. The temperature was then raised to 348 K and the pressure increased accordingly following the liquid-vapor equilibrium. Catalytic experiments were made at 24 h.

The reaction products were analyzed by gas chromatography using a chromatograph model Shimadzu GC-2010 equipped with a SupraWax-280 column and a FID detector.

Glycerol conversion and selectivity to MTBG (glycerol monoethers) were determined from calibration lines obtained from commercial products. For DTBG (glycerol diethers) and TTBG (glycerol triether), which were not available commercially, we isolated them from the products of the etherification reaction by column chromatography (1:9 Ethyl Acetate/Hexane) and identified them by ^{13}C and ^{1}H NMR for proper quantification with the assistance of the characterization data reported by Jamróz et al. [96]

Results and discussion

Catalysts characterization

XRD patterns of Na-Beta-10, H-Beta-10, H-Beta-27 and H-Beta-hierarchical are shown in Fig. 71. The four samples exhibited well-defined peaks corresponding to the Beta zeolite crystalline phase. Besides, XRD peaks of the sample with hierarchical porosity, prepared from silanized seeds, were less intense than those observed in the reference zeolite, H-Beta-27. This suggests the existence of either smaller crystals or a higher number of defects in the sample H-Beta-hierarchical.

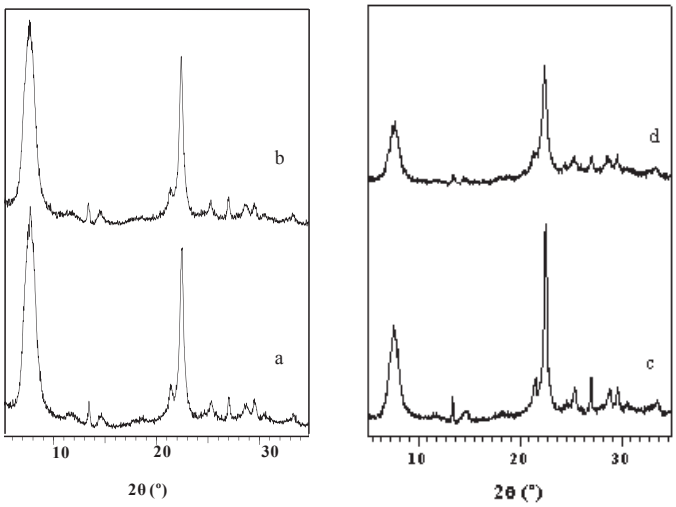

Figure 71. XRD patterns of the samples a) Na-Beta-10, b) H-Beta-10, c) H-Beta-27 and d) H-Beta-hierarchical.

The modification of Na-Beta-10 by protonation practically did not affect the zeolite structure except for some decrease in the crystallinity (Fig. 71, Table 14). H-Beta-10 showed slightly higher Si/Al ratio than commercial beta zeolite. Regarding IR results, a shift to higher frequency values of the IR bands assigned to symmetric and asymmetric stretching of the T-O bond (T= Si, Al) was observed for H-Beta-10 with respect to Na-Beta-10 (Table 14). This can be explained because some dealumination occurred at the temperature used during calcination, as reported by other authors. [45] The increase of the strength of the T-O bond when the Al content decreases was explained by the fact that Si-O bond is shorter than the Al-O bond, and Al has lower electronegativity than Si. [123]

Table 14. Characterization of commercial and modified zeolites by XRF, XRD, N_2 physisorption, FTIR, TGA and ^{1}H NMR techniques.

Catalyst	Si/Al (XRF)	Crystallinity [a] (%)	S_{BET} [b] (m^2/g)	V_{micro} (cc/g)	S_{EXT} (m^2/g)	IR bands (cm^{-1})[c]		Acidity capacity (mmol H^+/g)	^{1}H NMR (ppm)
						ν_1	ν_2		
Na-Beta-10	10.0	100	584	0.19	122	1068	629	0.41	4.2
H-Beta-10	11.0	89	608	0.17	175	1081	633	0.60	4.4
FH-Beta-10	10.6	82	496	0.15	120	1073	629	0.46	4.7
H-Beta-27	26.4	100	568	0.14	206	1096	621	0.34	4.0
FH-Beta-27	26.8	86	431	0.10	186	1097	621	0.30	4.1
H-Beta-hierarchical	27.5	100	750	0.18	301	1093	621	0.32	4.0
FH-Beta-hierarchical	27.7	68	503	0.12	215	1094	620	0.31	4.2

[a] Calculated from XRD patterns. [b] Calculated from N_2 physisorption results. [c]Frequencies of the main asymmetric stretch (υ_1), and the main symmetric stretch (υ_2) due to the T-O bond (T=Si, Al).

^{27}Al NMR spectra of commercial beta (Na-Beta-10) showed both tetrahedral Al and octahedral Al (in less amount) (Fig. 72a). The signals corresponding to tetrahedral and octahedral aluminum appear around 50 ppm and 0 ppm, respectively. The presence of octahedral Al in commercial beta can be attributed to extraframework aluminium species or to aluminium coordinated in defect sites taking into account the characteristic stacking faults of this zeolite structure. [103, 115] ^{27}Al NMR spectrum of the protonated sample (H-Beta-10) confirmed slight dealumination of this sample, according to IR results, since an increase in the octahedral Al due to the presence of Al-extraframework was observed (Fig. 72b).

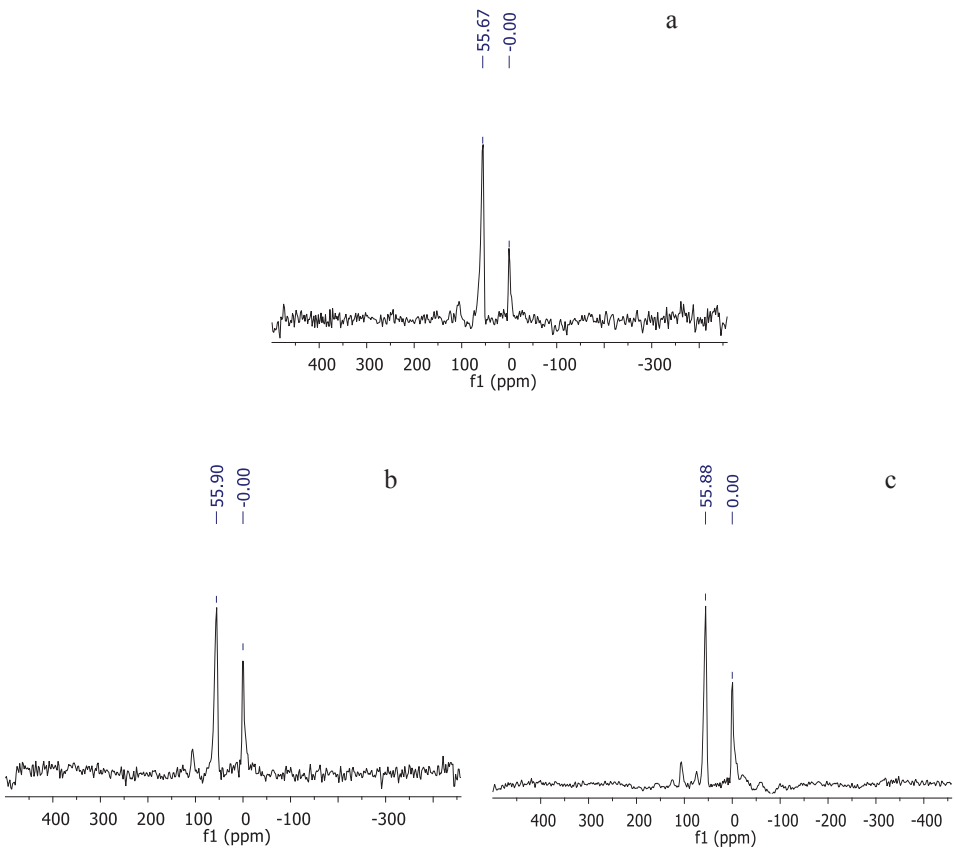

Figure 72. ^{27}Al MAS NMR spectra of a) Na-Beta-10, b) H-Beta-10 and c) FH-Beta-10 samples.

Fig. 73 showed the ^{27}Al NMR spectra of H-Beta-27 and H-Beta-hierarchical. As we can see, the sample with hierarchical porosity had slightly higher content of octahedral Al than its reference. Therefore, Al was incorporated into the zeolite framework in a similar extension for both samples.

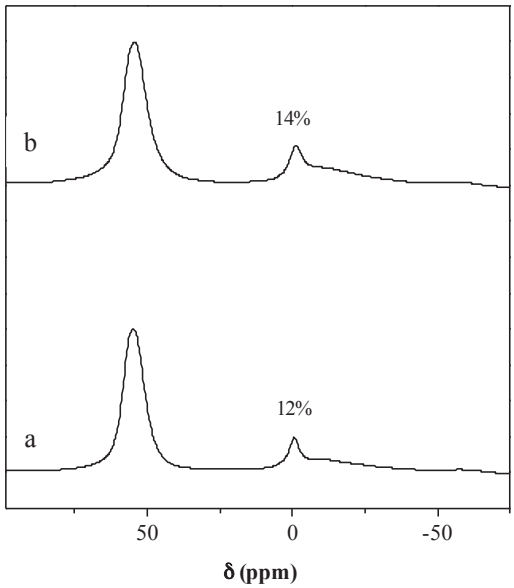

Figure 73. ^{27}Al MAS NMR spectra of a) H-Beta-27 and b) H-Beta-hierarchical samples.*

Fig. 74 compares the high-resolution SEM micrographs of the sample H-Beta-hierarchical with those obtained for its reference, H-Beta-27. As we can see, H-Beta-27 consisted of well formed particles with elliptic shape and size around 500-600 nm whereas for the sample prepared from silanized seeds (H-Beta-hierarchical), the particles had slightly lower particle sizes and their shape was less uniform. Interestingly, for the zeolite with hierarchical porosity, we can clearly distinguish different crystalline nanodomains. Therefore, the silanization treatment seems to enhance the voids existing between the nanounits, leading to supermicropores.

*These spectra were provided by Dr. María Linares from Universidad Rey Juan Carlos, Madrid.

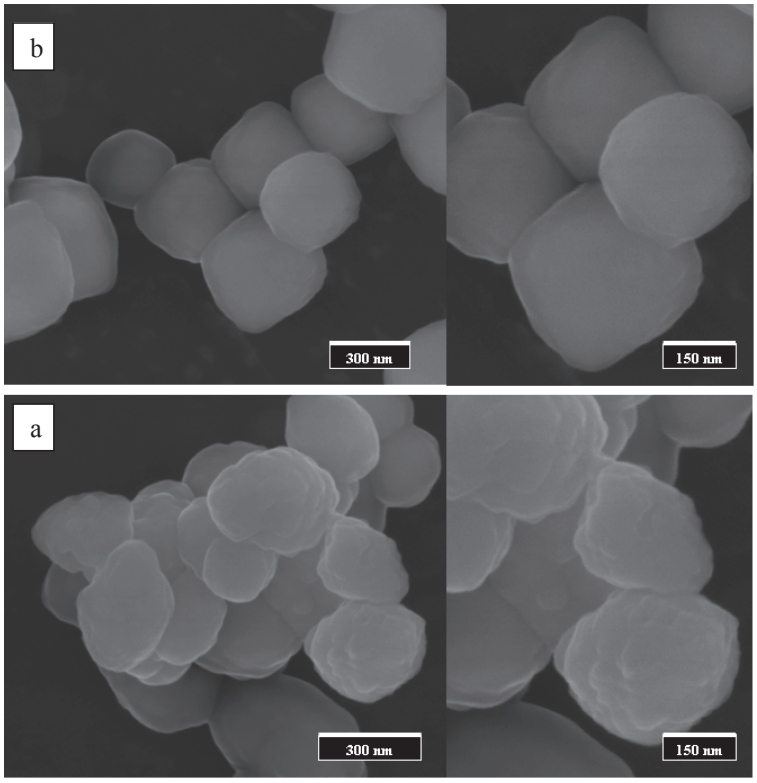

Figure 74. High-resolution SEM micrographs of a) H-Beta-hierarchical and b) H-Beta-27.*

In order to demonstrate that the silanization agent was incorporated in the H-Beta-hierarchical, ^{29}Si MAS-NMR spectra was taken for H-Beta-hierarchical and H-Beta-27 sample for comparison. For reference H-Beta-27, only the signals corresponding to silicon atoms linked either to others silicon or aluminium atoms are observed (Fig. 71a): Q^4 at –111 ppm, Q^3 at –105 ppm (silicon linked to aluminium atoms), Q^3 at –100 ppm (silicon linked to three silicon atoms and to one –OH group) and Q^2 at –90 ppm (silicon linked to two silicon atoms and to two –OH group). However, in the spectrum corresponding to the seed-silanized sample, an additional peak was observed at –67 ppm which is adscribed to silicon atoms linked to a carbon atom and to three silicon atoms (T^3). The almost total absence of T^2 and T^1 signals (they should appear at –57 ppm and –48 ppm, respectively) indicates that a strong linkage has been established between the silicon atoms of the zeolite structure. A decrease in the intensity of the Q^3 signal at –100 ppm is observed in the spectra of the seed-silanized

*These micrographs were provided by Dr. María Linares from Universidad Rey Juan Carlos, Madrid.

materials in regards to that the silanization agent is linked to the zeolite mainly though Q^3 species, causing their transformation into Q^4.

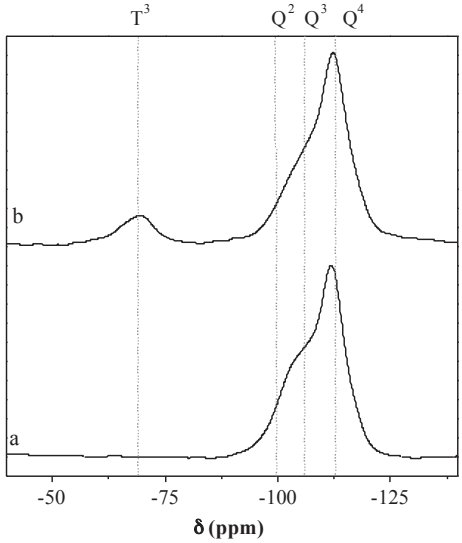

Figure 75. ^{29}Si MAS NMR spectra of a) H-Beta-27 and b) H-Beta-hierarchical.*

The incorporation of the silanization agent was also confirmed by FTIR (not shown here), since in the region 2900-3000 cm^{-1} a higher intensity of the bands corresponding to C-H bonds were observed for the sample H-Beta-hierarchical than for its reference H-Beta-27. This was consistent with the larger organic content of the sample obtained from sinalized seeds due to the presence of both silanized and structure directing agents. ^{29}Si MAS-NMR and FTIR results are in agreement with the results previously reported for similar seed-silanized samples. [179]

N_2 adsorption-desorption isotherms shapes of Na-Beta-10 and H-Beta-10 were very similar (Fig. 76) with just some slight higher mesoporosity for the protonated sample (Table 14, Fig. 76). The slight higher surface area of H-Beta-10 can be related to the slight dealumination occurred, as commented above. Interestingly, the zeolite obtained from silanized seeds presented an enhanced nitrogen adsorption compared to the reference sample H-Beta-27, as expected. This increase of the amount of adsorbed nitrogen was observed in two zones: the first one at low partial pressures ($P/P_0 < 0.2$), corresponding to micropore adsorption and the second one at high partial pressures ($P/P_0 > 0.9$) associated to interparticular adsorption. Therefore, the generation of a secondary microporosity was confirmed, as observed in the pore size distribution of H-

*These spectra were provided by Dr. María Linares from Universidad Rey Juan Carlos, Madrid.

Beta-hierarchical (Fig. 76) with the appearance of a peak centered around 1.8 nm, clearly within the supermicropore region. Consequently, H-Beta-hierarchical showed higher BET and external surface areas and higher micropore volume than the non-hierarchical Beta zeolites (Table 14).

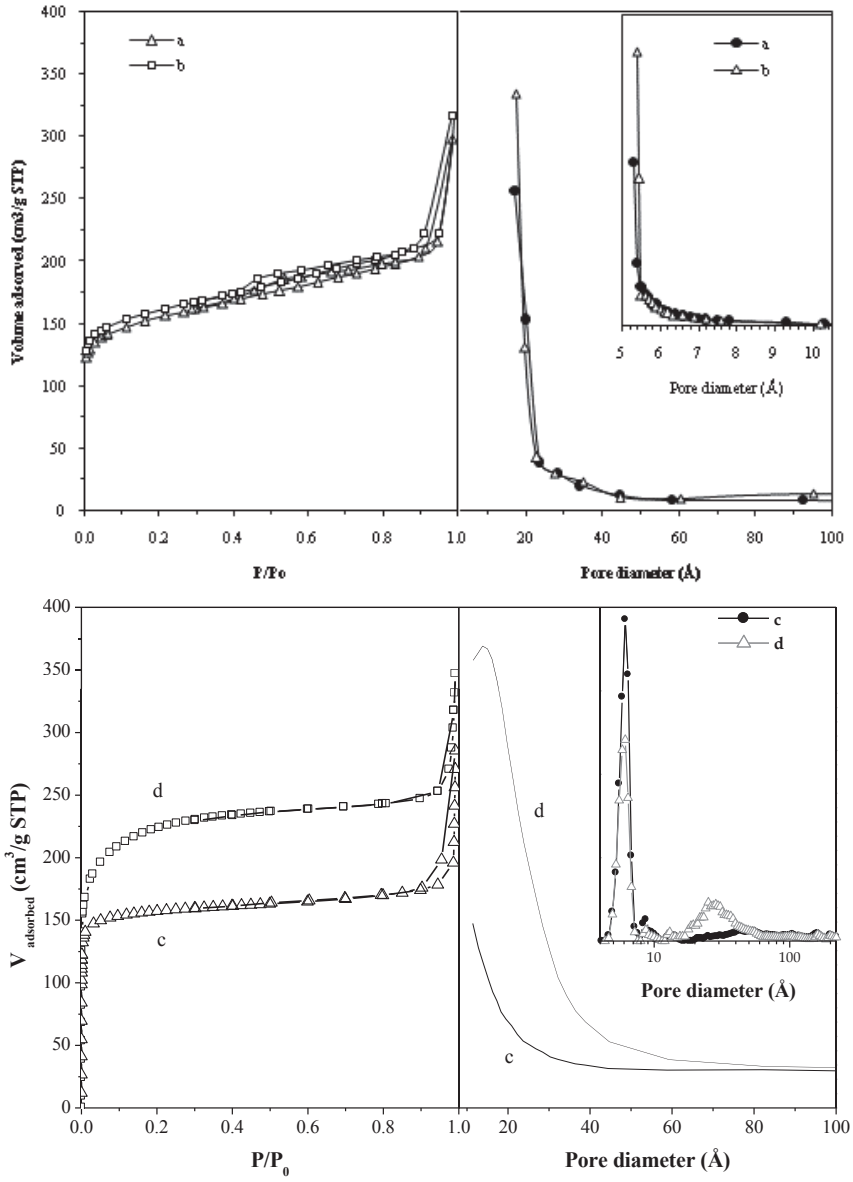

Figure 76. N_2 adsorption-desorption isotherms and pore size distribution of samples a) Na-Beta-10, b) H-Beta-10, c) H-Beta-27 and d) H-Beta-hierarchical.

The acidity capacity of H-Beta-10, determined by thermal desorption of cyclohexylamine, were higher than that of Na-Beta-10 (Table 14). This can be explained by the presence of H^+ compensating the negative charge of the zeolite framework. Moreover, the acidity capacity of the zeolites H-Beta-27 and H-Beta-hierarchical were lower than that of H-Beta-10, as expected, due to their higher Si/Al ratio. ^{1}H NMR spectrum of the commercial Na-Beta showed one peak around 4 ppm (Table 14), which can be associated to free Brønsted protons. [137, 171] After protonation, this peak, related to the protons formed during the treatment, shifted to higher ppm values (Table 14), indicating stronger acidity. [136] ^{1}H NMR spectra of the synthesized H-Beta-27 and H-Beta-hierarchical showed one peak at 4.0 ppm (Table 14), which can be associated to the Brønsted protons formed during their synthesis. Therefore, there are not great differences between the acidity strength of these two zeolites.

Fluorinated samples (FH-Beta-10, FH-Beta-27 and FH-Beta-hierarchical) also maintained their starting zeolitic structure, with some decrease of crystallinity (Table 14). Besides, the Si/Al ratio, the position for the symmetric and asymmetric TO_4 tetrahedra band in the mid-IR region (Table 14) and the nitrogen adsorption-desorption isotherm shapes of the fluorinated samples were very similar to those observed for their starting ones with just some higher mesoporosity (e.g. Figure 77). The lower BET and external surface areas, and the lower micropore volume of the fluorinated samples (Table 14) can be attributed to the loss of crystallinity observed for these samples by XRD due to the fluorination treatment.

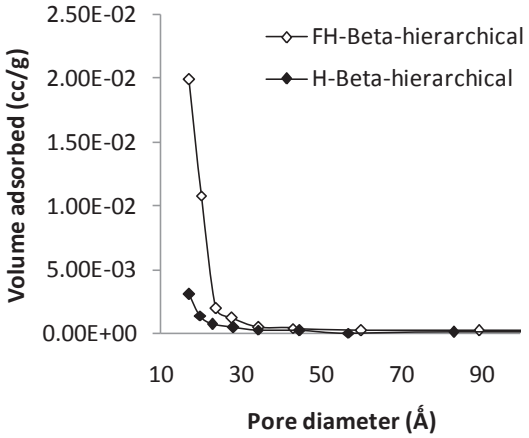

Figure 77. BJH pore size distribution of samples H-Beta-hierachical and FH-Beta-hierarchical.

^{27}Al NMR spectrum of the fluorinated sample FH-Beta-10 (Fig. 72c) was very similar to that of the starting zeolite (Fig. 72a). This confirms that fluorination at mild conditions did not cause appreciable dealumination, in agreement with IR results. The same behaviour was observed for FH-Beta-27 and FH-Beta-hierarchical samples. After fluorination, the acidity capacity values were slightly lower than those of their corresponding H-zeolites. However, the ^{1}H NMR peak attributed to Brønsted protons that are interacting with the zeolite framework, shifted to slightly higher ppm values (Table 14). This means that fluorinated samples had slightly stronger Brønsted acid sites. This only can be explained by an inductive effect by F confirming the introduction of fluorine atoms in the zeolite framework.

Catalytic Activity

Table 15 shows the catalytic activity results for the etherification reaction of glycerol with tert-butanol. One acid ion-exchange resin (Amberlyst 15, here named as A), which is a typical acid catalyst used for this reaction, has been also tested at the same reaction conditions for comparison. The reaction products obtained were mono-tert-butyl glycerol ether (MTBG), di-tert-butyl glycerol ether (DTBG) and some times low amounts of tri-tert-butyl glycerol ether (TTBG). No other reaction products were detected in any case.

Table 15. Catalytic activity of zeolitic materials for the etherification of glycerol with tert-butanol after 24 h of reaction.

Catalyst	Conversion (%)	Selectivity to MTBG (%)	Selectivity to h-GTBE (%)
A	81	64	35 (1)
Na-Beta-10	63	74	26 (0)
H-Beta-10	66	66	34 (0)
FH-Beta-10	75	63	36 (1)
H-Beta-27	27	82	18 (0)
FH-Beta-27	62	69	30 (0.3)
H-Beta-hierarchical	77	65	35 (0.5)
FH-Beta-hierarchical	65	60	40 (1.5)

MTBG: glycerol monoethers; h-GTBE: glycerol diethers + glycerol triether. In parenthesis, selectivity to glycerol triether (%).

H-Beta-10 showed higher conversion and higher selectivity to h-GTBE than Na-Beta-10, as expected, taking into account the higher amount and strength of its Brønsted acid sites (Table 14). One important feature to remark is that triether was not detected for these two catalysts. This has been attributed by other authors to steric hindrance effects because of the microporosity of the zeolites. [156] FH-Beta-10 showed higher conversion and higher selectivity to h-GTBE than Na-Beta-10 and H-Beta-10 due to the higher amounts of stronger acid sites generated because of the incorporation of fluorine in the zeolite framework. Interestingly, FH-Beta-10 allowed us to detect the presence of tri-tert-butyl glycerol ether (TTBG) in low amounts. Taking into account that this catalyst has similar porosity than Na-Beta-10 or H-Beta-10 (Table 14), we can conclude that the modification of the acidity of the zeolite through the introduction of low amounts of fluorine in the zeolite structure is more important than porosity to favour the obtention of the bulky triether. Interestingly, catalytic activity of this catalyst was comparable to that obtained with Amberlyst-15 (Table 15).

Catalysts H-Beta-27 and FH-Beta-27 showed lower conversion and lower selectivity to h-GTBE than H-Beta-10 and FH-Beta-10. This can be explained by the lower amount of acid sites, related to their higher Si/Al ratio, and slight lower strength of their Brønsted acid sites, as observed by ^{1}H NMR (Table 14). Catalyst FH-Beta-27 led to higher conversion and higher selectivity to h-GTBE, with the appearance of TTBG in very low amounts, than catalyst H-Beta-27. Again, this can be related to the presence of fluorine in the zeolite structure.

Regarding the activity results of the catalysts with hierarchical porosity, we observed that H-Beta-hierarchical yielded higher conversion and higher selectivity to h-GTBE than H-Beta-10 and H-Beta-27 catalysts. Taking into account that H-Beta-hierarchical had lower amount and slight lower strength of Brønsted acid sites than H-Beta-10 and similar acid sites amount and strength to those of H-Beta-27, these catalytic results only can be explained by the higher accessibility of the reactants to the acid sites in the zeolite with hierarchical porosity caused by the presence of the secondary porosity. This has been previously reported for other catalytic reactions. [179] FH-Beta-hierarchical showed lower conversion and slight higher selectivity to h-GTBE than H-Beta-hierarchical (Table 15). The lower conversion can be related to the lower surface area of this catalyst attributed to the loss of crystallinity of the zeolite structure during fluorination whereas the slight higher selectivity to h-GTBE can be explained because of its slight stronger acidity together with its slight higher mesoporosity (Table 14).

Table 16 shows the catalytic activity results obtained for the etherification reaction of glycerol with isobutene. The reaction products obtained were mono-tert-butyl glycerol ether (MTBG), di-tert-butyl glycerol ether (DTBG) and some times low amounts of tri-tert-butyl glycerol ether (TTBG). No other reaction products were detected in any case (diisobutylene).

Table 16. Catalytic activity of zeolitic materials for the etherification of glycerol with isobutene at 24 h of reaction.

Catalyst	Conversion (%)	Selectivity to MTBG (%)	Selectivity to h-GTBE (%)
A	99	23	77 (19)
Na-Beta-10	49	39	61 (0)
H-Beta-10	95	35	65 (0)
FH-Beta-10	98	30	70 (1.5)
H-Beta-27	50	30	70 (1)
FH-Beta-27	48	26	74 (3)
H-Beta-hierarchical	97	43	57 (2)
FH-Beta-hierarchical	96	37	63 (8)

MTBG: glycerol monoethers; h-GTBE: glycerol diethers + glycerol triether. In parenthesis, selectivity to glycerol triether (%).

All catalysts showed higher conversion and higher selectivity to h-GTBE values than when the etherification was performed with tert-butanol, as expected, having in mind the results reported by other authors. [155, 158]

The differences observed between beta zeolites followed the same tendencies than those observed in the reaction with tert-butanol. It is important to remark the high conversion, near total activity, achieved with H-Beta-10, FH-Beta-10, H-Beta-hierarchical and FH-Beta hierarchical. The higher selectivity values to the bulky triether were again obtained for the catalysts with fluorine atoms in their structure. This can be mainly related to the higher amount and higher strength of the Brønsted acid sites that these catalysts had when compared with those without fluorine (Table 14). Interestingly, the higher selectivity to the triether obtained for H-Beta hierarchical and FH-Beta hierarchical can be explained because of their hierarchical porosity, which favor the diffusion of the reactants to the acid sites, since these catalysts showed lower acidity amount and strength than H-Beta-10 and FH-Beta-10 catalysts.

Table 17 shows the BET surface areas of the catalysts with hierarchical porosity before and after reaction compared with those obtained for the catalysts with the same Si/Al ratio but without hierarchical porosity.

Table 17. BET surface areas of several catalysts before and after 24 h of reaction for the etherification of glycerol with isobutene.

Catalyst	BET area before reaction (m^2/g)	BET area after reaction (m^2/g)
H-Beta-27	568	48
FH-Beta-27	431	37
H-Beta-hierarchical	750	474
FH-Beta-hierarchical	503	356

All catalysts suffered a loss of surface area during reaction due to the partial blocking of the pores by the reaction products formed. It is important to note that the catalysts with hierarchical porosity lost surface area in less extent than those without hierarchical porosity. This also can explain the higher amounts of glycerol triether obtained with these catalysts.

Conclusions

Catalytic glycerol etherification results obtained with isobutene were better than those obtained with tert-butanol but the differences observed in the catalytic behavior between the catalysts were in the same way for both reactions.

Beta zeolites with hierarchical porosity yielded higher selectivity to the bulky triether than conventional Beta zeolites. This only can be explained because of its additional porosity, which favors the accessibility of the reactants to the acid sites, since these catalysts with hierarchical porosity, showed lower amount and strength of Brønsted acid sites than a conventional beta zeolite with lower Si/Al. The presence of fluorine in the zeolitic structures resulted in slight higher strength of Brønsted acid sites, which led to higher selectivity to h-GTBE.

Acknowledgments

The authors are grateful for the financial support of the Ministerio de Ciencia e Innovación and FEDER funds (CTQ2008-04433/PPQ). Dolores González acknowledges Ministerio de Educación y Ciencia for a FPU grant (AP2007-03789).

4.2.3 Boosted selectivity towards high glycerol tertiary butyl ethers by microwave-assisted sulfonic functionalization of SBA-15 and Beta zeolite

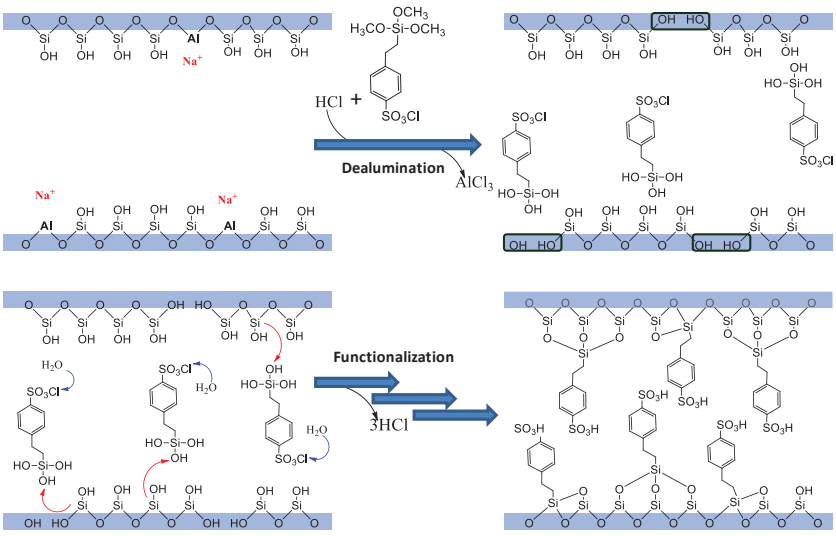

Abstract

Microwave-assisted sulfonated samples showed remarkably higher selectivity towards di and tri-ethers of glycerol than those sulfonated by conventional heating due to the higher acidity and/or accessibility of their Brønsted acid sites.

Introduction

During biodiesel production, glycerol is formed as by-product. The price of glycerol is falling as fast as biodiesel plants are being built. Research is currently starting to find new outlets to convert the surplus of glycerol into high-added value products that improve the economy of the whole process. [2-3]

One challenging option is the catalytic etherification of glycerol with isobutene to obtain di- and tri- tertiary butyl ethers of glycerol (h-GTBE), which can be used as oxygenated fuels replacing the highly toxic to the environment methyl tertiary butyl ether (MTBE) and reducing remarkably the emissions of particulate matter, hydrocarbons, CO and unregulated aldehydes in the exhaust gases. [145] Regarding heterogeneous catalysis, the best activity results were achieved with acid ion-exchange resins (Amberlyst) [154-157] and with silicas functionalized with organosulfonic groups introduced by conventional heating. [5, 158] When H-Beta zeolite was tested, the formation of the triether was not observed. This has been attributed to steric hindrance effects due to the microporosity of zeolites. [156]

The use of microwaves for the synthesis or modification of materials is becoming an important tool to reduce the synthesis time (energy saving). [132, 171] However, there are no studies about the use of microwaves for the sulfonation of zeolites or mesoporous silicas.

For the first time, we report the post-synthesis sulfonation of commercial Beta-zeolite in one-step, by conventional heating as well as with microwaves, and the introduction of high amount of sulfonic groups during functionalization of SBA-15 with microwaves. Acid functionalized samples resulted in outstanding activity and selectivity to h-GTBE catalysts for the etherification of glycerol with isobutene.

Experimental

Catalysts preparation

SBA-15 sulfonated by conventional heating (SBA-15-CS) was prepared with a molar composition of 1.2 SiO_2: 0.2 chlorosulfonylphenylethyltrimethoxy-silane (CSPTMS, Gelest): 6.5 HCl: 180 H_2O. [85] The sulfonation step was made at 313 K for 24 h by traditional refluxing. SBA-15 sulfonated with microwaves (SBA-15-MwS) was prepared at the same conditions than SBA-15-CS but the sulfonation step was made at

313 K for 2 h by refluxing with microwaves (Milestone ETHOS-TOUCH CONTROL). 2 g of commercial Na-Beta (Zeochem, Si/Al=10) were treated with 1.4 g of CSPTMS in 150 mL of 2 M HCl at 313 K for 2 h by conventional refluxing (Beta-CS) or by refluxing with microwaves for 2 h (Beta-MwS). Amberlyst-15, was supplied by Aldrich (39 m^2/g, pore size of 103 Å).

Catalysts characterization

XRD patterns were obtained with a Siemens D5000 diffractometer. BET areas were calculated from N_2 adsorption isotherms using a Quadrasorb SI surface analyser. TGA were performed with a TA instruments equipment from 323 K to 1073 K at 10 K/min under airflow. X-ray photoelectron spectra were taken with a SPECS system equipped with an Al anode XR50 source and a Phoibos 150 MCD-9 detector with pass energy of 25 eV at 0.1 eV steps at a pressure below $6 \cdot 10^{-9}$ mbar. Acid capacities were determined potentiometrically using 2M NaCl as cationic-exchange agent, and a dropwise addition of 0.01 NaOH as titration agent.

Catalytic activity

Etherification of glycerol with isobutene (glycerol/isobutene molar ratio of 0.25) was carried out in a stainless steel stirred autoclave batch reactor at 348 K using 0.5 g of catalyst. Reaction products were analyzed by gas chromatography. Glycerol conversion and selectivity to MTBG were determined from calibration lines obtained from commercial products. For glycerol diethers (DTBG) and triether (TTBG), which were not available commercially, we isolated them from the reaction products by column chromatography and identified by ^{13}C and ^{1}H NMR for proper quantification. [96]

Results and discussion

X-ray diffraction (XRD) patterns of SBA-15 samples showed the typical hexagonal structure whereas sulfonation of beta did not cause drastic changes in the zeolite structure. N_2 adsorption-desorption isotherms were type I for the zeolite samples, attributed to microporous materials, and type IV for the SBA-15 samples, associated to mesoporous materials.

X-ray photoelectron spectroscopy (XPS) is useful for evaluating qualitatively the type of sulfur species and measuring quantitatively the sulfonic groups near the surface region. [77, 87] The S 2p XP spectra of sulfonated SBA-15 samples only showed one peak at ca. 168-169 eV associated with sulfate (S^{6+}) species due to sulfonic ($-SO_3H$) groups, [77, 87] with higher intensity for SBA-15-MwS (Fig. 78).

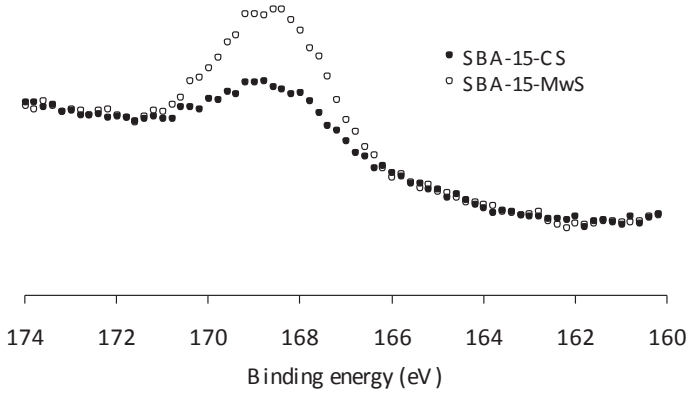

Figure 78. XP spectra of samples SBA-15-CS (conventional heating) and SBA-15-MwS (microwaves) in the S 2p core level region.*

Therefore, the use of microwaves for the sulfonation of SBA-15 allowed us a faster introduction of higher amount of sulfonic groups in the mesoporous silica, according to the higher S/Si atomic ratio, higher sulfur content due to sulfonic groups, [83] determined by TGA, lower BET area and higher acidity observed for SBA-15-MwS (Table 18).

Table 18. Characterization of the samples.

Catalyst	S/Si atomic ratio[a]	Sulfur content[b]	BET area (m^2/g)	Pore volume (cm^3/g)	Acid capacity (meq H^+/g)[c]
SBA-15	----	----	1082	1.68	----
SBA-15-CS	0.03	0.83	640	0.81	0.35
SBA-15-MwS	0.07	1.01	575	0.74	0.75
Beta	----	----	584	0.23	----
Beta-CS	0.06	0.74	330	0.14	0.75
Beta-MwS	0.06	0.70	505	0.24	0.72

[a] Determined from XPS; [b] (mmol organic sulfonic group/g sample) calculated from TGA; [c] Obtained by potentiometric titration.

XPS confirmed sulfonation of beta when using conventional heating as well as microwaves. Again, only one S 2p peak, corresponding to sulfonic groups, was

* XPS spectra were provided by Dr. Jordi Llorca from the Universitat Politècnica de Catalunya.

observed. The S/Si atomic ratio, the sulfur content and the acid capacity were similar for both samples (Table 18). With respect to Beta, Beta-CS showed a higher decrease of BET area, with some decrease of pore volume, than Beta-MwS. From these results, we believe that sulfonation in Beta-CS occurred largely at the micropores whereas the use of microwaves resulted in higher amounts of external sulfonic groups.

Taking into account that the main difficulty to introduce bulky organic species in a zeolite is the lack of reactant silanol groups, an important key to understand these good beta sulfonation results is the beta dealumination occurred under the acidic conditions used during sulfonation.

Zeolite beta is easier to dealuminate than ZSM-5 or mordenite.[45, 132, 171] This has been related to the flexibility of the zeolite framework, and the accessibility of the aluminium atoms depending on the pores arrangement and sizes. [45] The Si/Al atomic ratio of Beta-CS and Beta-MwS, calculated from XPS, were 53 and 69, respectively, confirming dealumination. We believe that zeolite dealumination during sulfonation favors the generation of new silanols than can react with the sulfonating agent to form sulfonic groups (Scheme 2).

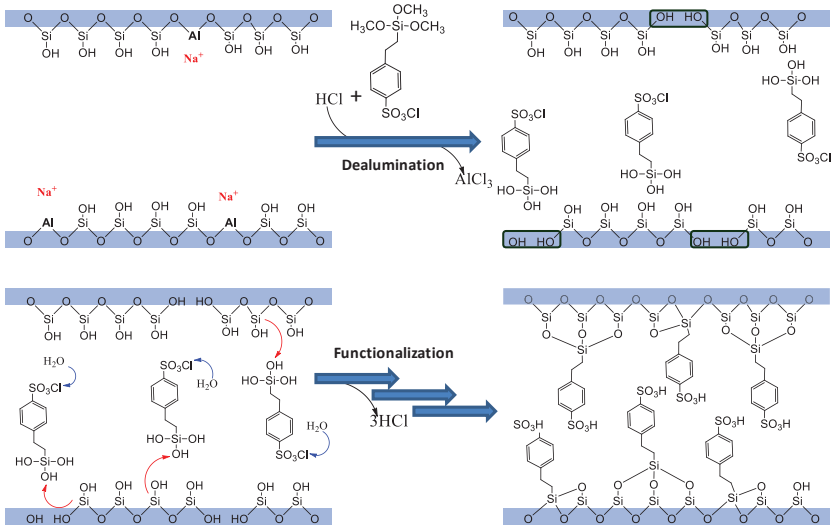

Scheme 2. Mechanism of sulfonic functionalization of zeolite beta.

Regarding catalytic activity, pure silica (SBA-15) and commercial beta zeolite had the lowest conversion and selectivity to h-GTBE (Table 19) due to their low amount of acid centres. However, functionalized catalysts were very active due to the presence of the sulfonic acid groups.

Table 19. Catalytic results for the glycerol etherification with isobutene

Catalysts	Reaction time (h)	Conversion (%)	Selectivity to MTBG[a] (%)	Selectivity h-GTBE[b] (%)
Amberlyst-15	4	73	65	35 (3)
	24	99	23	77 (19)
SBA-15	4	41	87	13 (0)
	24	62	86	14 (2)
SBA-15-CS	4	98	39	61 (5)
	24	99	15	85 (28)
SBA-15-MwS	4	99	9	91 (36)
	24	100	9	91 (39)
Beta	4	44	32	68 (1)
	24	49	39	61 (2)
Beta-CS	4	93	49	51(5)
	24	100	12	88 (32)
Beta-MwS	4	100	17	83 (15)
	24	100	9	91 (36)

[a]MTBG: glycerol monoethers; [b] h-GTBE: glycerol diethers + glycerol triether. In parenthesis, selectivity to glycerol triether (%).

Interestingly, the samples sulfonated with microwaves showed a remarkably higher selectivity to h-GTBE than those functionalized by conventional heating, especially at 4 h of reaction. This can be explained by the higher acidity and/or accessibility of Brønsted acid sites in these samples. The selectivity to triether obtained for Beta-MwS at 24 h (36 %) is the best result achieved for this reaction up to now using a zeolite as catalyst. This reveals the great importance of acidity in front of porosity for this etherification reaction.

Conclusions

For the first time, we report the post-synthesis sulfonation of commercial Beta-zeolite in one-step, by conventional heating as well as with microwaves. After 4 h of reaction catalyst Beta-MwS presented 99% of conversion and 91 % of selectivity to di- and triethers. Interestingly, after 24h this catalyst obtained 36 % of selectivity to triether, the best result using a zeolite for this reaction.

The use of microwave during functionalization of SBA-15 allowed us to introduce higher amount of sulfonic groups at shorter times than by using convetional heating.

Acknowledgments

The authors are grateful for the financial support of the Ministerio de Ciencia e Innovación and FEDER funds (CTQ2008-04433/PPQ and CTQ2009-12520). M.D.G. acknowledges FPU grant AP2007-03789. J.L. is grateful to ICREA Academia program. We thank Ms. Irene Marín for her help in the performance and interpretation of ^{13}C and ^{1}H NMR spectra.

Supporting information

X-ray diffraction (XRD)

The patterns of beta zeolite samples were recorded over a range of 2θ angles from 5º to 40º. Crystalline phases were identified using the Joint Committee on Powder Diffraction Standards (JCPDS) files (48-0074 corresponds to beta). For small-angle powder XRD patterns of SBA-15 samples, the scanning range was set from 0.5º to 10º with a step of 0.02º. Sulfonated SBA-15 samples exhibit three peaks assigned to the 100, 100 and 200 reflections of ordered 2D hexagonal (P6mm) mesostructure (Figure 79). Figure 80 shows the XRD patterns of the sulfonated beta-zeolites. The functionalization treatment did not cause drastic changes in the zeolite structure.

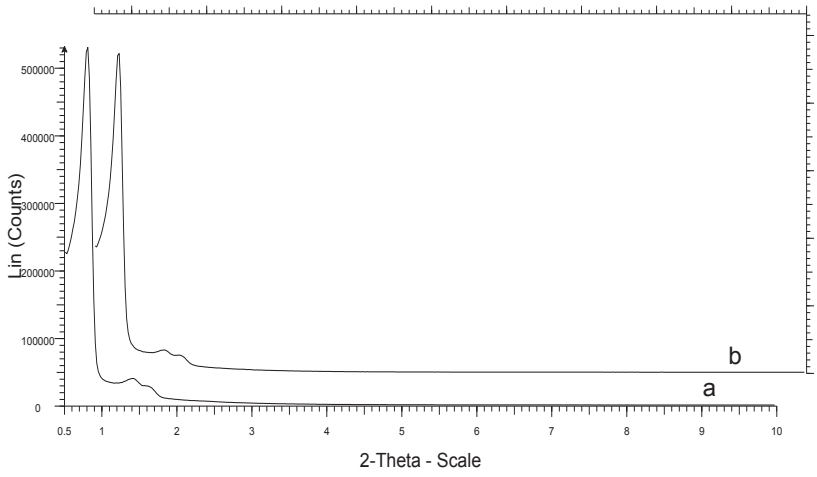

Figure 79. XRD patterns of SBA-15-CS (a) and SBA-15-CMwS (b).

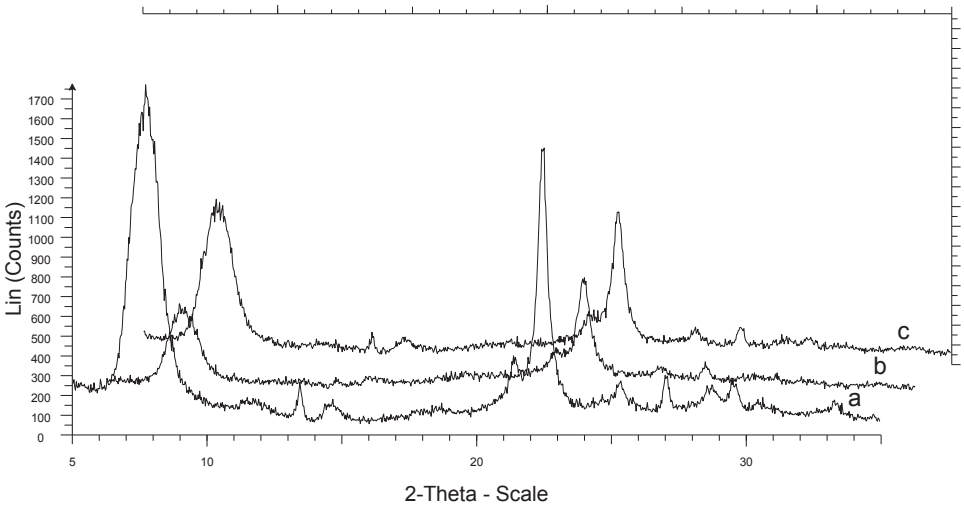

Figure 80. XRD patterns of Beta (a), Beta-CS (b) and Beta-CMwS (c).

N_2 Physisorption

Fig. 81 shows the N_2 adsorption-desorption isotherms of the sulfonated samples. N_2 adsorption-desorption isotherms were type I for the zeolite samples, attributed to microporous materials, and of type IV for the SBA-15 samples, associated to mesoporous materials, according to the Brunauer, Deming, Deming and Teller classification.

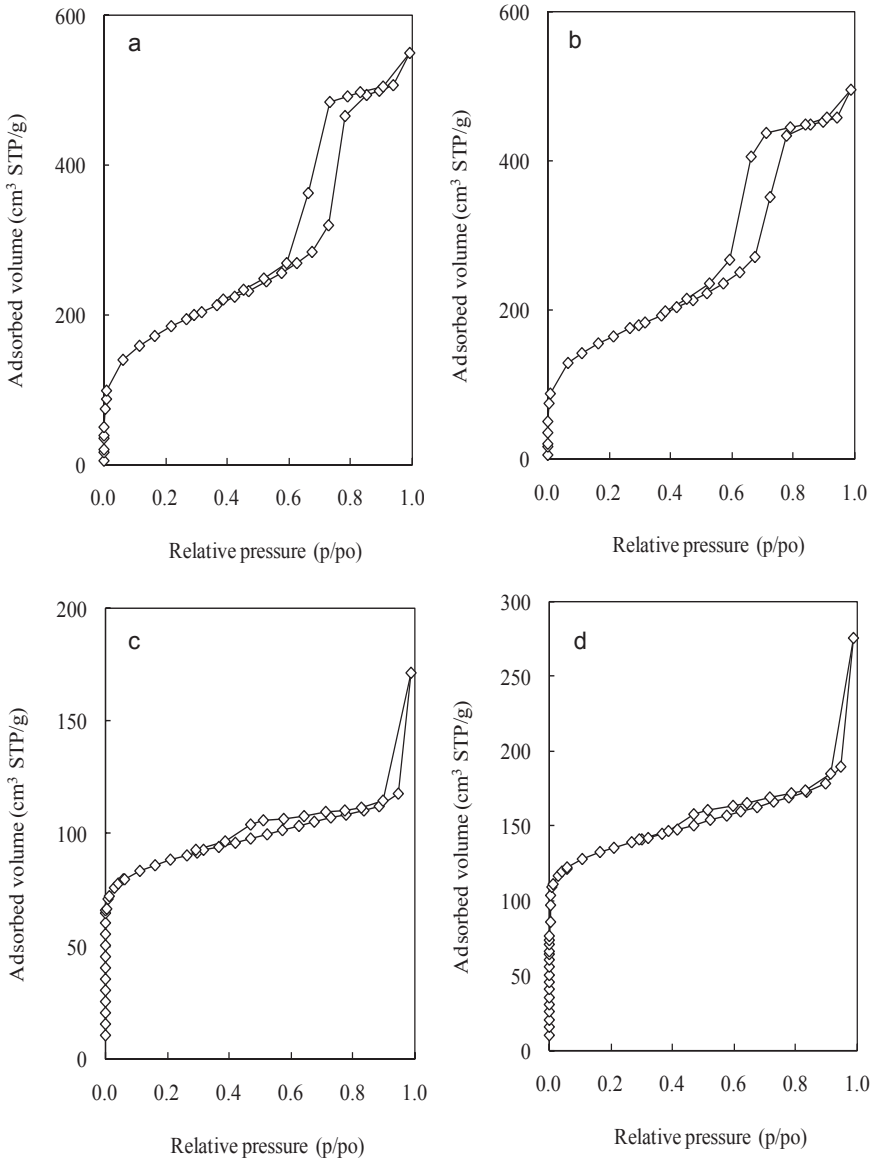

Figure 81. Nitrogen adsorption-desorption isotherms of SBA-15-CS (a), SBA-15-MwS (b), Beta-CS (c) and Beta-MwS (d).

Thermogravimetric Analysis (TGA)

Fig. 82 shows the thermogravimetric results obtained for the sulfonated samples. The weight loss observed between 360ºC and 660ºC, indicated between red bars on the figures, was related to the loss of sulfonic groups, according to the literature, [83] and allowed us to calculate the mmol organic sulfonic group/g sample.

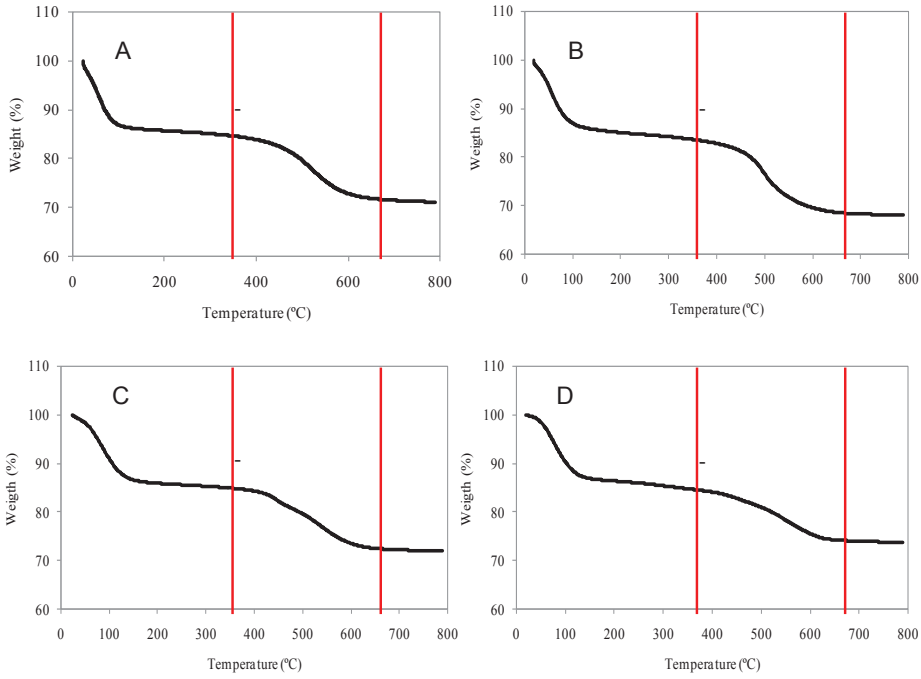

Figure 82. Thermogravimetric weight loss curves of SBA-15-CS (a), SBA-15-MwS (b), Beta-CS (c) and Beta-MwS (d).

Reaction conditions details

Etherification of glycerol with isobutene (glycerol/isobutene molar ratio of 0.25) was carried out in a stainless steel stirred autoclave (150 mL) equipped with temperature controller and a pressure gauge. Liquid phase pressurized isobutene was injected into the reactor, previously charged with glycerol and catalyst (0.5 g), using nitrogen at 10 bar as pushing agent. The temperature was then raised to 348 K and the pressure increased accordingly following the liquid-vapour equilibrium. Stirring was fixed for all experiments at 1200 rpm to avoid external diffusional limitations. Catalytic experiments were made at 4 and 24 h. Reaction products were analysed by gas chromatography using a SupraWax-280 column and a FID detector.

Identification of DTBG and TTBG

Glycerol conversion and selectivity to MTBG (glycerol monoethers) were determined from calibration lines obtained from commercial products. For DTBG (glycerol diethers) and TTBG (glycerol triether), which were not available commercially, we isolated them from the products of the etherification reaction by column chromatography (1:9 Ethyl acetate/Hexane) and identified them by ^{13}C and ^{1}H NMR for proper quantification with the assistance of the characterization data reported by Jamróz et al. [96]

^{1}H and ^{13}C NMR spectra were recorded on a 400 MHz and 100.6 MHz, respectively, using $CDCl_3$ as solvent, with chemical shifts (δ) referenced to internal standards $CDCl_3$ (7.26 ppm ^{1}H, 77.23 ppm ^{13}C). Figs. 35-38.

UNIVERSITAT ROVIRA I VIRGILI
REVALORIZACIÓN CATALÍTICA DE GLICERINA PARA UNA OBTENCIÓN MÁS RESPETUOSA CON EL MEDIO AMBIENTE DE ADITIVOS PARA COMBUSTIBLES
Mª Dolores González Candela
DL:T. 1715-2011

4.2.4 Microwave-assisted synthesis of sulfonic acid-functionalized microporous materials for the catalytic etherification of glycerol with isobutene

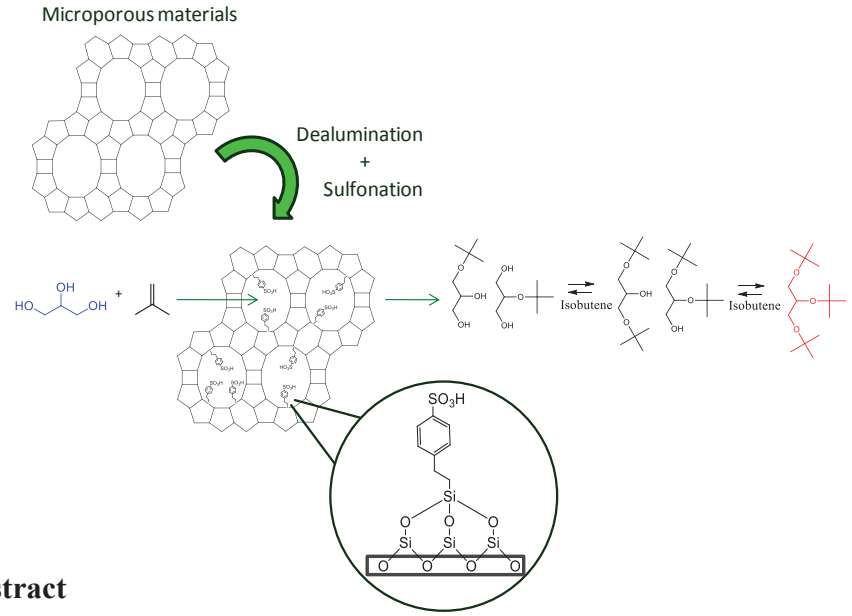

Abstract

Commercial beta, ZSM-5 and mordenite zeolites and commercial montmorillonite were successfully sulfonated by one-step simple method using microwaves. Different amounts of sulfonating agent were required to optimize the incorporation of sulfonic groups for each structure. This has been related to the different dealumination degree suffered by the starting samples during sulfonation together with the different accessibility of the silanols to the sulfonic groups depending on the arrangement and size of their pores. All optimised sulfonated catalysts showed total conversion and very high selectivity (79-91%) to h-GTBE (glycerol di- and tri-ethers), in spite of their microporosity, due to the incorporation of the sulfonic groups that led to high number and strength of Brønsted acid sites. Pore size and arrangement of the catalysts affected the accessibility of the reactants to the acid sites and the diffusion of the reactants through the pores explaining the evolution of the catalytic results with time for each structure.

Introduction

Glycerine (glycerol or 1,2,3-propanetriol) has over 1500 known end uses, including applications in cosmetics, pharmaceuticals and food products. [3, 168] During biodiesel manufacture, by transesterification of vegetable oils with methanol, glycerine is formed as by-product (10 weight % of the total product). [3, 11, 168] The price of glycerol is falling as fast as biodiesel plants are being built. Research is currently starting to find new outlets to convert the surplus of glycerol into high-added value products that improve the economy of the whole process. [2-3, 6, 9-10, 169]

One challenging option is the catalytic etherification of glycerol with tert-butanol or isobutene to obtain di- and tri- tertiary butyl ethers of glycerol, the so-called "higher ethers" (h-GTBE), which constitute an excellent additive with a large potential for diesel and biodiesel reformulation. [144-146] When h-GTBE was incorporated in standard 30-40% aromatic-containing diesel fuel, emissions of particulate matter, hydrocarbons, carbon monoxide, and unregulated aldehydes decreased significantly. [145-146] Etherification of glycerol with isobutene or with tert-butanol has been studied in the presence of acid catalysts. [5, 154-164, 166-167] Etherification with isobutene yielded higher conversion and selectivity to h-GTBE than etherification with tert-butanol. [155, 158]

In the first studies performed with zeolites as catalysts for this reaction, Klepáčová et al. reported that the formation of the triether was sterically hindered in H-Beta and H-Y zeolites due to their microporosity. [156] However, in a previous study, we observed the formation of this tri- tertiary butyl ether of glycerol (TTBG) in low amounts when using a fluorinated Beta zeolite for the etherification of glycerol with tert-butanol. [Section 4.2.1] Interestingly, the post-synthesis sulfonation of one commercial Beta zeolite in one step with microwaves resulted in a catalyst that yielded total conversion and 83 % of selectivity to h-GTBE, with 15 % of selectivity to TTBG, at 4 h of reaction for the etherification of glycerol with isobutene. [Section 4.2.3] Selectivity to h-GTBE and to TTBG increased at higher reaction time (24 h) with this catalyst (91 % and 36 %, respectively). The catalytic results were better than those obtained with the corresponding sample sulfonated by conventional heating. [Section 4.2.3] Besides, the selectivity values were much higher than those obtained by using a macroporous acid-ion exchange resin (Amberlyst-15) as catalyst for this reaction. From these results, we concluded that the acidity strength significantly influenced in the formation of di- and

specially tri-ethers of glycerol, independently of the porosity of the catalysts. However, the accessibility of the reactants to the acid sites must be guaranteed so that they can act.

Apart from the study commented above, [Section 4.2.3] there are not references about the post-synthesis sulfonation of zeolites in one step or about the use of microwaves for the sulfonation of zeolites although microwave irradiation has been extensively applied for the synthesis, dealumination, and cation-exchange of zeolites. [91, 139, 171] The use of microwaves considerably decreases the preparation times, with the subsequent energy saving, and modifies the samples properties, which can be of interest for catalysis.

The aim of this work was a) to explore the effect of using different amounts of sulfonating agent during the microwaves-assisted sulfonic acid-functionalization of three pentasyl-type zeolites (mordenite, ZSM-5 and beta) on the catalytic etherification of glycerol with isobutene. Several beta samples will be also sulfonated by conventional heating for comparison; b) to find the optimum extent of sulfonation for each zeolite to maximize the obtention of h-GTBE; and c) to correlate the possible zeolite dealumination occurred during functionalization with the extent of sulfonation, and the dimensionality and channels sizes of the three zeolite structures with the obtention of the bulkier triether. Also, one commercial microporous montmorillonite was sulfonated with microwaves and tested for this reaction.

Experimental

Catalysts preparation

Three commercial pentasyl-type zeolites were sulfonic acid-functionalized in one step by using microwaves (Milestone ETHOS-TOUCH CONTROL equipped with a temperature controller). Na-Mordenite (Zeolyst, Si/Al=6.5, CBV 10A Lot No. 1822-50), Na-Beta (Zeochem, Si/Al=10, PB Lot No. 6000186) and Na-ZSM-5 (Zeochem, Si/Al=20, PZ-2/40 Lot No. 6002827,01) were designated as M, B and Z, respectively.
2 g of commercial zeolite were treated with different amounts of 2-(4-chlorosulfonylphenyl) ethyltrimethoxysilane (CSPTMS) solution in methylene choride (50 wt %, Gelest) in 2 M HCl solution at 313 K for 2 h. Sulfonic acid-functionalized zeolites were called S-B(x), S-Z(x), S-M(x), where x is the amount (in grams) of CSPTMS used. Three more sulfonated beta samples were prepared by modifying some sulfonation parameters: one was prepared at the same sulfonating conditions as for preparing S-B(1.4) but using conventional heating instead of microwaves (sample CS-

B(1.4)), and two more samples were obtained by treatment of 2 g of commercial beta zeolite with 1.4 g of CSPTMS in 2 M HCl solution at 313 K for 30 min under microwaves (sample S-B(1.4)-30 min) or by conventional heating (sample CS-B(1.4)-30 min).

Besides, 2 g of commercial montmorillonite K-10 (Sigma-Aldrich, Si/Al=2.7), here named as Mont, were treated with 1.4 g of CSPTMS in 2 M HCl solution at 313 K for 2 h (sample S-Mont(1.4)). All samples were filtered, washed with deionised water and dried overnight.

Catalysts characterization

X-ray diffraction (XRD) patterns of the samples which were obtained with a Siemens D5000 diffractometer using nickel-filtered Cu Kα radiation. Samples were dusted on double-sided sticky tape and mounted on glass microscope slides. The patterns were recorded over a range of 2θ angles from 5º to 40º and crystalline phases were identified using the Joint Committee on Powder Diffraction Standards (JCPDS) files (43-0171, 48-0074, 37-359 corresponds to mordenite, beta and ZSM-5, respectively). Crystallinity of the modified mordenites was determined by comparing the sum of the peak areas of (150), (202), (350) and (402) (22-32º 2θ) with respect to commecial Na-mordenite. Crystallinity of the modified ZSM-5 samples was calculated using the (051) peak intensity compared with the parent zeolite sample. The integrated intensity of the signal at 2θ = 22.4º was used to evaluate the crystallinity of beta samples.

BET areas were calculated from the nitrogen adsorption isotherms at 77 K using a Quadrasorb surface analyser. Samples were pretreated in vacuum at 573 K for 6 h. Pore size distribution of micropores and meso-macropores were determined from isotherms using the Horvath-Kawazoe method and the BJH method, respectively.

X-ray photoelectron spectra (XPS) were taken with a SPECS system equipped with an Al anode XR50 source and a Phoibos 150 MCD-9 detector with pass energy of 25 eV at 0.1 eV steps at a pressure below $6 \cdot 10^{-9}$ mbar.

Infrared spectra were recorded on a Bruker-Equinox-55 FTIR spectrometer with an MCT detector using a DRIFT cell connected to a temperature controller. The spectra were acquired (at 623 K) by accumulating 64 scans at 4 cm^{-1} resolution in the range of 3500-4000 cm^{-1}. Previously, samples were dehydrated at 623 K for 2 h under N_2 flow.

Scanning electron microscopy (SEM) were performed on a scanning electron microscope, JEOL JSM6400, operating at accelerating voltage of 25 kV and work distances of 10 mm, and magnifications of 2,000-50,000x.

Thermogravimetric analyses (TGA) were performed with a TA instruments equipment from 323 K to 1073 K at 10 K/min under airflow.

Acid capacities were determined potentiometrically using 2 M NaCl as cationic-exchange agent, and a dropwise addition of 0.01 NaOH as titration agent.

Catalytic Activity

Etherification experiments were performed in the liquid phase in a stainless steel stirred autoclave (150 mL) equipped with temperature controller and a pressure gauge. Stirring was fixed for all experiments at 1200 rpm to avoid external diffusion limitations. Liquid phase pressurized isobutene (glycerol/isobutene molar ratio of 0.25) was injected into the reactor, previously charged with glycerol and catalyst (0.5 g), using nitrogen at 10 bar as pushing agent. The temperature was then raised to 348 K and the pressure increased accordingly following the liquid-vapour equilibrium. Catalytic experiments were made at 4, 24 and 48 h. The reaction products were analyzed by gas chromatography using a chromatograph model Shimadzu GC-2010 equipped with a SupraWax-280 column and a FID detector.

Glycerol conversion and selectivity to MTBG (glycerol monoethers) were determined from calibration lines obtained from commercial products. For DTBG (glycerol diethers) and TTBG (glycerol triether), which were not available commercially, we isolated them from the products of the etherification reaction by column chromatography (1:9 ethyl acetate/hexane) and identified them by ^{13}C and ^{1}H NMR for proper quantification with the assistance of the characterization data reported by Jamróz et al. [96]

Results and discussion

Catalysts characterization

Regarding XRD patterns of zeolites, we observed that, after sulfonation, the three zeolites maintained their structure (e.g. Fig. 83) although some decrease of crystallinity was detected for all the sulfonated samples (Table 20). This loss of crystallinity was more marked for the samples sulfonated by conventional heating (e.g. Fig. 84, Table 20).

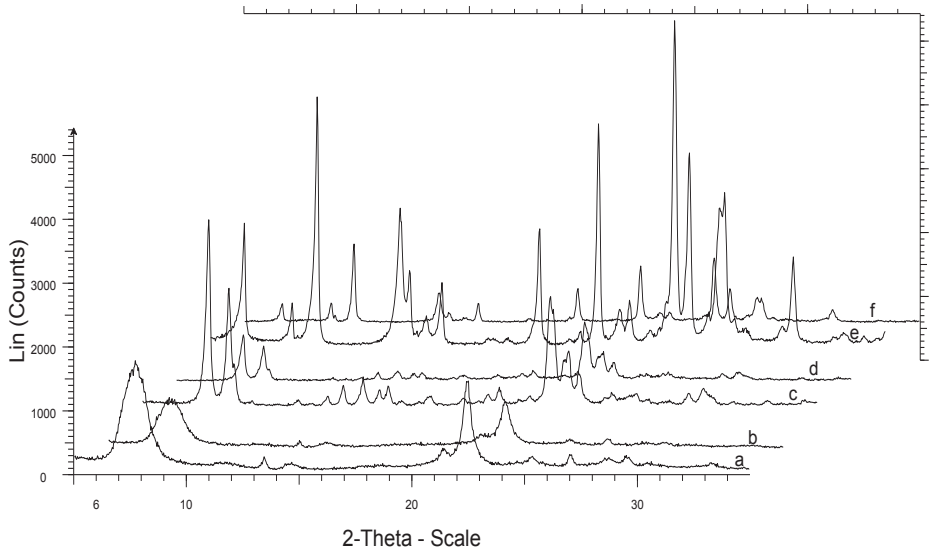

Figure 83. XRD patterns of (a) B, (b) S-B(1.4), (c) Z, (d) S-Z(1.8), (e) M and (f) S-M(1.6) samples.

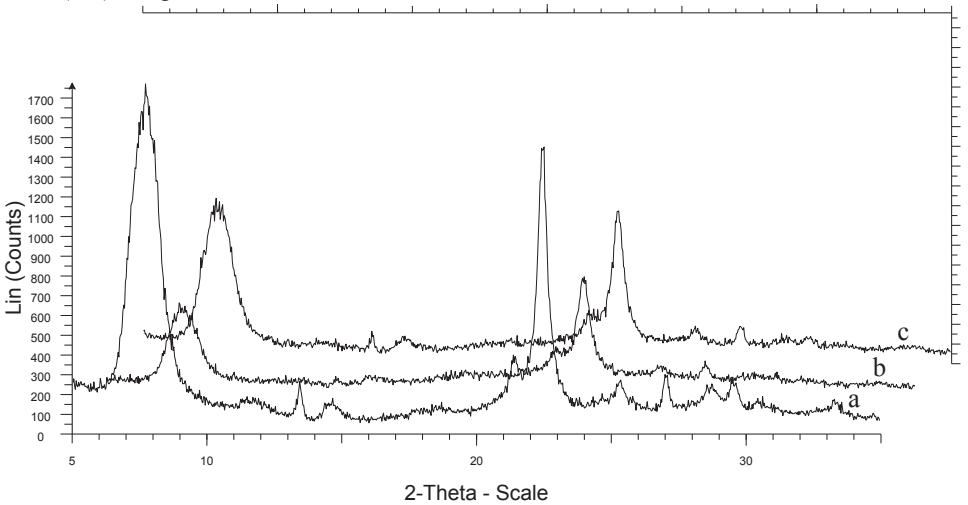

Figure 84. XRD patterns of (a) B, (b) CS-B(2.8) and (c) S-B(2.8).

Table 20. Characterization of catalysts.

Catalyst	Crystallinity[a] (%)	BET area (m^2/g)	Pore volume (cc/g)	Sulfur content[b]	Acid capacity[c] (meq H^+/g)
B	100	584	0.23	--	--
S-B(0.7)	50	502	0.20	0.31	0.30
S-B(1.0)	49	501	0.21	0.40	0.42
S-B(1.4)	45	505	0.24	0.70	0.72
S-B(2.8)	30	88	0.04	0.77	0.76
S-B(1.4)-30 min	35	395	0.13	0.40	0.39
CS-B(1.4)-30 min	36	372	0.09	0.43	0.42
Z	100	330	0.06	--	--
S-Z(0.7)	50	355	0.07	0.14	0.17
S-Z(1.4)	54	345	0.05	0.16	0.26
S-Z(1.8)	53	213	0.02	0.68	0.52
M	100	424	0.10	--	--
S-M(1.4)	31	529	0.15	0.14	0.62
S-M(1.6)	29	426	0.07	0.60	0.82
S-M(1.8)	32	500	0.12	0.72	0.77
S-M(2.2)	30	489	0.11	0.70	0.62
Mont	--	233	0.36	--	--
S-Mont (1.4)	--	125	0.19	0.71	0.77

[a]Calculated from XRD patterns; [b](mmol organic sulfonic group/g sample) calculated from TGA; [c]Obtained by potentiometric titration.

N_2 adsorption-desorption isotherms were type I for all the zeolite samples, before and after sulfonation (e.g. Fig. 85), as expected, attributed to microporous materials, according to the Brunauer, Deming, Deming and Teller classification. [180] All sulfonated beta samples showed lower surface areas, and on the whole, lower pore volumes than commercial beta (Table 20). In contrast, sulfonated mordenites exhibited higher surface areas and higher pore volumes than commercial mordenite (Table 20) whereas sulfonated ZSM-5 zeolites had just slightly higher surface areas than commercial ZSM-5 except for the ZSM-5 sulfonated with the highest amount of sulfonic agent where a considerable decrease of surface area and pore volume was observed (Table 20, Fig. 85). There are several factors that can contribute to explain

these results: the partial dealumination suffered by the zeolites because of the acidic medium used during sulfonation, the loss of crystallinity observed for the sulfonated samples, and the partial blockage of pores by the sulfonic groups.

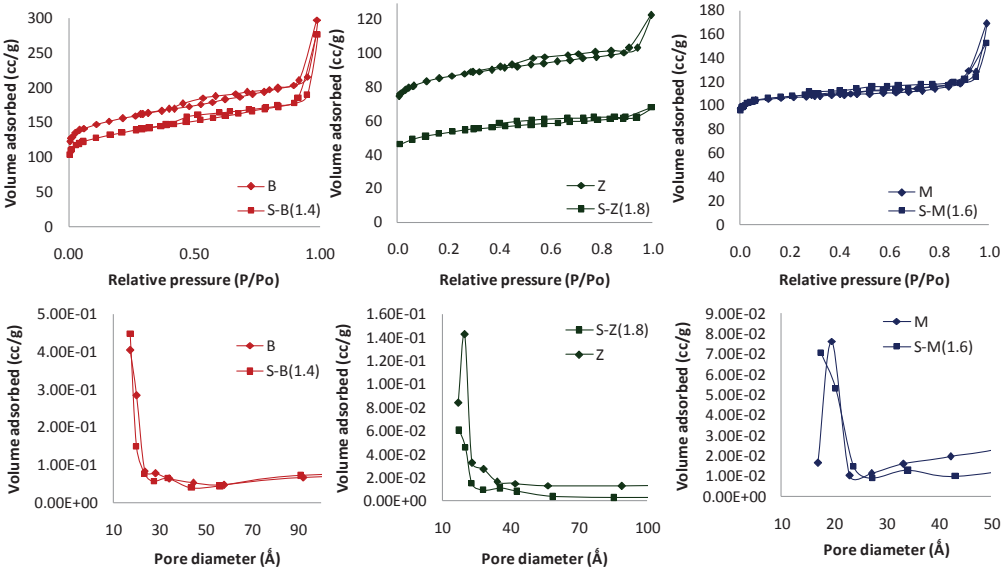

Figure 85. Nitrogen adsorption-desorption isotherms and pore size distribution graphics of B, S-B(1.4), Z, S-Z(1.8), M and S-M(1.6).

Zeolite beta has a three-dimensional 12-ring pore system (straight channels of diameter 6.6 x 6.7 Å and sinusoidal channels of diameter 5.6 x 5.6 Å) and, because of this property, the framework is very flexible. Zeolite mordenite has a one-dimensional pore system with main channels of diameter 6.7 x 7.0 Å and compressed channels of diameter 2.6 x 5.7 Å whereas ZSM-5 has a three-dimensional 10-ring pore system with channels of diameter 5.1 x 5.5 Å. Both these structures are less flexible than beta, and consequently, it is more difficult to dealuminate them. Additionally, zeolite beta crystallizes with many stacking faults [115] while mordenite samples, although less frequently, may also have structurally related stacking faults. [116] Stacking faults increase the probability of the presence of defect sites in the framework. Thus, beta zeolite is easier to dealuminate than mordenite and mordenite is easier to dealuminate than ZSM-5, which always shows very low dealumination. [45, 171] In a previous study, we also conclude that the use of microwaves led to faster dealumination than conventional heating for the three zeolites. [171]

Therefore, the higher surface areas observed for the sulfonated mordenite samples could be associated to the loss of aluminium in the zeolite structure, due to the acidic medium used during sulfonation, which results in higher mesoporosity, and therefore, higher surface area, as reported before for partially dealuminated mordenites. [33, 46, 171] However, the decrease of surface area observed for sulfonated beta samples can be attributed to the loss of crystallinity observed after acid treatment, as reported by other authors, [134] together with the easier introduction of the sulfonic groups in this more flexible zeolite framework. Finally, the low dealumination of ZSM-5 practically did not affect the surface areas and pore volumes of the sulfonated samples, and only when the amount of sulfonating agent was the highest, lower surface areas and lower pore volumes were observed.

By comparing the beta samples functionalised by conventional heating or by using microwaves at the same conditions we observed that those sulfonated by conventional heating had lower surface areas and lower pore volumes than those sulfonated under microwaves. This confirms the results obtained in a previous study. [Section 4.2.3] We believe that sulfonation in the beta samples conventionally heated occurred largely at the micropores whereas the use of microwaves resulted in higher amounts of external sulfonic groups. The effect of these differences on their catalytic behaviour will be correlated later.

Scanning electron microscopy was used to monitor the morphologies and sizes of the particles of the sulfonic acid-functionalized samples with respect to the starting commercial zeolites (Fig. 86). Sulfonated mordenite and beta samples appeared less agglomerated, with less densely packed crystallites, than their corresponding commercial ones, whereas the micrographs of ZSM-5 samples were very similar.

Table 20 also shows the sulfur content of the sulfonated samples obtained from TGA. All the sulfonated samples had sulfonic groups since a weight loss between 633 K and 933 K was observed in the TG curves for all of them. This weight loss has been related to the loss of sulfonic groups, according to the literature, [83] and allowed us to calculate the mmol organic sulfonic group/g sample (Table 20). This is the first time that post-synthesis sulfonation of commercial ZSM-5 and mordenite in one-step has been reported. Besides, this is also the first time that microwaves have been used for sulfonating these two zeolites. We recently applied this procedure for sulfonation of commercial beta. [Section 4.2.3] Similar sulfur content was observed when comparing the

beta zeolites sulfonated with microwaves with those sulfonated by conventional heating at the same conditions (Table 20).

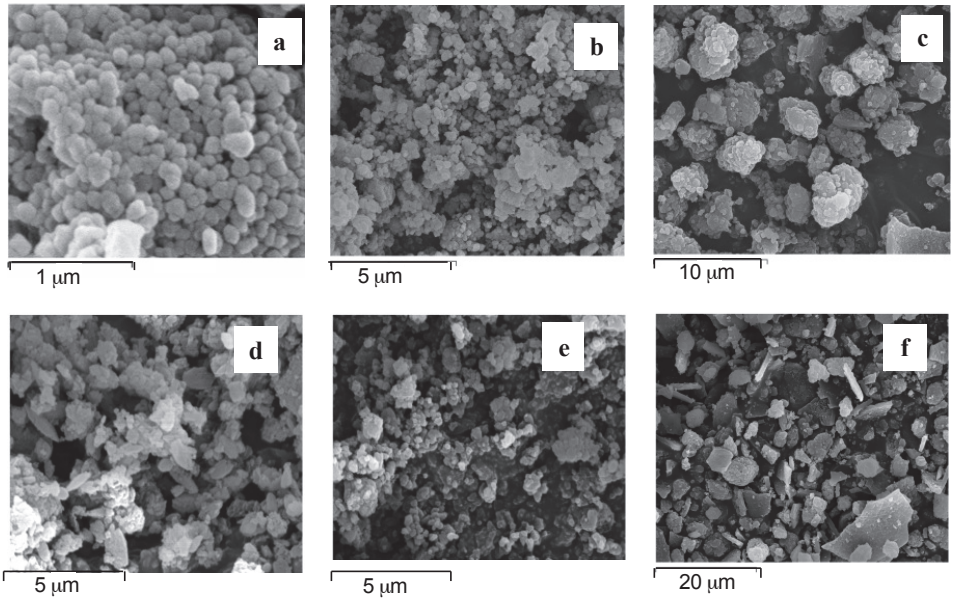

Figure 86. Scanning electron micrographs of samples: (a) M, (b) B, (c) Z, (d) S-M(1.6), (e) S-B(1.4) and (f) S-Z(1.8)

As we can observe, the optimum introduction of sulfonic groups was achieved with different amounts of sulfonating agent (CSPTMS) for each zeolite structure. Thus, for beta zeolite, the optimum amount of CSPTMS was 1.4, whereas for mordenite and ZSM-5 zeolites, the optimum CSPTMS amount was 1.6 and 1.8, respectively.

Taking into account that the main difficulty to introduce bulky organic species in zeolites is their microporous structure together with the lack of reactant silanol groups (≡Si-OH), [64] an important key to understand these good beta sulfonation results is the zeolite dealumination occurred under the acidic conditions used during sulfonation. It is well known that during dealumination, the loss of aluminum of the zeolite framework led to the formation of silanol groups. [97] We believe that these new silanol groups can react with the sulfonating agent to form the sulfonic groups (Scheme 3). This was confirmed by IR.

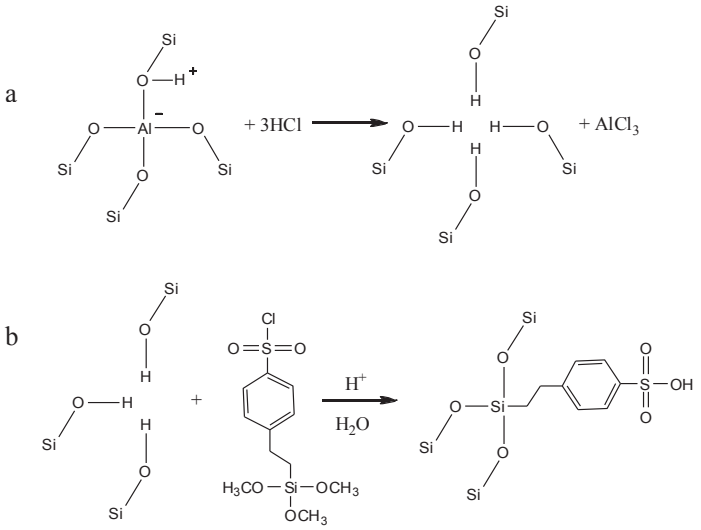

Scheme 3. a) Formation of silanols during dealumination in acidic medium and b) reaction of silanols with CSPTMS to form the sulfonating groups.

Fig. 87 shows the IR spectra of commercial beta, partially dealuminated beta, which was obtained by treatment of commercial beta in HCl 2M for 15 min at 373 K, and the sulfonated beta sample S-B(1.4).

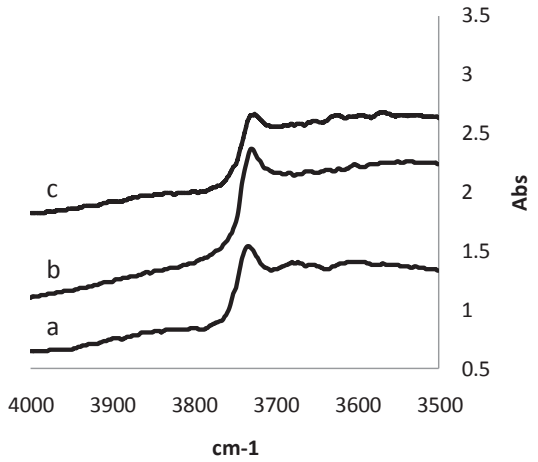

Figure 87. IR spectra of (a) B, (b) partially dealuminated B sample and (c) S-B(1.4).

As we can observe, after dealumination, there was a clear increase in the intensity of the silanol band (around 3745 cm^{-1}) whereas after sulfonation the silanol band decreased as a consequence of the reaction of the silanol groups formed during

dealumination with the sulfonating agent. Thus, zeolite beta, which is easier to dealuminate, can generate more silanol groups. Additionally, the arrangement and size of the pores in this zeolite allows a higher accessibility of the silanol groups to the sulfonating agent. This explains the lower amount of CSPTMS required to obtain the optimum extent of sulfonation for this zeolite. In the same way, mordenite is easier to dealuminate than ZSM-5, as commented above. This involves a higher formation of silanol groups in mordenite than in ZSM-5, and therefore, fewer amounts of CSPTMS (1.6) were necessary to obtain the optimum extent of sulfonation.

X-ray photoelectron spectroscopy (XPS) is useful for evaluating qualitatively the type of sulfur species and measuring quantitatively the sulfonic groups near the surface region. [77, 87] The S 2p XP spectra of the most representative sulfonated samples (not shown here) only showed one peak at ca. 168-169 eV associated with sulfate (S^{6+}) species due to sulfonic ($-SO_3H$) groups. [77, 87] Therefore, XPS confirmed sulfonation of zeolites in agreement with TGA results. The S/Si surface atomic ratio, calculated from XPS, was S-B(1.4) > S-Z(1.8) S-M(1.6) (Table 21) in agreement with the sulfur contents obtained by TGA (Table 20). The Si/Al surface atomic ratios, obtained from XPS, confirmed that beta suffered higher dealumination than mordenite and ZSM-5 during sulfonation.

XP spectra of several beta samples sulfonated at the same conditions with microwaves or by conventional heating again only showed one peak at ca. 168-169 eV associated to the sulfonic groups (not shown here). Moreover, the S/Si atomic ratios, calculated from XPS results, confirmed the similar sulfur contents obtained by TGA for CS-B(1.4)-30 min and S-B(1.4)-30 min.

Finally, the acidity of the zeolites, determined potentiometrically, agrees with the TGA results, since the sulfonated samples which had higher amounts of sulfonic groups, led to higher acidity, as expected (Table 20).

Table 21. Si/Al and S/Si atomic ratio calculated from XP spectra.

Catalyst	Si/Al atomic ratio[a]	S/Si atomic ratio
S-B(1.4)	69.1 (10.0)	0.062
S-Z(1.8)	19.8 (20.0)	0.055
S-M(1.6)	12.3 (6.5)	0.047
S-Mont (1.4)	4.5 (2.7)	0.061

[a] In parenthesis Si/Al ratio of the non-sulfonated commercial starting materials for comparison.*

Montmorillonite is a clay of the smectite group with general formula $[Si_8(Al_{4-x}Mg_x)(OH)_4O_{20}]M_{n+x/\ n}\cdot mH_2O$. These layered materials are microporous, as zeolites. Montmorillonite K-10 was used which derived from Montmorillonite that has been submitted to an acid treatment that provide a certain increase of porosity. There are not references in the literature about sulfonation of smectites with CSPTMS. Sulfonated montmorillonite maintained the starting smectite structure, as observed by XRD. After sulfonation, we observed a decrease of the surface area and the pore volume. This can be explained because of the introduction of sulfonic groups according to the sulfur content related to sulfonic groups, determined by TGA (Table 20), the S/Si surface atomic ratio obtained from XP spectrum (Table 21) and its higher acidity (Table 20) potentiometrically evaluated. This sample also exhibited slight dealumination after sulfonation (Table 21). The treatment acid used to obtain this sample can justifie this behaviour.

Catalytic Activity

Table 22, 23 and 24 show the catalytic activity results of beta, ZSM-5 and mordenite catalysts, respectively, for the etherification reaction of glycerol with isobutene. The reaction products obtained were mono-tert-butyl glycerol ether (MTBG), di-tert-butyl glycerol ether (DTBG) and tri-tert-butyl glycerol ether (TTBG). Besides, diisobutylene was detected in very low amounts for most of all the sulfonated samples.

*XP spectra were provided by Dra. Elena Taboada and Dr. Jordi Llorca from Universitat Politècnica de Catalunya

Table 22. Catalytic activity of Beta catalysts for the etherification of glycerol with isobutene after 4 h.

Catalyst	Conversion (%)	Selectivity to MTBG (%)	Selectivity to h-GTBE (%)[a]	DIB (wt.%)
B	44	32	68 (1)	5.3
S-B(0.7)	97	73	26 (1)	3.0
S-B(1)	93	60	40 (1)	1.9
S-B(1.4)	100	17	83 (15)	2
S-B(2.8)	98	33	67 (7)	1.0
B[a]	49	39	61 (2)	6.1
S-B(1.4)[a]	100	9	91 (36)	9.4
S-B(2.8) [a]	99	23	77 (18)	2.5
S-B-30min(1.4)[a]	99	29	71 (11)	0.6
CS-B-30min(1.4)[a]	96	45	55 (7)	1.1
S-B(1.4)[b]	100	10	90 (35)	9.3

MTBG: glycerol monoethers; h-GTBE: glycerol diethers + glycerol triether. In parenthesis, selectivity to glycerol triether (%). DIB: diisobutylene.
[a] Reaction time: 24 h
[b] Reaction time: 48 h

Zeolite Na-beta was more active and selective to h-GTBE than Na-ZSM-5 and Na-mordenite, as deduced by comparing the conversion values after 24 h of reaction (Table 22, 23 and 24). The differences in the activity between the three types of zeolites could be explained by the number of Brønsted acid sites (related to the Si/Al ratio) and their strength together with the higher accessibility of the reactants to the active sites in beta and ZSM-5 samples because of their three-dimensional pore structure compared with the one-dimensional pore structure of mordenite, as observed before when these zeolites were tested for the etherification of glycerol with tert-butanol. [Section 4.2.1] One important feature to remark is that triether was not detected for Na-mordenite or Na-ZSM-5 and in very low amounts (1%) for Na-Beta (Table 22). This has been attributed to steric hindrance effects because of the microporosity of the zeolites [156] but based on our previous results we believe that the formation of the glycerol triether can be mainly related to the presence of stronger Brønsted acid sites. [Sections 4.2.1-4.2.3]

All sulfonated zeolite catalysts showed higher conversion than their corresponding starting non-sulfonated zeolites due to the presence of the acid sulfonic groups. Sulfonated beta catalysts exhibited very high conversion (almost total) after just

4 h of reaction (Table 22). Selectivity to h-GTBE values increased when the acidity due to the sulfonic groups increased (Table 20). Thus, the best catalytic results were obtained with catalyst S-B(1.4), which showed total conversion and 83 % of selectivity to h-GTBE with 15 % of selectivity to the triether (Table 22). When this catalyst was tested at longer reaction time (24 h), the selectivity to h-GTBE improved until 91 % with 36 % of selectivity to the triether maintaining total conversion. This means that when glycerol conversion stopped the isobutene molecules remaining in the reaction medium react with monoethers and diethers formed previously evolving with time to higher selectivity to the di- and triether. At higher sulfur content (S-B(2.8)), the selectivity to h-GTBE decreased because of the lower acidity of the catalyst due to the excess of the sulfonating agent that are blocking the pores hindering the formation of the bulkier products, di- and triethers At higher reaction time (24 h), the selectivity to h-GTBE, and to the triether of this catalyst increased, following the same tendency to that observed for S-B(1.4). However, at 48 h of reaction, the selectivity values practically did not change.

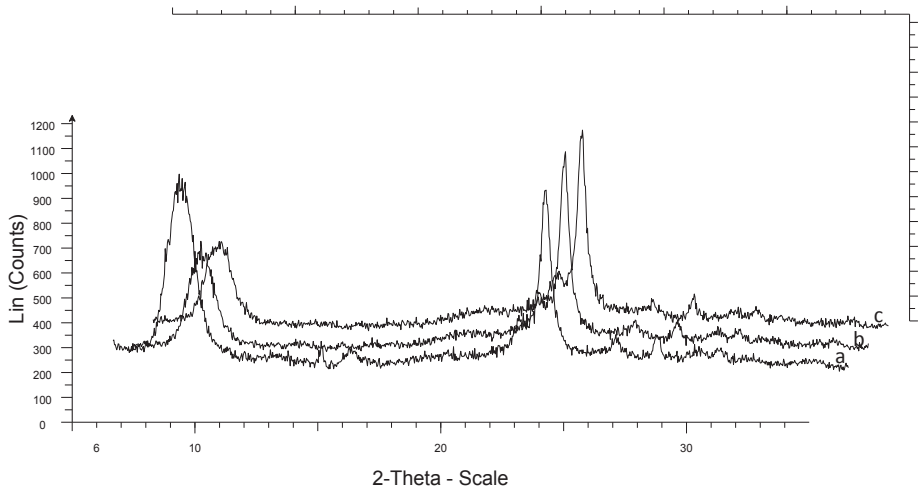

Figure 88. XRD patterns of (a) S-B(1.4) before reaction, (b) S-B(1.4) after 4 h of reaction and (c) S-B(1.4) after 24 h of reaction.

Fig. 88 showed the XRD patterns of catalyst S-B(1.4) before reaction and after reaction at 4 h and 24 h, respectively whereas Fig. 89 exhibits their N_2 adsorption-desorption isotherms. As we can observe, XRD did not show significant changes in the zeolite structure after reaction except for some decrease in the crystallinity. However, N_2 adsorption-desorption isotherms clearly showed a decrease of the adsorbed volume, and consequently, of the surface area after reaction. From these results, we can conclude that there is not collapse of the structure during reaction, but blocking of pores by reaction products.

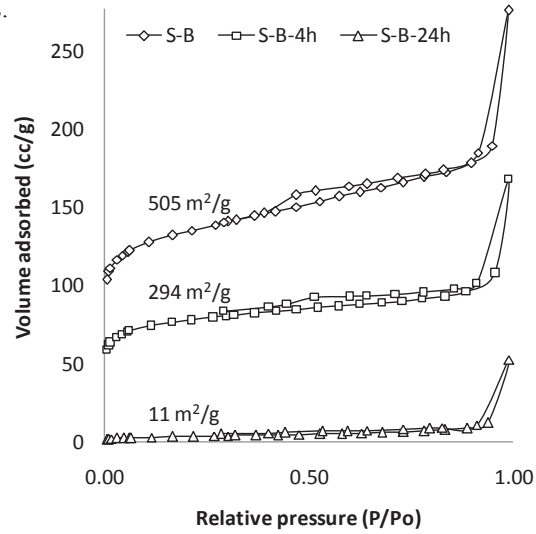

Figure 89. Nitrogen adsorption-desorption isotherms of (a) S-B(1.4) before reaction, (b) S-B(1.4) after 4 h of reaction and (c) S-B(1.4) after 24 h of reaction.

By comparing beta catalysts sulfonated with microwaves with those sulfonated by conventional heating at the same conditions, we observed that conversion was slightly higher while selectivity to h-GTBE and to the triether was clearly higher for the samples functionalised with microwaves. This can be related to the presence of higher amounts of external silanol groups, obtained for microwaved samples as commented before, which can be more accessible to the reagents.

Table 23. Catalytic activity of ZSM-5 catalysts for the etherification of glycerol with isobutene after 24 h.

Catalyst	Conversion (%)	Selectivity to MTBG (%)	Selectivity to h-GTBE (%)	DIB (wt.%)
Z	19	83	17 (0)	0
S-Z(0.7)	50	86	14 (2)	5.5
S-Z(1.4)	54	92	9 (0)	0.1
S-Z(1.8)	100	16	84 (28)	3.9
S-Z(0.7)[a]	37	90	10 (0)	0.9
S-Z(1.8)[a]	99	28	72 (9)	1.2
S-Z(1.8)[b]	98	17	83 (24)	4.5

MTBG: glycerol monoethers; h-GTBE: glycerol diethers + glycerol triether. In parenthesis, selectivity to glycerol triether (%). DIB: diisobutylene.
[a] Reaction time: 4 h
[b] Reaction time: 48 h

Regarding the catalytic activity of sulfonated ZSM-5 catalysts, the best catalytic results were obtained at 24 h of reaction with catalyst S-Z(1.8) with total conversion, selectivity to h-GTBE of 84 % and selectivity to the triether of 28 % (Table 23). These results can be explained by the higher acidity of this catalyst because of the presence of higher amounts of sulfur content due to the sulfonic groups (Table 20). At shorter or longer reaction times, the catalytic results did not improve. On the whole, these sulfonated ZSM-5 catalysts had lower conversion and lower selectivity to the desired products than sulfonated beta catalysts. It is important to note that beta catalysts achieved good catalytic results at lower reaction time than ZSM-5 catalysts. This can be related to the pore sizes and arrangement since beta has a 12-ring three-dimensional pore system and is a very flexible structure, as commented above, whereas ZSM-5 has a 10-ring three-dimensional pore system.

Table 24. Catalytic activity of mordenite catalysts for the etherification of glycerol with isobutene after 48 h.

Catalyst	Conversion (%)	Selectivity to MTBG (%)	Selectivity to h-GTBE (%)	DIB (wt.%)
M	37	84	16 (0)	0
S-M(1.4)	95	51	49 (8)	3.3
S-M(1.6)	99	21	79 (21)	1.6
S-M(1.8)	94	61	39 (7)	3.4
S-M(2.2)	98	50	50 (5)	3.7
S-M(1.6)[a]	71	73	27 (0)	0.7
S-M(1.8)[a]	34	95	5 (0)	0
M[b]	15	92	8 (0)	0

MTBG: glycerol monoethers; h-GTBE: glycerol diethers + glycerol triether. In parenthesis, selectivity to glycerol triether (%). DIB: diisobutylene.
[a] Reaction time: 4 h
[b] Reaction time: 24 h

Finally, sulfonated mordenite catalysts required 48 h of reaction to achieve almost total conversion and the highest selectivity to h-GTBE and to the triether values (79 % and 21 %, respectively) (Table 24). At lower reaction times, conversion and selectivity to h-GTBE were lower and TTBG was not detected. These results confirmed that depending on the zeolite structure, the diffusion of the reactants through the pores could be slower or faster. Thus, mordenite, which has a one-dimensional pore system, needs longer times of reaction to favour the accessibility of the reagents to the acid sites than ZSM-5 or Beta, which have three-dimensional pore systems.

Commercial montmorillonite K-10 showed high conversion but low selectivity to h-GTBE. However, after sulfonation, besides the increase of conversion, a high selectivity to h-GTBE was obtained from 4 h of reaction doubling the selectivity to TTBG after 24 h of reaction (Table 25).

Table 25. Catalytic activity of montmorillonite catalysts for the etherification of glycerol with isobutene after 24 h.

Catalyst	Conversion (%)	Selectivity to MTBG (%)	Selectivity to h-GTBE (%)[a]	DIB (%)
Mont	90	69	30 (1)	0.3
S-Mont(1.4)	100	16	84 (28)	4.5
S-Mont(1.4)[a]	99	16	84 (14)	15

MTBG: glycerol monoethers; h-GTBE: glycerol diethers + glycerol triether. In parenthesis, selectivity to glycerol triether (%). DIB: diisobutylene.
[a] Reaction time: 4 h

From these results, we can conclude that microporosity of the zeolites and smectites can be overcame increasing the number and, especially, the strength of the Brønsted acid sites together with the use of the appropriate reaction times that facilitate the diffusion of the reactants through the pores.

Conclusions

Three commercial Beta, ZSM-5 and mordenite zeolites and one commercial montmorillonite were successfully sulfonated by one-step simple method using microwaves.

The highest incorporation of sulfonic acid groups was achieved with different amounts of sulfonating agent for each structure. This has been explained by the different dealumination degree suffered by the starting samples at the acidic conditions used during sulfonation since higher dealumination involved the formation of higher amounts of silanol groups that can react with the sulfonating agent to form the sulfonic groups. Additionally, we observed that the arrangement and size of the pores also affected the accessibility of the silanol groups to the sulfonating agent.

The presence of the sulfonic groups, which led higher number and strength of Brønsted acid sites than those of the starting commercial materials, resulted in high active and high selective to h-GTBE catalysts, in spite of their microporosity, for the etherification of glycerol with isobutene. The optimised catalytic results were obtained by beta sulfonated with 1.4 g of sulfonating agent with total conversion and 91 % of selectivity to h-GTBE with 36 % of TTBG after 24 h of reaction followed by ZSM-5 sulfonated with 1.8 g of sulfonating and montmorillonite sulfonated with 1.4 g of sulfonating agent both with total conversion and 84 % of selectivity to h-GTBE with 28

% of TTBG after 24 h of reaction. Finally, mordenite sulfonated with 1.6 g of sulfonating agent led 99 % of conversion and 79 % of selectivity to h-GTBE with 21 % of TTBG after 48 h of reaction.

The size and arrangement of the pores also influenced in the catalytic results. Thus, sulfonated mordenite catalysts required higher reaction time than the other catalysts to achieve the optima conversion and selectivity to h-GTBE values. This can be related to the one-dimensional pore system of the mordenite, which difficult the accessibility of the reactants to the acid sites. Moreover, we observed higher selectivity to h-GTBE with a optimised sulfonated beta catalyst that had less acidity than a optimised sulfonated ZSM-5 catalyst at the same reaction conditions although both zeolites have tridimensional structure. This has been explained by the higher pore size and flexibility of the beta zeolite structure that favour the diffusion of the reactants. This was confirmed by the good catalytic results obtained for sulfonated beta catalysts from 4 h of reaction.

Therefore, microporosity of zeolites and smectites can be overcame increasing the number and strength of acid sites together with the use of the appropriate reaction times that facilitate the diffusion of the reactants through the pores.

Acknowledgments

The authors are grateful for the financial support of the Ministerio de Ciencia e Innovación and FEDER funds (CTQ2008-04433/PPQ). Dolores González acknowledges Ministerio de Educación y Ciencia for a FPU grant (AP2007-03789).

4.2.5 Successfully conventional and microwave-assisted preparation of sulfonic acid-functionalized aerogels and liogels by a simple post-synthesis method

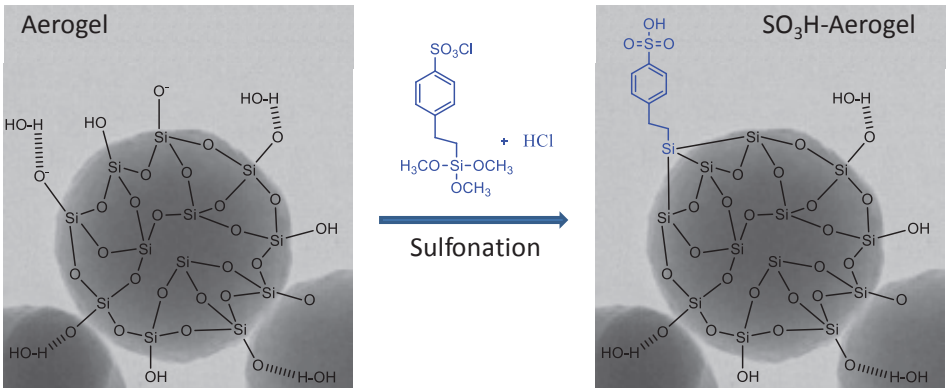

Abstract

For the first time, silica aerogels and liogels were successfully sulfonated in one step by a simple post-synthesis method using microwaves as well as conventional heating. The use of microwaves allowed us the introduction of higher amounts of sulfonic groups in the silicas, according to the higher S/Si atomic ratio, determined by XPS, higher sulfur content due to sulfonic groups, determined by TGA, lower surface area and higher acidity observed for the microwaved-sulfonated samples. Sulfonated aerogels were much more active and selective to h-GTBE (glycerol di- and tri-ethers) than sulfonated liogels for the acid-catalyzed etherification of glycerol with isobutene. This was related to the higher content of sulfonic groups, which led to higher and stronger Brønsted acidity, incorporated in aerogels due to their higher porosity. Interestingly, this higher porosity also avoided the partial blocking of the pores by the reaction products observed when microporous catalysts were tested for this reaction.

Introduction

Nanoporous materials can be applied for a wide range of applications, including energy storage and conversion, nanoeletronics or catalysis. [181]

Aerogels are unique low-density, open-cell porous materials consisting of submicrometer pores and ligaments that can be used as robust material platform for design novel nanoporous materials. Aerogels have a unique microstructure that consists of a branched skeleton of interlinked nanoparticles surrounding pores that are tens of nanometers in size. Characteristic properties of silica aerogels are high porosity and large surface areas, which make this material very appropriate for catalytic purposes, [181-186] besides low density, low thermal conductivity, high temperature stability and low dielectric constant.

Silica aerogels are usually synthesized by sol-gel chemistry to form solvent filled gels, which are then dried under supercritical conditions. [184-185] When the silica alcogels are dried by liophilization, silica liogels can be obtained. [187] Liogels also have high surface areas but lower and narrower pore size distribution. There are not references about the use of liogels in catalysis.

Sulfonic acid-functionalization of aerogels and liogels can generate effective solid acid catalysts with enhanced catalytic properties due to the increase of the number and strength of Brønsted acid sites through the incorporation of sulfonic groups. There is just one study about functionalization of silica aerogel with chlorotrimethylsilane (CTMS), which was added during the synthesis of the aerogel prior to supercritical extraction. This procedure involved many consecutive longer steps starting with solvent exchanges in ethanol (48 h) and hexane (24 h) followed by exposure to CTMS for 72 h to promote functionalization. [188] There are not references about the post-synthesis sulfonic acid-funcionalization of aerogels or liogels in one step.

Moreover, the use of microwaves for the synthesis or modification of materials is becoming an important tool to reduce the synthesis time, with the subsequent energy saving, and to modify the sample properties, which can be of interest for catalysis. [132, 171, 189] However, there are no studies about the use of microwaves for the sulfonation of aerogels or liogels.

Recently, special attention is focused in the obtention of di- and tri-tertiary butyl ethers of glycerol, the so-called “higher ethers” (h-GTBE), by catalytic etherification of glycerol (glycerine, 1,2,3-propanetriol) with tert-butanol or isobutene in the presence of

acid catalysts. [5, 155-158] h-GTBE can be used as oxygenated fuels replacing the highly toxic to the environment methyl tertiary butyl ether (MTBE) and reducing remarkably the emissions of particulate matter, hydrocarbons, CO and unregulated aldehydes in the exhaust gases. [144-145] Moreover, this reaction constitutes a valuable green process since it allows the revalorization of glycerine, which is formed as by-product in considerable amounts during biodiesel production (10% wt % of the total product). [2-3, 11]

For the first time, we report the post-synthesis sulfonation of aerogels and liogels by a simple one-step method using microwaves as well as conventional heating. Samples were widely characterized by XRD, N_2 physisorption, TGA, XPS, ^{29}Si NMR, FTIR and potentiometric titration techniques. Sulfonated aerogels and liogels were tested as catalysts for the acid-catalyzed etherification of glycerol with isobutene to obtain selectively h-GTBE.

Experimental

Silica gels were synthesized by the sol-gel method [90] based on the hydrolysis and condensation of a silicon alkoxide, in our case tetramethoxysilane (TMOS).

TMOS was first dissolved in ethanol and stirred magnetically. Then, an aqueous solution of NH_3 0.65 M was added dropwise. The resulting solution, called sol, was stirred during 10 minutes, then poured into plastic tubes and closed to avoid the solvent evaporation. After 40 minutes they gelified, giving rise to colourless and transparent alcogels. Additionally, some extra ethanol was added to the gels to avoid their drying. The TMOS/H_2O/EtOH molar ratio was 1/4/12.25.

The silica alcogels were dried following one of these two methods: lyophilisation or supercritical drying. [190] The lyophilisation required a pre-treatment of the alcogels: the ethanol inside the gel pores had to be exchanged by water. This was done by immersing the alcogels in water baths and changing the water at least 4 times during two days. The resulting hydrogels were then frozen in liquid nitrogen and connected to a lyophilisator, to reduce the pressure down to 0.05 mbar. The frozen water inside the silica pores was sublimated. The final material was a white and fluffy powder, denoted as liogel (LG). On the other hand, the supercritical drying consisted of placing the wet gels inside an autoclave and increasing the pressure and temperature over the supercritical point of ethanol (543 K, 200 bar). Then, the autoclave was depressurized,

venting out the ethanol. The final materials, aerogels (AG), were transparent and very light monoliths.

Aerogel and liogel were sulfonic acid-functionalized in one step by a simple method. Thus, 2 g of aerogel or liogel were treated with 1.4 g of 2-(4-chlorosulfonylphenyl) ethyltrimethoxysilane (CSPTMS) solution in methylene choride (50 wt %, Gelest) in 2 M HCl solution at 313 K for 2 h using microwaves (Milestone Ethos-Touch Control equipped with a temperature controller) (SMw-AG(1.4) and SMw-LG(1.4)) or conventional heating (SC-AG(1.4) and SC-LG(1.4)). Two more sulfonated aerogel samples were prepared with microwaves by using lower (0.7) and higher (2.8) amounts of CSPTMS (SMw-AG(0.7) and SMw-LG(2.8)) All samples were filtered, washed with deionised water and dried overnight.

XRD patterns were obtained with a Siemens D5000 diffractometer. BET areas were calculated from N_2 adsorption isotherms using a Quadrasorb SI surface analyser. TGA were performed with a TA instruments equipment from 323 K to 1073 K at 10K/min under airflow. X-ray photoelectron spectra were taken with a SPECS system equipped with an Al anode XR50 source and a Phoibos 150 MCD-9 detector with pass energy of 25 eV at 0.1 eV steps at a pressure below $6 \cdot 10^{-9}$ mbar. Acid capacities were determined potentiometrically using 2 M NaCl as cationic-exchange agent, and a dropwise addition of 0.01 NaOH as titration agent.

Etherification experiments were performed in the liquid phase in a stainless steel stirred autoclave (150 mL) equipped with temperature controller and a pressure gauge. Stirring was fixed for all experiments at 1200 rpm to avoid external diffusion limitations. Liquid phase pressurized isobutene (glycerol/isobutene molar ratio of 0.25) was injected into the reactor, previously charged with glycerol and catalyst (0.5 g), using nitrogen at 10 bar as pushing agent. The temperature was then raised to 75 ºC and the pressure increased accordingly following the liquid-vapour equilibrium. Catalytic experiments were made at 4, 24 and 48 h. The reaction products were analyzed by gas chromatography using a chromatograph model Shimadzu GC-2010 equipped with a SupraWax-280 column and a FID detector.

Glycerol conversion and selectivity to MTBG (glycerol monoethers) were determined from calibration lines obtained from commercial products. For DTBG (glycerol diethers) and TTBG (glycerol triether), which were not available commercially, we isolated them from the products of the etherification reaction by column chromatography (1:9 ethyl acetate/hexane) and identified them by ^{13}C and ^{1}H

NMR for proper quantification with the assistance of the characterization data reported by Jamróz et al. [96]

Results and Discussion

X-ray diffraction (XRD) patterns of the sulfonated samples were very similar to those of their starting materials showing a typical amorphous structure.

N_2 adsorption-desorption isotherm of the initial non-sulfonated aerogel (AG) was mainly of type II (Fig. 90a) corresponding to macroporous materials, as confirmed in the pore size distribution graphic (Fig. 90b) where some mesoporosity was also observed. On the other hand, N_2 adsorption-desorption isotherm of the initial non-sulfonated liogel (LG) (Fig. 90a) was of type IV associated to mesoporous materials, as observed in the pore size distribution graphic (Fig. 90b)

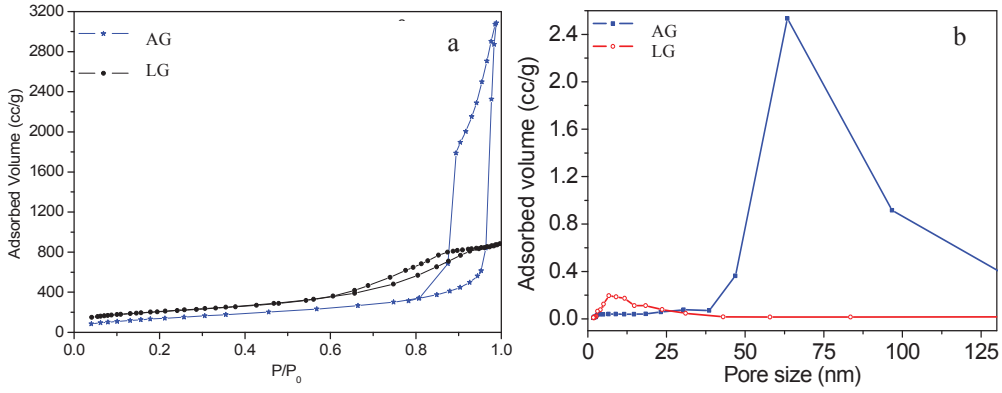

Figure 90. a) N_2 adsorption-desorption isotherms and b) pore size distribution of samples AG and LG.*

* N_2 physisorption results were provided by Dra. Elena Taboada and Dr. Jordi Llorca from Universitat Politècnica de Catalunya

After aerogel sulfonation, there was a considerable decrease of the adsorbed volume and in the pore size, more marked for the sample sulfonated with microwaves (Fig. 91b). Thus, N_2 adsorption-desorption isotherms of the sulfonated samples were mainly of type IV attributed to mesoporous materials (Fig. 91a). These variations can be related to the incorporation of the sulfonic groups.

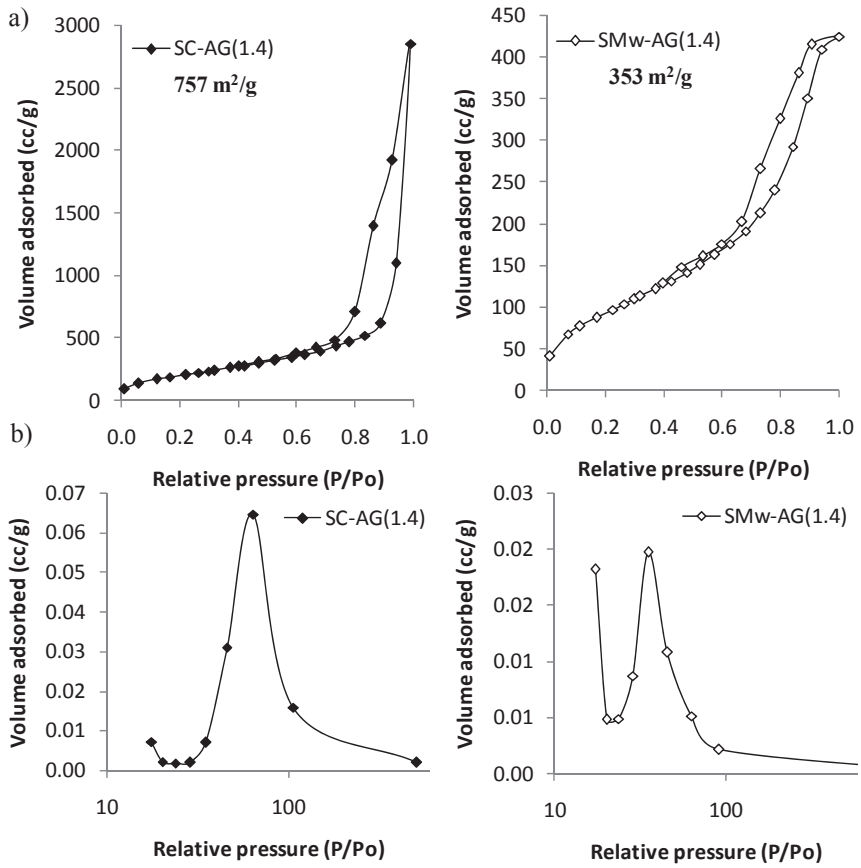

Figure 91. a) N_2 adsorption-desorption isotherms and b) pore size distribution of samples SMw-AG(1.4) and SC-AG(1.4).

After liogel sulfonation, there was a slight decrease of the adsorbed volume and in the pore size, due to the incorporation of the sulfonic groups. This variation again appeared more marked for the sample sulfonated with microwaves (Fig. 92a and b),

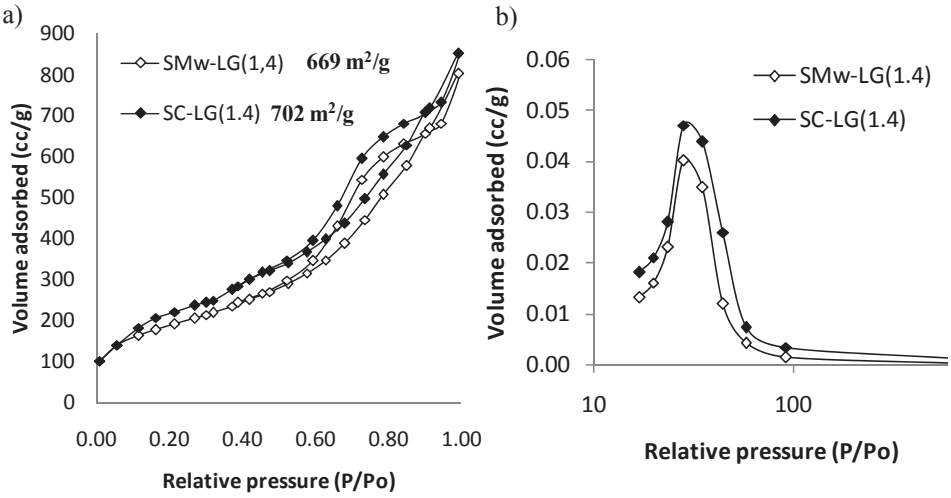

Figure 92. a) N_2 adsorption-desorption isotherms and b) pore size distribution of samples SMw-LG(1.4) and SC-LG(1.4).

X-ray photoelectron spectroscopy (XPS) is useful for evaluating qualitatively the type of sulfur species and measuring quantitatively the sulfonic groups near the surface region. [77, 87] The S 2p XP spectra of the sulfonated aerogels and liogels samples only showed one peak at ca. 168-169 eV associated with sulfate (S^{6+}) species due to sulfonic ($-SO_3H$) groups, [77, 87] with higher intensity for the microwaved samples (e.g. Fig. 93), as confirmed by regarding the S/Si atomic ratios calculated from XP spectra.

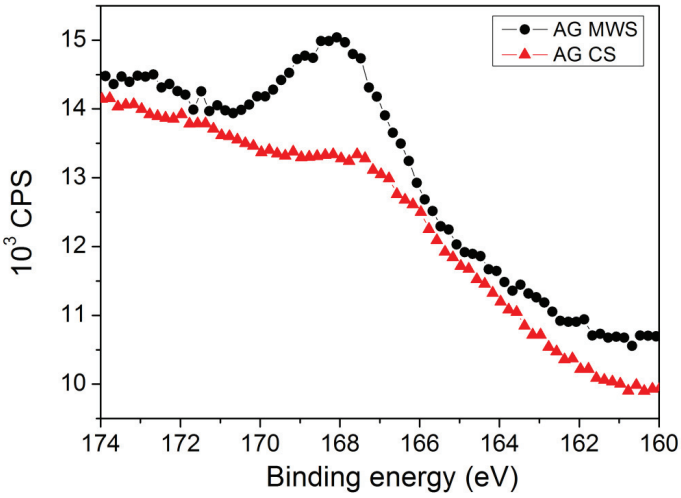

Figure 93. XP spectra of samples SC-AG(1.4) (conventional heating) and SMw-AG(1.4) (microwaves) in the S 2p core level region.*

Therefore, the use of microwaves for the sulfonation of aerogels or liogels allowed the introduction of higher amounts of sulfonic groups in the silica than conventional heating, according to the higher S/Si atomic ratio, higher sulfur content due to sulfonic groups, determined by TGA, [83] lower BET area and higher acidity observed for the samples sulfonated with microwaves (Table 26).

Table 26. Characterization of the samples

Samples	S/Si atomic ratio [a]	Sulfur content[b]	BET area (m^2/g)	Pore volume (cc/g)	Acid capacity[c]
AG	---	---	526	4.77	---
SC-AG(1.4)	0.003	0.05	759	4.50	0.06
SMw-AG(1.4)	0.03	0.22	353	0.62	0.24
SMw-AG(0.7)	--	0.04	537	3.20	0.03
SMw-AG(2.8)	--	0.27	211	0.48	0.30
LG	---	---	751	1.60	---
SC-LG(1.4)	--	0.03	702	1.47	0.02
SMw-LG(1.4)	--	--	669	1.16	0.05

[a] Determined from XPS; [b] (mmol organic sulfonic group/g sample) calculated from TGA; [c] Acid capacity obtained by potentiometric titration (meq H^+/g).

*XP spectra were provided by Dra. Elena Taboada and Dr. Jordi Llorca from Universitat Politècnica de Catalunya

^{29} Si NMR spectra of aerogel and liogel samples showed two peaks related to the siloxane [Q^n = $Si(OSi)_n(OH)_{4-n}$, n=2-4; Q^3 at -100 ppm; Q^4 at -110 ppm] species (Fig. 88). After sulfonation, two additional peaks appeared corresponding to the organosiloxane [T^m = $RSi(OSi)_m$-$(OH)_{3-m}$, m=1-3; T^3 at -65 ppm and T^2 at -57 ppm] species introduced during sufonation, with higher intensity for the microwaved samples (not show here). This confirmed the acid sulfonic functionalization of the samples in agreement with the XPS and TGA results commented above.

The higher content of sulfonic groups introduced in the aerogel with respect to the liogel sample using microwaves as well as conventional heating (Table 26) can be explained by the large pore size (meso-,macropores) of aerogel, and therefore, the higher accessibility of the sulfonating agent to the silanol groups (Scheme 4).

Sulfonation of aerogel with lower or higher amounts of sulfonating agent (CSPTMS) with microwaves (SMw-AG(0.7) and SMw-AG(2.8)) did not increase the incorporation of sulfonic groups, as confirmed by the lower sulfur content and lower acidity observed for both samples when compared with SMw-AG(1.4) (Table 26). For SMw-AG(0.7) the amount of CSPTMS was not enough to sulfonate all the available silanols whereas for SMw-AG(2.8) the excess of sulfonating agent partially blocked the pores. This explains the BET area values obtained for both samples.

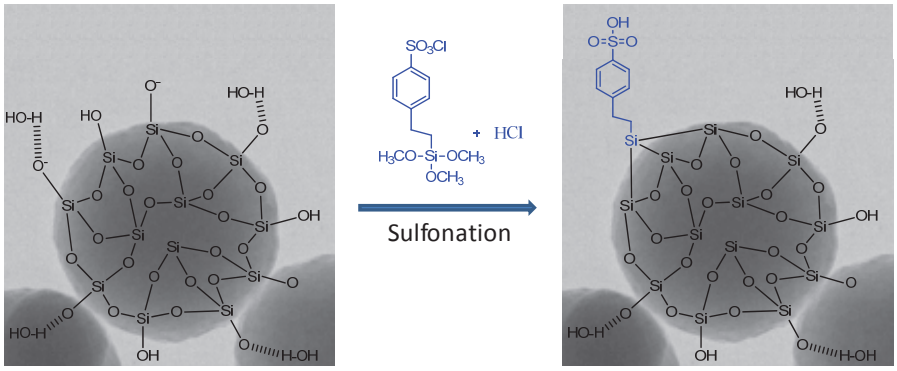

Scheme 4. Reaction of silanols with CSPTMS to form the sulfonating groups.

Table 27 shows the catalytic results for the etherification of glycerol with isobutene. The reaction products obtained were mono-tert-butyl glycerol ether (MTBG), di-tert-butyl glycerol ether (DTBG) and tri-tert-butyl glycerol ether (TTBG). Besides, diisobutylene was detected in very low amounts for sulfonated aerogel samples.

Table 27. Catalytic results for the glycerol etherification with isobutene

Catalysts	Conversion (%)	Selectivity to MTBG[a] (%)	Selectivity to h-GTBE[b] (%)
AG	53	83	17 (0)
SC-AG(1.4)	96	56	39 (4)
SMw-AG(1.4)	99	25	75 (17)
SMw-AG(0.7)	72	78	22 (0.1)
SMw-AG(2.8)	97	41	59 (7)
LG	0	--	--
SC-LG(1.4)	37	100	0
SMw-LG(1.4)	57	87	13 (0.3)

[a] MTBG: glycerol monoethers; [b] h-GTBE: glycerol diethers + glycerol triether. In parenthesis, selectivity to glycerol triether (%).

After 24 h of reaction, AG showed moderate conversion but low selectivity to h-GTBE whereas LG was not active for this reaction. These results can be related to the low acidity of these materials.

However, acid-functionalized aerogels and liogels were more active due to the presence of the sulfonic groups. Sulfonated aerogels showed much higher conversion (almost total) and much higher selectivity to h-GTBE than sulfonated liogels. Besides, the glycerol triether was formed in sulfonated aerogels but only in very low amounts for sulfonated liogels. These results can be mainly explained by the lower acidity of the sulfonated liogels (Table 26).

Aerogel sulfonated with the optimum amount of CSPTMS with microwaves (SMw-AG(1.4)) exhibited the best catalytic result with 99 % of conversion and 75 % of selectivity to the desired product, h-GTBE. This agrees with the higher acidity, due to the incorporation of higher amounts of sulfonic groups, obtained for this sample (Table 26). This catalytic result was comparable to that obtained, in a previous work, with one acid ion-exchange resin, Amberlyst-15, [Section 4.2.3] which is a typical acid catalyst often used for this reaction.

Regarding the catalytic results of the aerogels sulfonated with lower or higher amounts of sulfonating agent than 1.4 g, we observed lower conversion and lower selectivity to h-GTBE, as expected, due to their lower acidity, for the sample sulfonated with lower CSPTMS amounts and to the less accessibilities to the acid sites for the sample sulfonated with higher sulfonating agent amount due to the partial blockage of pores because of the excess of sulfonating agent.

Figure 94 shows the N_2 adsorption-desorption isotherms of the sample SMw-AG(1.4) before and after reaction.

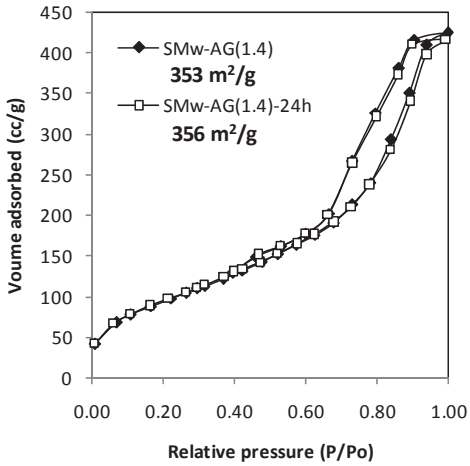

Figure 94. N_2 adsortion-desorption isotherms of the sample SMw-AG(1.4) before and after 24 h of reaction.

Interestingly, after 24 h of reaction, this sample did not show appreciable changes in the N_2 adsorption-desorption isotherms and in the BET area values. This means that the higher porosity of aerogels avoids the partial blocking of pores by the reaction products formed during the etherification reaction in contrast with other microporous materials, which showed a considerable decrease of the surface area after reaction. [Section 4.2.1 and Section 4.2.4]

Conclusions

Silica aerogels and liogels were successfully sulfonated in one step by a simple post-synthesis method using microwaves as well as conventional heating. The incorporation of the sulfonic groups was much higher in aerogels than in liogels because of their higher porosity, which favoured the accessibility of the sulfonating agent to the silanols groups to form the sulfonic groups. Samples sulfonated with microwaves showed higher incorporation of sulfonic groups than those sulfonated by conventional heating according to the higher S/Si atomic ratio, higher sulfur content, lower surface area and higher acidity observed for the microwaved-sulfonated samples.

Sulfonated aerogels were much more active and selective to h-GTBE (glycerol di- and tri-ethers) than sulfonated liogels for the acid-catalyzed etherification of glycerol

with isobutene. This was related to the higher content of sulfonic groups, which led to higher and stronger Brønsted acidity. The best catalytic result was achieved with aerogel sulfonated with the optimum sulfonating agent amount, which yielded almost total conversion and high selectivity to h-GTBE (75 %). The large meso-, macropores of aerogel also avoided the partial blocking of the pores by the reaction products observed when microporous catalysts were tested for this reaction.

Acknowledgments

The authors are grateful for the financial support of the Ministerio de Ciencia e Innovación and FEDER funds (CTQ2008-04433/PPQ and CTQ2009-12520). M.D.G. acknowledges FPU grant AP2007-03789. J.L. is grateful to ICREA Aca

4.2.6 Synthesis of modified MCM-41, SBA-15 and HMS to be used as catalysts for the catalytic etherification of glycerol with isobutene

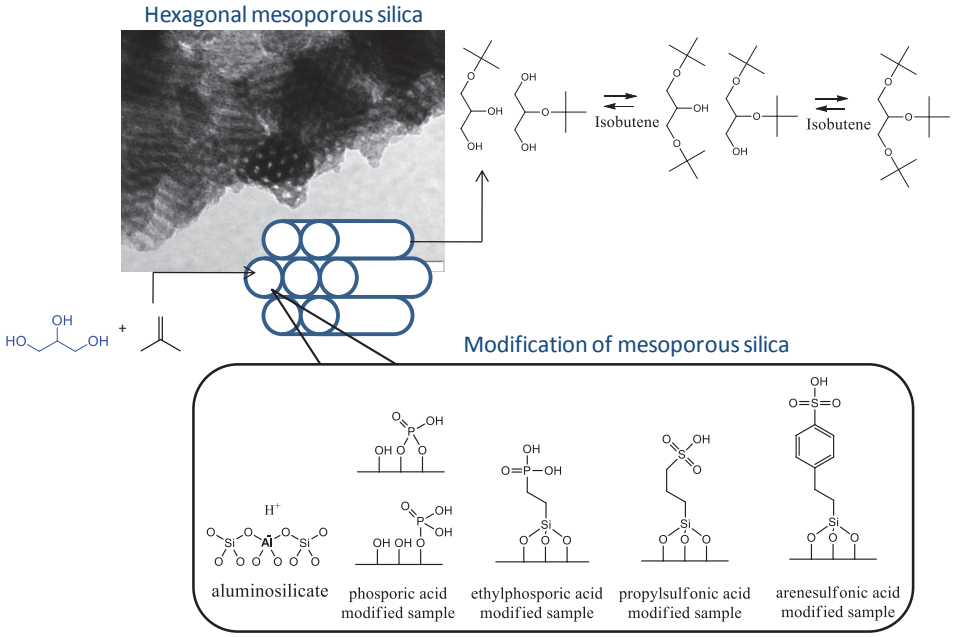

Abstract

MCM-41, SBA-15 and HMS were modified by the incorporation of aluminium, phosphoric and sulfonic acid groups to generate Brønted acid site which can be active for glycerol etherification. Mesoporous aluminosilicates and phosphoric acid-functionalized samples showed lower catalytic activity whereas sulfonic acid-functionalized HMS, which had complementary textural porosity, exhibited higher conversion (100%) and higher selectivity to di- and tri-ethers (84%). This confirms the important role of the strength of Brønsted acid sites. The degree of complementary textural porosity in mesoporous silica HMS depended on the surfactant used during the synthesis. Moreover, the generation of textural mesoporosity reduced diffusion limitations and, consequently, increased the incorporation of sulfonic groups into HMS.

Introduction

The catalytic etherification of glycerol, in the presence of tert-butanol or isobutene, to obtain di- and tri- tertiary butyl ethers of glycerol (h-GTBE) has been extensively investigated. [5,153-163] h-GTBE can be used as oxygenated fuels replacing the highly toxic to the environment, methyl tertiary butyl ether (MTBE), and reducing remarkably the emissions of particulate matter. [2] In the first studies, the best catalysts reported for glycerol etherification (with isobutene or tert-butanol) were strong acid ion-exchange resins (Amberlyst type). Mesoporous silicas functionalized with organosulfonic acid groups, introduced by conventional heating, have been tested as catalysts for the glycerol etherification with isobutene resulting in high conversion and moderate selectivity values to h-GTBE. [158]

Interestingly, in a previous study, we prepared a organosulfonic acid-functionalized SBA-15 with microwaves. This catalyst yielded total conversion and 91 % of selectivity to h-GTBE, with 36 % of selectivity to the glycerol triether, at 4 h of reaction for the etherification of glycerol with isobutene. [181] The catalytic results were better than those obtained with the corresponding sample sulfonated by conventional heating. [181] Besides, the selectivity values were much higher than those obtained by using a macroporous acid-ion exchange resin (Amberlyst-15) as catalyst for this reaction. From these results, we concluded that the acidity strength significantly influenced in the formation of di- and specially tri-ethers of glycerol, independently of the porosity of the catalysts. However, the accessibility of the reactants to the acid sites must be guaranteed so that they can act.

Apart from the study of organosulfonic acid-functionalized SBA-15, there are not references about the use of other mesoporous silicas, such as MCM-41 or HMS modified by incorporation of Al, phosphorus species or sulfonic groups, as catalysts for glycerol etherification.

The incorporation of Al into the walls of MCM-41 or SBA-15 generates active sites for adsorption, ion exchange and catalysis as aluminosilicate zeolites. Zeolites are extensively applied as catalysts, adsorbents and ion exchanges but their microporosity limits their applications to small molecules, and not larger organic or biological molecules. Mesoporous molecular sieves have attracted much interest because of their potential application in reactions or separations involving bulky molecules.

Aluminium is usually introduced into MCM-41 and SBA-15 by direct synthesis [191-192] or by post-synthesis grafting methods. [193-194] In general, the extremely acidic medium for SBA-15 synthesis does not favour the introduction of Al into the "framework" or wall, since Al species are very soluble at these synthesis condition.

Another alternative to improve the acidity in mesoporous materials and zeolites is to introduce phosphorus species. S. Kawi proposed their incorporation by impregnating MCM-41 in H_3PO_4 solution. [76] More recently, J. C. McKeen and co-workers incorporated organic sulfonic, carboxylic and phosphoric acid groups into zeolite Beta, MCM-41 and MCM-48. [63]

HMS is a hexagonal mesoporous silica which shows significant differences with MCM-41. HMS can exhibit complementary mesopores, in addition to framework pores. The textural mesopores are important because they greatly facilitate mass transport to the framework. For this reason the catalytic reactivity of HMS is usually superior to MCM-41, specially for reactions involving large substrates in a liquid reaction medium where the reaction rates are limited by diffusion. [21-22] It is now apparent that the degree of textural mesoporosity is quite sensitive to both the solvent and the nature of the S^o surfactant used in the synthesis of HMS. [22]

The aim of this work was to generate Brønsted acid sites with different strength in mesoporous silicas to be tested as catalysts for the glycerol etherification with isobutene. We modified their acidic properties by a) incorporation of aluminium during the synthesis or post-synthesis of MCM-41 and SBA-15, b) incorporation of phosphorus species in MCM-41 and SBA-15, c) sulfonation by direct synthesis of MCM-41 and d) post-synthesis sulfonation of mesoporous silica HMS.

Experimental

Catalysts preparation

Synthesis of mesoporous aluminosilicates: Al-MCM-41 and Al-SBA-15

Direct synthesis: Tetramethylammonium hydroxide (TMAOH) and cetyltrimethylammonium bromide (CTAB) were dissolved in distilled water by stirring at 308 K. Fumed silica and aluminium isopropoxide were added to the template solution under stirring for 1 h to have a composition of 1 Si: x Al: 0.25 CTAB: 0.2 TMAOH: 40 H_2O (where x=0.1, 0.05 or 0.025). After further stirring for 1 h the resulting gel was aged at room temperature for 20 h. Then, the gel was transferred to a teflon autoclave and heated at 423 K for 48 h. The solid was filtered, washed, dried in air at room temperature, and calcined at 823 K for 8 h. Sample were denoted as Al-MCM-41(40), Al-MCM-41(20) and Al-MCM-41(10), in parenthesis Si/Al ratio. *Post-synthesis:* Pure silica MCM-41 was also prepared using the procedure described above except but without Al. For alumination, 1.0 g of calcined pure silica MCM-41 was added to 50 ml hexane(dry) containing the required amount of aluminium isopropoxide and stirred at room temperature for 24 h. The resulting powder was obtained by filtration, washed with dry hexane, dried at room temperature and calcined at 823 K for 4 h (Al-MCM-41(5)-ps sample, in parenthesis Si/Al ratio).

Direct synthesis: Al-SBA-15 was prepared by adding 4.0 g triblock copolymer poly(ethylene glycol)-block-poly(propylene glycol)-block-poly(ethylene glycol) ($EO_{20}PO_{20}EO_{20}$) to a solution of 25 g HCl (35% wt.-%) and 125 g water under stirring. After stirring for 2 h, the copolymer was completely dissolved after which 8.6 g TEOS and $Al(O\text{-}i\text{-}Pr)_3$ were added. Following continuous stirring at 313 K for 20 h, the reaction mixture was transferred to a Teflon-lined autoclave and heated at 373 K for 24 h. The resulting product was obtained by filtration, washed repeatedly with a large amount of water, air dried at room temperature and calcined at 773 K for 6 h to remove the surfactant (Al-SBA-15(40) and Al-SBA-15(5) samples, in parenthesis Si/Al ratio). *Post synthesis:* Pure silica SBA-15 was also prepared using the procedure outlined above but without Al. Al-SBA-15 was prepared by adding 1.0 g of calcined pure silica SBA-15 to 50 ml hexane (dry) containing the required amount of aluminium isopropoxide and stirring at 343 K for 24 h. The resulting powder was obtained by

filtration, washed with dry hexane, dried at room temperature and calcined at 823 K for 4h (Al-SBA-15(5)-ps sample, in parenthesis Si/Al ratio).

Synthesis of phosphoric acid-functionalized MCM-41, SBA-15

Surface phosphorus species were introduced onto the surface of samples by impregnating 1 g of sample in 4.5 ml of H_3PO_4 solution (Si/P=25). The phosphoric acid impregnated sample was rapidly dried under stirring. It was then dried in the oven at 373 K for 8 h and calcined at 673 K for 3 h. Samples were named P-MCM-41 and P-SBA-15.

Synthesis of ethylphosporic acid-functionalized SBA-15

Direct synthesis: Another phosphoric acid-functionalized SBA-15 sample was prepared by direct synthesis. 4.0 g triblock of copolymer poly(ethylene glycol)-block-poly(propylene glycol)-block-poly(ethylene glycol) ($EO_{20}PO_{20}EO_{20}$) was added to 125 ml of 2 M HCl at room temperature under stirring. Then, the solution was heated to 313 K and TEOS (9 g) was added dropwise. After 45 min, 2.8 g of diethylphosphatoethyltriethoxy silane (DEPTES, Gelest) was added dropwise (to prevent phase separation). After that, sample was heated under continuous stirring at 313 K for 2 h by refluxing under microwaves. The reaction mixture was transferred to a Teflon-lined autoclave and heated in a conventional oven at 373 K for 24 h. The resulting product was filtered, washed repeatedly with a large amount of water, and dried in air overnight. The surfactant template was removed by extraction with ethanol under reflux for 24 h. Finally, diethylphosphatoethyl groups were cleaved and converted to phosphonic acid groups by refluxing 1 g of diethylphosphatoethyl functionalized SBA-15 in 21 ml of concentrated HCl at 313 K for 24 h. Sample was called Ethyl-P-SBA-15-MW.

Synthesis of propylsulfonic acid-functionalized MCM-41

Direct synthesis: Tetramethylammonium hydroxide (TMAOH) and cetyltrimethylammonium bromide (CTAB) were dissolved in distilled water by stirring at 308 K. The silica source, fumed silica, and (3-mercaptopropyl)trimethoxy silane (MPTMS) was then added to the template solution under stirring for 1 h. After further

stirring for 1h the resulting synthesis gel of composition 1 Si: 0.1 MPTMS: 0.25 CTAB: 0.2 TMAOH: 40 H_2O aged at room temperature for 20 h. Then, the gel was transferred to a Teflon-lined autoclaved and heated at 423 K for 48 h. The solid was filtered, washed, dried in air at room temperature, and reflux in ethanol for 24 h. Material with immobilized mercaptopropyl groups was oxidized with H_2O_2 in a methanol-water mixture. Tipically, 2.04 g of aqueous 35% H_2O_2 dissolved in three parts of methanol was used per g of material. After 24 h, the suspension was filtered and washed with water and EtOH. The wet material was resuspended (1 wt%) in acidified H_2O (H_2SO_4 0.1M) for another 4 h. Finally, the solid was extensively rinsed with H_2O, dried at 333 K, and stored in a dessicator (Propyl-S-MCM-41 sample).

Synthesis of arenesulfonic acid-functionalized HMS

HMS was synthetized at 338 K from a gel containing 0.02 TEOS, 0.005 amine 0.088 EtOH and 2.56 H_2O. The amine (dodecylamine (dda), hexadecylamine (hda) or octadecylamine (oda)) was first dissolved in the alcohol-water mixture. TEOS was added and the mixture was stirred at 338 K for 24 h. The amine template was extracted by calcining at 873 K for 4 h. Starting materials were named: HMS(dda), HMS(hda) and HMS(oda). Then, mesoporous silica was treated with 1.5 g of CSPTMS at 313 K by refluxing for 2 h to introduce sulfonic groups. Sulfonated samples were called as S-HMS(dda), S-HMS(hda) and S-HMS(oda).

Catalysts characterization

Powder X-ray diffraction (XRD) analysis was performed using a Bruker AXS D8 Advance powder diffractometer with Cu KR radiation (40 kV, 40 mA), a 0.020º step size, and a 1 s step. The elemental composition (Si/Al ratio) was determined by a Philips MiniPal PW4025 X-ray fluorescence (XRF) instrument. Textural properties were determined via nitrogen sorption analysis at -196 ºC using a conventional volumetric technique by a Micromeritics ASAP 2020 sorptometer. Before analysis the samples were oven-dried at 150 ºC and evacuated overnight at 150 ºC under vacuum. The Brunauer-Emmett-Teller (BET) specific surface area was calculated using the standard BETmethod for adsorption data in the relative adsorption range from 0.05 to 0.2. The total pore volume was estimated on the basis of the amount of nitrogen adsorbed at a relative pressure (P/Po) of ca. 0.99. The acid content was determined

using established procedures that employ thermal desorption of cyclohexylamine (CHA). [92] Samples were exposed to liquid CHA at room temperature, after which they were kept overnight (at room temperature) and then in an oven at 353 K for 2 h to allow the base to permeate the samples. Thermogravimetric analysis (TGA) curves were then obtained for the CHA-containing samples. The mass loss associated with desorption of the base from acid sites was used to calculate the total the acid content (mmol of CHA/g of sample) assuming that each acid site interacts with one base molecule. To obtain the content of strong acid sites, the CHA-containing samples dried at 353 K were further heated in an oven at 523 K prior to TGA analysis.

Catalytic Activity

Etherification experiments were performed in the liquid phase in a stainless steel stirred autoclave (150 mL) equipped with temperature controller and a pressure gauge. Stirring was fixed for all experiments at 1200 rpm to avoid external diffusion limitations. Liquid phase pressurized isobutene (glycerol/isobutene molar ratio of 0.25) was injected into the reactor, previously charged with glycerol and catalyst (0.5 g), using nitrogen at 10 bar as pushing agent. The temperature was then raised to 348 K and the pressure increased accordingly following the liquid-vapour equilibrium. Catalytic experiments were made at 24 h. The reaction products were analyzed by gas chromatography using a chromatograph model Shimadzu GC-2010 equipped with a SupraWax-280 column and a FID detector.

Glycerol conversion and selectivity to MTBG (glycerol monoethers) were determined from calibration lines obtained from commercial products. For DTBG (glycerol diethers) and TTBG (glycerol triether), which were not available commercially, we isolated them from the products of the etherification reaction by column chromatography (1:9 ethyl acetate/hexane) and identified them by ^{13}C and ^{1}H NMR for proper quantification with the assistance of the characterization data reported by Jamróz et al. [96]

Results and discussion

Catalysts characterization

Mesoporous aluminosilicates

Figure 95 shows the powder XRD patterns of MCM-41 samples. XRD pattern of the pure silica, MCM-41 (Fig. 95a), was typical of well-ordered hexagonal materials. The incorporation of Al, by direct synthesis, resulted in a drastic reduction in the intensity of the (100) peak. XRD patterns of Al-MCM-41(40), Al-MCM-41(20) and Al-MCM-41(10) clearly illustrate that the incorporation of Al via direct mixed-gel synthesis since a decrease in the long-range structural ordering was observed (Fig. 95b, 95c and 95d). However, the structural ordering of the pure silica MCM-41 maintained after post-synthesis alumination (Fig. 95e).

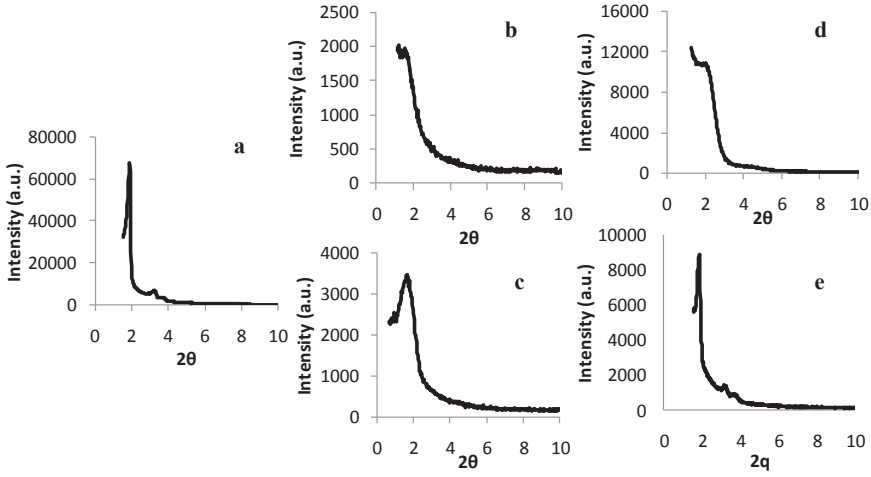

Figure 95. Powder XRD patterns of samples: (a) MCM-41, (b) Al-MCM-41(40), (c) Al-MCM-41(20), (d) Al-MCM-41(10) and Al-MCM-41(5)-ps.

N_2 adsorption-desorption isotherms and pore size distribution graphics are shown in Figure 96. The capillary condensation step was much higher and steeper for the pure silica sample. The Al-MCM-41(10) sample showed low mesoporous structural ordering and a narrow pore size distribution. On the other hand, the Al-MCM-41(20) exhibited a wide pore size distribution. It is interesting to note that the presence of Al, during the direct synthesis, led to a significant adsorption at high partial pressures (P/Po=0.9) which was totally absent in the pure silica sample (Fig. 96b2 and 96c2).

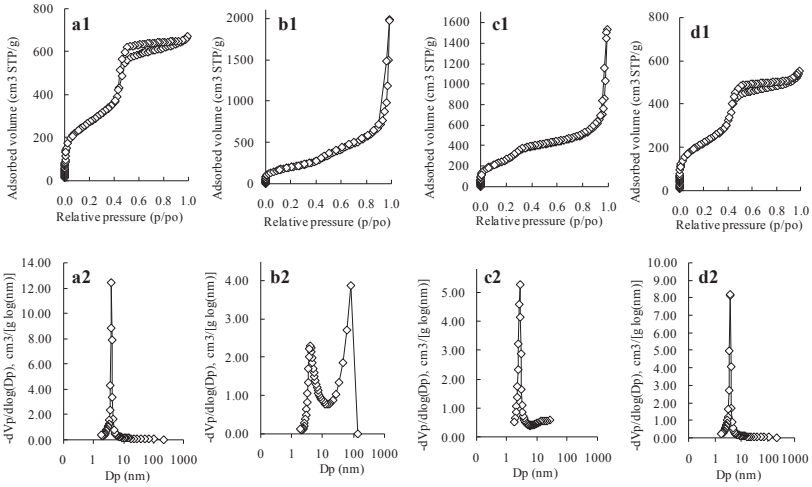

Figure 96. N_2 adsorption-desorption isotherms of samples: (a1) MCM-41, (b1) Al-MCM-41(20), (c1) Al-MCM-41(10), (d1) Al-MCM-41-ps and pore size distribution graphics of samples: (a2) MCM-41, (b2) Al-MCM-41(20), (c2) Al-MCM-41(10), (d2) Al-MCM-41(5)-ps.

The N_2 adsorption-desorption isotherm (Fig. 96d1) of Al-MCM-41(5)-ps indicates that this sample retained good mesostructural ordering and a narrow pore size distribution after incorporation of Al (Fig. 96d2). However, Al-MCM-41(5)-ps exhibited lower surface area and lower pore volume than the parent Si-MCM-41 which had a surface area of 989 m^2/g and pore volume of 1.04 cm^3/g (Table 28). The thicker pore walls of the Al-grafted materials, together with the presence of non-framework Al in the pores may be responsible for this decrease. In contrast, samples modified by direct synthesis showed higher pore volume than pure silica MCM-41.

Table 28. Elemental analysis, N_2 physisoportion and acidity of MCM-41 samples.

Sample	Si/Al	BET area (m^2/g)	Pore volume (cc/g)	Acid capacity (meq H^+/g)
Si-MCM-41	--	989	1.04	--
Al-MCM-41 (40)	16	823	3.12	0.23
Al-MCM-41 (20)	13.5	723	3.07	0.38
Al-MCM-41 (10)	10.6	995	2.36	0.86
Al-MCM-41(5)-ps	7.8	808	0.86	0.81

Table 28 also gives the elemental composition (Si/Al ratio) and acidity of Al-MCM-41 materials. The Si/Al ratios of the solid products were found lower than the gel

ratios except for Al-MCM-41(10) sample. With respect to the acidity, by increasing the Al content, the acidity increased as expected.

The structural ordering of SBA-15 maintained after Al insertion by direct as well as by post-synthesis alumination as shown in Figure 97.

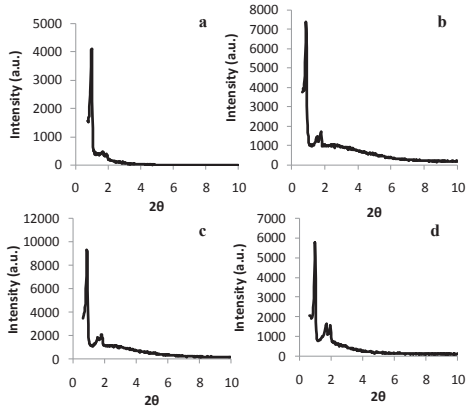

Figure 97. Powder XRD patterns of the samples: (a) SBA-15, (b) Al-SBA-15(40), (c) Al-SBA-15(5) and (d) Al-SBA-15-ps.

N_2 adsorption-desorption isotherms indicate the good mesostructural ordering and narrow pore size distribution of Al-SBA-15(5)-ps (Figure 98). However, this post-aluminated sample had lower surface area and lower pore volume than SBA-15 as previously observed for Al-MCM-41(5)-ps when compared with MCM-41. This can be attributed to the presence of non-framework Al in the pores.

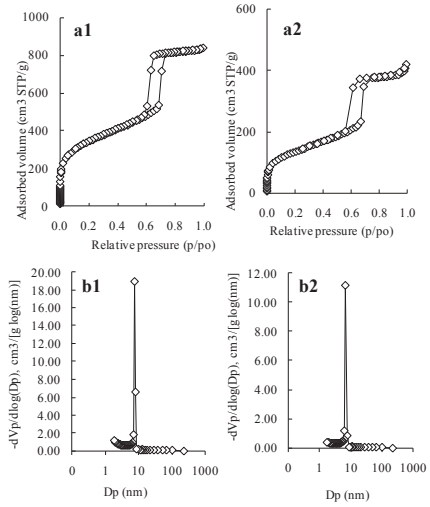

Figure 98. N_2 adsorption-desorption isotherms of samples: (a1) SBA-15, (b1) Al-SBA-15(5)-ps and pore size distribution graphics of samples: (a2) SBA-15, (b2) Al-SBA-15(5)-ps.

The Si/Al ratio of the samples aluminated by direct synthesis indicates that mostly Al was not incorporated probably due to acid medium used during reaction. Sample Al-SBA-15(5)-ps showed the lowest Si/Al ratio although some aluminium can be in non-framework positions (Figure 29). Acidity increased, when increasing the Al content, as expected (Table 29).

Table 29. Elemental analysis, N_2 physisoportion and acidity of SBA-15 samples.

Sample	Si/Al	BET area (m^2/g)	Pore volume (cc/g)	Acid capacity (meq H^+/g)
SBA-15	--	1212	1.30	--
Al-SBA-15 (40)	21.3	707	1.03	0.30
Al-SBA-15 (5)	20.1	689	1.04	0.31
Al-SBA-15(5)-ps	7.3	488	0.65	0.55

Functionalized mesoporous silicas

MCM-41, SBA-15 and HMS were functionalized by introduction of phosphoric and sulfonic acid groups using different methodologies to prepare acid catalysts with higher Brønsted acidity strength. Figure 99 shows the different acid groups incorporated into mesoporous silicas.

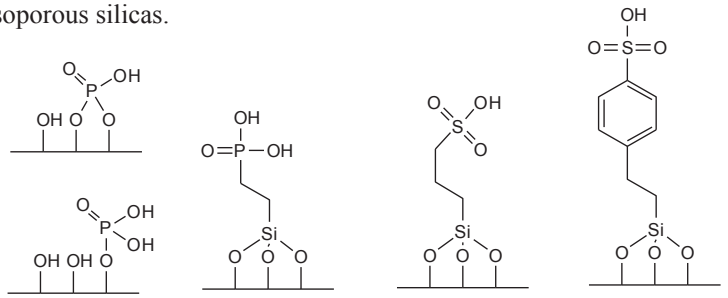

Figure 99. Schematic representation of the acid groups incorporated into mesoporous materials.

Phosphoric acid-functionalized MCM-41 and SBA-15

Figure 100 shows XRD patterns of P-MCM-41 and P-SBA-15. These results indicate that the structure of the samples maintained after treatment. Therefore phosphoric acid did not degrade the mesoporous framework.

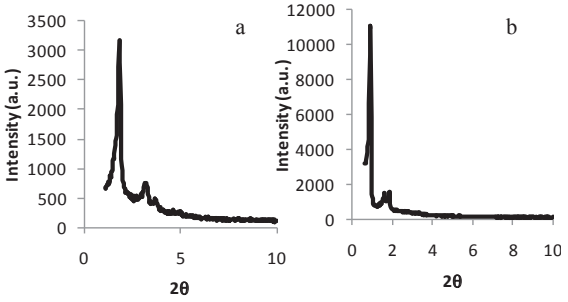

Figure 100. Powder XRD patterns of samples: (a) P-MCM-41, (b) P-SBA-15 and (c) P-ZY(15).

N_2 adsorption-desorption isotherms of P-MCM-41 and P-SBA-15 are shown in Figure 101. As we can observe, after treatment, the samples maintained their porosity. However, there is a decrease in adsorbed volume probably due to the presence of phosphorus species in the pores. Both samples presented a narrow pore size distribution (Fig. 102).

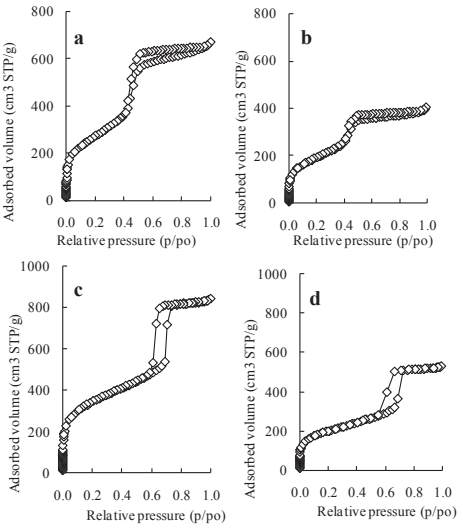

Figure 101. N_2 adsorption-desorption isotherms of samples: (a) MCM-41, (b) P-MCM-41, (c) SBA-15 and (d) P-SBA-15.

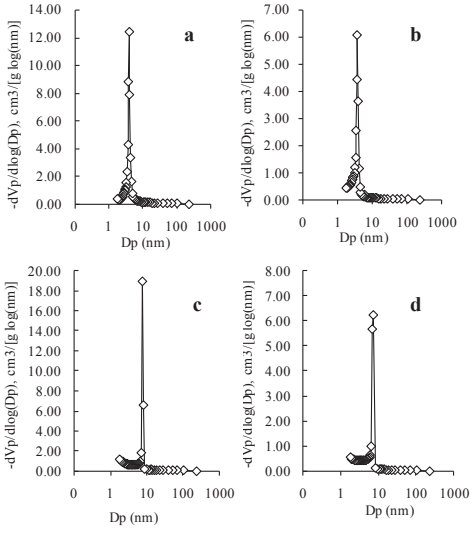

Figure 102. Pore size distribution graphics of samples: (a) MCM-41, (b) P-MCM-41, (c) SBA-15 and (d) P-SBA-15.

Sulfonic acid-functionalized samples

Powder X-ray diffraction patterns of the modified HMS samples showed only one peak typical of a wormhole pore structure although some loss in the ordering was observed for all of them. N_2 adsorption-desorption isotherms were type IV for all samples, before and after modification, as expected, attributed to mesoporous materials, according to the Brunauer, Deming, Deming and Teller classification. [182] Although sulfonated HMS samples presented similar N_2 adsorption-desorption isotherms to starting materials observed a decrease in the adsorbed volume and surface area. (Figure 103, table 30). This can be associated to the incorporation of sulfonic groups.

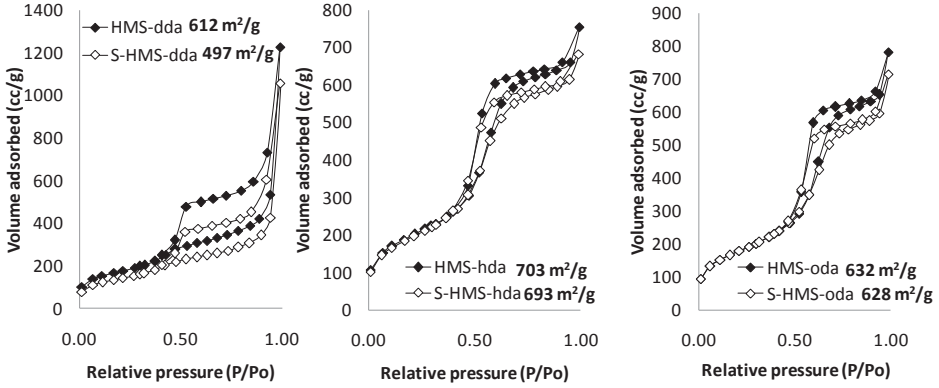

Figure 103. Nitrogen adsorption-desorption isotherms of HMS(dda), S-HMS(dda), HMS(hda), S-HMS(hda), HMS(oda) and S-HMS(oda).

Interestingly, sulfonated HMS synthesized using dodecylamine as surfactant showed a higher decresase in surface area than the rest of samples. This can be related to a higher introduction of sulfonic groups. Moreover, S-HMS(dda) exhibited additional capillary condensation at partial pressures > 0.90 due to the filling of textural mesopores (Figure 103). The textural mesopores are important because they greatly facilitate mass transport to the framework mesopores.[21-22]

Table 30. Characterization results.

Catalyst	BET area (m^2/g)	Pore volume (cc/g)	Sulfur content[b]	Acid capacity[c] (meq H^+/g)
HMS(dda)	612	1.96	--	--
S-HMS(dda)	497	1.65	0.64	0.63
HMS(hda)	703	1.27	--	--
S-HMS(hda)	693	1.10	0.13	0.15
HMS(oda)	632	1.30	--	--
S-HMS(oda)	628	1.15	0.11	0.10

[a]Calculated from XRD patterns; [b](mmol organic sulfonic group/g sample) calculated from TGA; [c]Obtained by potentiometric titration.

Pore size distributions are shown in Figure 104. We can observe that when using longer surfactant chain, pore size slightly increased. After sulfonation, all samples showed a decrease in pore volume.

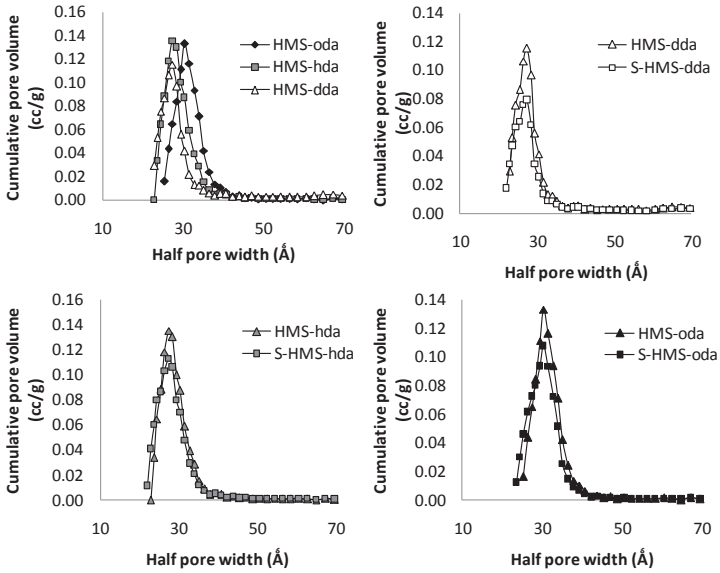

Figure 104. Pore size distribution graphics of HMS(dda), Arene-S-HMS(dda), HMS(hda), Arene-S-HMS(hda), HMS(oda) and Arene-S-HMS(oda).

Figure 105 shows the morphology of the particles of sulfonated HMS samples. Sulfonated HMS synthesized with dodecylamine exhibited smaller particles sizes than sulfonated HMS synthesized with hexadecylamine or octadecylamine. Small particles

sizes (< 200 nm) result in complementary textural mesoporosity, as confirmed by N_2 physisorption.

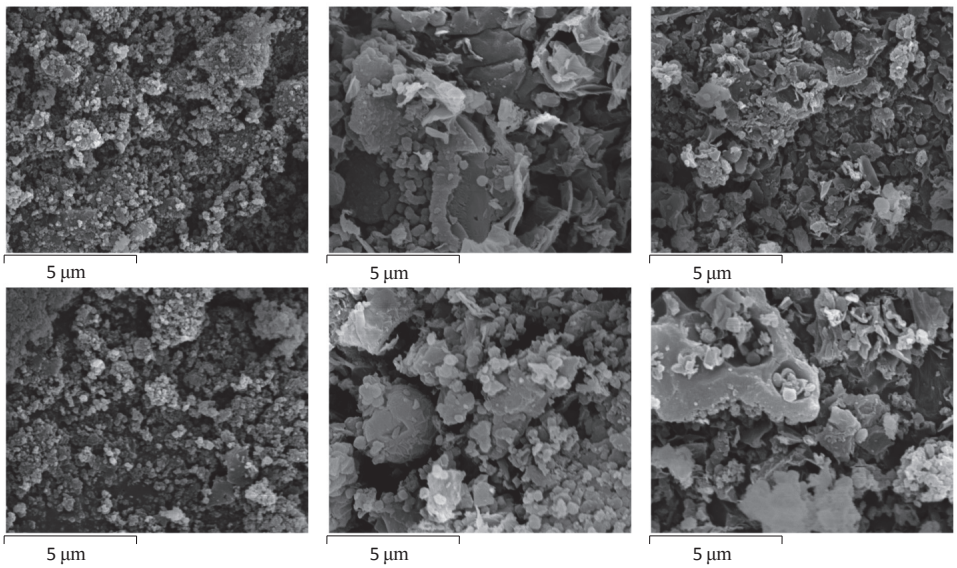

Figure 105. Scanning electron micrographs of samples: (a) S-HMS(dda), (b) S-HMS(hda) and (c) S-HMS(oda).

All sulfonated HMS samples showed lower surface areas, and on the whole, lower pore volumes than their corresponding starting HMS (Table 30). Sulfonated HMS(dda) exhibited a considerable decrease of surface area and pore volume because of its higher content of sulfonic groups. The presence of higher amount of textural mesoporosity favours the accessibility of the reagents to the acid sites.

Table 30 also shows the sulfur content of the sulfonated samples obtained from TGA. All the sulfonated samples had sulfonic groups since a weight loss between 633 K and 933 K was observed in the TG curves for all of them. This weight loss has been related to the loss of sulfonic groups, according to the literature, [83] and allowed us to calculate the mmol organic sulfonic group/g sample (Table 30). We recently applied this procedure for sulfonation of SBA-15. [181]

Finally, the acidity of the zeolites, determined potentiometrically, agrees with the TGA results, since the sulfonated samples which had higher amounts of sulfonic groups, led to higher acidity, as expected (Table 30).

Catalytic Activity

Table 31 shows the catalytic activity results of modified MCM-41, SBA-15 and HMS catalysts for the etherification reaction of glycerol with isobutene. The reaction products obtained were mono-tert-butyl glycerol ether (MTBG), di-tert-butyl glycerol ether (DTBG) and tri-tert-butyl glycerol ether (TTBG). Besides, diisobutylene was detected in very low amounts for all samples.

Al-MCM-41 and Al-SBA-15 samples exhibit low conversion and low selectivity to h-GTBE. Although the incorporation of aluminium in the structure of MCM-41 and SBA-15 increased the amount of Brønsted acid sites, they had lower. The acid strength influences significantly in the catalytic performance, both conversion and selectivity to h-GTBE, as previously reported. [180-181] The incorporation of phosphoric groups allows us to detect the tri-tert-butyl ether of glycerol in low amounts. However, long times were required to obtain high conversion and the acid strength of phosphoric groups were not enough to obtain high selectivity to di- and tri-ethers. All sulfonated HMS samples showed higher conversion and higher selectivity to h-GTBE than their starting materials.

This confirms the important role of the strength of Brønsted acid sites. Interestingly, S-HMS(dda) exhibited total conversion and 84 % of selectivity to h-GTBE (26% to triether) after 24 h of reaction. The differences in the activity between the three types of sulfonated HMS could be explained by the different amount of sulfonic groups. HMS synthesized with dodecylamine presented additional mesoporosity which facilitate the diffusion of the sulfonic agent obtaining higher incorporation of sulfonic groups.

From these results, we can conclude that complementary textural mesoporosity of sulfonated HMS samples favours the incorporation of higher amount of sulfonic groups resulting in catalysts with high catalytic activity for glycerol etherification.

Table 31. Catalytic activity of modified MCM-41, SBA-15 and HMS catalysts for the etherification of glycerol with isobutene after 24 h.

Catalyst	Conversion (%)	Selectivity to MTBG (%)	Selectivity to h-GTBE (%)[a]
MCM-41	20	87	13 (0)
Al-MCM-41(40)	32	85	15 (0)
Al-MCM-41(20)	35	80	20 (0)
Al-MCM-41 (10)	45	78	22 (0)
Al-MCM-41(5)-ps	47	80	20 (0)
P-MCM-41	45	70	30 (2)
Propyl-S-MCM-41	60	45	55 (3)
SBA-15	23	89	11 (0)
Al-SBA-15(40)	30	88	12 (0)
Al-SBA-15(5)	32	80	20 (0)
Al-SBA-15(5)-ps	41	78	22 (0)
P-SBA-15	40	67	43 (4)
Ethyl-P-SBA-15-MW[a]	43	65	35 (13)
Ethyl-P-SBA-15-MW[b]	96	50	45 (5)
HMS(dda)	30	88	12 (0)
HMS(hda)	25	93	7 (0)
HMS(oda)	23	95	5 (0)
Arene-S-HMS(dda)	100	16	84 (26)
Arene-S.HMS(hda)	64	85	15 (0)
Arene-S-HMS(oda)	43	86	14 (0)

MTBG: glycerol monoethers; h-GTBE: glycerol diethers + glycerol triether. In parenthesis, selectivity to glycerol triether (%).
[a] 18 h of reaction.
[b] 48 h of reaction.

Conclusions

The incorporation of aluminium in the structure of MCM-41 and SBA-15 increase the amount of Brønsted acid sites but their lower strength resulted in low catalytic activity. The incorporation of phosphoric groups allows us to detect the tri-tert-butyl ether of glycerol in low amounts. However, long times were required to obtain high conversion. The strength of phosphoric groups were not enough to obtain high

selectivity to di- and tri-ethers. On the other hand, sample S-HMS(dda), which shows textural mesoporosity, exhibited total conversion and 84 % of selectivity to h-GTBE (26% to triether) after 24 h of reaction. This confirms the important role of the strength of Brønsted acid sites.

The degree of complementary textural porosity in mesoporous silica HMS depends on the surfactant used during the synthesis. Moreover, the generation of textural mesoporosity reduces diffusion limitations and consequently increase the incorporation of sulfonic groups into HMS.

Acknowledgments

The authors are grateful for the financial support of the Ministerio de Ciencia e Innovación and FEDER funds (CTQ2008-04433/PPQ). Dolores González acknowledges Ministerio de Educación y Ciencia for a FPU grant (AP2007-03789).

5. CONCLUSIONES

UNIVERSITAT ROVIRA I VIRGILI
REVALORIZACIÓN CATALÍTICA DE GLICERINA PARA UNA OBTENCIÓN MÁS RESPETUOSA CON EL MEDIO AMBIENTE DE ADITIVOS PARA COMBUSTIBLES
Mª Dolores González Candela
DL:T. 1715-2011

5. Conclusiones

Efecto de la radiación microondas en la desaluminación de zeolitas

El uso de la radiación microondas en la desaluminación de zeolitas mediante tratamiento en medio ácido dio lugar a una mayor desaluminación en menor tiempo de tratamiento además de diferencias significativas en las propiedades ácidas y superficiales de estos materiales:

- ✓ La desaluminación de una zeolita mordenita, tanto en autoclave como a reflujo, utilizando radiación microondas generó una mayor desaluminación que mediante calentamiento convencional para un mismo tiempo de tratamiento.

- ✓ La utilización de la radiación microondas en la desaluminación de mordenita a tiempos cortos (15 min) en autoclave dio lugar a un material con centros de acidez intermedia, no presentes en el resto de muestras parcialmente desaluminadas, además de tener una menor cantidad de centros ácidos fuertes de Lewis.

- ✓ La ampliación del estudio de desaluminación a otras dos zeolitas, beta y ZSM-5, mediante su tratamiento en medio ácido en autoclave a tiempos cortos (15 min) confirmó el mayor grado de desaluminación cuando el calentamiento se realiza con microondas. La estructura de la zeolita también influye decisivamente en el grado de desaluminación siguiendo el orden: beta > mordenita > ZSM-5.

- ✓ La desaluminación de las zeolitas beta y ZSM-5 en medio ácido en autoclave durante 15 minutos en presencia de microondas dio lugar a la formación de grupos silanoles no presentes en las mismas muestras tratadas mediante calentamiento convencional.

Efecto de la radiación microondas en la sulfonación de materiales micro-, meso- y macroporosos

Se han incorporado grupos sulfónicos, por primera vez, mediante post-síntesis en una etapa en diferentes materiales: micro-, meso- y macroporosos utilizando radiación microondas y también mediante calentamiento convencional. Además, la utilización de la radiación microondas durante la sulfonación da lugar a la obtención de catalizadores que han mostrado mayor conversión y selectividad a di- y tri-éteres de glicerol que los sulfonados mediante calentamiento convencional debido al mayor número y/o accesibilidad de los centros ácidos de Brønsted incorporados.

- ✓ Se han funcionalizado por primera vez zeolitas (beta, mordenita, ZSM-5) mediante post-síntesis en una única etapa tanto mediante calentamiento convencional como con microondas. La incorporación de grupos $–SO_3H$ en zeolitas podría estar facilitada por la desaluminación que se produce durante el tratamiento en medio ácido, ya que dicha desaluminación da lugar a la formación de grupos silanoles, que podrían reaccionar con el agente sulfonante, para formar los grupos sulfónicos. También se ha sulfonado una montmorillonita K10 en presencia de microondas mediante post-síntesis en una etapa.
- ✓ La cantidad necesaria de agente sulfonante para la incorporación óptima de grupos sulfónicos en zeolitas es inversamente proporcional a la facilidad de desaluminación de las zeolitas.
- ✓ El uso de la radiación microondas durante la sulfonación de un material mesoporoso ordenado SBA-15 permitió incorporar una mayor cantidad de grupos sulfónicos ($-SO_3H$) en tiempos más cortos que mediante el uso de calentamiento convencional.
- ✓ La presencia de porosidad textural en una sílica mesoporosa HMS reduce los límites de difusión aumentado la incorporación de grupos sulfónicos. En este caso también es la primera vez que se incorporan grupos sulfónicos mediante post-síntesis en una etapa y utilizando radiación microondas.
- ✓ Se han incorporado, por primera vez, grupos sulfónicos en un aerogel y un liogel de sílica mediante post-síntesis en una única etapa utilizando microondas y mediante calentamiento convencional. La utilización de microondas permitió la incorporación de una mayor cantidad de grupos sulfónicos en ambos materiales.

Actividad catalítica en la eterificación de glicerol con tert-butanol o isobuteno

La cantidad y fuerza de los centros ácidos de Brønsted afectan a la conversión mientras que la fuerza ácida influye significativamente en la formación de los di- y tri-éteres de glicerol, independientemente de la porosidad del catalizador. Sin embargo, la accesibilidad de los reactivos a los centros ácidos se debe garantizar para que éstos puedan ser activos:

- ✓ Los resultados catalíticos utilizando isobuteno fueron mejores que los obtenidos utilizando tert-butanol de acuerdo con lo encontrado en la bibliografía debido a la formación de agua durante la reacción que puede competir con los reactivos por la adsorción en los centros activos.

- ✓ Los catalizadores beta presentaron una mayor actividad catalítica que los catalizadores ZSM-5 y mordenita. Este comportamiento se ha relacionado con el diferente número de centros ácidos (inversamente proporcional a la relación Si/Al) así como a la diferente accesibilidad de los reactivos a los centros ácidos en las diferentes estructuras.

- ✓ La parcial desaluminación, parcial desilicación o la incorporación de lantano en la estructura de las zeolitas dio lugar a menores conversiones y menor selectividad a di- y tri-éteres de glicerol que las zeolitas protonadas debido a una menor cantidad de centros ácidos, una menor fuerza de los centros ácidos o a efectos estéricos, respectivamente.

- ✓ La presencia de flúor en la estructura de la zeolita permitió observar la formación del triéter de glicerol en pequeñas cantidades obteniéndose mejores conversiones debido al efecto inductivo del flúor que aumenta la fuerza ácida de los centros de Brønsted presentes en la zeolita. Este mismo efecto del flúor se observó en una zeolita con porosidad jerarquizada fluorada, detectándose la formación de una cantidad algo mayor de triéter debido a la mayor accesibilidad de los reactivos a los centros ácidos de este material.

- ✓ La incorporación de grupos sulfónicos en la superficie de materiales de diferente porosidad (micro-, meso- o macroporosos) influye significativamente en los resultados catalíticos dando lugar a elevadas conversiones y selectividades hacia los productos de interés.

- ✓ La microporosidad de zeolitas y esmectitas se puede superar aumentando el número y fuerza de centros ácidos de Brønsted junto con la utilización de un tiempo adecuado de reacción que favorezca la difusión de los reactivos hacia los centros activos.

- ✓ La incorporación de aluminio en dos sílicas mesoporosas genera centros ácidos de Brønsted pero su poca fuerza ácida dio lugar a una baja actividad catalítica.

- ✓ La incorporación de grupos fosfóricos en materiales mesoporosos permitió la obtención del triéter en moderadas cantidades. Sin embargo, se necesitan tiempos largos de reacción para obtener elevada conversión y la fuerza de los grupos fosfóricos no es suficiente para mejorar la selectividad hacia la formación de los productos de interés.

- ✓ La utilización de materiales con mayor porosidad (zeolita con porosidad jerarquizada, aerogeles y liogeles) favorece la accesibilidad de los reactivos a los centros activos y reduce el bloqueo de los poros por los reactivos y productos, disminuyendo así su desactivación.

- ✓ Los mejores resultados catalíticos se han conseguido con un material mesoporoso ordenado SBA-15 y con una zeolita beta sulfonados mediante calentamiento con microondas obteniéndose total conversión y selectividad a di- y tri-éteres de glicerol del 91 % (con un 39 % y 36 % de selectividad al triéter, respectivamente) después de 24 h de reacción. Estos resultados están muy por encima de los conseguidos con un catalizador Amberlyst (resina de intercambio iónico ácida) que es un típico catalizador comercial utilizado en este tipo de reacciones.

6. REFERENCIAS BIBLIOGRÁCICAS

UNIVERSITAT ROVIRA I VIRGILI
REVALORIZACIÓN CATALÍTICA DE GLICERINA PARA UNA OBTENCIÓN MÁS RESPETUOSA CON EL MEDIO AMBIENTE DE ADITIVOS PARA COMBUSTIBLES
Mª Dolores González Candela
DL:T. 1715-2011

6. Referencias bibliográficas

[1] *The Future of glycerol: 2nd Edition*, Mario Pagliaro and Michele Rossi, RSC Green Chemistry **2010**.

[2] A. Behr, J. Eilting, K. Irawadi, J. Leschinski, F. Lindner, *GreenChem.*, **2008**, 10, 13.

[3] M. Pagliaro, R. Ciriminna, H. Kimura, M. Rossi, C. D. Pina, *Angew. Chem. Int. Ed.,* **2007**, 46, 4434.

[4] L. Bournay, D. Casanave, B. Delfort, G. Hillion, J. A. Chodorge, *Catal. Today,* **2005**, 106, 190.

[5] J. A. Melero, J. Iglesias, G. Morales, *Green Chem.*, **2009**, 11, 1285.

[6] N. Rahmat, A. Z. Abdullah, A. R. Mohamed, *Renewable and Sustainable Energy Reviews,* **2010**, 14, 987.

[7] S. S. Yazdani, R. Gonzalez, *Current Opinion in Biotechnology,* **2007**, 18, 213.

[8] C. H. Zhou, J. N. Beltramini, Y.-X. Fan, G. Q. Lu, *Chem. Soc. Rev.*, **2008**, 37, 527.

[9] J. Barrault, F. Jerome, *Eur. J. Lipid Technol.*, **2008**, 110, 825.

[10] M. Pagliaro, R. Ciriminna, H. Kimura, M. Rossi, C. D. Pina, *Eur. J. Lipid Technol.,* **2009**, 111, 788.

[11] J. Feng, M. Yuan, H. Chen, X. Li, Progress in Chemistry, **2007**, 19, 651.

[12] L. Smart, E: Moore, "Química del estado sólido". Addison-Wesley **1995**.

[13] L.V. Interrante, M.J. Hampden-Smith (eds),"Chemistry of Advanced Materials: An overview", Wiley-VCH, **1998**.

[14] D. W.Breck, Zeolite Molecular Sieves, Wiley, New York, **1974**.

[15] J. Weitkamp, L. Puppe (eds). E: Springer, " Catalysis and zeolites: fundamentals and applications". Springer-Verlag Berlin Heidelberg, **1999**.

[16] R. Xu, W. Pang, J. Yu, Q. Huo, J. Chen,"Chemistry of Zeolites and Related Porous Materials: synthesis and structure". John Wiley & sons **2007**.

[17] G. de A. A. Soler- lllia, C. Sanchez, B. Lebeau, J. Patarin, *Chem. Rev.,* **2002**, 102, 4093.

[18] J. S. BeckJ. C. Vartuli, W. J. Roth, M. E. Leonowicz, C. T. Kresge, K. D. Schmitt, C. T. W. Chu, D. H. Olson, E. W. Sheppard,S. B. McCullen, J. B. Higgins, J. L. Schlenkert, *J. Am. Chem. Soc.,* **1992**, 114, 10834.

[19] Q. HuoD. I. Margolese, U. Ciesla, D. G. Demuth, P. Feng, T. E. Gier, P. Sieger, A. Firouzi, B. F. Chmelka, F. Schüth, G. D. Stucky, *Chem. Mater.,***1994**, 6, 1176.

[20] P. T. Tanev, T. J. Pinnavaia, *Science,* **1995**, 267 (5199), 865.

[21] T. R. Pauly, Y. Liu, T. J. Pinnavaia, S. J. L. Billinge, T. P. Rieker, *J. Am. Chem. Soc.,* **1999***,* 121*,* 8835.

[22] W. Zhang, T. R. Pauly, T. J. Pinnavaia, *Chem. Mater.*, **1997**, 9, 2491.

[23] M. M. Olken, J. M. Garces, in: von Ballmoos, J. B. Higgings, M. M. J. Treacy (Eds.), Proc. 9th Int. Zeolite Conf., Butterworth-Heinemann, Boston, MA, **1993**, Montreal, Canada, **1992**, p. 559.

[24] G. J. Lee, J. M. Garces, G.R. Meima, M. J. M. Van der Aalst, US patent 32517, **1989**.

[25] N. Viswanadham, M. Kumar, *Micropor.Mesopor.Mater.* **2006**, 92, 31.

[26] F. Raatz, C. Marcill, E. Freund, *J. Chem. Soc. Faraday Trans.* **1983**, 79, 2299.

[27] J. Nagano, T. Eguchi, T. Asanuma, M. Nakayama, N. Nakamura, E. G. Derouance, *Micropor. Mesopor. Mater.* **1999**, 33, 249.

[28] S. van Donk, A. Broersma, O. L. J. Gijzeman, J. A. Van Bokhoven, J. H. Bitter, K. P. De Jong, *J. Catal.* **2001**, 204, 272.

[29] B. L. Meyers, T. H. Fleisch, G. J. Ray, J. T. Miller, J. B. Hall, *J. Catal.* **1998**, 110, 82.

[30] M. J. A. van Tromp, M. T. Garriga Oostenbrink, J. H. Bitter, K. P. de Jong, D. C. Koningsberger, *J. Catal.* **2000**, 190, 209.

[31] N. S. Nesterenko, F. ThibaultStarzyk, V. Montouillout, V. V. Yuschenko, C. Fernandez, J. P. gilson, F. Fajula, Ivanova II, *Micropor. Mesopor. Mater.* **2004**, 71, 157.

[32] K. H. Lee, B. H. Ha, *Micropor. Mesopor. Mater.* **1998**, 23, 211.

[33] S.Moreno and G.Poncelet, *Micropor. Mat.* **1997**, 12, 197.

[34] D. Vergani, R. Prins, H. W. Kouwenkoven, *Appl. Catal. A: Gen.* **1997**, 163, 71.

[35] P. O. Fritz, J. H. Lunsford, *J. Catal.* **1989**, 118, 85.

[36] M. H. W. Sonnemans, C. den Heijer, M. Crocker, *J. Phys. Chem.* **1993**, 97, 440.

[37] A. Corma, *Chem. Rev.* **1995**, 95, 559.

[38] R. A. Van Santen, G. J. Kramer, *Chem. Rev.* **1995**, 95, 637.

[39] M. Sawa, M. Niwa, Y. Murakami, *Zeolites* **1992**, 12, 175.

[40] M. J. Van Niekerk, J. C. Q. Fletcher, C. O'Connor, *J. Catal.* **1992**, 138, 150.

[41] G.J. Hutchings, A. Burrows, C. Rhodes, C. J. Kely, R. McClung, *J. Chem. Soc., Faraday Trans*. **1997**, 93, 3593.

[42] Y. Hong, V. Gruver, J. J. Fripiat, *J. Catal.* **1994**, 150, 421.

[43] W. O. Haag, R. M. Lago, US Pat. 4 326 994, **1982**.

[44] Z. M. Magrioti Noronha, J. L. Fontes Monteiro, P. Gélin, *Micropor. Mesopor. Mater.* **1998**, 23, 331.

[45] M. Müller, G. Harvey, R. Prins, *Micropor. Mesopor. Mater.* **2000**, 34, 135.

[46] K. H. Chung, *Micropor. Mesopor. Mater.* **2008**, 111, 544.

[47] M. Boveri, C. M. Álvarez , M. A. Laborde, *Catalysis Today* **2006**, 114, 217.

[48] R. M. Barrer, M. B. Makki, *Can. J. Chem.* **1964**, 42, 1481.

[49] A.Rivera, T. Farías, L. C. de Ménorval, G. Autié-Castro, H. Yee-Madeira, J. L. Contreras, M. Autié-Pérez, *Journal of Colloid and Interface Science*, **2011**, 360, 220.

[50] H. van Bekkum, E.M. Flanigen, P.A. Jacobs and J.C. Jansen, "Introduction to zeolite science and practice", Elsevier **2001**.

[51] S. A. Peter, J. Sebastian, R. V. Jasra, *Ind. Eng. Chem. Res.,* **2005**, 44, 6856.

[52] B. Yuan, Z. Li, Y. Liu, S. Zhang, *J. Molec. Catal. A: Chem.*, **2008**, 280, 210.

[53] Q. Shu, B. Yang, H. Yuan, S. Qing, G. Zhu, *Catal. Comm.*, **2007**, 8, 2159.

[54] M. Ogura, S. Y. Shinomiya, J. Tateno, Y. Nara, E. Kikuchi, H. Matsukata, *Chem. Lett.* **2000**, 29, 882.

[55] J. C. Groen, J. A. Moulijn, J. Pérez-Ramírez, *Ind. Eng. Chem. Res.* **2007**, 46, 4193.

[56] J. C. Groen, T. Sano, J. A. Moulijn, J. Pérez-Ramírez, *J. Catal.* **2007**, 251, 21.

[57] J. C. Groen, L. A. A. Peffer, J. A. Moulijnm J. Pérez-Ramírez, *Chem. Eur. J.* **2005**, 11, 4983.

[58] J. C. Groen, S. Abelló, L. A. Villaescusa, J. Pérez-Ramírez, *Micropor. Mesopor. Mater.* **2008**, 114, 93.

[59] I. Salla, O. Bergadà, P. Salagre, Y. Cesteros, F. Medina, J. E. Sueiras, T. Montanari, *J. Catal.,* **2005**, 232, 239.

[60] A. G. Panov, V. Gruver, J. J. Fripiat, *J. Catal.*, **1997**, 168, 321.

[61] R. B. Borade, A. Clearfield, *J. Chem. Soc. Faraday Trans.* **1995**, 91, 539.

[62] C. W. Jones, K. Tsuji, M. E. Davis, *Nature,* **1998**, 393, 52.

[63] J. C. Mckeen, Y. S. Yan, M. E. Davis, *Chem. Mat.*, **2008**, 20, 5122.

[64] D. H. Lee, M. Choi, B. W. Yu, R. Ryoo, *Chem. Comm.,* **2009**, 74.

[65] Y. Tão, H. Kanoh, L. Abrams, K. Kaneko, *Chem. Rev.* **2006**, 106, 896.

[66] J. Pérez-Ramírez, C. H. Christensen, K. Egeblad, C. H. Christensen, J. C. Groen, *Chem. Soc. Rev.* **2008**, 37, 2530.

[67] J. Peréz-Ramírez, D. Verboekend, A. Bonilla, S. Abelló, *Advanced Functional Materials*, **2009**, 19 (24), 3972.

[68] J. Aguado, D. P. Serrano, J. M. Escola, J. M. Rodríguez, Eur. Pat. ES2004000407, **2004**.

[69] D. P. Serrano, J. Aguado, J. M. Escola, J. M. Rodríguez, A. Peral, *Chem. Mater.* **2006**, 18, 2462.

[70] E. G. Derouane, I. Schemidt, H. Lachas, C. J. H. Christensen, *Catal. Lett.* **2004**, 95, 13.

[71] J. Aguado, D. P. Serrano, J. M. Escola, E. Garagorri, J. A. Fernández, *Polym. Degrad. Stabil.* **2000**, 69, 11.

[72] J. M. Escola, J. Aguado, D. P. Serrano, A. García, A. Peral, L. Briones, R. Calvo, E. Fernandez, *Applied Catalysis B: Environmental*, **2011**, 106 (3-4), 405

[73] K. Cho., H. S. Cho., L.-C. de Mérnorval, R. Ryoo, *Chem. Mat.,* **2009**, 21 (23),5664.

[74] D. P. Serrano, R. A. García, G. Vicente, M. Linares, D. Procházková, J. Čejka, *J. Catal.* **2011**, 279 (2), 366.

[75] E. Taarning, K. Egeblad, C. H. Christensen, *Catal. Today*, **2011**, 168 (1), 3.

[76] S. Kawi, S. C. Shen and P. L. Chew, *J. Mater. Chem.* **2002**, 12, 1582.

[77] E. Cano-Serrano, G. Blanco-Brieva, J. M. Campos-Martin, J. L. G. Fierro, *Lagmuir*, **2003,** 19**,** 7621.

[78] B. Karimi, M. Khalkhali, *J. Molec. Catal. A: Chem* **2007**, 271, 75.

[79] L. M. Yang, Y. J. Wang, G. S. Luo, Y. Y. Dai, *Micropor. Mesopor. Mater.* **2005**, 84. 275.

[80] P. F. Siril, N. R. Shiju, D. R. Brown, K. Wilson, *Appl. Catal. A: Gen.* **2009**, 364, 95.

[81] W. D. Bossaert, D. E. De Vos, W. M. Van Rhijn, J. Bullen, P. J. Grobet, P. A. Jacobs, **1999**, 182, 156.

[82] D. Margolese, J. A. Melero, S. C. Chistiansen, B. F. Chmelka, G. D. Stucky, *Chem. Mater.* **2000**, 12, 2448.

[83] J. A. Melero, G. D. Stucky, R. van Grieken, G. Morales, *J. Mater. Chem.* **2002**, 12, 1664.

[84] I. K. Mbaraka, D. R. Radu, V. S.-Y. Lin, B. H. Shanks, *J. Catal.* **2003**, 219, 329.

[85] W. Zhao, P. Salame, F. Launay, A. Gédéon, Z. Hao, *J. Porous Mater.* **2008**, 15, 139.

[86] C. H. Rhee, H. K. Kim, H. Chang, J. S. Lee, *Chem. Mater.* **2005**, 17, 1691.

[87] Y. Kim, Y. Choi, H. K. Kim, J. S. Lee, *J. Power Sources*, **2010**, 195, 4653.

[88] Krijn P. de Jong (Ed), "Synthesis of Solid Catalysts", Wiley-VCH, **2009**.

[89] G. Ertl, H. Knözinger, J. Weitkamp (Eds), "Handbook of Heterogeneous Catalysis", volume 1, Wiley-VCH, **1997.**

[90] C. Jeffrey Brinker and George W. Scherer, "Sol-Gel Science: The Physics and Chemistry of Sol-Gel Processing", Academic Press, Elsevier Science, **1989**

[91] H. M. Kingston, S. J. Haswell, " Microwave-Enhanced Chemistry: Fundamentals, Sample Preparation and Applications". American Chemical Society, Washington DC **1997**.

[92] R. Mokaya, W. Jones, S. Moreno, G. Poncelet, *Catal. Lett.* **1997**, 49, 87.

[93] G. L. Woolery, G. H. Kuehl, H. C. Timken, A. W. Chester, J. C. Vartuli, *Zeolites* **1997**, 19, 288.

[94] M. Müller, G. Harvey and R. Prins. *Micropor. Mesopor. Mater.* **2000**, 34, 281.

[95] S. M. Auerbach, K. A. Carrado, P. K. Dutta (Eds), Handbook of zeolite Science and Technology, **2003**.

[96] M. E. Jamróz, M. Jarosz, J. Witowska-Jarosz, E. Bednarek, W. Tecza, M. H. Jamróz, J. C. Dobrowolski, J. Kijenski, *Spectrochim. Acta, Parta A*, **2007**, 67, 980.

[97] I. E. Marxwell, W. H. J. Stork, in: H. Van Vekkum, E. M. Flanigen, P. A. Jacobs, J. C. Jansen (Eds.), Introduction to zeolite science and practice, Studies in Surface Science and Catalysis vol. 137, Elsevier Science, Amsterdam, **2001**.

[98] T. E. Whyte, R. D. Betta, E. G. Derouane, R. T. K. Baker, Catalytic materials: relationship between structure and reactivity, American Chemical Society, Washington, DC, **1984**.

[99] A.K. Chandra, A. Goursot and F. Fajula, *J. Mol. Catal. A: Chem.*, **1997**, 119, 45.

[100] Z. M. M. Noronha, J. L. F. Monteiro and P. Gélin, *Micropor. Mesopor. Mater.*, **1998**, 23, 331.

[101] N. Viswanadham, L. Dixit, J. K. Gupta and M. O. Garg, *J. Mol. Catal. A: Chem.*, **2006**, 258, 15.

[102] R. Srivastava, N. Iwasa, S. Fujita and M. Arai, *Catal. Lett.*, **2009**, 130, 655.

[103] J. P. Marques, I. Gener, P. Ayrault, J. C. Bordado, J. M. Lopes, F. R. Ribeiro and M. Guisnet, *C. R. Chimie*, **2005**, 8, 399

[104] M. M. L. R. Carrott, P. A. Russo, C. Carvalhal, P. J. M. Carrott, J. P. Marques, J. M. Lopes, I. Gener, M. Guisnet and F. R. Ribeiro, *Micropor. Mesopor. Mater.*, **2005**, 81, 259.

[105] J. P. Marques, I. Gener, J. M. Lopes, F. R. Ribeiro and M. Guisnet, *Catal. Today*, **2005**, 107-108, 726.

[106] J. P. Marques, I. Gener, J. M. Lopes, F. R. Ribeiro and M. Guisnet, *Appl. Catal. A: Gen.*, **2006**, 301, 96.

[107] S. M. Maier, A. Jentys and J. A. Lercher, *J. Phys. Chem. C*, **2011**, 115, 8005.

[108] J. Kornatowski, W. H. Baur and G. Pieper, *J. Chem. Soc. Faraday Trans.*, **1992**, 88, 1339.

[109] S. Kumar, A. K. Sinha, S. G. Hegde and S. Sivasanker, *J. Mol. Catal. A: Chem.*, **2000**, 154, 115.

[110] C. S. Triantafillidis, A. G. Vlessidis, N. P. Evmiridis, *Ind. Eng. Chem. Res.*, **2000**, 39, 307.

[111] S. Shu, S. Husain, J. Koros, *Ind. Eng. Chem. Res.*, **2007**,46, 767.

[112] H. K. Beyer, I. Belenykaja, in: B. Imelik, C. Naccache, Y. Ben Taarit, J. C. Vedrine, G. Coudurier, H. Praliaud (Eds.), Catalysis by Zeolites, Studies in Surface Science and Catalysis vol. 5, Elsevier, Amsterdam, **1980**.

[113] J. Weitkamp, M. Sakuth, C. Chen, S. Ernst, J. *Chem. Commun.*, **1989**, 1908.

[114] M. Lenarda, M. Da Ros, M. Casagrande, L. Storaro, R. Ganzerla, *Inorg. Chim. Acta*, **2003**, 349, 195.

[115] J. M. Newsam, M. M. Treacy, W. T. Koetsier, C. B. DeGruyter, *Proc. R. Soc. London Ser. A*, **1988**, 420, 375.

[116] W. M. Meiwer, Z. Kristallogr. **1961**, 115, 439.

[117] S. Ban, A. N. C. van Laak, J. Landers, A. V. Neimark, P. E.de Jongh, K. P. de Jong and T. J. H. Vlugt, *J. Phys. Chem. C*, **2010**, 114, 2056.

[118] Y. Kuroda, T. Okamoto, R. Kumashiro, Y. Yoshikawa and M. Nagao, *Chem.Comm.* **2002**, 1758.

[119] M. D. Romero, G. Ovejero, M.A. Uguina, A. Rodríguez and J.M. Gómez, *Catal. Commun.,* **2004**, 5, 154.

[120] I. E. Maxwell, *Catal. Today* **1987**, 1, 385.

[121] J. Scherzer and J.M.Bass, *J. Catal.* **1973**, 28, 115.

[122] P.E. Eberly, C.N. Kimberlin and A.Voorhies, *J.Catal.* **1971**, 22, 419.

[123] B. Imelik and J.C. Vedrine, "Catalyst Characterization, Physical Techniques for Solid Materials", Plenum Press, New York, **1994**.

[124] M. Niwa and N. Kertada, Catal. *Surveys from Japan* **1997**, 1, 215.

[125] F.Lónyi and J. Valyon, *Micropor. Mesopor. Mat.* **2001**, 47, 293.

[126] H. Igi, N. Katada, M. Niwa, in: M.M.J. Treacy, B.K. Marcus, M.E.Bisher, J. B. Higgins (Eds.), Proceedings of the 12th International Zeolite Conference, Materials Research Society, Warrendale, PA, **1999**, 2643.

[127] N.Y.Topsoe, K. Pedersen and E. G. Derouane, *J. Catal.* **1981**, 70, 41.

[128] N. R. Meshram, S.G. Hegde and S. B. Kulkarni, *Zeolites* **1986**, 6, 434.

[129] H. G. Karge and V. Dondur, *J. Phys. Chem.* **1990**, 94, 765.

[130] T. Ohgushi, S. Komarneni, and A. S. Bhalla, *J. Porous Mater* **2001**, 8, 23.

[131] T. Ohgushi, and Mg. Nagae*, J. Porous Mater.* **2003**, 10, 139.

[132] M. D. González, Y. Cesteros, P. Salagre, F. Medina and J. E. Sueiras, *Micropor. Mesopor. Mater.* **2009**, 118, 341.

[133] B. M. Chandra Shekara, B. S. Jai Prakash and Y. S. Bhat, *ACS Catal.* **2011**, 1, 193.

[134] D. M. Roberge, H. Hausmann and W. F. Hölderich, *Phys. Chem. Chem. Phys.* **2002**, 4, 3128.

[135] C. Gabriel, S. Gabriel, E. H. Grant, B. S. J. Halstead, and D. M. P. Mingos, *Chem.Soc.Rev.* **1998**, 27, 213.

[136] S. Hayashi and N. Kojima, *Micropor. Mesopor. Mater.* **2011**, 141, 49.

[137] A. A. Gabrienko, I. G. Danilova, S. S. Arzumanov, A. V. Toktarev, D. Freude and A. G. Stepanov, *Micropor. Mesopor. Mater.* **2010**, 131, 210.

[138] C. S. Triantafillidis, A. G. Vlessidis, L. Nalbandian, and N. P. Evmiridis, *Micropor. Mesopor. Mater.* **2001**, 47, 369.

[139] O. Bergadà, E. Boix, P. Salagre, Y. Cesteros, F. Medina and J. E. Sueiras, *Appl. Catal. A: Gen.* **2009**, 368, 163.

[140] I. Batonneau-gener, A. Yonli, S. Hazael-pascal, J. P. Marques, J. M. Lopes, M. Guisnet, F. R. Ribeiro and S. Mignard. *Micropor. Mesopor. Mater.* **2008**, 110, 480.

[141] V. V. Ordomsky, V. Y. Murzin, Y. V. Monakhova, Y. V. Zubavichus, E. E. Knyazeva, N. S. Nesterenko and I. I. Ivanova. *Micropor. Mesopor. Mater.* **2007**, 105, 101.

[142] A. Vimont, F. Thibault-Starzyk and J. C. Lavalley. *J. Phys. Chem. B.* **2000**, 104, 286.

[143] M. Guisnet, P. Ayrault, C. Coutanceau, M. F. Alvarez and J. Datka, *J. Chem. Soc. Faraday Trans.* **1997**, 93, 1661.

[144] T. S. Viinikainen, R. S. Karinen, A. O. Krause, Ed: G. Centi, R. A. van Santen. "Conversion of Glycerol into traffic Fuels" Catalysis for Renewables: From Feedstock to Energy Production" **2007** Wiley-VCH Verlag GmbH and Co. KgaA, Weinheim.

[145] F. J. Liotta, Jr., L. J. Karas, H. Kesling, US Patent 5308365, **1994**, to ARCO Chemical Technology, L.P.

[146] M. Marchionna, R. Patrini, D. Sanfilippo, A. Paggini, F. Giavazzi, L. Pellegrini, *Stud. Surf. Sci. Catal.* **2001**, 136, 489.

[147] V. P. Gupta, US Patent 5476971, **1995**, to ARCO Chemical Technology, L.P.

[148] C. Dewattines, H. Hinnekens, EP 0649829, **1995**, to Fina Research S.A.

[149] D. S. Bradin, US Patent 5578090, **1996** to BRI, Macon.

[150] A. Behr, H. Schmidke, C. Lohr, M. Schneider, DE 4222183, **1994**, to Henkel KGaA.

[151] R. Wessendorf, Erdöl, Erdgas, *Petrochem.* **1995**, 48 (3) 138.

[152] H.Noureddini, W. R. Dailey, B. A. Hunt, "Production of ethers of glycerol from crude glycerol", Chem. Biomolecul. Engineer. Res. Publ., 1998. http://digitalcommons.unl.edu/

[153] A.Behr, L. Obendorf, *Eng. Life Sci.* **2003**, 2, 185.

[154] K. Klepáčová, D. Mravec, E. Hájeková, M. Bajus, *Petrol. Coal*, **2003**, 45, 54.

[155] K. Klepáčová, D. Mravec, M. Bajus, *Appl. Catal. A: Gen.* **2005**, 294, 141.

[156] K. Klepáčová, D. Mravec, A. Kaszony, M. Bajus, *Appl. Catal. A: Gen.* **2007**, 328, 1.

[157] R. S. Karinen, A. O. I. Krause, *Appl. Catal. A: Gen.* **2006**, 306, 128.

[158] J. A. Melero, G. Vicente, G. Morales, M. Paniagua, J. M. Moreno, R. Roldán, A. Ezquerro, C. Pérez, *Appl. Catal. A: Gen.* **2008**, 346, 44.

[159] M. Di Serio, L. Casale, R. Tesser, E. Santacesaria, *Energy Fuels* **2010**, 24, 4668.

[160] H. J. Lee, D. Seung, K. S. Jung, H. Kim, I. N. Filimonov, *Appl. Catal. A: Gen.* **2010**, 390, 235.

[161] L. Xiao, J. Mao, J. Zhou, X. Guo, S. Zhang, *Appl. Catal. A: Gen.* **2011**, 393, 88.

[162] W. Zhao, B. Yang, C. Yi, Z. Lei, J. Xu, *Ind. Eng. Chem. Res.* **2010**, 49, 12399.

[163] P. M. Slomkiewicz, *Appl. Catal. A: Gen.* **2006**, 313, 74.

[164] F. Frusteri, F. Arena, G. Bonura, C. Cannilla, L. Spadaro, O. Di Blasi, *Appl. Catal. A: Gen.* **2009**, 367, 77.

[165] R. van Grieken, J. A. Melero, G. Morales, *J. Mol. Catal. A: Chem.* **2006**, 256,29.

[166] R. Luque, V. Budarin, J. H. Clark, D. Macquarrie, *Appl. Catal. B: Environ.* **2008**, 82, 157.

[167] N. Ozbay, N. Oktar, N. A. Tapan, *Int. J. Chem. Reac. Engin.* **2010**, 8 A18, 1.

[168] R. D'Aquino, G. Ondrey, *Chem. Engineering* **2007**, 114, 31.

[169] M.O. Guerrero-Pérez, J. M. Rosas, J. Bedia, J. Rodríguez-Mirasol, T. Cordero, *Recent Patents on Chemical Engineering*, **2009**, 2, 11.

[170] C. Breen, *Clay Miner.* **1991**, 26, 487.

[171] M. Dolores González, Y. Cesteros, P. Salagre, *Micropor. Mesopor. Mater.* **2011**, 144, 162.

[172] V. Paixão, A. P. Carvalho, J. Rocha, A. Fernandes, A. Martins, *Micropor. Mesopor. Mater.* **2010**, 131, 350.

[173] B. O Dalla Costa, C. A. Querini, *Appl. Catal. A: Gen.* **2010**, 385, 144.

[174] C. Sievers, J. S. Liebert, M. M. Stratmann, R. Olindo, J. A. Lercher, *Appl. Catal. A: Gen.* **2008**, 336, 89.

[175] J. A. Van Bokhoven, A. Roest, D. C. Konigsberger, J. T. Miller, G. H. Nachtegaal, A. P. M. Kentgents, *J. Phys. Chem. B* **2000**, 104, 6743.

[176] F. Ancilloti, F. Mauri, E. Pescarollo, *J. Catal.* **1977**, 46, 49.

[177] A. Gicquel, B. Torck, *J. Catal.* **1983**, 83, 9.

[178] V. N. Shetti, J. Kim, R. Srivastava, M. Choi, R. Ryoo, *J. Catal.* **2008**, 254, 296.

[179] J. Aguado, D. P. Serrano, J. M. Rogríguez, *Micropor. Mesopor. Mater.* **2008**, 115, 504.

[180] J.H. De Boer, The Structure and Properties of Porous Materials, Butterwoth, London, **1958**.

[181] J. Weissmüller; R. N. Viswanath; D. Kramer; P. Zimmer; R. Würschum; H. Gleiter, *Science* **2003**, 300, 312.

[182] S. Chan; S. Kwon; T. W. Koo; L. P. Lee; A. A. Berlin, *Adv. Mater.* **2003**, 15, 1595.

[183] X. He; D. Antonelli, *Angew. Chem. Int. Ed.* **2002**, 41, 214.

[184] M. Moner-Girona; A. Roig; M. Benito; E. J. Molins, *J. Mater. Chem*, **2003**, 13, 2066.

[185] A. Vallribera; E. Molins, *In Nanoparticles and Catalysis*; Astruc, D.; Ed.Wiley-VCH: Weinheim, **2007**.

[186] M. Domínguez; E. Taboada; H. Idriss; E. Molins; J. Llorca, *J. Mater. Chem.*, **2010**, 20, 4875.

[187] M. V. Landau. In Handbook of Heterogeneous Catalysis; Ertl, G.; Knözinger, H.; Schüth, F.; Weitkamp, J. Eds; Wiley-VCH, Weinheim, **2008**.

[188] S. Ghosal; T. F. Baumann; J. S. King; S. O. Kucheyev; Y. Wang; M. A. Worsley; J. Biener; S. F. Bent; A. V. Hamza, *Chem. Mater.* **2009**, 21, 1989.

[189] I. Vicente; P. Salagre; Y. Cesteros; F. Medina; J. E. Sueiras, *Appl. Clay Sci.* **2010**, 48, 26.

[190] N. Hüsing; U. Schubert, Angew. Chem. Int. Ed. **1998**, 37, 22.

[191] R. Mokaya, *J. Phys. Chem. B* **2000,** 104*,* 8279.

[192] Y. Yue, A. Gédéon, J.-L. Bonardet, N. Melosh, J.-B. D'Espinose*,* J. Fraissard, *Chem. Commun.* **1999**, 1967.

[193] R. Mokaya, *Chem. Phys. Chem.* **2002**, 4, 360.

[194] J. Połtowicz, K. Pamin, L. Matachowski, E.M. Serwicka, R. Mokaya, Y. Xia, Z. Olejniczak, *Catal. Today* **2006**, 114, 287.